Potential utilization of fly ash for CO_2 sequestration and acid mine drainage (AMD) wastewater treatment

by

Sibulele Zide

A thesis submitted in fulfillment of the requirements for the degree Master of Engineering: Chemical Engineering

in the

Faculty of Engineering and the Built Environment

at the

Cape Peninsula University of Technology

Supervisor: Prof. Tunde Victor Ojumu

Co-supervisor: Prof. Leslie Felicia Petrik

December 2023

Declaration

I, Sibulele Zide, declare that the contents of this dissertation represent my own unaided work, and that the dissertation or thesis has not previously been submitted for academic examination towards any qualification. Furthermore, it represents my own opinions and not necessarily those of the Cape Peninsula University of Technology.

Signed

17/ 07/ 2023

Date

ABSTRACT

The continued use of fossil fuels to meet the world's energy demands contributes largely to the emissions of greenhouse gases. In South Africa, a considerable amount of carbon dioxide (CO_2) is emitted annually from burning coal to produce electricity. To mitigate the adverse environmental effects arising from the continual increase in CO_2 concentration ($MtCO_2$) in the atmosphere, which in turn gives rise to global warming, this work investigated carbon capture and storage (CCS) using accelerated mineral carbonation (MC). Accelerated MC is emerging as a promising technology for the permanent storage of CO_2 based on its high storage potential (> 10 000 Gt of CO_2) because of the abundance of natural silicates worldwide. The accelerated MC process involves reacting captured CO_2 from a CO_2 emission source with an alkaline-rich feedstock to produce a mineral carbonate, thereby storing the CO_2 permanently. Despite the high storage potential displayed by MC, the relatively high energy consumption (MW) and costs ($/tonne CO_2) associated with the process continue to hinder its widespread implementation. Hence, the focus for accelerated MC in this work was the optimization of several process parameters and the use of coal fly ash (CFA) to improve the carbonation performance thereby reducing the energy consumption (MW) of the process. A preliminary study was first conducted to determine the amount of calcium (Ca^{2+}) leachable from the fly ash (FA). The parameters investigated for the calcium (Ca^{2+}) extraction study were the temperature (^0C), time (min), and particle size (μm). Conditions resulting in the maximum concentration of calcium (Ca^{2+}) extracted were considered the optimum conditions from the leaching study and these process conditions were subsequently used for the carbonation process. The optimum temperature was determined to be 70 ^0C and the optimum reaction times were 30 min, 90 min, and 120 min due to the lower calcium (Ca^{2+}) concentration obtained after 60 min, which from the Dixon's Q-Test proved to be an outlier potentially caused by errors while conducting the experiment. The particle size (μm) was not considered for carbonation experiments based on the trade-off between the maximum calcium (Ca^{2+}) leached and the potential additional energy requirement (MW) due to sieving. Following the carbonation experiments, the carbonation performance was measured through the percentage of $CaCO_3$ formed, the carbonation efficiency CE (%), and the maximum CO_2 storage capacity (kg/kg fly ash). It was found that the maximum % $CaCO_3$ formed after a reaction time of 120 min at 4 Mpa from direct carbonation with AMD wastewater was higher compared to the maximum % $CaCO_3$ formed of 2.43 % from direct aqueous carbonation under the same conditions of time (min) and CO_2 pressure (Mpa). This was attributed to the lower S/L ratio of 0.2 g/mL used for experiments involving AMD wastewater, which improved the calcium (Ca^{2+}) extraction, the additional calcium (Ca^{2+}) concentration of 362.5 ppm from the AMD wastewater, and the increase in the stirring speed from 100 rpm up to 400 rpm upon process optimization.

The highest CE (%) was 63 % and was achieved from direct carbonation with AMD wastewater after 120 min of direct carbonation at 4 Mpa, followed by 53.9 % achieved from indirect carbonation with AMD under the same process conditions. The higher CE (%) through the direct carbonation route was possibly due to the continued extraction of calcium (Ca^{2+}) from the fly ash during the direct carbonation reaction. A lower CE (%) was achieved when pure water was used as the reaction solvent compared to when AMD wastewater was utilized, again attributed to the lower S/L ratio, the additional calcium (Ca^{2+}) concentration provided by the AMD wastewater, as well as the higher stirring speed (rpm) used for the AMD carbonation study. The CE (%) achieved from direct aqueous carbonation was 29.4 % while the CE (%) achieved from the indirect aqueous route was found to be 35.2 % after 120 min of carbonation at 4 Mpa. The higher CE (%) achieved from indirect aqueous carbonation compared to direct aqueous carbonation was due to the higher stirring rate (rpm) used for indirect aqueous carbonation, which improved calcium (Ca^{2+}) extraction. The maximum CO_2 storage capacity which gave an indication of the maximum CO_2 storage potential of the fly ash per 1 kg of fly ash used, was also measured, and it was found to be 0.026 kg/kg fly ash which was expected for fly ash material with a lower calcium oxide (CaO wt. %) content of 4.06 wt. % such as the one used in this study. The study demonstrated a relatively effective storage of CO_2 considering the lower CaO (wt. %) in the fly ash used. From material balance considerations, there was a higher concentration of undissolved CO_2 (i.e., $\sum CO_{2(out)}$ 22.89 g) in the liquid phase from the total CO_2 introduced into the reaction system (i.e., $\sum CO_{2(in)}$ 36.97 g). The mass of dissolved CO_2 was 14.08 g, and 2.08 g was stored as $CaCO_3$. 0.068 MW was consumed from the process, and a high amount of the energy from the total energy output was due to the power for heating, which suggested that lower temperatures (^0C) could be applied for the carbonation process. The energy consumption of 0.068 MW was relatively low due to the non-pre-treatment (i.e., crushing, grinding, sieving, etc.) of the FA. Effective neutralization of the AMD was achieved after 120 min of carbonation at a CO_2 pressure of 4 Mpa for both direct and indirect carbonation with AMD. A pH of 7.1 was achieved under these conditions, which was close to a neutral pH of 7. The percentage (%) removal of most toxic elements was close to 100 % in all cases investigated, which suggests that most of the concentrations after treatment met the target water quality range (TWQR).

ACKNOWLEDGEMENTS

I wish to thank my supervisor, Professor Tunde Victor Ojumu, for his incredible and constant support throughout my master's journey. He has equipped me with invaluable technical skills within chemical engineering during my master's that will serve me throughout my career as an engineer. His supervision was of a high standard, and he ensured that I gained as much as I could from the feedback given during weekly progress meetings. He was always available to assist me whenever required, at whatever time. His supervision was not only confined to academics but stretched to other key areas of life as he was able to frequently give personal support and prudent advice. He has been a great parent to me, and his hardworking, diligent, and stern nature has motivated me throughout the tenure of my master's and life in general.

I also wish to thank my co-supervisor, Professor Leslie Felicia Petrik, whose vast knowledge and expertise in the field provided me with the necessary tools to ensure a full understanding of all concepts pertaining to my master's work and also to ensure that I upheld the required standard throughout my work. Her detailed explanation of concepts during weekly progress meetings and also outside of scheduled progress meetings was outstanding and has helped me enormously in putting this work together. Her kind and wise nature are principles I will always admire and apply throughout my daily life.

I also wish to thank Dr. Emmanuel Ameh, who assisted me immensely during my experimental work carried out at the University of the Western Cape (UWC) Environmental Nanoscience (ENS) laboratories. His ability to oversee my experimental setup and some of my experimental work ensured that I carried out my experiments effectively and accurately. I also wish to thank Mrs. Ilse Wells for ensuring that I had all the necessary resources within the laboratory to carry out my work and for assisting me throughout all the administrative issues I faced. I also wish to thank Mrs. Hannelene Small for ensuring that I had all the necessary laboratory equipment. Her constant follow-ups on administrative matters relating to equipment orders and analyses carried out externally were pivotal in ensuring that I completed my postgraduate work. I would also like to extend my gratitude to the University of the Western Cape (UWC), especially the Technical Services team, for providing the necessary facilities for my laboratory work to be carried out successfully, as well as the University of Cape Town and Stellenbosch for providing me with the necessary analytical equipment for the analysis of my samples.

Given the collaboration with Tohoku University for this work, I would therefore also like to thank Professor Atsushi Iizuka and Dr. Hsing Jung Ho who have assisted me during the course of my master's work, especially during their visits to the Republic of South Africa as well as my return student visit to Tohoku University. I also wish to thank other project collaborators namely Professor Jochen Peterson, Dr Ravi Vadapalli, and Dr Henk Coetzee who thoroughly availed their priceless time for relevant progress meetings, workshops etc.

I also would like to thank the National Research Foundation (NRF) and the Cape Peninsula University of Technology (CPUT) for providing me with bursary opportunities that ensured the covering of my tuition fees including daily expenses. Lastly, I wish to thank my entire family in particular my brother Dr. Mawande Zide who has given me his devoted support emotionally, financially, and otherwise throughout my studies until this higher level. His support has made this achievement possible.

DEDICATION

This thesis is dedicated to my late father (Michael Ndyebo Zide) and late mother (Buyiswa Cynthia Zide). May their souls continue to overlook my hard work and dedication towards my career, and I am certain they are proud of this moment.

Table of Contents

List of Tables

List of Figures

NOMENCLATURE

List of Abbreviations

AMD	Acid Mine Drainage
CCS	Carbon Capture and Storage
C & DW	Construction and Demolition Waste
CE	Carbonation Efficiency
CFA	Coal Fly Ash
CSIR	Council for Scientific and Industrial Research
IPCC	Intergovernmental Panel on Climate Change
ICP-OES	Inductively Coupled Plasma Optical Emission Spectroscopy
MC	Mineral Carbonation
MCT	Mineral Carbonation Technology
MEA	Monoethanolamine
Mt	Megatonne
MW	Megawatt
PCC	Pure Calcium Carbonate
TWQR	Target Water Quality Range
XRD	X-Ray Diffraction
XRF	X-Ray Fluorescence

List of symbols

Definition	Units
Energy	MJ/s
Pressure	Mpa
Particle size	μm
Temperature	℃/K
Time	min
Tonne	t
Stirring speed	rpm
Specific heat capacity (C_p)	J/g ℃
Ideal gas law constant (R)	$L\ bar/K\ mol$
Viscosity	Pa.s

Chemical Formulae

$CaCO_3$	Calcium Carbonate
CO_2	Carbon Dioxide
CO	Carbon Monoxide
CaO	Calcium Oxide
Fe^{2+}	Iron
H_2	Hydrogen
Mg^{2+}	Magnesium
Mn^{2+}	Manganese
N_2	Nitrogen
O_2	Oxygen

Greek symbols

μ	Micron
θ	Theta

Glossary

CO_2 sequestration

The process of capturing and storing atmospheric carbon dioxide (CO_2) with the goal of reducing global climate change.

Carbon Capture and Storage

Carbon capture and storage is a method of reducing carbon emissions from industrial processes by capturing CO_2 and storing it permanently.

Exothermic reaction

A chemical reaction that releases energy from the system to the surroundings.

Law of conservation of energy

Energy can neither be created nor destroyed but can only be altered in its form.

Mineral Carbonation

Mineral carbonation is a process whereby CO_2 is chemically reacted with metal oxide-bearing materials to produce insoluble mineral carbonates.

Hydrolysis

A chemical reaction in which water interacts with a substance and breaks down the molecular bonds of the substance.

Le Chatelier's Principle

Le Chatelier's principle states that if dynamic equilibrium is disturbed by changing the process conditions, equilibrium will shift towards the side that opposes the change.

CHAPTER 1

1. Introduction

1.1 Background

South Africa has a coal-based economy and relies heavily on coal for power generation. This contributes largely to the emission of carbon dioxide (CO_2) into the atmosphere through coal combustion (Kaliyavaradhan & Ling, 2017; Mathieu, 2006). Increasing energy demands result in an increased concentration of atmospheric CO_2 which poses a serious environmental threat because of its contribution to global warming (Neeraj & Yadav, 2020). A promising strategy to reduce CO_2 emissions to mitigate the adverse effects of global warming includes the use of renewable energy sources. Renewable energy sources include wind power, hydropower, solar energy, and biofuels. (Neeraj & Yadav, 2020). The potential use of renewable energy will ensure diversification in our energy mix and reduce CO_2 emissions. Fossil fuels like coal are expected to continue to meet our primary energy demands for the foreseeable future, nevertheless, given the economic benefits provided by the South African coal mining industry (Cloete, 2010).

Carbon Capture and Storage (CCS) is thus becoming one of the more practical methods sought for lowering CO_2 concentrations in the atmosphere (Sikhakhane, 2020). CCS can be done using several CO_2 capture and storage techniques. CO_2 capture methods include pre-combustion capture, post-combustion capture, and oxyfuel combustion, while subsequent storage techniques include biological storage, geological storage, oceanic storage, and mineral carbonation (MC) storage (Bandilla, 2020; Ncongwane, 2016). In South Africa, plans for the implementation of CCS technology started in 2004. Around this time, the Council for Scientific and Industrial Research (CSIR) published a report that indicated that South Africa could have considerable storage capacity in geological formations (Cloete, 2010). CO_2 can be captured and collected from emitters, where it can then be transported and stored underground for long periods of time (Ngwenya, 2019).

Furthermore, the South African Centre for Carbon Capture and Storage (SACCCS) has since conducted extensive research on the technical feasibility of CCS in South Africa (Beck et al., 2013). The research conducted indicates that geological sequestration has the problem of limited storage sites for storage, and the selection of more suitable storage sites requires increased expenditure (Cloete, 2010). In addition, potential CO_2 leakages and transport costs associated with the method present further problems (Mortezaei et al., 2017; Smith et al., 2021).

Oceanic sequestration is another CO_2 sequestration method that has been considered. The method involves the injection of CO_2 into the ocean and has a relatively higher potential for CO_2 sequestration (Neeraj & Yadav, 2020). However, the method presents similar problems to geological sequestration which include limited storage sites, potential CO_2 leakages, and transport costs due to offshore basins being far from CO_2 emitters (Lal, 2008; Smith et al., 2021). Another issue associated with the method is that of ocean acidification (Gupta, 2011). Given the limitations, costs, and environmental impact associated with geological and oceanic sequestration methods, the use of these technologies in South Africa may not be worthwhile. The amounts sequestered may not be significant enough to justify the costs and potential negative environmental impact (Ncongwane, 2016).

An alternative to these methods is the permanent storage of CO_2 through accelerated MC. Due to the high CO_2 storage potential (i.e., > 10 000 Gt of CO_2) and the permanent storage of CO_2 provided by accelerated MC, which is also regarded as being safer, accelerated MC is becoming a potential solution for the long-term storage of CO_2 (Sanna et al., 2014). Accelerated MC follows the process of natural MC. MC for the storage of atmospheric CO_2 is a known process that occurs naturally through silicate weathering, whereby natural silicate rocks react with atmospheric CO_2, which later becomes stored in mineral carbonate form on a geological time scale (Pan et al., 2012). However, the process occurs too slowly in nature to achieve effective CO_2 storage. Hence, accelerated MC using engineered processes for more effective consumption of atmospheric CO_2 was then proposed by Seifritz (1990).

For accelerated MC, captured CO_2 from a process plant is stored permanently by reacting the captured CO_2 with calcium (Ca^{2+}) or magnesium (Mg^{2+}) bearing natural silicate minerals, often in the form of wollastonite ($CaSiO_3$), serpentine ($Mg_3Si_2O_5(OH)_4$), or olivine (Mg_2SiO_4), or by reacting the captured CO_2 with alkaline-rich waste materials such as coal fly ash (Nyambura et al., 2011), demolished concrete waste, steel slag, etc. This is done under conditions (i.e., temperature, pressure, etc.) that favour a faster rate of carbonation for the formation of mineral carbonates, e.g., calcium carbonate ($CaCO_3$) or magnesium carbonate ($MgCO_3$), thereby permanently storing CO_2 in mineral carbonate form (Gerdemann et al., 2007; Yadav & Mehra, 2021). MC can follow ex-situ (above ground level) or in-situ (below ground level) routes (Madzivire et al., 2019; Muriithi et al., 2013). The former route involves the already described approach of using industrial chemical processes for CO_2 storage, where captured CO_2 from a process plant is reacted with natural silicate minerals or industrial alkaline wastes to form mineral carbonates thereby storing CO_2, while the latter route involves the captured CO_2 being injected below the ground where it can react with alkaline minerals in geological formations to form mineral carbonates (Olajire, 2013). The ex-situ route is often preferred for accelerated

MC due to the limited availability of suitable geological sites for the in-situ route (Yadav & Mehra, 2021). Although the method of accelerated MC displays higher CO_2 storage potential and better safety, it still proves costly (Neeraj & Yadav, 2020). Hence, the current focus for the accelerated MC process is improving the rate of carbonation by determining the optimum set of process parameters for carbonation such as temperature (^0C), time (min), particle size (μm), S/L ratio, CO_2 pressure (Mpa), etc. Optimizing process parameters that significantly affect the rate of carbonation can ensure a more efficient CO_2 storage process and in turn, reduce energy consumption and process costs (Pan et al., 2012). The other important area of focus for achieving reduced process costs for accelerated MC is investigating the use of suitable feedstocks for the process. Given that natural silicate minerals such as wollastonite ($CaSiO_3$), serpentine ($Mg_3Si_2O_5(OH)_4$), and olivine (Mg_2SiO_4) require mining and expensive pre-treatment (i.e., thermal, chemical, or mechanical) to achieve effective reactivity, industrial waste materials such as fly ash, demolished concrete waste, steel slag, etc. offer an attractive alternative to natural silicate minerals as the main feedstocks for accelerated MC (Pan et al., 2012).

Alkaline waste materials have high reactivity because they contain active metal oxide elements including calcium oxide (CaO) and magnesium oxide (MgO) and are chemically less stable than natural silicate minerals (Ji et al., 2017; Pan et al., 2012). They require less expensive pre-treatment, and in some cases, no pre-treatment is required. In addition, alkaline industrial by-products such as fly ash have the benefit of being abundant and are easily accessible near CO_2 emission sources, unlike natural minerals, which require mining, which is an additional process cost (Bauer et al., 2011; Mathieu, 2006). Research on accelerated MC using alkaline waste materials has mostly focused on the direct carbonation of these feedstocks. The advantage of the direct carbonation route is the simplicity of the process, as it is a single-step process, unlike indirect carbonation, which takes place in two steps. For the accelerated carbonation of alkaline-rich wastes, whether through the direct or indirect route, water has mostly been used as the reaction medium, although the use of wastewater reaction mediums such as brine (Muriithi et al., 2009), or acid mine drainage (AMD) wastewater has also been investigated (Ji et al., 2017; Ukwattage et al., 2015). By adding calcium (Ca^{2+}) from AMD or brine, effective CO_2 storage can be achieved, and the wastewater can also be neutralized as a result (Lee et al., 2016; Madzivire et al., 2019). This makes it desirable to employ these wastewaters as reaction media for CO_2 storage.

The neutralization of environmentally hazardous wastewater, particularly AMD, is a critically concerning environmental issue. AMD wastewater is environmentally hazardous, and the wastewater is generated when groundwater comes into contact with sulfide-bearing minerals that are undergoing oxidation (Akcil & Koldas, 2006). The generation of AMD wastewater is promoted by mining activity from both active and abandoned coal and gold mines in South Africa (Akcil & Koldas, 2006; Vellemu, 2017). Potgieter-Vermaak et al. (2006) mentioned that gold-bearing mines contain a significant amount of conglomerates that contain pyrite (FeS_2) together with several other sulfide-containing minerals, such as pyrrhotite. When mining activity becomes economically unfavourable, mines become abandoned. Abandoned mines become flooded with groundwater, and the water becomes acidic pH (2 to 4) with a high concentration of sulfates and dissolved metals as a result of being in contact with sulfide-bearing minerals that are undergoing oxidation due to exposure to atmospheric oxygen (O_2) (CSIR, 2009).

AMD wastewater emanating from sulfide-containing minerals which is highly acidic with toxic metal contaminants such as copper (Cu^{2+}), lead (Pb^{2+}), zinc (Zn^{2+}), etc (Akcil & Koldas, 2006; Tomiyama et al., 2019), therefore presents a serious threat to water quality and aquatic life as it can enter into rivers, lakes, etc (Nkongolo, 2020). AMD neutralization and remediation have mostly been done using limestone although several other methods of treatment have been studied (Gitari et al., 2018; Jones & Cetin, 2017). Notable disadvantages of limestone for AMD neutralization are mainly its limited efficiency and the sludge that is generated in large volumes and requires disposal (Gitari et al., 2018).

The environmental threat posed by the increase in atmospheric CO_2 concentration coupled with AMD wastewater concerns provides the need for the development of processes that can ensure effective CO_2 storage and simultaneous AMD wastewater treatment. The simultaneous treatment of AMD and CO_2 storage can ensure both effective neutralization of AMD and CO_2 sequestration (Ji & Yu, 2018). Hence, this study focuses on determining the most effective method between direct carbonation and indirect carbonation using different reaction mediums (i.e., water and AMD wastewater) for efficient storage of CO_2 and simultaneous neutralization of environmentally hazardous AMD wastewater with coal fly ash used as the feedstock.

1.2 Problem Statement

South Africa relies heavily on coal for power generation, and this contributes largely to the emission of CO_2 through coal combustion (Kaliyavaradhan & Ling, 2017). CO_2 is one of the most problematic greenhouse gases, and although renewable energy sources are available, South Africa's economy still relies heavily on the coal mining industry (Cloete, 2010). Hence, there is a growing need to develop effective CCS methods that will mitigate the threat posed by vast CO_2 emissions coming from coal power plants in South Africa (Beck et al., 2013). Current CO_2 storage techniques such as geological and oceanic sequestration are relatively costly, with safety and environmental issues continuing to hinder their application (Lal, 2008). The method of accelerated MC for the permanent storage of CO_2 is attractive due to its higher CO_2 storage potential and ability to ensure permanent storage of CO_2. However, the method is still costly with strategies required around ensuring optimum carbonation performance using less energy to reduce process costs ($/tonne of CO_2 stored). In addition to the problem posed by CO_2 emissions from coal power plants, there is also the issue of acid mine drainage (AMD) wastewater generated from mining activity in South Africa. AMD is highly acidic (pH 2-4) and poses a serious environmental threat (Gitari et al., 2018). There is thus a clear need for the development of processes that can help achieve effective CO_2 capture and storage with the simultaneous treatment of AMD wastewater.

1.3 Aim

The aim of this study is to investigate the potential of Durapozz fly ash to permanently store CO_2 and simultaneously neutralize AMD wastewater. Furthermore, the study also aims to investigate whether using AMD wastewater enhances the overall carbonation performance.

1.4 Objectives

1. Conducting leaching (i.e., preliminary) experiments to determine the effect of temperature (^{0}C), time (min), and particle size (μm) on the amount of calcium (Ca^{2+}) leachable from fly ash.

2. Performing direct and indirect carbonation experiments with water and AMD for CO_2 storage and AMD neutralization.

3. Investigating the effects of temperature (^{0}C), reaction time (min), S/L ratio, stirring speed (rpm), and CO_2 pressure (MPa) on carbonation efficiency (CE %) and $CaCO_3$ formed for CO_2 storage.

4. Investigating the effects of reaction time (min) and CO_2 pressure (MPa) on the pH and the percentage (%) removal of metals from AMD during AMD neutralization.

5. Performing material balance calculations around a 600 mL high-pressure reactor to determine the total CO_2 uptake of the reaction system.

6. Determining the energy (MW) requirement for the process.

1.5 Research questions

The study will answer the following research questions:

1. How effective is the fly ash used in the storage of CO_2 in mineral carbonate form?

2. What parameters have the most significant effect on the overall carbonation performance for CO_2 storage and AMD neutralization?

3. Which process route between direct and indirect carbonation is more effective for CO_2 storage and AMD neutralization?

4. Which reaction medium between water and AMD is more effective for CO_2 storage?

5. How much energy does the procedure use?

1.6 Research Approach

This study will focus on the direct and indirect carbonation approaches for CO_2 sequestration and AMD neutralization:

1.6.1 Direct Carbonation

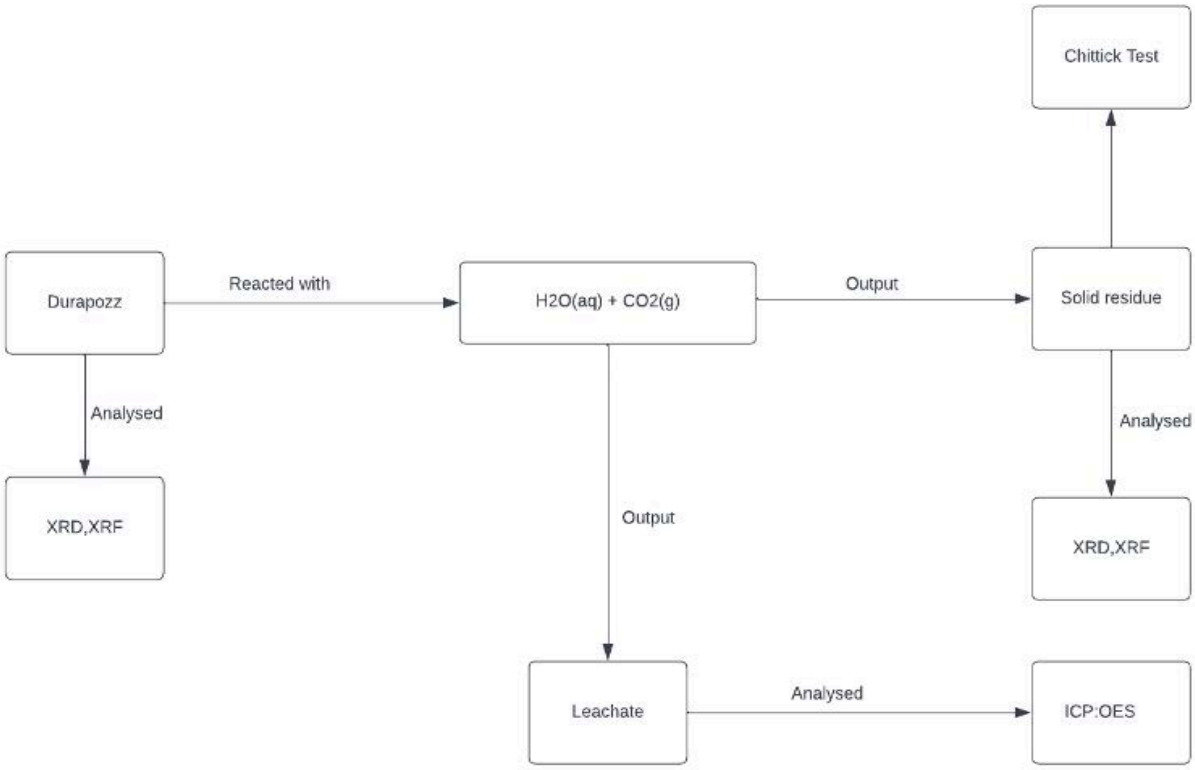

Figure 1.1: Block Flow Diagram (BFD) for direct carbonation approach

Figure 1.1 illustrates the various steps taken during direct aqueous carbonation experiments and the appropriate characterisation techniques used at each stage. An identical approach was taken for direct carbonation experiments involving AMD neutralization, where the feedstock (i.e., fly ash) was reacted with AMD wastewater.

1.6.2 Indirect Carbonation

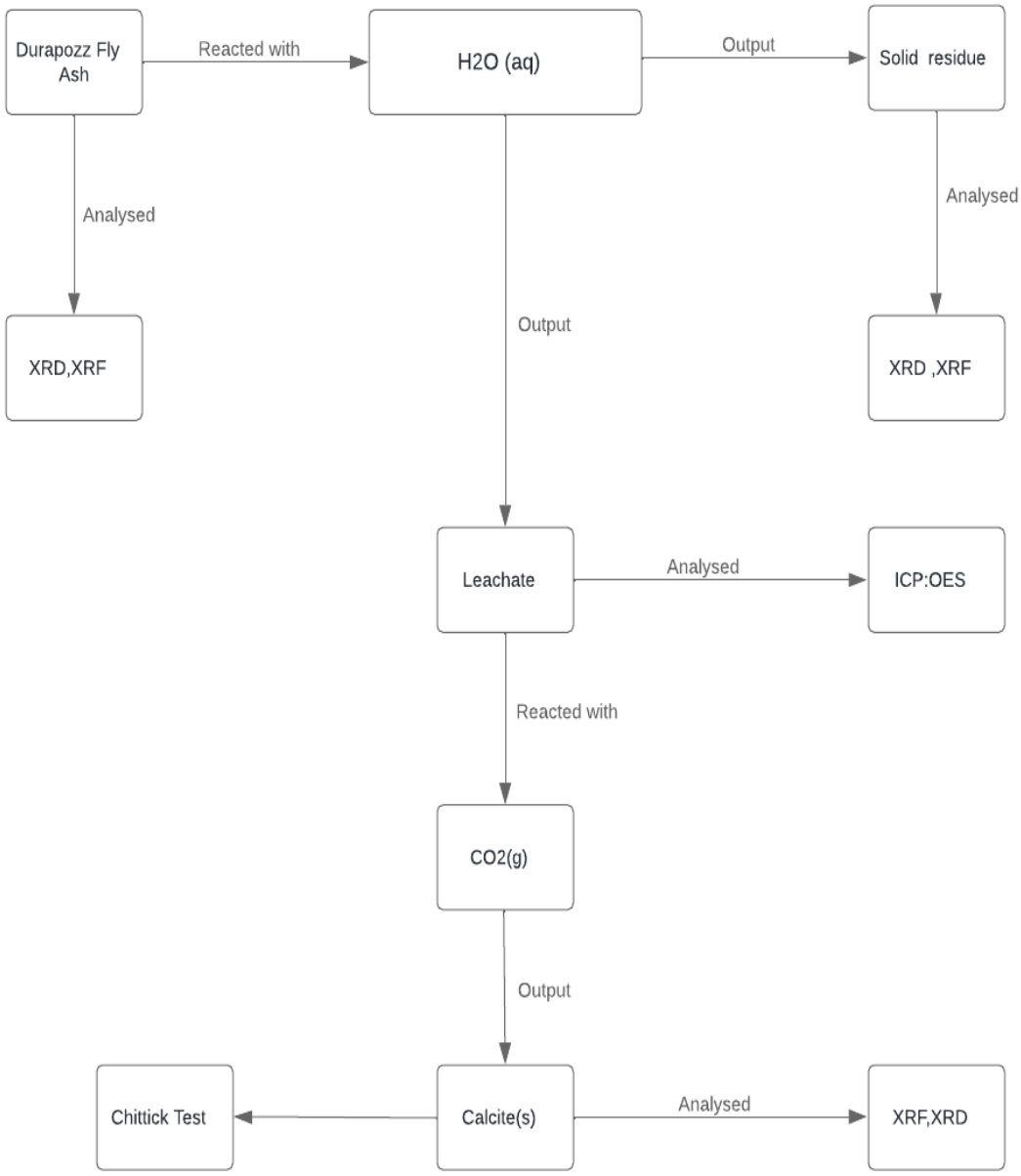

Figure 1.2: Block flow diagram for indirect carbonation approach

Figure 1.2 illustrates the various steps taken during indirect aqueous carbonation experiments and the appropriate characterisation techniques used at each stage. An identical approach was taken for indirect carbonation experiments involving AMD neutralization, where the feedstock (i.e., fly ash) was reacted with AMD wastewater.

1.7 Hypothesis

From the metal oxide species available in fly ash that can store CO_2 as a mineral carbonate, calcium oxide (CaO wt. %) is predominantly responsible for CO_2 storage as calcium carbonate ($CaCO_3$). Optimizing key process parameters results in effective carbonation performance and the use of AMD wastewater as a solvent is more effective for CO_2 storage compared to water.

1.8 Scope and Delineation

This study focuses mainly on the CO_2 sequestration potential of fly ash. The study focuses specifically on direct and indirect carbonation using water and AMD wastewater for CO_2 sequestration. The CO_2 sequestration process will also neutralize the AMD wastewater. The $CaCO_3$ product from the process can also be utilized for AMD neutralization, as AMD wastewater can be neutralized using $CaCO_3$. However, this study only focuses on the neutralization of AMD wastewater through the CO_2 sequestration process using fly ash as the reaction feedstock. Only one type of fly ash (Class F) material was considered for the study. The use of additives and enhancing extraction reagents such as hydrochloric acid (HCl) and sodium hydroxide (NaOH) for indirect carbonation was not considered.

1.9 Thesis Outline

Six more chapters are present in this study. Their sequence and content are as follows:

- **Chapter 2: Literature Review**

This chapter focuses on CO_2 sequestration by the methods of mineral carbonation (MC) and AMD neutralization using fly ash as a feedstock. By using previous literature, the chapter highlights and compares relevant experimental parameters influencing the carbonation performance of CO_2 sequestration experiments, as well as parameters influencing AMD neutralization.

- **Chapter 3: Methodology**

This chapter presents the materials used in the study. It also describes the methodology and analytical methods used to achieve the objectives of the study.

- **Chapters 4, 5, and 6: Results and Discussion, Material Balance, and Energy Balance**

These chapters present results obtained from experiments, analytical techniques, and material and energy balances. The results are discussed in relation to previous literature.

- **Chapter 7: Conclusions, Recommendations, and Implications**

  This chapter presents the final conclusions drawn from the study based on the results obtained. Relevant recommendations and the implications thereof are provided.

CHAPTER 2

2. Literature Review

This chapter provides a review of the Carbon Capture and Storage (CCS) process, focusing mainly on the utilization of accelerated mineral carbonation (MC) as the storage method and the subsequent neutralization of acid mine drainage (AMD) wastewater. This literature review section essentially highlights and compares the key process parameters that influence the carbonation performance for the storage of captured carbon dioxide (CO_2) by accelerated CO_2 mineralization from previous studies.

2.1 Carbon Capture and Storage (CCS) process

There are currently 26 operational CCS facilities worldwide in a range of industries, including power generation, hydrogen, steel, cement, etc (Global CCS Institute (GCCSI), 2020). CCS involves the capture and permanent storage of CO_2, mainly from the combustion of fossil fuels. The initial stage of any CCS process involves capturing CO_2 using one of the following capture methods (Bandilla, 2020):

1. Post-combustion capture involves the separation of CO_2 from the products of the combustion process (i.e., flue gases).
2. Pre-combustion capture is the method of decarbonizing of the fuel (i.e., coal, gas, or biomass) prior to combustion.
3. Oxyfuel combustion is re-engineering the combustion process in order to produce pure CO_2, thereby eliminating the need for its separation.

Figure 2.1 shows the various options for CO_2 capture from power generation. From Figure 2.1, it is evident that CO_2 separation is not required for oxyfuel combustion, while pre-combustion and post-combustion capture require the separation of CO_2 from a gas mixture containing CO_2 and hydrogen (H_2) and CO_2 and nitrogen (N_2), respectively:

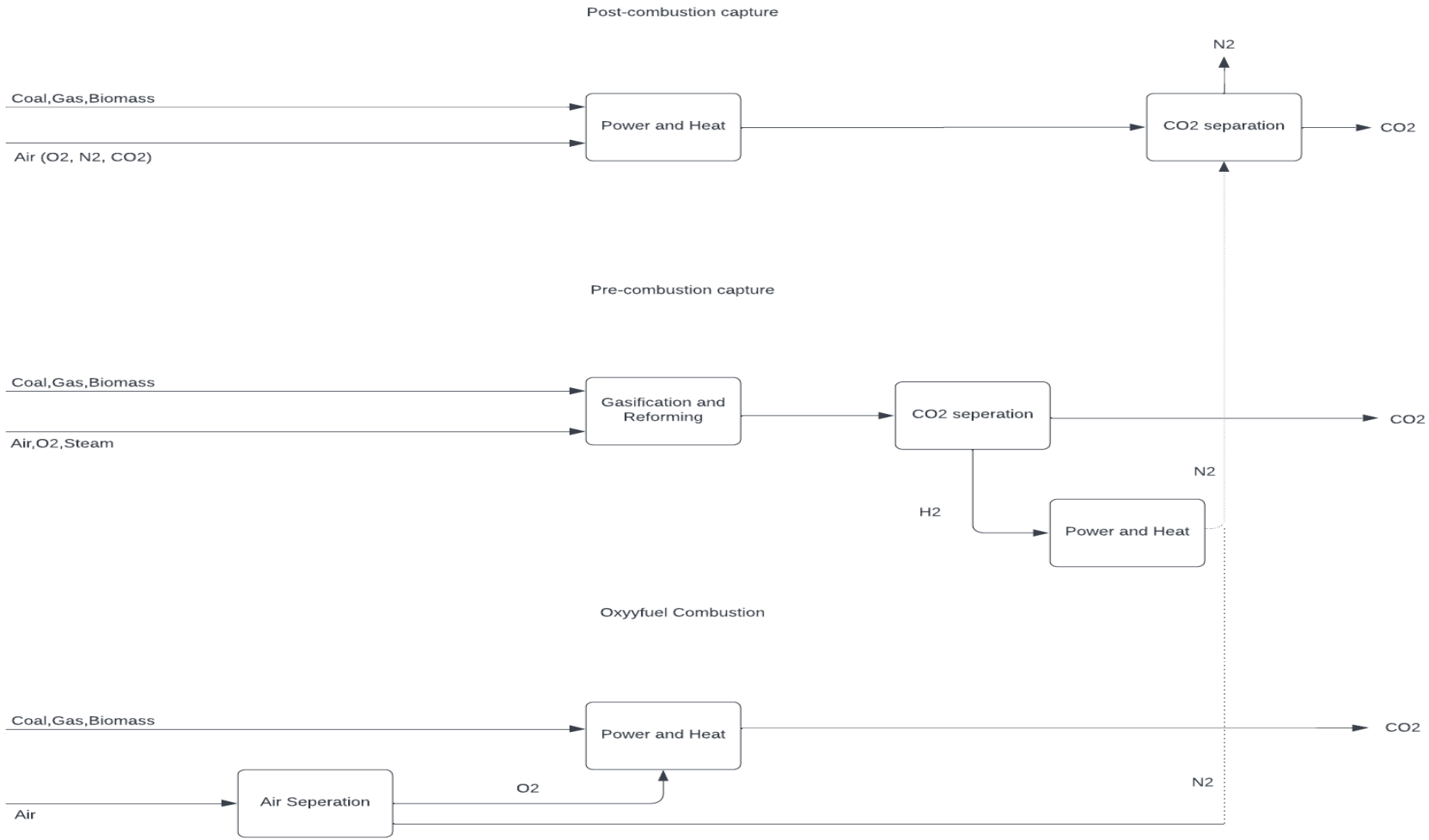

Figure 2.1: Various options for CO_2 capture from power generation (Bandilla, 2020)

2.1.1 Post-combustion capture

Post-combustion systems separate CO_2 from part of the flue gases, as shown in Figure 2.1. There are currently several technologies available for the process of CO_2 capture from flue gases, but based on the higher capture efficiency, selectivity, lower energy requirements, and the overall process costs, the absorption process, which typically uses the solvent monoethanolamine (MEA), is the most preferred method (Kheirinik et al., 2021; Mathieu, 2006).

2.1.2 Pre-combustion capture

There are also pre-combustion capture techniques used industrially. The primary fuel is processed in a reactor with steam, air, or oxygen (O_2) for the pre-combustion process to create a mixture that primarily contains carbon monoxide (CO) and hydrogen (H_2) (Jansen et al., 2015). Additional H_2 and CO_2 are produced by reacting the CO with steam in a second reactor, with the resulting mixture of H_2 and CO_2 separated into a CO_2 and H_2 gas stream. If the CO_2 is stored, then H_2 is a carbon-free energy carrier that can be combusted to generate power and heat (Mathieu, 2006).

2.1.3 Oxyfuel combustion

Oxyfuel combustion requires the delivery of oxygen rather than air to the combustion chamber. This ensures that the gaseous combustion reaction product is near-pure CO_2 rather than a mixture from which CO_2 needs to be separated (Bandilla, 2020).

2.1.4 Preferred CO_2 capture method

Kheirinik, Ahmed and Rahmanian (2021) assessed the capital and investment costs of a 230 MW powerplant and found that the total costs were lower for the post-combustion method. Additionally, post-combustion technologies can be integrated into existing power plants without major disruption to the operation of the plant (Bandilla, 2020). For these reasons, post-combustion CO_2 capture methods are preferred over pre-combustion and oxyfuel combustion systems.

2.1.5 CO_2 Storage

Neeraj and Yadav (2020) observed that after CO_2 has been effectively captured, the existing storage techniques have their individual advantages and disadvantages to consider. These are presented in Table 2.1:

Table 2.1: Characteristics of CO_2 storage methods (Neeraj and Yadav 2020)

Storage Type	**Advantages**	**Drawbacks**	**Storage potential (Gt)**	**Cost ($/tonne CO_2 stored)**
Geological	Well developed technology	Risk of leakage	1800	0.5-8
	Economical	Requires constant monitoring		
		Shortage of suitable storage sites		
Oceanic	High storage potential	Environmental risk	>100	6-31
	No monitoring required	More expensive that geological storage		
		Ocean acidification		
MC	Environmentally safe	High process costs in some cases	>1000 to >1 000 000	50-100
	Exothermic reactions	Slow reaction kinetics		
	Abundance of feedstock	Pre-treatment of feedstock required in some cases		
	Permanent storage	High energy consumption in some cases		

Table 2.1 shows the various CO_2 storage methods and although geological storage is currently the most developed technology for large CO_2 emitters, it can be seen that MC has the highest CO_2 sequestration potential (i.e., >10 000 Gt) due to the abundance of natural silicates worldwide (Sanna et al., 2014). However, MC currently still has the highest process cost of 50-100 $/tonne CO_2 (Bobicki et al., 2012). This is notably the most significant drawback for accelerated MC as the process can prove energy-intensive (Pan et al., 2012). If the process is to be considered for widespread implementation, it therefore needs to find strategies for minimizing its energy consumption, which would lead to reduced process costs. One of the major strategies to ensure the process of accelerated MC is more efficient and hence more cost-effective is by improving the kinetics of the carbonation process by optimizing process parameters (Huijgen et al., 2005).

When using natural silicates as the feedstock for accelerated MC, such as wollastonite ($CaSiO_3$), serpentine ($Mg_3Si_2O_5(OH)_4$), or olivine (Mg_2SiO_4), the process can be kinetically improved by activating the material to make it more reactive. This activation can be achieved through pre-treatment of the mineral which includes crushing, grinding, and milling to ensure a reduced particle size (μm) which increases the surface area of particles contacting CO_2 during the carbonation process and results in a more effective carbonation process (Mathieu, 2006). The other form of activation is through heat treatment. The heat treatment ensures more effective leaching of calcium (Ca^{2+}) or magnesium (Mg^{2+}) from these natural silicates. The effective leaching of metal ions yields a higher concentration of metal ions available for the reaction with CO_2, which in turn improves the rate of the carbonation process (Yadav & Mehra, 2021). All of these activation processes are energy intensive and need to be avoided for the accelerated MC process to become viable (IPCC, 2005).

Most research efforts have been aimed at optimizing process parameters that overall result in a more effective carbonation process, such as the temperature (^0C), time (min), particle size (μm), S/L ratio, CO_2 pressure (Mpa), etc. In this way, the MC process can then have the potential to be less energy-intensive and therefore less costly (Ji & Yu, 2018). Recent studies have mainly focused on the use of calcium-rich industrial waste materials such as coal fly ash, demolished concrete, steel slag, etc., for accelerated MC due to the high costs associated with mining and pre-treatment of natural silicates (Huntzinger et al., 2009). The costs of mining and activating natural silicates are estimated at around 10 $ per tonne of CO_2 with an additional 2 % of CO_2 emissions (Bobicki et al., 2012).

2.2 Mineral Carbonation (MC)

The permanent storage of CO_2 through MC is a naturally occurring process where atmospheric CO_2 reacts with natural silicates to form carbonates, thereby storing the CO_2 permanently (Pan et al., 2012). In nature, MC for CO_2 sequestration is a slow process. The MC process can be accelerated through the carbonation of pre-treated natural silicates or alkaline-rich materials to help reduce the rate of CO_2 emissions, from power plants and other emission sources thus preventing the further increase of atmospheric CO_2 (Ukwattage et al., 2013). Accelerated MC for permanent CO_2 storage involves the reaction of captured CO_2 from a process plant with calcium (Ca^{2+}) or magnesium (Mg^{2+}) metal oxide-bearing feedstocks in order to form a stable mineral carbonate (Sanna et al., 2014).

2.2.1 Natural MC

MC is a naturally occurring process that occurs on a geological time scale through silicate weathering. The process involves the reaction of natural silicates with atmospheric CO_2, as shown (Pan et al., 2012):

Olivine

$$Mg_2SiO_4 + CO_2 \rightarrow 2MgCO_3 + SiO_2 \ \Delta H = +89\ kJ/mol \quad (1)$$

Serpentine

$$Mg_3Si_2O_5(0H)_4 + 3CO_2 \rightarrow 3MgCO_3 + 2SiO_2 + 2H_2O \ \ \Delta H = +64\ kJ/mol \quad (2)$$

Wollastonite

$$CaSiO_3 + CO_2 \rightarrow CaCO_3 + SiO_2 \ \Delta H = +90\ kJ/mol \quad (3)$$

When atmospheric CO_2 comes into contact with the natural silicate after being dissolved in rainwater, the rainwater leaches the calcium (Ca^{2+}) and magnesium (Mg^{2+}) from the silicate into rivers and, subsequently, the ocean, where it precipitates to form stable mineral carbonates that store CO_2 permanently over time (Bobicki et al., 2012).

2.2.2 Accelerated MC

Following the separation of CO_2 from flue gas in a power plant, permanent storage of CO_2 can then be achieved through the accelerated MC process. Accelerated MC, used to achieve more effective CO_2 storage, is a process whereby CO_2 from the capture step is brought into contact with a metal oxide-bearing material with the purpose of fixing the CO_2 as a carbonate under conditions that promote a faster rate of carbonation (Board et al., 2012; Mathieu, 2006). Table 2.2 presents some of the metal oxide-bearing materials used for the accelerated MC process:

Table 2.2: Feedstocks for accelerated MC (Mathieu, 2006)

Feedstock	Examples
Natural silicates	Wollastonite, olivine, serpentine etc
Industrial wastes	Coal fly ash (CFA), construction and demolition waste (C&DW), steel slag, cement kiln dust etc.

The accelerated MC method has been studied using some of the reaction feedstocks shown in Table 2.2. For the accelerated MC process, CO_2 reacts with metal oxides (MO) available in natural minerals or industrial wastes. The corresponding mineral carbonate forms through the exothermic reaction shown in Equation 4 (Bobicki et al., 2012):

$$MO + CO_2 \rightarrow MCO_3 + heat \quad (4)$$

It is important to note that interest in MC comes from the following unique features (Mathieu, 2006):

- The abundance of materials that contain metal oxides.
- The ability of the method to permanently store CO_2 in a stable solid form.
- High storage potential.

2.3 Material balance considerations for MC

Figure 2.2 shows material and energy balances through the system boundaries for a power plant with integrated CCS, and accelerated MC used for the storage process:

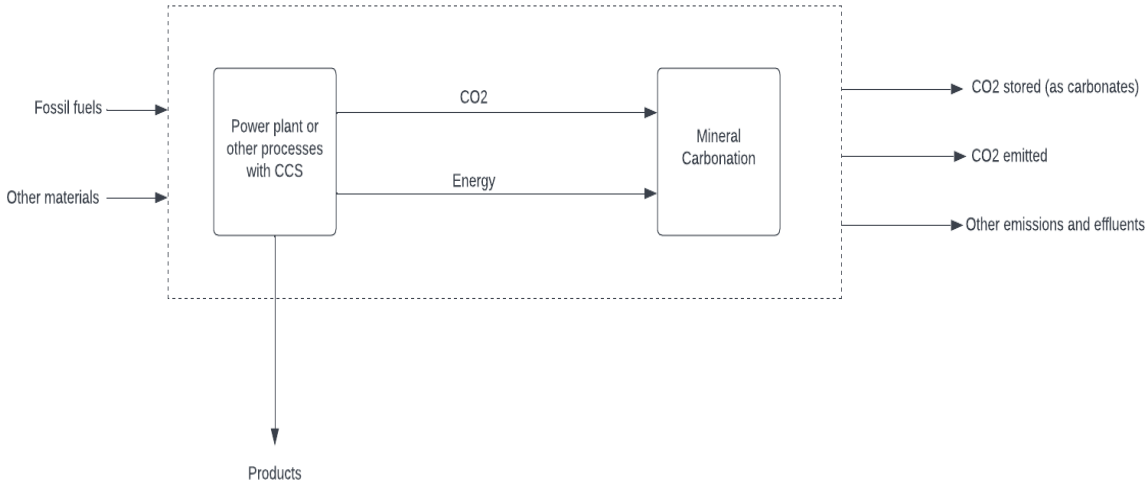

Figure 2.2: Material and energy balance through the system boundaries for a power plant with CCS with accelerated MC used as the storage method (Mazzotti et al., 2005)

For a power plant with integrated CCS that uses accelerated MC as the storage method such as the one presented in Figure 2.2, the fossil fuel provides energy both to the power plant that produces CO_2 and to the mineralization process (Mazzotti et al., 2005). Given that the accelerated MC process can also produce CO_2, the amount of CO_2 that can be emitted from the overall process is important to determine. A significantly higher amount of CO_2 stored than that emitted indicates an effective CO_2 sequestration process.

The amount of CO_2 captured by the power plant, together with the amount of CO_2 emitted and stored through the mineralization process, can be determined using the law of conservation of mass through material balance calculations. The overall material balance around any system is given by (Himmelblau & Riggs, 2004):

$$\begin{matrix}\text{Accumulation} \\ (\text{Build up} \\ \text{within system})\end{matrix} = \begin{matrix}\text{Mass in} \\ (\text{Enters through} \\ \text{system boundaries})\end{matrix} - \begin{matrix}\text{Mass out} \\ (\text{Leaves through} \\ \text{system boundaries})\end{matrix} + \begin{matrix}\text{Generation} \\ (\text{Produces within} \\ \text{system})\end{matrix} - \begin{matrix}\text{Consumption} \\ \text{Consumed} \\ \text{within system}\end{matrix} \quad (5)$$

For a system without reaction and at steady state (i.e., no accumulation of mass within the process), the general mass balance reduces to (Reklaitis & Schneider, 1986)**:**

$$\cancel{Accumulation} = Material\ In - Material\ Out + \cancel{generation} - \cancel{consumption}$$

$$\therefore Material\ In = Material\ out \quad (6)$$

The accelerated MC process can be batch or continuous in nature. A continuous process is one that has the feed streams and product streams moving in and out of the process all the time, whereas a batch process is one where no mass is added or removed from the vessel.

Iizuka et al. (2013) investigated the amount of CO_2 that could be sequestered from a CCS process using accelerated MC for storage with an alkaline waste material (i.e., waste concrete) utilized as the reaction feedstock. The study showed that by using alkaline wastes such as waste concrete, high CO_2 storage capacities can be achieved at lower sequestration costs ($/tonne), as their process estimated an annual CO_2 storage capacity of 1.4 million tonne/year.

2.4 Energy balance considerations for MC

Determining the amount of energy consumed for accelerated MC is critical because the potential of the accelerated MC process depends on the trade-off between costs associated with the energy-consuming steps (i.e., mining and pre-treatment of the feedstock) and benefits (i.e., the large potential capacity due to the abundance of natural metal oxide bearing silicates and the permanence of CO_2 storage) (IPCC, 2005). The overall energy consumption for the accelerated MC processes can be determined by an application of the law of conservation of energy through energy balance calculations, where the total energy consumed for the process is determined from the general energy balance (Himmelblau & Riggs, 2004):

$\Delta E_{system} = Q + W$ (assuming a closed system) where; (7)

ΔE_{system} is the total energy of the system. For a stationary and unelevated closed system, $\Delta E_{system} = \Delta U$ (internal energy).

Q is the energy due to heat given by $Q_{in} - Q_{out}$;

and W is the energy due to work given by $W_{in} - W_{out}$

2.4.1 Energy consumption for MC

MC using natural silicates is a slow process that can be kinetically enhanced by raising parameters such as temperature (^{0}C). Metal ion extraction is considered the main rate-limiting step, and most research efforts have been devoted to finding ways to speed up the metal extraction from the solid input materials. This can be achieved by activating the mineral to make it more reactive (Mathieu, 2006). Activation takes different forms, such as heat treatment at 650 (^{0}C) for serpentine and ultra-fine grinding for olivine and wollastonite. The energy requirement for activation has been estimated to be 300 kWh/tonne and 70–150 kWh/tonne for thermal and mechanical activation, respectively. MC for CO_2 storage has been performed after such pre-treatment ; however, the process is expensive and energy-intensive, and its feasibility is questionable (IPCC, 2005).

Introducing CCS technology can result in a 30-50% energy penalty on the original power plant. When accounting for the 10-40% energy penalty in the capture plant as well, a full CCS system with mineral carbonation would need 60-180% more energy than a power plant with equivalent output without the implementation of CCS which shows the implications of the CCS process on the total energy consumption of a power plant (Mazzotti et al., 2005). Iizuka et al. (2004) determined a minimum power consumption of 25.9 MW/100 MW for the sequestration process from a CO_2 emitting thermal power plant on the basis of laboratory-scale experimental results using an alkaline industrial waste feedstock. The energy requirement resulted in an overall cost of 22 $/tonne of CO_2 stored, which is still competitive with costs obtained for sequestration methods such as oceanic, which are between 6-31 $/tonne of CO_2 stored (Neeraj and Yadav 2020).

2.4.1 Cost considerations for MC based on energy consumption

A commercial process for accelerated MC would require mining, crushing, and milling of the mineral-bearing ores and transporting them to a processing plant that receives CO_2 from a power plant. As mentioned previously, there are additional costs associated with such pre-treatment processes, and the costs of mining and preparing natural silicates are estimated at around 10 US$/tonne of CO_2, with an additional 2 % of CO_2 emissions (Bobicki et al., 2012). The energy requirements associated with mineral pre-treatment can be reduced by exploiting options such as the exothermic nature of the MC reaction, where energy in the form of heat can be recovered from the process and reused, thereby reducing the energy requirements and process costs. The case studied for MC on an industrial scale for the wet carbonation of the natural silicate olivine, found the cost associated with the process to be between 50 and 100 US$/t$CO_2$ (Mathieu, 2006).

Due to such high costs, current studies have focused on the use of industrial alkaline waste materials such as fly ash, demolished concrete, steel slag, etc. to effectively reduce process costs for accelerated MC and hence the overall costs for the CCS process. These waste materials have the benefit of requiring a lower degree of pre-treatment and less energy-intensive operating conditions to enhance carbonation yields. Iizuka et al. (2013) performed a cost evaluation for accelerated MC under aqueous conditions using waste concrete. The lowest estimated CO_2 sequestration cost for the process was -232 $/tonne CO_2 and was found to be highly competitive with other sequestration methods such as geological and oceanic sequestration that have reported CO_2 storage costs between 0.5-8 and 5-30 $/tonne CO_2 net injected, respectively, thus proving that the use of alkaline waste feedstocks is well suited for making the accelerated MC process economically feasible (Mathieu, 2006).

2.5 Suitable feedstocks for MC

Ncongwane (2016) noted that considering the energy penalty associated with accelerated MC, the key goal of research has been to enhance the reaction kinetics of the process. This is necessary if the technology is to be justified for mass industrial deployment. Therefore, it is essential in the endeavor to make accelerated MC economically practical and, as a result, for the technology to have widespread industrial implementation, to employ industrial waste materials instead of natural silicate minerals. Examples of such materials are fly ash, demolished concrete debris, steel slag, etc. Compared to natural silicate minerals, industrial waste materials have several advantages as feedstock for accelerated MC. These waste materials offer higher reactivity because they are chemically less stable than geologically derived minerals (Huijgen & Comans, 2003). They are also typically fine-grained with high reactive surface areas, thus, they require a lower degree of pre-treatment and less energy-intensive operating conditions for enhancing the carbonation performance (Sanna et al., 2014). Sanna et al. (2014) further mention that these materials are often associated with CO_2 point source emissions, and they supply a readily available source of calcium (Ca^{2+}) without the need for mining. There are several industrial waste materials currently being investigated for accelerated MC, most of which are rich in CaO (wt. %) content. This study focuses on the use of one such industrial waste material in the form of fly ash.

2.5.1 Coal Fly ash (CFA)

The industrial by-product coal fly ash has been used as a feedstock for CCS by MC in several studies. Ji et al. (2017) mentioned that the advantages of using fly ash include relatively high material reactivity, no pre-treatment requirements, abundance, ease of availability near CO_2 emission sources, and the possibility of reusing the end product of the CO_2 sequestration step in construction materials.

2.5.1.1 Coal fly ash generation and global recycling

Coal is a fossil fuel that can be classified into four main groups, namely bituminous coal, sub-bituminous coal, lignite, and anthracite, depending on the carbon content and energy released when burnt (Nkongolo, 2020). The burning of coal gives rise to coal fly ash, and this by-product of coal combustion is produced in significant quantities worldwide. Countries such as India are regarded as one of the world's leading coal producers and given that Indian coal has a high ash content, 120 - 150 million metric tons of coal fly ash are generated in India (Jain & Dwivedi, 2014). This coal fly ash is mostly stored as waste heaps or landfill deposits and thus becomes a pollutant that poses a serious environmental threat (Sett, 2017). Of the 120 – 150 Mt of coal fly ash produced in India, only about 38 % is reused in various industries, such as the construction industry (Jain & Dwivedi, 2014). Other countries such as the United States of America (USA), produce around 122 Mt of coal fly ash annually of which approximately 35 – 40 % is used beneficially (Reddy et al., 2010). Gianoncelli et al. (2013) identified that although coal fly ash poses a certain environmental threat, coal fly ash can be used as an important raw material for the cement and construction industries with various other applications such as wastewater treatment, zeolite synthesis, etc.

2.5.1.2 Fly ash generation and recycling in South Africa

South Africa produces around 100 Mt of low-grade bituminous coal each year and of this 100 Mt, approximately 28 Mt of coal fly ash is produced as a by-product (Gitari et al., 2018). The principal components of this fly ash are silica (SiO_2), aluminium oxide (Al_2O_3), and calcium oxide (CaO), with varying amounts of carbon as indicated by the loss of ignition (LOI) (Gitari et al., 2005). Reynolds-Clausen & Singh (2019) reported that between 2014 and 2015, 119.2 Mt of coal were produced, with only 7 % of the coal fly ash reused constructively. In South Africa, many power stations are running out of storage space to accommodate coal fly ash waste, which explains Eskom's initiative of recently reviving its Ash Utilisation Project to advocate for the use of coal as a beneficial resource (Funston et al., 2021).

The constructive reuse of coal fly ash could play a vital role in mitigating the negative environmental impact of stockpiled fly ash, as leachates from fly ash are highly siliceous and alkaline (pH>12) and can contaminate soil and groundwater (Gitari et al., 2006). It can also play a key role in business development as it benefits the construction industry. Moreover, its new applications will help in the effort towards reducing CO_2 emissions and treating environmentally hazardous wastes such as AMD wastewater (Reynolds-Clausen & Singh 2019).

2.5.2 Chemical and mineralogical properties of fly ash (FA)

Table 2.3: Elemental and mineralogical phases of a typical fly ash sample

	Fly Ash
Elemental Composition	SiO_2>Al_2O_3>Fe_2O_3> CaO>MgO
Mineralogical Composition	Quartz (SiO_2), mullite ($Al_6O_{13}Si_2$), magnetite ($FeFe_2O_4$)

Table 2.3 shows the chemical and mineralogical compositions of a typical fly ash sample. Fly ash is classified into two main groups, namely Class C and Class F as claimed by the American Society for Testing and Materials (ASTM). The characterisation is based upon the maximum and minimum percentages of quartz (SiO_2), aluminium oxide (Al_2O_3), and hematite (Fe_2O_3) available (Alterary & Marei, 2021). Class F fly ash is pozzolanic, arising from either anthracite or bituminous coal. The total amount of SiO_2, Al_2O_3, and Fe_2O_3 must be greater than 70%. Class C ashes are pozzolanic, and cementitious and are produced from sub-bituminous or lignite coal burning. The overall quantity of SiO_2, Al_2O_3, and Fe_2O_3 must be greater than 50% (American Coal Ash Association, 2013). Notably, fly ash with more than 20% CaO (wt. %) is classified as Class C and lower calcium-bearing fly ash is characterised as Class F fly ash. Therefore, a distinction can be made between Classes C, and F fly ash based on the percentage of CaO (wt. %), with Class C having greater than 10% and Class F having less than 10% of CaO (Wardhono, 2018).

2.5.2.1 Characterisation of fly ash

The percentage composition of each mineral and element present in fly ash can be determined by analytical methods such as X-Ray Diffraction (XRD) and X-Ray Fluorescence (XRF). It also becomes important to determine the elemental composition of the resulting leachates from the carbonation of fly ash, and the elemental compositions can be determined using Inductively Coupled Plasma: Optical Emission Spectrometry (ICP-OES) analysis. Table 2.4 provides a summary of the purpose of each of the analytical methods, namely XRD, XRF, and ICP-OES.

Table 2.4: Various analytical techniques used for analysis

Analytical Method	Purpose
• XRD	According to Kruse et al. (2012), the XRD analytical technique is used to determine the mineralogical phases present in various solids. In the case of fly ash, X-ray diffraction (XRD) qualitatively identifies the crystalline phases of the fly ash sample. Within an XRD machine setup, electrons hit a solid sample, and X-rays are emitted. When the X-rays hit a crystal structure, some X-rays diffract based on this crystal structure, but other X-rays penetrate further into the sample until colliding into a crystal. The machine reads all the angles of diffracted, scattered X-rays and their intensities to create a pattern. With a high-intensity scan, major and minor crystalline phases can be identified.
• XRF	The XRF analytical technique is used to determine the elemental composition (wt.%) of major, minor, or trace elements in various solids. In the case of fly ash, XRF is used to evaluate the bulk oxide content (Alterary & Marei, 2021). High-energy X-rays excite the fly ash, and this process emits fluorescent, or secondary X- rays. These secondary X-rays are used to identify the oxides qualitatively and quantitatively in the sample (Kruse et al., 2012). XRF can be used to determine amorphous content by subtracting the crystalline amount from the total bulk oxide amount found with XRF. XRF spectrometers are available in different designs. The simplest are handheld devices that are used for routine analysis of materials and most analyse circular areas with diameters of ~10 mm, although some models can also analyse areas of 1 mm diameter (Goodman et al., 2015).

• ICP-OES	ICP-OES is used to determine the elemental composition of major and minor elements for varying types of liquid solutions. The technique derives its analytical data from the emission spectra of elements excited in a high-temperature plasma. The ICP-OES optical system separates element-specific wavelengths of light emitted from the excited sample and focuses the resolved light onto the detector as efficiently as possible. The spectrometer is comprised of two sections, the fore-optics, and the polychromator. When the light exits the polychromator, it is focused on the detector (Hannan, 2017). The technique gives very high sensitivity for the determination of elements in solution and is sensitive in detecting small concentrations to even very low parts per billion (ppb) levels (Muriithi, 2009).

2.5.3 Coal fly ash compared to other alkaline waste feedstocks for CO_2 storage

According to the South African Coal Fly Ash Association, South Africa only produces Class F fly ash which typically contains low CaO (wt. %) content (Vilakazi et al., 2022). Table 2.5 shows the percentage (%) chemical composition of a typical South African Class F fly ash sample:

Table 2.5: Chemical composition of South African fly ash (Vilakazi et al., 2022)

SiO_2	Al_2O_3	Fe_2O_3	CaO	TiO_2	Na_2O	SO_3	MgO	P_2O_5	MnO	LOI
49.92-56.29	27.21-31.52	2.58-5.91	4.80-9.47	1.39-2.25	0.03-0.81	0.05-4.78	1.47-2.69	0.45-0.90	-	1.54-7.81

According to Nyambura et al. (2011), the overall calcium (Ca^{2+}) content of fly ash has a significant impact on the degree of carbonation, even though the presence of other mineral phases may affect the reactivity of CO_2 during carbonation. Recently, several other researchers have investigated the use of construction waste for the CO_2 storage process. Ben Ghacham et al. (2015) demonstrated that 34.6 % of the introduced CO_2 converted to thermodynamically stable calcite ($CaCO_3$) when using concrete waste with the chemical composition presented in Table 2.6:

Table 2.6: Chemical composition of construction waste material (Ben Ghacham et al., 2015)

SiO_2	Al_2O_3	Fe_2O_3	CaO	TiO_2	Na_2O	SO_3	MgO	K_2O	MnO	LOI
45.2	8.1	2.1	26.8	0.34	1.39	1.2	0.63	2.18	-	17.2

From Table 2.6, the concrete waste from the study conducted by Ben Ghacham et al. (2015) contains lower compositions of SiO_2, Al_2O_3 and Fe_2O_3 compared to typical Class F fly ash, but more importantly, the material contains a high CaO (wt. %) content, which was responsible for the high CO_2 storage in mineral form (i.e., $CaCO_3$) (Bobicki et al., 2012). Previous work conducted by using cement waste with a high calcium (Ca^{2+}) content of 27.6 % showed that a high amount of CO_2 can be converted to $CaCO_3$, as a maximum conversion to $CaCO_3$ of more than 67% was achieved in their study at a lower CO_2 pressure of 0.1 Mpa which favoured $CaCO_3$ precipitation.

2.6 Process routes for MC

Several approaches for accelerated MC have been studied, ranging from direct gas-solid approaches to more complex multi-stage MC routes as shown in Figure 2.3 (Olajire, 2013):

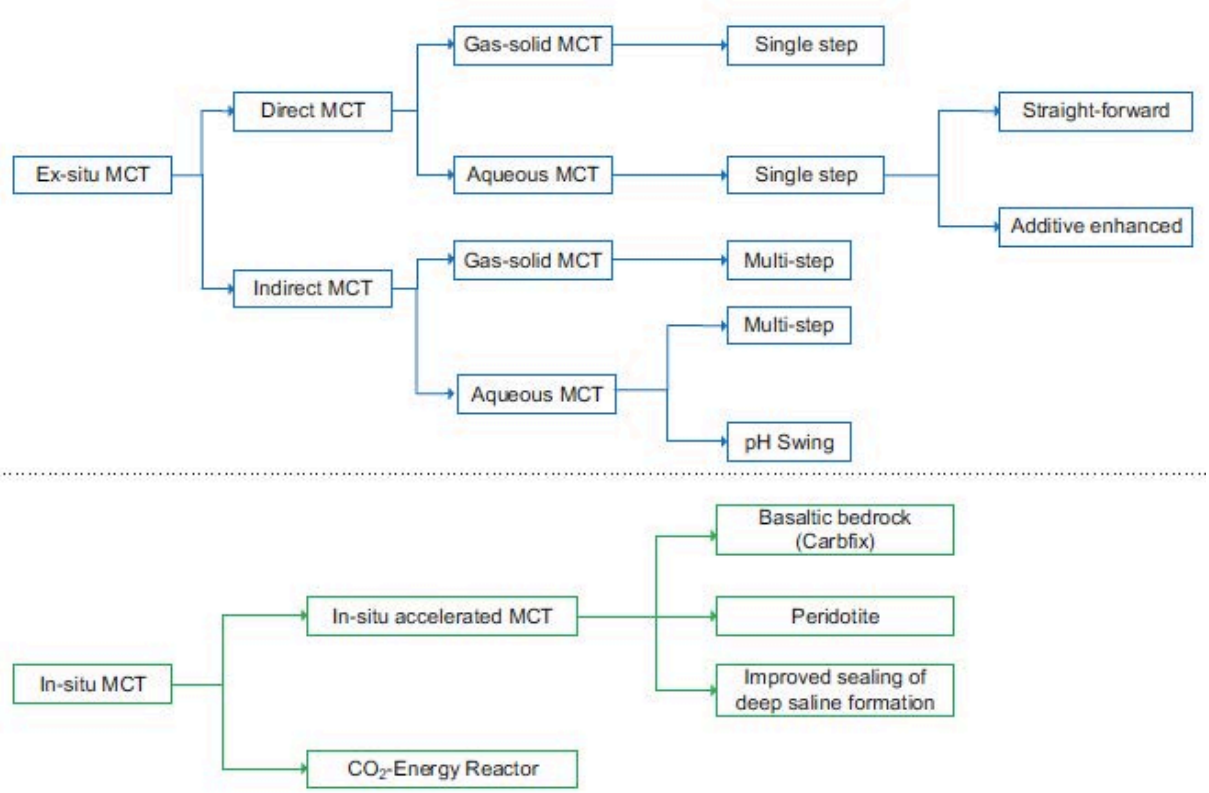

Figure 2.3: Classification of MC routes (Olajire, 2013)

Figure 2.3 illustrates the division of accelerated MC processes into ex-situ (outside of its native environment, i.e. above ground) and in-situ (in deposit) groups. For these categories, research interest has been given to ex-situ Mineral Carbonation Technology (MCT), with a focus on direct and indirect mineral carbonation routes for accelerated MC (Olajire, 2013).

2.6.1 Direct aqueous route for MC using fly ash

MC processes can be divided into two routes namely direct and indirect carbonation. The direct carbonation process occurs in a single step as shown in Figure 2.4:

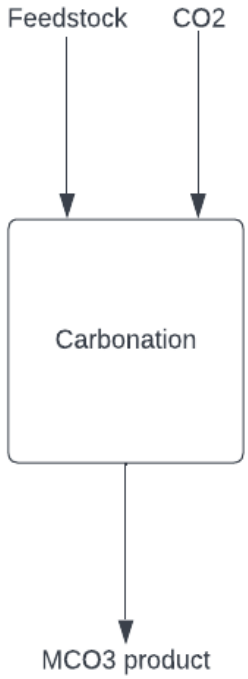

Figure 2.4: Direct MC process route

Ji & Yu (2018) mentioned that direct carbonation is a single-step process that can be achieved through both gas-solid carbonation and the aqueous carbonation route. The direct reaction of gaseous CO_2 with a suitable feedstock, e.g., fly ash, is the most basic form of direct mineral carbonation:

$$CaO_{(s)} + CO_{2(aq)} \rightarrow CaCO_{3(s)} \quad (8)$$

Previous studies confirmed that the gas-solid carbonation of dry fly ash under low-pressure conditions was technically viable and promising. However, due to the slow reaction kinetics, elevated temperature (^{0}C) and pressure (Mpa) are normally required in gas-solid carbonation (Doeff et al., 2008). Previous studies used temperatures up to 500 ^{0}C, which proves energy intensive. Hence, direct aqueous MC is more promising than gas-solid approaches because an effective carbonation process can be achieved by adding water to the fly ash. This is attributed to the water's ability to achieve effective extraction of calcium (Ca^{2+}) from the solid matrix of fly ash particles (Mazzotti et al., 2005; Patel et al., 2017).

2.6.1.1 Process chemistry

Ji & Yu (2018) observed that the process of accelerated MC using fly ash through the direct aqueous route is based on three reaction steps namely:

- The dissolution of CO_2 into solution from the gaseous phase.
- The extraction of calcium (Ca^{2+}) ions from the solid matrix of the fly ash particles.
- Lastly, the precipitation and crystal growth of calcium carbonate ($CaCO_3$).

The CO_2 dissolution from the gaseous phase into the liquid phase and the extraction of calcium (Ca^{2+}) ions from fly ash constitute the rate-limiting steps for the carbonation reaction. This is because the concentration of dissolved CO_2 and the amount of calcium (Ca^{2+}) extracted and dissolved affects the overall carbonation performance (Ji & Yu, 2018). However, most studies identify the leaching of calcium (Ca^{2+}) as the main rate-limiting step (Ukwattage et al., 2015). The rate-limiting steps are controlled by process parameters including temperature (^{0}C), time (min), particle size (μm), S/L ratio, stirring speed (rpm), CO_2 pressure, etc. These process parameters are known to significantly affect the dissolution of CO_2 in the liquid phase and also the leachability of calcium (Ca^{2+}) from the fly ash (Mazzotti et al., 2005). The carbonation reaction for the Ca-H_2O-CO_2 system is controlled by the state of equilibrium, and the reaction mechanism of the process is as follows:

Initially, CO_2 gas is hydrated and dissolved in the liquid phase to form carbonic acid (H_2CO_3) (Ukwattage et al., 2015):

$$CO_{2(g)} + H_2O \rightarrow H_2CO_{3(aq)} \quad (9)$$

The equilibrium concentration of dissolved CO_2 follows Henry's law where the solubility of CO_2 is directly proportional to its partial pressure at a given temperature (^{0}C) (Dananjayan et al., 2016):

$$[CO_2] = K_H \times P_{CO_2} \quad (10)$$

Where;

K_H is the Henry's law constant (mol/atm) and P_{CO_2} is the partial pressure.

H_2CO_3 then dissociates in solution, producing bicarbonate (HCO_3^-), carbonate (CO_3^{2-}), and protons (H^+), which results in a reduced solution pH of approximately 3 units. Typically, pH is reduced from 11 to 8 (Bertos et al., 2004). According to Le Chatelier's principle, the dissolution of CO_2 in the Ca-H_2O-CO_2 system is thus favourably favoured under alkaline conditions (Ho et al., 2020):

$H_2CO_{3(aq)} \overset{K_a}{\rightarrow} HCO_3^- + H^+$ and;

$HCO_3^- \overset{K_b}{\rightarrow} H^+ + CO_3^{2-}$

Where;

K_a and K_b are the equilibrium constants expressed by:

$K_a = \frac{[HCO_3^-]\,[H^+]}{[H_2CO_3]}$ and;

$K_b = \frac{[CO_3^{2-}]\,[H^+]}{[HCO_3^-]}$

According to Ji & Yu (2018), alkaline oxides are hardly present in pure forms but instead tend to be locked up in silicate, aluminate, and ferrite amorphous phases. The calcium (Ca^{2+}) extraction step from fly ash causes an increase in pH during the leaching process due to the release of OH^- ions into the aqueous phase (Ho et al., 2020). When CaO interacts with the water in solution, calcium hydroxide ($Ca(OH)_2$) dissociates to form Ca^{2+} and OH^- ions (Ji & Yu, 2018):

$CaO + H_2O \rightarrow Ca(OH)_2$ then; (11)

$Ca(OH)_{2(s)} \rightarrow Ca^{2+} + 2OH^-$

Calcium carbonate is then formed through the reaction between calcium (Ca^{2+}) ions and carbonate (CO_3^{2-}) ions (Iizuka et al., 2004b):

$Ca^{2+} + CO_3^{2-} \rightarrow CaCO_3$

Finally, the crystal growth occurs spontaneously until the equilibrium between calcite and the solution is reached. The carbonation reaction is regulated by solution equilibrium (Ji & Yu, 2018):

$$CaCO_3(nuclei) \leftrightarrow CaCO_3(calcite)$$

Ji & Yu (2018) mentioned that from the point of view of process chemistry, the challenge of mineral carbonation by fly ash is that the dissolution of calcium (Ca^{2+}) from fly ash is favoured at lower pH, whereas lower pH does not favour the precipitation of carbonates. Therefore, there is a need to find a balance between conditions that favour an effective rate of carbonation without hindering the precipitation of $CaCO_3$ (Ji & Yu 2018). The precipitation of $CaCO_3$ products can be related to the solubility product constant of $CaCO_3$ (Bauer et al., 2011):

$$K_{sp} = [Ca^{2+}] \times [CO_3^{2-}] \quad (12)$$

Where;

K_{sp} is the solubility product constant at a given temperature (℃), $[Ca^{2+}]$, and $[CO_3^{2-}]$ are the equilibrium concentrations of calcium and carbonate ions respectively.

The saturation index S_I can be used to estimate the saturation with respect to $CaCO_3$ and can be calculated by (Montes-Hernandez et al., 2009):

$$S_I = \frac{[Ca^{2+}]\,[CO_3^{2-}]}{K_{sp}} > 1 \quad (13)$$

$S_I > 1$ represents oversaturation while $S_I < 1$ represents undersaturation (Bauer et al., 2011).

Ji & Yu (2018) mentioned that an oversaturation of metal ions may hinder the leaching and dissolution of calcium (Ca^{2+}) which can result in a slower rate of $CaCO_3$ formation.

2.6.2 Indirect aqueous route for MC using fly ash

Indirect aqueous carbonation is another process route that exists for accelerated MC. The process can produce high-purity and marketable precipitated calcium carbonate (PCC) due to the separation of the precipitation step and dissolution of raw materials. This can help offset the total costs of the accelerated MC process (Chang et al., 2017; He et al., 2013). Indirect mineral carbonation takes place in more than one stage, as shown in Figure 2.5:

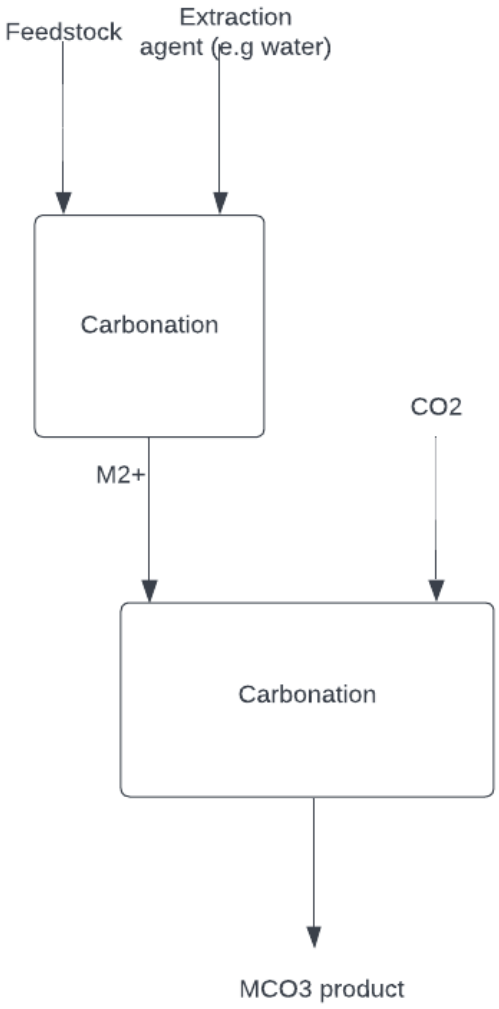

Figure 2.5: Indirect MC process route

The indirect aqueous carbonation method takes place in two steps. The first step involves the extraction of the reactive component from fly ash, namely calcium (Ca^{2+}), and the second step is the reaction of CO_2 with the calcium-rich solution obtained from the extraction step (Saran et al., 2018).

As mentioned, the first step for indirect aqueous carbonation is the extraction of calcium ions from the dissolution of CaO:

$CaO + H_2O \rightarrow Ca(OH)_2$ then;

$Ca(OH)_{2(s)} \rightarrow Ca^{2+} + 2OH^-$

After the calcium (Ca^{2+}) is extracted and leached, the calcium (Ca^{2+}) rich water is then carbonated. The CO_2 first interacts with the water to form carbonate ions (Sun et al., 2012):

$CO_{2(g)} + H_2O \rightarrow H_2CO_{3(aq)}$

H_2CO_3 then dissociates in solution, producing bicarbonate (HCO_3^-), carbonate (CO_3^{2-}), and protons (H^+), which results in reduced pH of the solution:

$H_2CO_{3(aq)} \overset{K_a}{\rightarrow} HCO_3^- + H^+$ and;

$HCO_3^- \overset{K_b}{\rightarrow} H^+ + CO_3^{2-}$

Carbonate (CO_3^{2-}) ions that form react with the calcium (Ca^{2+}) ions found in solution to form calcium carbonate ($CaCO_3$):

$Ca^{2+} + CO_3^{2-} \rightarrow CaCO_3$

Finally, crystal growth occurs until the equilibrium between calcite and the solution is reached:

$CaCO_3(nuclei) \leftrightarrow CaCO_3(calcite)$

Pure carbonates can be produced using indirect methods, due to the removal of impurities in previous carbonate precipitation stages (Sanna et al., 2014). However, Chang et al. (2017) found that the formation of the desired polymorph of $CaCO_3$,which is calcite, from the indirect aqueous carbonation route is still a practical challenge that strongly depends on synthesis variables such as temperature (^{0}C), pressure (Mpa), solution pH, reaction time (min), the degree of saturation in solution, ionic concentration and ratio, ionic strength, and also stirring speed (rpm).

2.7 Carbonation performance

There are several methods that can be used to determine the efficiency of the carbonation process. The actual maximum CO_2 storage capacity of fly ash can be used to determine the amount of CO_2 that can be sequestered for a given amount of fly ash, and it depends on the theoretical maximum CO_2 storage capacity, which can be determined from Stenoir's formula. From the resulting theoretical maximum CO_2 storage capacity, the maximum CO_2 storage capacity can be determined (Montes-Hernandez et al., 2009). The percentage of $CaCO_3$ formed can be used to determine the actual amount of CO_2 stored in the fly ash by considering the volumetric evolution of CO_2 using Chittick tests. The carbonation efficiency (CE %) can also be used to determine the amount of CO_2 consumed due to the carbonation reaction. Previous work relates this CO_2 sequestration measure to the pressure drop due to carbonate precipitation (Muriithi, 2009). These methods for determining the carbonation performance all provide an indication of how effective the fly ash material is for capturing CO_2.

2.7.1 Maximum CO_2 storage capacity

For pure oxides such as CaO and $Ca(OH)_2$, the theoretical extent of carbonation is a function of basic stoichiometry:

$$CaO_{(s)} + CO_{2(aq)} \rightarrow CaCO_{3(s)}$$

Given that $mass = moles \times molar\ mass$ and considering that the molar ratio of the reaction of $CaO_{(s)}$, and $CO_{2(aq)}$ to form $CaCO_{3(s)}$ is 1:1, it follows that every tonne of CaO can potentially sequester up to 0.799 metric tons of CO_2 (Muriithi, 2009). The theoretical extent of carbonation for fly ash can also be calculated as a function of stoichiometry, though in this case the extent of carbonation also depends on the availability of the oxides for reaction. Theoretically, the maximum CO_2 storage capacity can be calculated as a function of the chemical composition of the raw fly ash using Stenoir's formula (Rushendrarevathy et al., 2014):

$$CO_2\ (\%) = 0.785 \times (\%\ CaO - 0.7\ \%\ SO_3) + 1.09\ \%\ Na_2O + 0.93\ \%\ K_2O \quad (14)$$

Where;

$\%\ CaO$, $\%\ SO_3$, Na_2O *and* $\%\ K_2O$ are the elemental compositions from the raw fly ash.

2.7.2 % $CaCO_3$ formed

Muriithi et al. (2009) used a Chittick test to quantify the amount of $CaCO_3$ in each sample based on the volumetric evolution of CO_2 when carbonates react with dilute hydrochloric acid. The amount of CO_2 fixed in the solid phase as $CaCO_3$ is an important indicator of how much CO_2 is stored from the process (Ho et al., 2020).

The percentage of $CaCO_3$ formed can be calculated by first calculating a correction factor for each reading with respect to pure calcium carbonate ($CaCO_3$). The correction factor is given as:

$$f = \frac{W \times T}{1.22 \times V} \quad (15)$$

Where;

W = 0.10 grams weighed of pure $CaCO_3$
T = temperature of measurement in K
V = ml produced CO_2

The above correction factor was used to calculate the % $CaCO_3$ (based on 1.7 g of fly ash samples) as follows:

$$F = CR_1 - (0.04)\,(CR_{20} - CR_1) \quad (16)$$

Where;

CR_1 = reading at 1 minute $\times$ f

CR_{20} = reading at 20 minutes $\times$ f

$\therefore \%\, CaCO3 = 0.232F$

2.7.3 Carbonation Efficiency (CE%)

By knowing the pressure drop, which is directly proportional to the CO_2 consumption within the reaction system for the carbonation reaction, the carbonation efficiency (CE %) can thus be used to determine the CO_2 consumption in the reaction system due to $CaCO_3$ formation. The carbonation efficiency (CE %) can be measured by:

$$CE\% = \frac{n_{CO_2} M_{CO_2}}{\left(\frac{w_{Cao}}{M_{CaO}}\right) M_{CO_2}} \times 100 \quad (17)$$

Where;

M_{CO_2} is the molar mass of CO_2, w_{Cao} is the starting mass of CaO in the reactor and M_{CaO} is the molar mass of CaO. Finally, n_{CO_2} is the number of moles of consumed CO_2 (Montes-Hernandez et al., 2009):

$$n_{CO_2} = \frac{P_{carbonation\_pressure\ drop} V}{RT} \quad (18)$$

Where;

V is the reactor volume, T is the temperature of the reaction and R is the gas constant (0.08314472 L bar/K mol). Montes-Hernandez et al. (2009) found the $P_{carbonation\_pressure\ drop}$ estimates the pressure drop produced from the process of CaO carbonation and hence the pressure drop due to $CaCO_3$ formation.

Muriithi et al. (2009) reported that the volume (V) is actually the reactor volume occupied with gas, and for an autoclave reaction system that uses a teflon liner such as the one used in the study with no tight fit between the teflon liner and the reactor steel jacket, the volume of the gas can be calculated by:

$$Volume\ of\ the\ steel\ jacket - volume\ of\ the\ teflon\ liner - the\ volume\ occupied\ by\ the\ solid\ and\ liquid\ mixture\ in\ the\ teflon\ liner\ (calculated\ using\ the\ formula\ of\ the\ volume\ of\ a\ cylinder\ \pi r^2 h)$$

The volume of the teflon liner was calculated by a simple displacement experiment where, the volume displaced by the teflon was taken to be its volume. The volume of the steel jacket was calculated from the equation for the volume of a cylinder (i.e., $\pi r^2 h$).

2.8 Approaches to enhancing carbonation performance for accelerated MC

Effective calcium (Ca^{2+}) leaching from the alkaline feedstock, effective dissolving of gaseous CO_2 in the liquid phase, and effective precipitation to create calcium carbonate ($CaCO_3$) are all required to effectively improve the carbonation reactions (Veetil et al., 2021). As mentioned previously, the CO_2 dissolution into the liquid phase and the extraction of calcium (Ca^{2+}) ions from fly ash constitute the rate-limiting steps for the carbonation reaction because a higher amount of dissolved CO_2 molecules from the gaseous phase and a higher amount of calcium (Ca^{2+}) extracted increase the rate of the carbonation reaction as the reaction rate ($-r_A$) is concentration dependent. This can thus lead to more CO_2 storage through higher $CaCO_3$ formation. However, the overall formation of $CaCO_3$ also depends on the precipitation step of the reaction, which is influenced by solution pH. The solution pH depends on the calcium (Ca^{2+}) concentration and also the concentration of CO_2 available (Katsuyama et al., 2005).

Hence, the accelerated MC process has been focused on determining the optimum set of conditions that are suitable for effective calcium (Ca^{2+}) extraction, CO_2 dissolution, and $CaCO_3$ precipitation to maximize the carbonation rate, thereby achieving high maximum carbonation efficiency (CE %) and effective CO_2 storage as a result of the higher $CaCO_3$ formed. Other approaches to enhancing the rate of carbonation for accelerated MC include the potential use of catalysts, although catalyst recovery is known to be a key hurdle for the approach (Mathieu, 2006).

2.8.1 Optimization of process parameters

Parameters that have an effect on carbonation performance are important to understand as they are critical to the reaction kinetics and rate of carbonation for accelerated MC. Tables 2.7 and 2.8 show the optimum set of parameters affecting the maximum CO_2 storage capacity (kg/kg fly ash), the % $CaCO_3$ formed during the carbonation process, and also the maximum carbonation efficiency (CE %) achieved from some previous studies, with the viewpoint of comparing the effect of these parameters on the carbonation performance.

Table 2.7: Experimental parameters that resulted in optimum carbonation performance from various studies

Author	(Muriithi, 2009)	(Ukwattage et al., 2013)	(Reddy et al., 2010)	(Ji et al., 2017)	(He et al., 2013)
Material	Secunda Fly Ash	Fly Ash	Fly Ash	Fly Ash	Fly Ash
Particle size (μm)	Bulk	900	40	-	< 100
CaO (wt. %)	9.198	~40	7.5	11.7	30.5
Carbonation route	Direct	Direct	Direct	Direct	Indirect
Reactor type	Autoclave/Batch	Batch	Packed bed	Semi Batch	Batch
Temperature (℃)	90	40	60	60-90	25
S/L ratio (g/mL)	1	0.2	-	0.05	0.05
Initial CO_2 Pressure (Mpa)	4	5	0.115	2	-
Stirring speed (rpm)	-	-	-	500	500
Time (min)	120	600	120	90	60
Maximum CO_2 storage capacity (kg /kg fly ash)	0.062	0.0076	0.207	0.045	-
CE (%)	75.5	-	-	34	47
% $CaCO_3$ increase	6.5	1.82	~3	-	-

Table 2.8: Experimental parameters that resulted in optimum carbonation performance from various studies (cont.)

Author	(Montes-Hernandez et al., 2009)	(Bauer et al., 2011)	(Dananjayan et al., 2016)	(Jo, Ahn, et al., 2012)	(Jo, Kim, et al., 2012)
Material	Fly Ash	Fly Ash	Fly Ash	Fly Ash	Fly Ash
Particle size (μm)	40	< 200	-	20	20
CaO (wt. %)	4.1	28.4	6.74	15	7.2
Carbonation route	Direct	Direct	Direct	Direct	Indirect
Reactor type	Batch	Batch	Batch	Column	Batch
Temperature (℃)	30	> 50	30	~25	~25
S/L ratio (g/mL)	0.05 - 0.15	8.3	0.07	0.33	0.1
Initial CO_2 Pressure (Mpa)	4	0.098-0.1	0.4	0.1	0.1
Stirring speed (rpm)	450	1500	900	150	-
Time (min)	1080	120	120	1080	~162
Maximum CO_2 storage capacity (kg/kg fly ash)	0.026	0.21	0.05	0.071	0.008
CE (%)	82	53	67.9	54.5	0.11
% $CaCO_3$ increase	-	-	-	16.1	-

2.8.1.1 Effect of initial CO_2 pressure (Mpa) and CaO (wt. %) content

The effect of initial CO_2 pressure (Mpa) on the carbonation process that has been previously studied indicates that applying a higher initial CO_2 pressure (Mpa) can enhance carbonation performance. The effect of initial CO_2 pressure (Mpa) on the carbonation process can be explained using Henry's law (Dananjayan et al., 2016):

$$[CO_2] = K_H \times P_{CO_2}$$

According to Henry's law, the concentration of CO_2 molecules that dissolve in the liquid phase is directly proportional to its pressure (Mpa) at a given temperature (^{0}C). Ji & Yu (2018) explained that a higher initial CO_2 pressure (Mpa) results in a large amount of dissolved CO_2 in the liquid phase leading to more carbonate (CO_3^{2-}) ions available to react with calcium (Ca^{2+}) during the carbonation process. The higher availability of CO_2 that dissolves in the liquid phase promotes a faster rate of carbonation due to an increased amount of CO_3^{2-} ions available for the reaction with calcium (Ca^{2+}), and this results in a more effective storage of CO_2 due to the higher $CaCO_3$ formed (Ji et al., 2017). In the study conducted by Dananjayan et al. (2016) (refer to Table 2.8), it was found that the net carbon gain in the coal fly ash (CFA) increased with increasing initial CO_2 pressure up to 10 bar (1 Mpa) and that an increase in initial CO_2 pressure (Mpa) also resulted in a higher CO_2 sequestration capacity. However, increasing the initial CO_2 pressure beyond 0.4 Mpa to a maximum pressure of 1 Mpa did not significantly affect the maximum CO_2 sequestration capacity as the system reached equilibrium due to the water reaching its saturation level with CO_2 molecules that it can hold at room temperature (^{0}C).

Ji et al. (2017) also found that increasing the initial CO_2 pressure from 1 Mpa to 2 Mpa resulted in a higher carbonation efficiency (CE %) due to the higher amount of CO_2 molecules dissolved in the liquid phase at the higher initial CO_2 pressure of 2 Mpa. This resulted in more carbonate (CO_3^{2-}) ions available for the carbonation reaction to react with calcium (Ca^{2+}) for a more effective carbonation reaction. Ukwattage et al. (2013), however, found that increasing the initial CO_2 pressure had a minor effect on the CO_2 that was sequestered into the fly ash. Results from their titrimetric tests showed that increasing the initial CO_2 pressure (Mpa) had a minor effect on the amount of CO_2 that was sequestrated into the fly ash as $CaCO_3$ for their process and that the initial CO_2 pressure gave an indication of the rate of CO_2 consumption rather than the amount of CO_2 stored in the fly ash in mineral carbonate form.

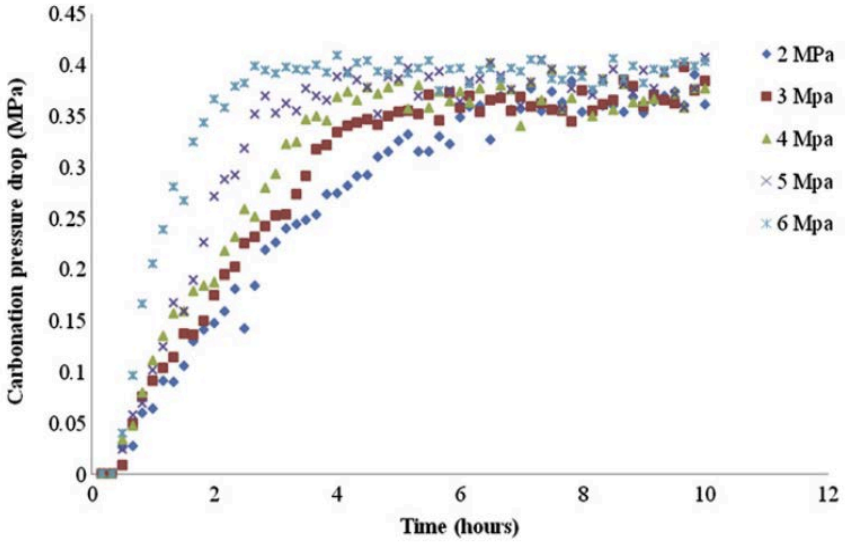

Figure 2.6: Pressure drop due to carbonation over reaction time (Ukwattage et al., 2013)

From Figure 2.6, the carbonation reaction is completed in less than 90 min and the pressure drop reaches a plateau after 90 min. However, for each initial CO_2 pressure, the maximum pressure drop achieved at the end of the 600-minute reaction is approximately the same (around 0.35 - 0.4 MPa). This implies that increasing the initial pressure of CO_2 inside the reactor for the study by Ukwattage et al. (2013) had an insignificant effect on the total amount of CO_2 sequestered in the fly ash. This indicates the increase in pressure is not favourable for effective $CaCO_3$ precipitation, as mentioned by Ji et al. (2017).

Tables 2.7 and 2.8 show that Jo, Ahn, et al. (2012) achieved a higher % $CaCO_3$ than the one obtained from the study conducted by Muriithi (2009). The higher % $CaCO_3$ achieved by Jo, Ahn, et al. (2012) compared to the one obtained by Muriithi (2009) can be explained through observations made by Montes-Hernandez et al. (2009), who from their study found that under isothermal conditions, although an increase in the initial CO_2 pressure (Mpa) produces an increase in the global pressure drop $P_{global\_pressure\ drop}$ (i.e., total pressure drop) due to higher CO_2 dissolution from hydration, which produces a pressure drop $(i.e., P_{water\_pressure\ drop})$, the amount of CO_2 that is sequestrated into the fly ash as $CaCO_3$ depends on the pressure drop produced due to calcium carbonate ($CaCO_3$) formation $(i.e.,\ P_{carbonation\_pressure\ drop})$.

This means that there is a pressure drop owing to the interaction of calcium (Ca^{2+}) and CO_2 in the system, which determines the amount of CO_2 fixed as $CaCO_3$ (Nyambura et al., 2011). Therefore, the amount of CO_2 that gets sequestered into the fly ash as $CaCO_3$ depends on the calcium (Ca^{2+}) extraction step and the amount of calcium (Ca^{2+}) available to react with CO_2 to form $CaCO_3$, because the higher the amount of calcium (Ca^{2+}) available in solution, the more calcium (Ca^{2+}) can react with CO_3^{2-} ions, resulting in an increase in the percentage of $CaCO_3$ formed (Veetil et al., 2021). Ho et al. (2020) mentioned that because the dissolution of CO_2 into water causes the lowering of solution pH, due to Le Chatelier's principle, the dissolution of CO_2 in the Ca-H_2O-CO_2 system is therefore favoured at alkaline conditions. Given that the calcium (Ca^{2+}) extraction step for the Ca-H_2O-CO_2 system increases the alkalinity of the solution as OH^- ions are released, thus causing higher CO_2 dissolution, using fly ash material with a higher CaO (wt. %) content generally results in higher CO_2 dissolution and more calcium (Ca^{2+}) ions leached into solution owing to the higher CaO (wt. %) in the feedstock. This results in an increase in the rate of carbonation and, overall, a higher % $CaCO_3$ formed as more calcium (Ca^{2+}) ions and CO_2 molecules become available for the reaction to form $CaCO_3$.

The study conducted by Jo, Ahn, et al. (2012) made use of coal fly ash with a higher CaO (wt. %) content of 15 %, while the CaO (wt. %) content in the Secunda fly ash used by Muriithi (2009) was reported at 9.2 % which explains the higher % $CaCO_3$ achieved from the study conducted by Jo, Ahn, et al. (2012) . The findings from these studies also show why the research literature considers calcium (Ca^{2+}) extraction to be the main rate-limiting step of the carbonation reaction because the rate of the carbonation reaction highly depends on the calcium (Ca^{2+}) concentration available in the carbonation reaction (Ukwattage et al., 2015). The higher percentage of $CaCO_3$ formed in the study conducted by Jo, Ahn, et al. (2012) compared to the study conducted by Muriithi (2009) was also possibly due to the lower initial CO_2 pressure used because, according to Iizuka et al. (2004), there is a high solubility of $CaCO_3$ under high- pressure CO_2 conditions, and Katsuyama et al. (2005) further mentioned in their publication that higher pressure conditions increase the solubility of calcium (Ca^{2+}) which decreases the rate of $CaCO_3$ precipitation.

The carbonation efficiency CE (%) determined from the study by Montes-Hernandez et al. (2009) showed that the CE (%) also provides a measure of the extent of CO_2 consumption due to $CaCO_3$ formation and that the pressure drop produced $(i.e.,\ P_{carbonation\_pressure\ drop})$ due to CO_2 consumption to form $CaCO_3$ depends on the initial CaO (wt. %) of the fly ash material. From Tables 2.7 and 2.8, it can be seen that Muriithi (2009) achieved a similar CE (%) (i.e., 75.5 %) compared to the CE (%) achieved by Montes-Hernandez et al. (2009) (i.e.,

82 %), and a higher CO_2 storage capacity (kg/kg fly ash) of 0.062 % using a shorter reaction time of 120 min compared to the 1080 min used by Montes-Hernandez et al. (2009) to achieve a lower CO_2 storage capacity of 0.026 kg/kg fly ash. The shorter reaction time (min) used by Muriithi (2009) to achieve a similar CE (%) and higher CO_2 storage capacity (kg/kg fly ash) than Montes-Hernandez et al. (2009) shows that the process from the study by Muriithi (2009) was more effective. Even though both studies used an equivalent and relatively higher initial CO_2 pressure (i.e., 4 Mpa), the difference in the efficiencies of the two processes is due to the fact that the CE (%) and hence, the maximum CO_2 storage capacity (kg/kg fly ash) depend on the amount of CaO (wt. %) content present in the feedstock, in this case fly ash (FA). The process by Muriithi (2009), was more effective compared to the one by Montes-Hernandez et al. (2009) because of the type of fly ash used in the study by Muriithi (2009), which had a higher CaO (wt. %) content of 9.2 % compared to the 4.1 % used by Montes-Hernandez et al. (2009). It is also important to note the role of the reaction mediums used in the two studies as Muriithi (2009) made use of brine with additional calcium (Ca^{2+}) as the reaction medium instead of water, which could also explain the higher maximum storage capacity achieved.

According to Ukwattage et al. (2015), brine solutions increase the retention of CO_2 in the fly ash due to the additional calcium (Ca^{2+}) provided by the brine solution which, leads to an enhanced carbonation efficiency CE (%). Soong et al. (2006) also used brine as a reaction medium for CO_2 sequestration and achieved a high % $CaCO_3$ formation of 52 % for the fly ash/brine/CO_2 system compared to the lower % $CaCO_3$ formation of 11 % achieved for the fly ash/water/CO_2 system.

The pilot scale study conducted by Reddy et al. (2010) made use of flue gas CO_2 with a 12.14 % concentration of CO_2 and the process managed to mineralize significant amounts of CO_2. The process required low pressures to achieve the optimum percentage of $CaCO_3$ formed, and overall, the process was found to be cost-effective. However, the process still achieved a lower % $CaCO_3$ formed compared to studies such as the one conducted by Jo, Ahn, et al. (2012), and this was possibly due to the lower CaO content in the fly ash used by Reddy et al. (2010). Ukwattage et al. (2013) achieved a lower storage capacity despite using fly ash with a higher CaO (wt. %) content. This can be attributed to the lower S/L ratio used in the study. When the S/L ratio is too low, this causes a higher amount of water to be present in the solution. According to Dananjayan et al. (2016), a high amount of water can obstruct the carbonation process by blocking the pathway of the dissolved gas molecules toward the pore system of the feedstock. Thus, a large amount of water limits the carbonation process as it reduces the permeability of gas molecules and their effective access to reaction sites (Bertos et al., 2004).

Jo, Kim, et al. (2012) carried out their CO_2 storage process using the two-stage indirect aqueous carbonation route, and from their study, it was found that the carbonation efficiency (CE %) was directly proportional to the calcium (Ca^{2+}) extraction efficiency. However, the CO_2 storage capacity (kg/kg fly ash) achieved from the study was three times lower than the CO_2 storage capacity obtained from the study conducted by Montes-Hernandez et al. (2009), who used the direct aqueous carbonation route. This can be attributed to the longer reaction time (min) and higher energy input used by Montes-Hernandez et al. (2009) compared to the energy input from the study conducted by Jo, Kim, et al. (2012). He et al. (2013) also used the indirect carbonation route for the CO_2 storage process but found a lower maximum carbonation efficiency (CE %) of ~47 % compared to the higher carbonation efficiencies reported in studies using the direct carbonation route.

2.8.1.2 Effect of reaction temperature (^{0}C)

An increase in the reaction temperature (^{0}C) can lead to an increase in the rate of carbonation because of the higher average kinetic energy of molecules and the better leaching of calcium (Ca^{2+}) ions (Bertos et al., 2004; Ji et al., 2017).

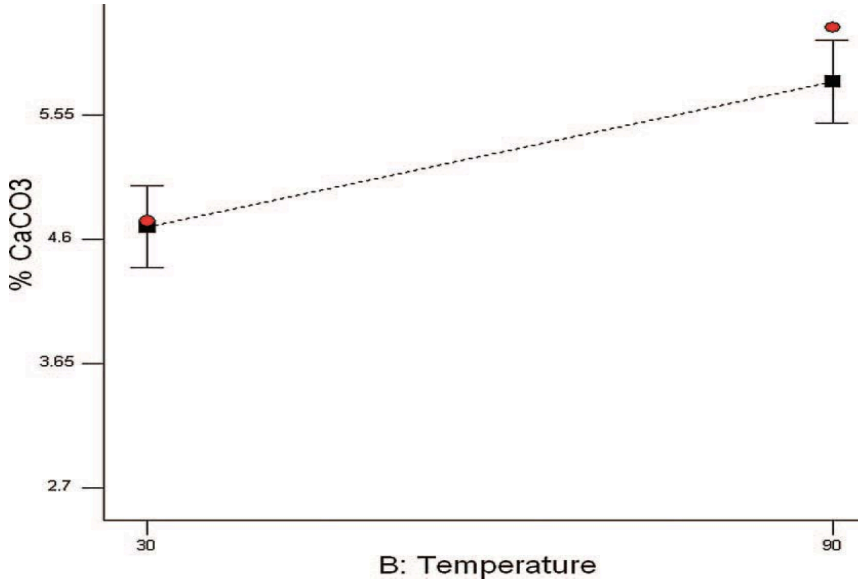

Figure 2.7: Effect of temperature (^{0}C) on % $CaCO_3$ for all factor combinations (Muriithi, 2009)

From the study conducted by Muriithi (2009) shown in Figure 2.7, the percentage of $CaCO_3$ formed increased with increasing reaction temperature (^{0}C). However, from Table 2.8, Montes-Hernandez et al. (2009) achieved a higher carbonation efficiency (CE %) of 81.4% using a lower temperature of 30 ^{0}C as compared to the carbonation efficiency (CE %) of 75.54% achieved by Muriithi (2009) for a higher temperature of 90 ^{0}C.

This is due to the opposing effect of temperature because the leaching of calcium (Ca^2) from the solid matrix is likely to proceed faster at higher temperatures (^oC), but higher temperatures (^0C) hinder the solubility of CO_2 in the liquid phase (Huijgen et al., 2005). Patel et al. (2017) found the CO_2 storage level increased up to 50 ^0C, but the solubility of CO_2 reduced beyond 50 ^0C. According to Bertos et al. (2004), CO_2 uptake increases at an increasing temperature (^0C) up to 60 ^0C, and to obtain the desired polymorph from the carbonation process, namely calcite ($CaCO_3$), a lower temperature (^0C) should be maintained for the carbonation. Ji et al. (2017) attempted to counter the opposing effects of temperature (^0C) by using a higher initial CO_2 pressure to maintain the CO_2 or CO_3^{2-} solubility in the liquid phase while simultaneously increasing the reaction temperature (^0C). The study found this to be effective, as the highest carbonation efficiency (CE %) for batch experiments was achieved at a higher temperature (^0C) and initial CO_2 pressure (Mpa).

2.8.1.3 Effect of reaction time (min)

The reaction time (min) is another key process parameter affecting carbonation performance. According to Dananjayan et al. (2016), the sequestration capacity increases with time (min). However, the findings from the study reported a similar CO_2 sequestration capacity (kg/kg fly ash) after 120 min and after 600 min of the reaction, which indicated that the process proceeds very slowly beyond a certain reaction time (min). This is because the carbonation reaction occurs on the outer surface of the fly ash, and as the reaction proceeds over time (min), the outer carbonate layer starts growing, which causes the alkaline oxide (CaO) in the inner core of the fly ash to stay within, thus creating a barrier that hinders the leaching of calcium (Ca^{2+}) which results in a slower rate of carbonation (Ji & Yu, 2018; Nyambura et al., 2011).

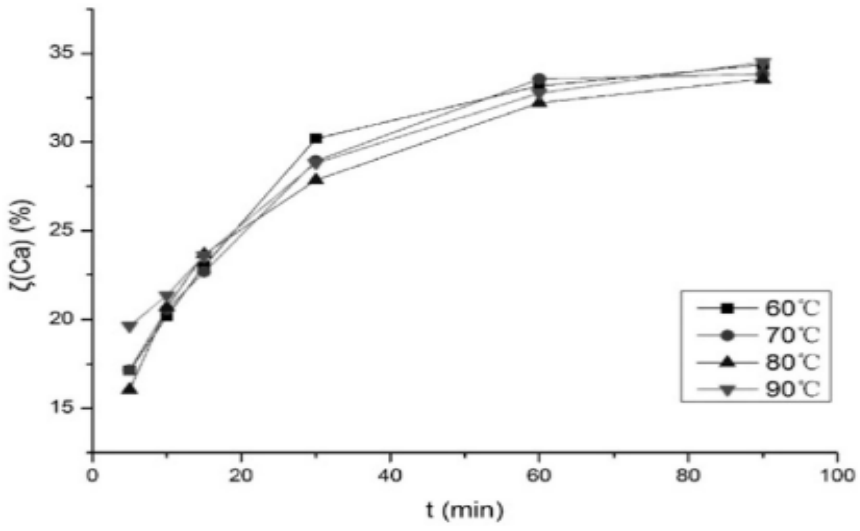

Figure 2.8: Effect of time (min) on carbonation efficiency at various temperatures (^0C) (Ji et al., 2017)

Figure 2.8 shows the effect of the reaction time (min) on the carbonation efficiency ζ (%) from the study conducted by Ji et al. (2017), and it can be observed that the carbonation efficiency ζ (%) increases sharply at the initial stages but then starts to increase slowly as the reaction proceeds, which is consistent with the findings from the study by Dananjayan et al. (2016), who found the sequestration capacity to increase with increasing reaction time (min) before the reaction reaching equilibrium after 120 min. Again, the decline in the CE (%) formed over time (min) can be attributed to the decrease in the rate of calcium (Ca^{2+}) extraction, which causes the reaction to reach completion after a certain point (Jo, Kim, et al., 2012).

2.8.1.4 Effect of S/L ratio (g/mL)

Previous studies indicate that a lower S/L ratio is required for an effective carbonation process due to the dilution effect. Back et al. (2008) found that lower S/L ratios increase the rate of calcium (Ca^{2+}) extraction and the rate of CO_2 uptake through the dilution effect because the greater the volume of water, the larger is the solubility of calcium (Ca^{2+}) and the ability to dissolve CO_2 in solution. The higher solubility of calcium (Ca^{2+}) therefore results in higher dissolution of calcium (Ca^{2+}) ions and more calcium (Ca^{2+}) ions, are then made available for the reaction with CO_2 which increases the rate of carbonation and leads to a higher percentage of $CaCO_3$ formed for a given reaction time (Veetil et al., 2021). Dri et al. (2014) investigated the effect of the S/L ratio and found that the carbonation efficiency increased with a decrease in the S/L ratio owing to the dilution effect.

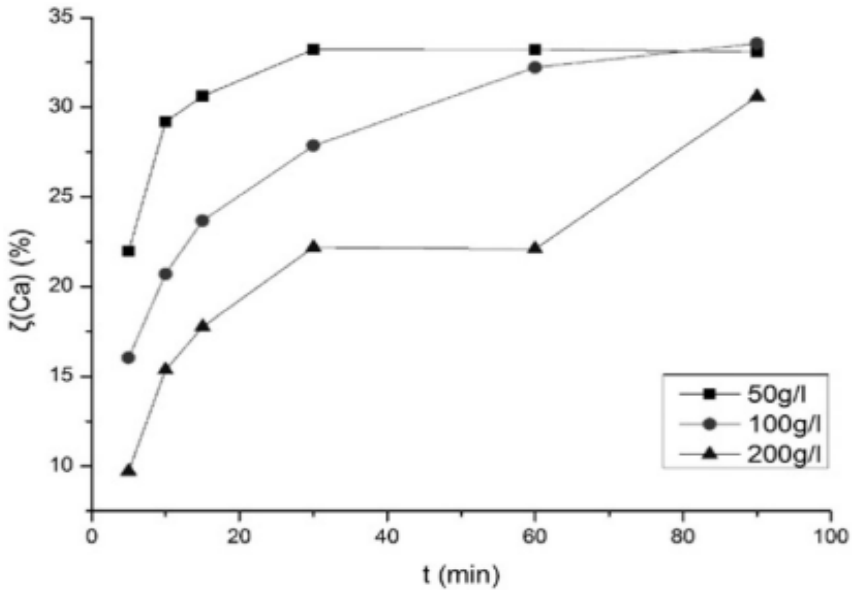

Figure 2.9: Effect of S/L ratio on carbonation efficiency for various reaction times (min) (Ji et al., 2017)

Ji et al. (2017) considered the effect of the S/L ratio on the carbonation efficiency ζ (%), and from Figure 2.9, it can be observed that a lower S/L ratio resulted in the highest carbonation efficiency ζ (%),which is consistent with the findings from the study conducted by Back et al. (2008), who found that a decrease in the S/L ratio resulted in an increase in the CO_2 uptake.

2.8.1.5 Effect of particle size (μm)

The particle size (μm) affects the overall reaction kinetics of the carbonation process, and a reduced particle size (μm) can improve the overall carbonation performance. Reduced particle size (μm) for the feedstock means there is an increased surface area of particles contacting CO_2 and also an enhanced extraction of calcium (Ca^{2+}) ions from the fly ash, which leads to an enhanced rate of carbonation. This results in higher CO_2 consumption through an effective carbonation process (Ji et al., 2017). Muriithi (2009) studied the effect of particle size (μm) on the % $CaCO_3$ formed. Four particle sizes were considered: bulk ash, >150μm, 20-150μm, and < 20μm, with the 20-150 μm fractions having the highest effect on the percentage of $CaCO_3$ formed. The least favourable fraction for carbonation was >150μm, indicating that fly ash samples with relatively smaller particle sizes (μm) favour the formation of $CaCO_3$. Studies such as the one conducted by Bertos et al. (2004) also show that carbonation is higher at smaller particle sizes (μm).

2.8.1.6 Effect of stirring speed (rpm)

Increasing the stirring rate (rpm) can improve the carbonation rate as it limits the formation of carbonate shells that can surround the fly ash particles, which leads to better mass transfer of CO_2 and diffusion of metal ions from the fly ash into solution (Ji et al., 2017). In the study conducted by Dananjayan et al. (2016), increasing the stirring speed up to 900 rpm resulted in a higher CO_2 storage capacity, while Mayoral et al. (2013) also found the optimum stirring speed (rpm) for their process to be between a range of 500 – 1000 rpm. However, Ji & Yu (2018) reported that increasing the stirring speed (rpm) above a certain stirring speed has no observable effect on the carbonation rate and that considering the energy consumption due to stirring, increasing the stirring speed (rpm) beyond a certain stirring speed (rpm) was not worth the trade-off between the CO_2 sequestered and the amount of energy expended due to stirring.

2.9 Alternative CO_2 sequestration methods

2.9.1 Geological storage

Geological storage involves the capture, liquefaction, transportation, and injection of industrial CO_2 into deep geological strata. For CO_2 to be geologically stored, it must be compressed to a dense fluid state called supercritical CO_2 (Lal, 2008). Geological storage can be undertaken in a variety of geological settings in sedimentary basins, as presented in Figure 2.10 below:

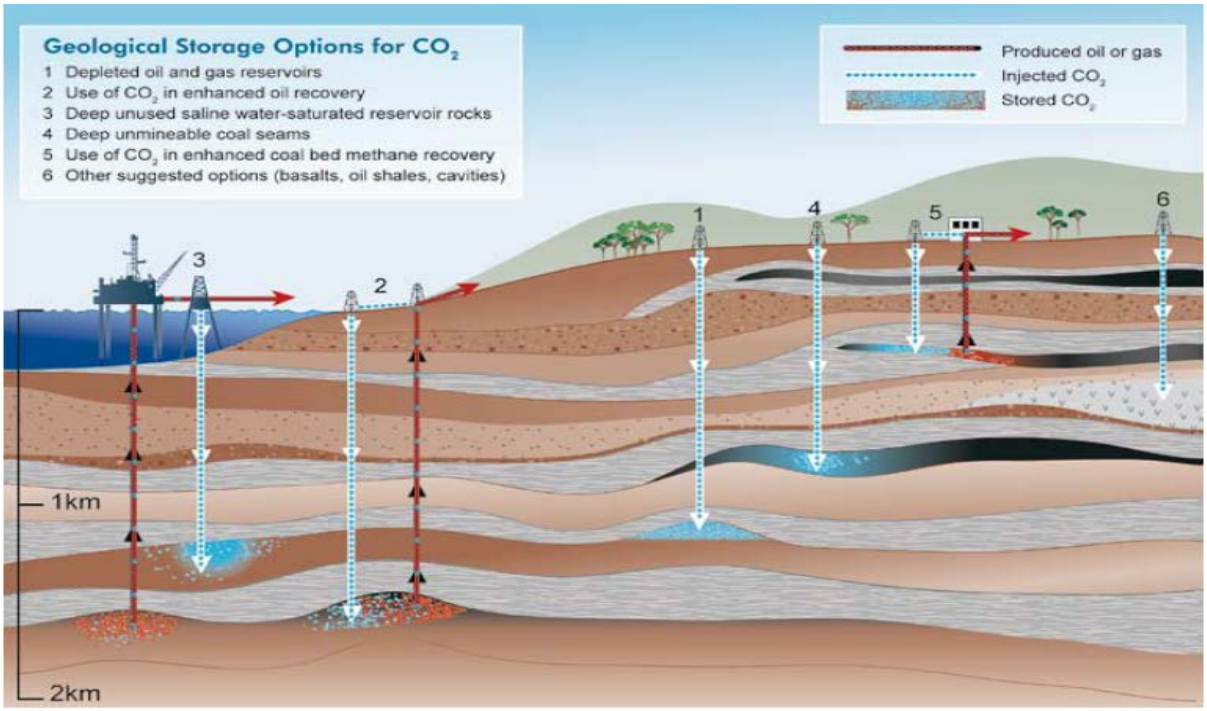

Figure 2.10: Options for storing CO_2 in deep underground geological formations (Mathieu, 2006)

Within these basins, oil fields, depleted gas fields, deep coal seams, and saline aquifers all form part of possible storage formations (Mathieu, 2006). Deep saline aquifers display the highest levels of geological sequestration when compared to those offered by exhausted oil and gas reserves and impassable coal beds. According to Ajayi et al. (2019), the basins best suited for CO_2 storage typically have thick sediment accumulations, permeable rock formations, saturated saline water, vast covers with low porosity, as well as structural simplicity.

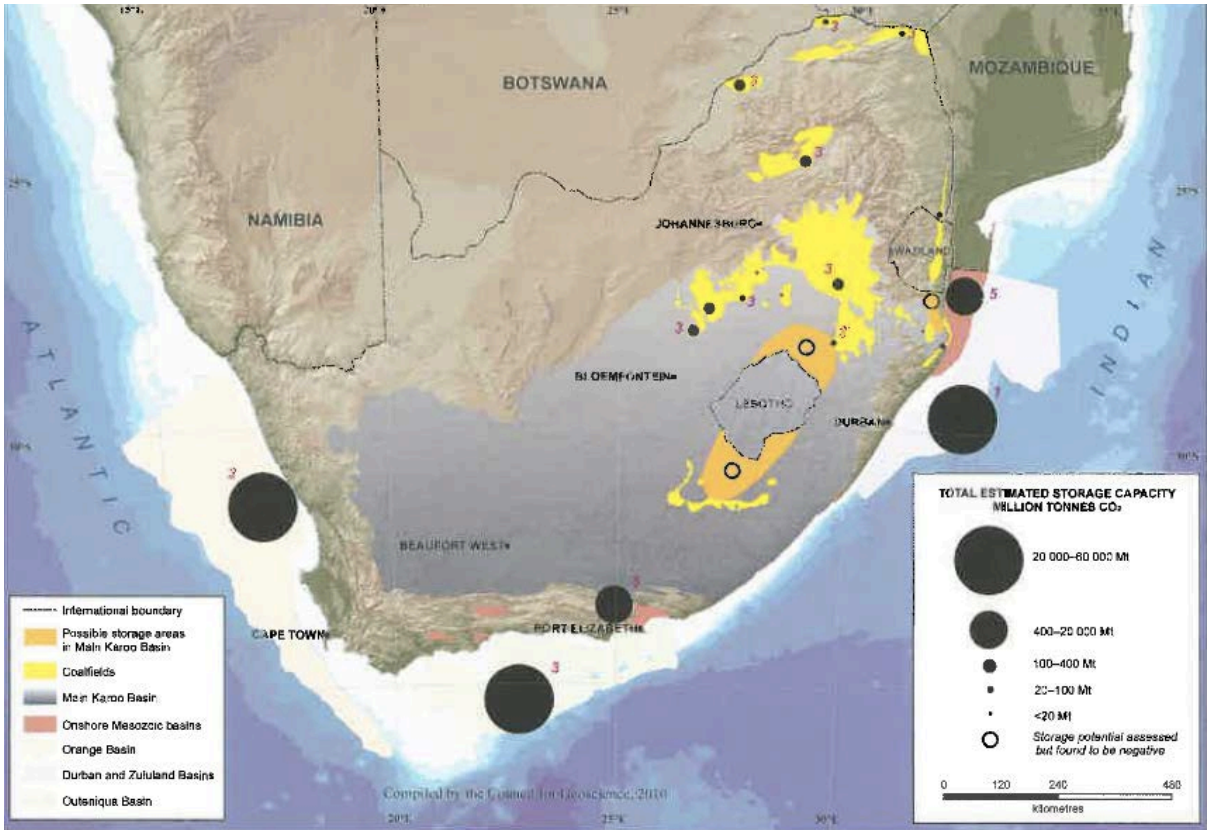

Figure 2.11: Geological storage opportunities in South Africa

Figure 2.11 presents the areas in which geological storage can be achieved in South Africa, and from the 150 Gt storage capacity estimated from geological storage in the country, 98 % of the total storage potential is present in the Mesozoic basins along the coast of South Africa. There is evidently limited onshore storage capacity for geological storage in the country as only around 2 % of the total estimated storage capacity occurs onshore (Cloete, 2010). The potential for onshore deep saline formations in the Karoo basin is often presented with the disadvantage of low permeability, and dolomite intrusions, which negatively impact the containment of the injected CO_2. Although geological storage possesses a high storage potential for large emitters, the method has significant drawbacks because of the issues around the containment of the injected CO_2, which pose an environmental issue. In addition, monitoring for offshore storage presents logistical and methodological challenges while costs associated with offshore storage remain high (Lichtschlag et al., 2021).

2.9.2 Oceanic storage

Liquefied CO_2 separated from industrial sources can be injected into the ocean using strategies illustrated in Figure 2.12:

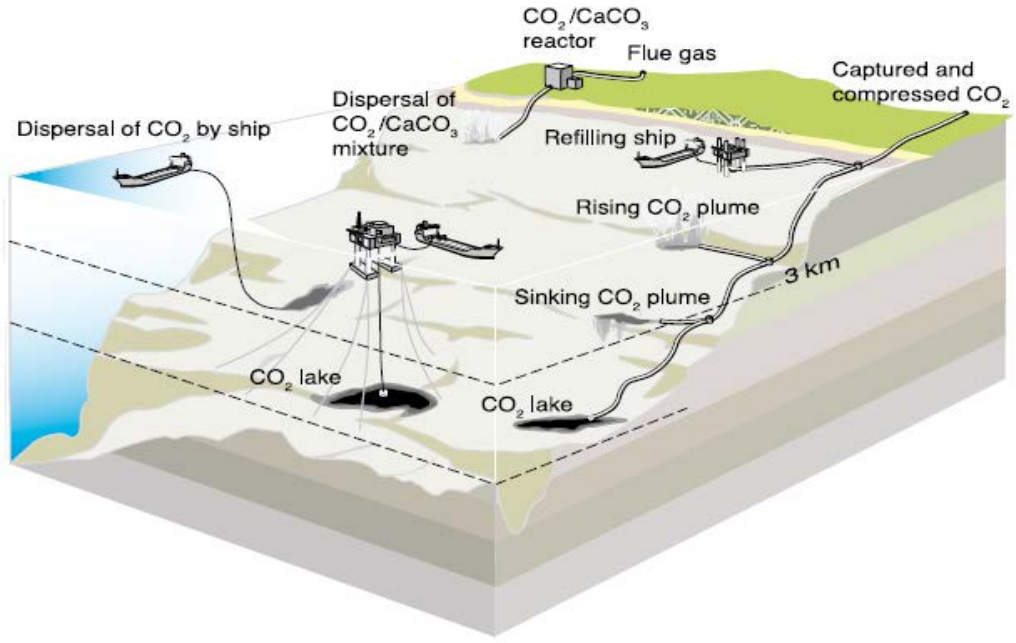

Figure 2.12: Illustration of some of the ocean storage strategies (Mathieu, 2006)

From Figure 2.12, the liquefied CO_2 can be injected into the ocean by the following techniques (Lal, 2008):

- It is injected below 1000 m from a manifold lying on the ocean floor, and being lighter than water, it rises to approximately 1000 m depth forming a droplet plume.
- It is also injected as a denser CO_2 seawater mixture at 500–1000 m depth, and the mixture sinks into the deeper ocean.
- It is discharged from a large pipe towed behind a ship.
- It is pumped into a depression at the bottom of the ocean floor, forming a CO_2 lake.
- Liquefied CO_2 injected at approximately 3 km depth is believed to remain stable.

Although the capacity of oceanic sequestration of CO_2 worldwide is approximately 20 000 Gt, there is still a critical environmental issue that surrounds oceanic sequestration that makes it unsuitable as a storage method. When CO_2 is stored in the ocean, the dissolved CO_2 can react with the oceanic water and form carbonic acid (H_2CO_3), which increases the acidity of the oceanic water and decreases the pH, thus making the ocean unsuitable for living organisms (Rabiu et al., 2017).

2.10 CO_2 storage with AMD wastewater

The use of wastewater solutions such as AMD or brine solutions as reaction mediums for CO_2 storage results in enhanced CO_2 storage capacities as a result of the wastewater being an additional calcium (Ca^{2+}) source and the AMD wastewater being effectively neutralized in the process (Ukwattage et al., 2015). In their study on AMD neutralization and subsequent CO_2 storage, Madzivire et al. (2019) used the neutralization step of AMD wastewater for CO_2 storage wherein the recovered calcium (Ca^{2+}) rich leachate from the AMD neutralization step was carbonated with CO_2. The study found that the carbonation of the leachate with CO_2 resulted in further neutralization of AMD while also storing the CO_2. Lee et al. (2016) also used AMD wastewater for their CO_2 storage process, and the highest amount of CO_2 sequestered was 33.46 %, although the higher percentage of $CaCO_3$ formed can also be attributed to the use of hydrated lime with a high CaO (wt. %) content.

2.10.1 Acid Mine Drainage (AMD)

AMD is acidic wastewater that results from mining activity when the mining activity exposes sulfur-bearing minerals (mostly iron sulfides) to oxygen, thus causing these sulfur-bearing minerals to undergo oxidation. When sulfur-bearing minerals come into contact with oxygen and water, this results in an acidic pH solution that contains high concentrations of sulfates (SO_4^{2-}), iron (Fe^{2+}), aluminium (Al^{3+}), calcium (Ca^{2+}), manganese (Mn^{2+}), magnesium (Mg^{2+}), etc. (Gitari et al., 2006; Madzivire et al., 2019). Abandoned coal and gold mines in South Africa that have become financially unfavourable continue to produce hazardous AMD wastewater, which contains many dissolved metals that are considered toxic (Potgieter-Vermaak et al., 2006). Figure 2.13 shows an old abandoned metalliferous mine in South Africa where mining activity ceased in 1980 but still continues to release a considerable amount of acidic water:

Figure 2.13: Example of a metalliferous mine in South Africa (Akcil & Koldas, 2006)

Considering AMD wastewater has an acidic pH (i.e., pH 2-4), its discharge into local streams poses a serious environmental hazard and causes a serious threat to aquatic life (Gitari et al., 2018).

2.10.2 Formation of AMD

The reactions of AMD wastewater formation are best described by examining the oxidation of pyrite (FeS_2) which is the most common sulfide (Akcil & Koldas, 2006). The oxidation of pyrite to form AMD wastewater in the presence of oxygen and water has been illustrated using the set of reactions presented (Maleka, 2015):

$$FeS_2 + \frac{15}{2}O_2 + \frac{7}{2}H_2O \rightarrow Fe(OH)_3 + 2H_2SO_4 \quad (19)$$

$$4Fe^{2+} + O_2 + 4H^+ \rightarrow 4Fe^{3+} + H_2O \quad (20)$$

$$4Fe^{3+} + 12H_2O \leftrightarrow 4Fe(OH)_3 + 12H^+ \quad (21)$$

$$FeS_2 + 14Fe^{3+} + 8H_2O \rightarrow 15Fe^{2+} + 2SO_4^{2-} + 16H^+ \quad (22)$$

The first equation shows the reaction of pyrite with oxygen and water to produce sulfuric acid (H_2SO_4), ferric iron (Fe (III), and the resulting solution is acidic (Akcil & Koldas, 2006). The oxidation of FeS_2 enhances the solubility of several base metals such as lead (Pb^{2+}), zinc (Zn^{2+}), cobalt (Co^{3+}), nickel (Ni^{2+}), aluminium (Al^{3+}), magnesium (Mg^{2+}), etc (Maleka, 2015). The conversion of Fe^{2+} to Fe^{3+}, which is the second step of the process is considered the rate-controlling step of the overall reaction sequence, because at pH < 5 under abiotic conditions, the reaction proceeds slowly (Nkongolo, 2020). The third step is the hydrolysis of Fe^{3+}, forming $Fe(OH)_3$ precipitates that produce additional acidity in solution, while the fourth step involves the autocatalytic oxidation of additional FeS_2 by Fe^{3+} in the presence of water (Maleka, 2015). According to Nkongolo (2020), the overall sequence of pyrite reactions is considered one of the most acid-producing of any weathering process.

2.10.2.1 Chemical properties of AMD wastewater

There are several elements contained in AMD wastewater and Table 2.9 presents some of the major elements present in the wastewater:

Table 2.9: Elemental composition of AMD wastewater (Kalombe et al., 2020)

	Acid mine drainage (AMD) wastewater
Elemental Composition	SO_4^{2-}, Ca, Al, Mg, Fe, Na, Mn K, Zn, Ni, Co, Sr, Ba. Cu

The elemental composition of a typical AMD wastewater sample is provided in Table 2.9. The neutralization and removal of the toxic contaminants from AMD wastewater have mostly been done using several available conventional methods that have been well studied, which include passive and active AMD treatment techniques (Gitari et al., 2005). Fly ash and other alkaline-rich materials, such as lime, have also been utilized in AMD remediation (Jones & Cetin, 2017).

2.11 AMD treatment

2.11.1 Conventional AMD treatment methods

AMD treatment methods can be generally classified into two categories namely: active and passive treatment. Both methods comprise physical, biological, and chemical approaches for AMD treatment (Maleka, 2015). Passive treatment methods involve treating AMD wastewater by passing it through an environment whereby geochemical and biological processes help in the treatment of the mine wastewater without the addition of any chemicals or intense labour requirements. In contrast, regular reagent and labour inputs are required during the active treatment process of AMD wastewater (Taylor et al., 2005).

2.11.1.1 Passive treatment

The passive treatment of mine water is a technique that uses natural resources to facilitate chemical and biological procedures to extract pollutants from mine water. Passive treatment is a process that does not require the continuous addition of chemicals or monitoring. Below are some different types of passive treatment methods for AMD wastewater (Taylor et al., 2005):

Constructed Wetlands (CW)

According to Taylor et al. (2005), wetlands have the capacity to improve water quality through physical, chemical, microbial, and plant-mediated processes. These processes involve mechanisms such as oxidation, reduction, precipitation, sedimentation, filtration, adsorption, complexation, chelation, and microbial conversion. Constructed wetlands mimic the functions of natural wetlands with the objective of treating wastewater (Pat-Espadas et al., 2018). Pat-Espadas et al. (2018) provided a comprehensive review of constructed wetland systems, and according to them, typical components of constructed wetlands are soil bottom, vegetation, and water surface, and they can also contain media (rock, gravel, soil, or others).

According to the flow direction of the influent, CW systems are categorized into surface and subsurface with the latter divided into horizontal and vertical flow (Perdana et al., 2018). There are also hybrids or combined systems that incorporate different types of constructed wetlands with the aim of exploiting the specific advantages of the different system arrangements. Constructed wetland systems are currently the most widely used passive mine water treatment technology for several reasons, including their low cost compared to active treatment systems (Pat-Espadas et al., 2018).

There are two categories of constructed wetlands namely: aerobic and anaerobic, with the latter being the most widely used passive treatment method for acidic mine water (Nkongolo, 2020). In general, net alkaline water is needed for an aerobic wetland, and anaerobic wetlands are used to neutralize the acidity and reduce metal concentrations in the AMD wastewater. The chemistry and flow of the wastewater discharge are critical to the proper selection of a CW system (Ford, 2003). Smith (1997) mentioned that biochemical processes have to be carefully considered when planning the construction of a wetland to treat acid mine drainage, and the maximum ability of a constructed wetland to treat AMD is determined by the loading rate. Smith (1997) further mentioned that slope and vegetation are important factors to consider in wetland designs.

Anaerobic Wetland

An anaerobic system is one that requires water from mines to run through an organic layer under anaerobic conditions. The organic material must have sulfate-reducing bacteria for metal sulfide precipitates to form (Nkongolo, 2020). Microorganisms facilitate this reaction by first consuming oxygen. Alkalinity and H_2S are produced. If the system is improperly sized, if flow dries up, or if extended low temperatures are encountered, the microorganisms will die and the performance will be decreased (Ford, 2003). According to Nkongolo (2020), anaerobic wetlands are the most commonly used passive treatment for net acid mine water, and alkalinity in the wetland must be developed and added to the water before dissolved metals can precipitate. The wetland substratum may contain a calcareous layer at the bottom, or it may be mixed with organic matter. Wetland plants are then transplanted into the substrate of the organic matter. Insoluble precipitates such as hydroxides, carbonates, and sulfides constitute a significant metal sink in the wetlands.

2.11.1.2 Active treatment

Active treatment requires continuous inputs such as artificial energy, biochemical or chemical reagents, and regular maintenance of a water treatment plant. The advantage of using active treatment methods is that they have the capability to handle changes in mine water quality and quantity due to the precise process control in response to these changes (Taylor et al., 2005). The method does not require a huge quantity of land compared to passive treatment. However, the cost of nonstop energy input (MW), reagents, and the need for skilled operators to operate and maintain the treatment plant make the technique more expensive (Kirby, 2014).

Different neutralization technologies that can be applied for the treatment of mine water are necessary because of the vast differences in the chemistry of acidic waters (Nkongolo, 2020). The selection of a suitable method of treatment can be based on the quality of the mine water, its quantity, the desired treated water quality, and the cost of the treatment techniques (Ford, 2003).

2.12 Treatment of AMD with coal fly ash

The use of fly ash for neutralization and removal of toxic metals from AMD is advantageous because of the abundance and alkalinity of the feedstock (Jones & Cetin, 2017). As a result, coal fly ash is currently one of the most widely used industrial waste products for the AMD wastewater neutralization process (Pérez-López et al., 2007). Moreover, power-generating plants that use coal are situated near the coal mines that service them with coal in South Africa thus making the treatment of AMD wastewater with fly ash economically viable because of reduced transport costs. The percentage removal of various elements during the treatment of AMD wastewater is a comprehensive indicator of the efficiency of the treatment process. The percentage removal of metals is given by:

$$\%\, removal = \left(\frac{conc.of\ ionic\ species\ in\ raw\ AMD - conc.of\ species\ after\ reaction\ time\ (hr)}{concentration\ of\ ionic\ species\ in\ raw\ AMD}\right) \times\ 100 \quad (23)$$

Kalombe et al. (2020) carried out treatment of AMD with fly ash using a 1500 L jet loop reactor system. Results from the study showed that reaction time had a significant effect on reducing the concentration of major contaminants, namely sulfate (SO_4^{2-}), Al^{3+}, Fe^{2+}, Ca^{2+}, Mg^{2+} and that the treated water met the required target water quality range (TWQR) limit for agricultural irrigation in South Africa.

Jones & Cetin (2017) evaluated the neutralization potential of three different types of fly ashes and found that the pH of the AMD wastewater was most significantly buffered by the fly ash with the highest calcium oxide (CaO wt. %) content of 12.5 %. They attributed this to increased hydroxyl ions (OH^-) caused by the dissolution of lime and calcium hydroxide $Ca(OH)_2$ in the fly ash material.

Gitari et al. (2018) treated AMD wastewater with coal fly ash at different fly ash to AMD ratios with the pH monitored over time (min) and found that the treatment of AMD depended on the amount of fly ash used, the AMD chemistry, and the treatment time. The pH was observed to increase in a stepwise manner when AMD was used, with buffer zones observed at 4 - 4.5, 4.5 – 7, and 6-8. However, due to the lower concentration of Al^{3+}, Fe^{2+}, Fe^{3+}, and Mn^{2+} in another source of AMD, the treatment process with this AMD source did not exhibit such buffer zones as there was a lack of stepwise decrease in pH. Two competing processes were observed to control the evolving pH of process water: the dissolution of basic oxides (i.e., CaO, MgO) from fly ash, which led to a pH increase, and the hydrolysis of AMD species such as Al^{3+}, Fe^{2+}, $Fe^{3+,}$ and Mn^{2+} which resulted in a decrease in solution pH.

The two processes further initiated mechanisms such as precipitation, adsorption, and ion exchange that led to a decrease in inorganic contaminants as the treatment progressed. The attenuation of inorganic contaminants in the study was directly related to the amount of fly ash involved in the reaction. The precipitation of insoluble hydroxides and Al^{3+} contributed to the removal of major and minor chemical species. The precipitation of gypsum was found to contribute largely to the removal of sulfate (SO_4^{2-}). Na, K, and Mg remained largely in solution after the initial decrease, while the leaching of B, Sr, Ba, and Mo from the fly ash was observed and was directly linked to the amount of fly ash in the reaction media. Gitari et al. (2018) identified this as a potential shortcoming of the treatment process since other processes may be required to polish up the product water. Maleka (2015) investigated the efficiency of fly ash in the removal of metal ions from AMD wastewater and found the neutralization process to be very effective as a high removal percentage of Fe, Al, Mn, and Mg was achieved. The study also found that the process of sparging CO_2 at certain periods during the reaction resulted in a further neutralization of the pH.

Nkongolo, (2020) considered the use of Lethabo and Kendal coal fly ash for AMD wastewater remediation and found that the neutralization process was characterized by a strong buffer zone around the pH of 12.83 to 8.37 from the Lethabo leachate and between 8.37 and 7.28 for the leachate from the Kendal column, and that this buffer zone could be explained by the hydrolysis of Al^{3+} which forms a hydroxide phase until all the Al^{3+}, was totally hydrolyzed. Findings from the study also indicated that the concentration of SO_4^{2-} was reduced to up to 88% in the effluent from Lethabo coal fly ash and 56% in the effluent from Kendal coal fly ash. Metals such as Fe, Mg, Mn, and Al were significantly removed from the AMD wastewater in the Lethabo and Kendal leachate.

2.13 Adherence to target water quality range (TWQR)

There are certain water quality standards that treated wastewater needs to adhere to upon discharge. Table 2.10 presents the targeted concentration of certain elemental species upon treatment of the wastewater:

Table 2.10: Target water quality range for treated wastewater: NL: No limit detected, NA: Not applicable (Kalombe et al., 2020)

	TWQR	
Element	Irrigation (mg/L)	Domestic (mg/L)
pH	6.5–8.4	6–9
SO_4^{2-}	NL	0–500
Al	0–5	0–0.15
Ca	NL	0–32
Fe	0–5	0–0.1
Mg	NL	0–30
Si	NL	NA
Na	0–70	0–100
Mn	0–0.	0–0.05
Zn	02 0–1	0–3
Ni	0–0.2	NA
K	NL	0–50
Co	0–0.05	NA
Cu	0–0.2	0–1
Pb	0–0.2	0–0.01
Ti	NA	0–0.01
Sr	NL	NA
Cd	0–10	0–5
Cr	0–0.1	0–0.05
As	0–0.1	0–0.001
Mo	0–0.01	0–0.07
Se	0–0.02	0–0.02
P	0–0.2	NA
Li	0–2.5	NA

Table 2.10 presents the TWQR as provided by the Department of Water and Forestry, which encourages the maintenance of water quality in South Africa. It is therefore imperative that the TWQR be met for treated AMD water in order to ensure that it is safe for discharge and, in turn, irrigation and domestic use (DWAF, 1996).

Chapter Summary

Carbon Capture and Storage (CCS) can be achieved first through the capture of CO_2 using post-combustion, pre-combustion, or oxyfuel combustion, although the former method is preferred due to the lower costs associated with the capture method. When CO_2 is captured, the captured CO_2 is then stored using either geological storage, oceanic storage, or accelerated MC. The literature review presented focused mainly on the storage method that was investigated in this study, which was accelerated MC. The accelerated MC method offers a high storage capacity while also ensuring the permanent storage of CO_2. However, the cost associated with this method has been the main challenge for the process. To minimize the energy consumption (MW) and, in turn, the costs (\$/t CO_2 stored) associated with accelerated MC, several process parameters that lead to an enhanced rate of carbonation for accelerated MC through effective calcium (Ca^{2+}) extraction, CO_2 dissolution, and effective $CaCO_3$ precipitation have been investigated in previous studies.

These process parameters include temperature (^{0}C), reaction time (min), particle size (μm), CO_2 pressure (Mpa), stirring speed (rpm), S/L ratio, etc. For the reaction temperature, previous studies have found that a temperature of around 60 ^{0}C is ideal for the carbonation reaction as it enhances the extraction of calcium (Ca^{2+}) while also ensuring that the solubility of CO_2 is not hindered. In terms of particle size, a smaller particle size increases the surface area of particles interacting with CO_2 thereby increasing the rate of carbonation as a result of the collision effect. A higher CO_2 pressure generally results in a higher rate of carbonation due to the higher amount of CO_2 molecules that get dissolved into solution, however, if the pressure is too high, this decreases the rate of $CaCO_3$ precipitation. For the S/L ratio, lower solid-to-liquid ratios tend to improve the extraction of calcium (Ca^2) through the dilution effect, thereby improving the rate of the carbonation reaction.

The use of alkaline-rich waste feedstocks with higher calcium oxide (CaO wt. %) content also proves beneficial in achieving an enhanced rate of carbonation. CFA has been used mainly because of its abundance and because it contains other elements besides calcium, such as iron and magnesium, that can contribute to the overall storage of CO_2 in the material. Another method of enhancing the storage capacity for accelerated MC is through the use of AMD wastewater as a solvent, which provides additional calcium (Ca^{2+}) source, thus increasing the overall CO_2 storage potential of the process. The CO_2 storage process by using of an alkaline-rich material such as CFA provides the added benefit of neutralizing the AMD wastewater, while the process also ensures the removal of toxic elements in the wastewater.

CHAPTER 3

3. Methodology

This chapter provides details of the experimental and analytical methods used to achieve the objectives of the study.

3.1 Materials and methods

A list of chemicals used in this study is given in Table 3.1, while an analysis of the CO_2 gas used is given in Section 3.1.1.

Table 3.1: Summary of chemicals used in the study

Chemical	Supplier	Purity
Hydrochloric acid (HCl)	Merck	37 %
Sodium chloride (NaCl)	Alfa Aesar	99 %
Sodium hydrogen carbonate ($NaHCO_3$)	Merck	99.7 %
Methyl orange indicator	Merck	55 %
Pure calcium carbonate ($CaCO_3$)	Kimix	98.8
Sulfuric acid (H_2SO_4)	Merck	95 – 97 %

3.1.1 CO_2 analysis

The CO_2 used for carbonation and AMD neutralization experiments was pure CO_2 obtained from Afrox and had the following properties:

- Molecular weight = 44.011 g/mol
- Specific volume at 20 ºC, 325 kPa = 5471 m^3/kg
- Critical temperature = 31 ºC
- Relative density at 1 atmosphere = 1.53
- Density at 0 ºC, 325 kPa = 1.977 kg/m^3

3.1.2 Sample collection and preparation

South Africa has a wide range of fly ash waste at its disposal due to coal burning by power utilities. The fly ash used in this study for CO_2 storage and AMD neutralization experiments was Durapozz fly ash, which is processed and classified fly ash from Lethabo power station. The material belongs to Class F fly ash and was obtained from Ash Resources. The fly ash obtained from the supplier was then placed into a tightly sealed container to avoid contact with air. The sealed container containing the fly ash was kept in a dark, cool cupboard away from sunlight and fluctuating temperatures, which could have affected the properties of the raw material (i.e., fly ash).

For the preliminary experiments, the Durapozz fly ash was sieved and separated into different size fractions $25\ \mu m, 45\ \mu m\ and\ 125\ \mu m$ to determine the effect of particle size (μm) on the leachability of calcium (Ca^{2+}) from the fly ash. The AMD wastewater was Penstock AMD obtained from the Navigation Coal Mine in Mpumalanga, South Africa. Given the levels of toxic metals in the AMD wastewater, it was kept safely in a sealed tank that was placed in an area positioned away from sunlight.

3.2 Analytical Methods

3.2.1 X-Ray Diffraction (XRD)

XRD was carried out to identify the different mineralogical phases present in the raw fly ash and the carbonated solid residues.

3.2.1.1 Sample preparation for qualitative XRD

The samples, supplied as fine powder, were mounted on a flat (low-background) sample holder.

3.2.1.2 Instrumental setup for qualitative XRD

XRD data were recorded on a Bruker D2 Phaser Diffractometer using Cu Kα radiation (l = 1.5418 Å) generated at 30 kV and 10 mA. Each sample was scanned from 4-80° in 2θ steps of ~0.02° with a 0.5 second exposure time per step, : the total scanning time is about 40 minutes.

3.2.2 X-Ray fluorescence (XRF)

The chemical makeup of uncarbonated solid residues from carbonation studies, carbonated solid residues from leaching tests, and solid residues from leaching experiments for all size fractions used were all quantified using X-ray fluorescence analysis.

3.2.2.1 Sample preparation for XRF

Samples were crushed into a fine powder (particle size < 70 μm) with a jaw crusher and milled in a tungsten-carbide Zibb mill prior to the preparation of a fused disc for major and trace element analysis. The jaw crusher and mill were cleaned with clean, uncontaminated quartz between 2 samples to avoid cross-contamination.

3.2.2.2 Instrumental setup for XRF

Glass disks were prepared for XRF analysis using 7 g of high-purity trace elements and rare earth element-free flux ($LiBO_2$ = 32.83%, $Li_2B_4O_7$ = 66.67%, LiI = 0.50%) mixed with 0.7 g of the powder sample. A mixture of sample and flux was fused in platinum crucibles using a Claisse M4 gas fluxer at a temperature between 1100 ^{0}C – 1200 ^{0}C. Whole-rock major element compositions were determined by XRF spectrometry on a PANalytical Axios Wavelength Dispersive Spectrometer. The spectrometer was fitted with an Rh tube and with the following analyzing crystals: LIF200, LIF220, PE 002, Ge 111, and PX1. The instrument was fitted with a gas-flow proportional counter and a scintillation detector. The gas-flow proportional counter used a 90% Argon-10% methane mixture of gas. Major elements were analyzed on a fused glass disk using a 2.4 kW Rhodium tube. Matrix effects in the samples were corrected by applying theoretical alpha factors and measured line overlap factors to the raw intensities measured with SuperQ PANalytical software. The concentrations of the control standards that were used in the calibration procedures for major element analyses adequately fit the range of concentrations of the samples. Amongst these standards were NIM-G (Granite from the Council for Mineral Technology, South Africa) and BE-N (Basalt from the International Working Group). The XRF equipment was located at Stellenbosch University.

3.2.3 Inductive Coupled Plasma: Optical Emission Spectroscopy (ICP-OES)

ICP-OES was used to determine the ionic species present in leachate samples.

3.2.3.1 Sample preparation for ICP-OES

A 10 times dilution was performed on raw AMD wastewater samples before ICP-OES analysis could be conducted. All leachate samples used in the study were filtered through a $0.45\ \mu m$ pore filter paper to ensure proper filtration for the separation of solids from liquids.

3.2.3.2 Instrumental setup for ICP-OES

The instrument used for ICP-OES analysis was a Varian 710. The instrument contains an axial torch, and the instrument uses Ar gas. The instrument was calibrated with a blank and 1 ppm, 5 ppm, 10 ppm, and 100 ppm LGC 1586 spectra-scan multi-element standard. The sample was analysed in triplicate, and the average reading is taken using a 10 % deviation.

3.2.4 Chittick test for determining % $CaCO_3$ formed

The determination of the percent $CaCO_3$ formed was made using the Chittick apparatus, and the method was based on the volumetric evolution of carbon dioxide (CO_2) when carbonate in this case calcium carbonate, ($CaCO_3$), reacts with dilute hydrochloric acid.

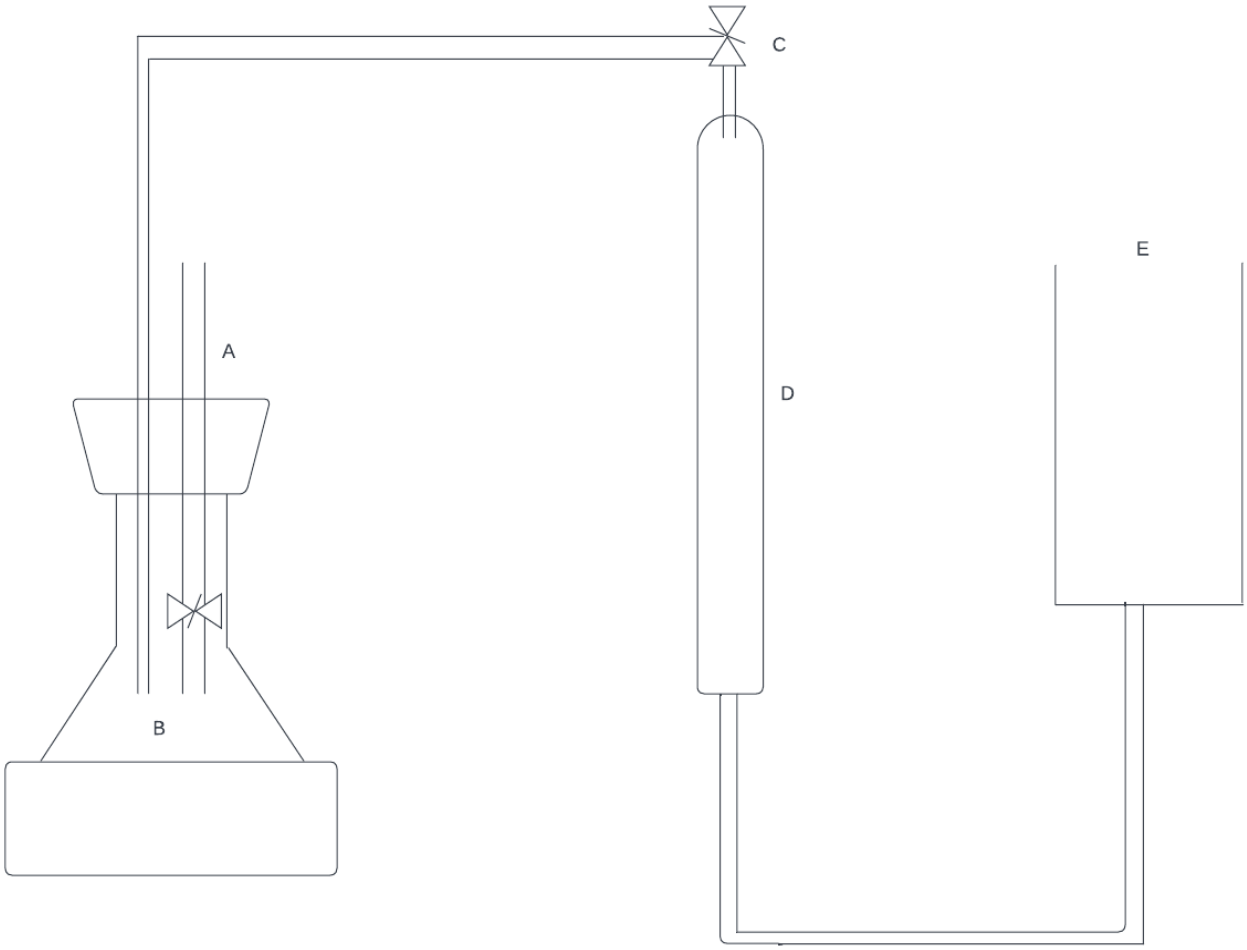

Figure 3.1: Schematic diagram for Chittick apparatus

A. Pipette with acid
B. Reaction vessel
C. Stop cork
D. Burette
E. Reservoir fluid

3.2.4.1 Methodology

Two solutions were required for the test, and these were diluted hydrochloric acid (HCl) and coloured reservoir fluid. The two solutions were prepared as follows:

- **Dilute Hydrochloric acid**

A 6 N solution of hydrochloric acid (HCl) was made by adding 109.4 g of concentrated hydrochloric acid (HCl) to 1 L of deionized water.

- **Reservoir fluid**

In a 1 L Erlenmeyer flask, 100 g of sodium chloride (NaCl) was dissolved in 800 mL of distilled water and 1 g of sodium hydrogen carbonate ($NaHCO_3$) was added. 2 mL (dropwise) of methyl orange solution was then added and the solution stirred.

A 1:5 dilute sulfuric acid (H_2SO_4) solution was prepared and then added to the solution prepared in the 1 L Erlenmeyer flask until the solution turned a deep pink colour. The solution was topped up to the 1 L mark in the flask and poured into the reservoir fluid point (E) to also reach a level in the burette (D). 1.70 g of fly ash was weighed and placed in the reaction vessel (B), which was then tightly capped. The level of the coloured liquid/reservoir fluid in the burette (D) and the reservoir was leveled by opening the stop cork (C). A slight negative pressure was created by lowering the reservoir level (E) by about 3 mL of the level in the burette. The stop cork had to be closed for the negative pressure to be created. 20 mL of 6 N hydrochloric acid (HCl) was introduced from the pipette (A) into the fly ash in the reaction vessel (B), and the mixture was agitated.

As the acid was introduced, the stop cork (C) was also opened to allow CO_2 to enter the burette, and then it was closed again to allow for the volumetric displacement of the reservoir fluid resulting from the CO_2 evolution. The valve on the pipette that held the acid was also closed to ensure no CO_2 escaped the system. Simultaneously, a stopwatch was started as the acid was introduced, and the displacement of the reservoir fluid in the burette by evolving CO_2 was read after 1 minute and after 20 minutes. The reading at 1 minute was recorded as R_1, while that at 20 minutes was recorded as R_{20}. A schematic of the Chittick apparatus is provided in Figure 3.1, while Figure 3.2 displays the full assembly of the Chittick apparatus.

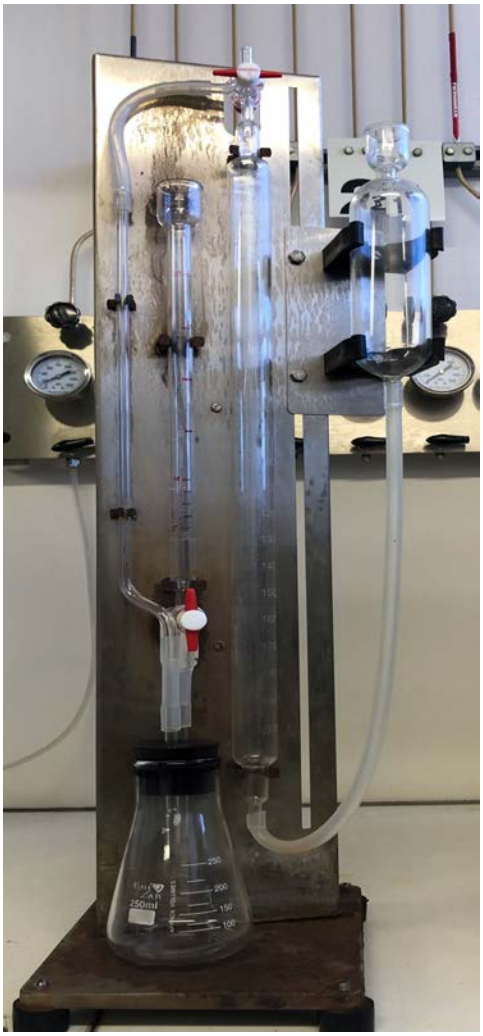

Figure 3.2: Chittick apparatus setup

To determine the % $CaCO_3$ formed, correction factors to account for errors associated with the calculation were calculated for each reading and subsequently used to determine the % $CaCO_3$ formed. The method for reacting the carbonated fly ash samples previously described was used to react 0.10 g of pure $CaCO_3$ in order to calculate the correction factor. The factor is specified as previously mentioned as follows:

$$f = \frac{W \times T}{1.22 \times V}$$

Where;

W = 0.10 grams weighed of pure $CaCO_3$
T = temperature of measurement in K
V = mL produced CO_2

The correction factor was used to calculate the % $CaCO_3$ (based on 1.7 g of fly ash samples) as follows:

$F = CR_1 - (0.04)(CR_{20} - CR_1)$ and $\% CaCO_3 = 0.232F$

Where;

CR_1 = reading at 1 minute × f

CR_{20} = reading at 20 minutes × f

3.3 Equipment

Preliminary and carbonation experiments were carried out using an autoclave reactor made of stainless-steel material (model 4560). The steel jacket of the reactor (with a teflon liner inside) had a height of 14.7 cm and an internal diameter of 6.3 cm as shown in Figure 3.3:

Figure 3.3: Reactor steel jacket

Figure 3.3 above shows the reactor assembly while Figure 3.4 provides a detailed schematic representation of the 600 mL Parr high-pressure/high-temperature reactor:

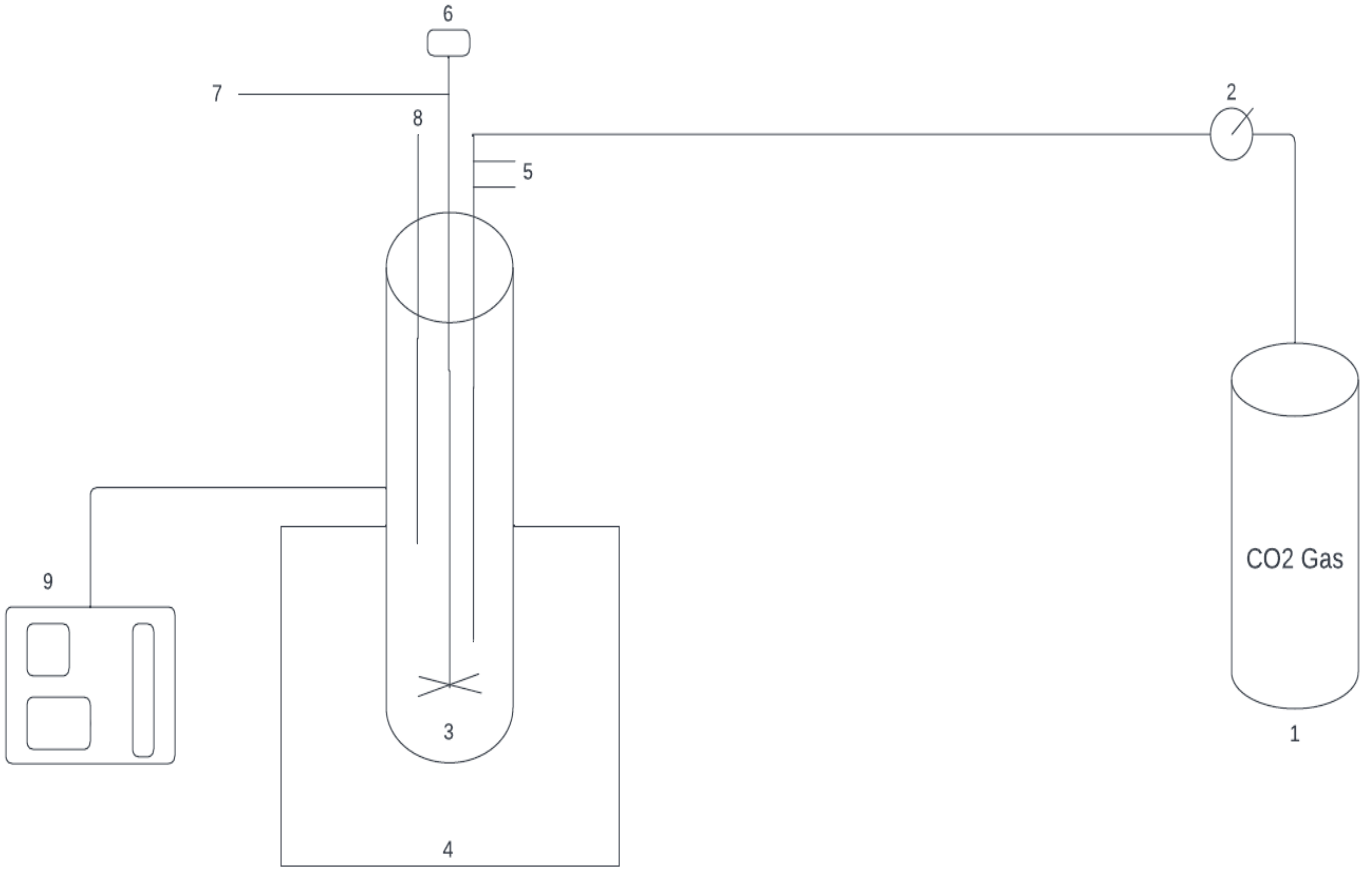

Figure 3.4: Schematic representation of 600 mL Parr high pressure/high temperature reactor

1) Carbon dioxide cylinder
2) Pressure regulator
3) Stainless steel reactor vessel (maximum temperature = 350 ºC with a teflon liner, maximum pressure = 345 bar)
4) Heating jacket
5) Pressure relief valve
6) Stirrer powered by a magnetic drive
7) Cooling water supply
8) Thermocouple
9) Monitor

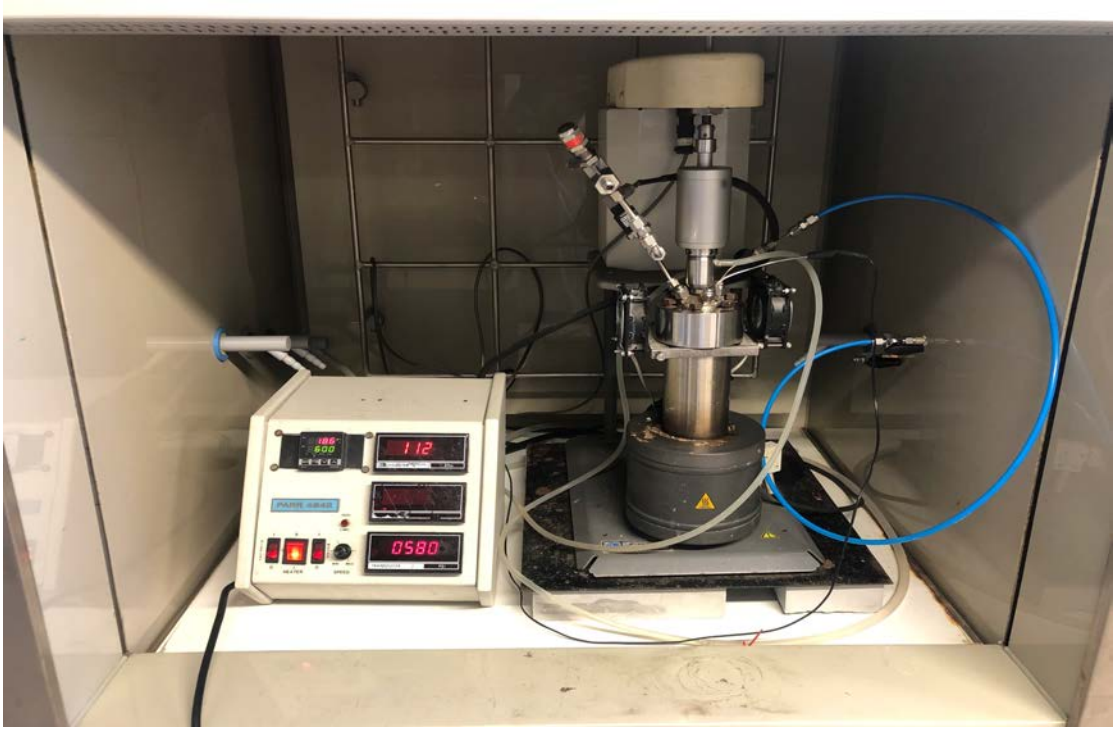

Figure 3.5: 600 mL Parr high-pressure/high-temperature reactor setup

As stated previously, all necessary experiments were conducted using a 600 mL Parr high-pressure reactor. The reactor used was temperature and pressure controlled, with a maximum pressure capacity of 34.5 Mpa. Initially, a teflon liner was sized to a height of 13.6 cm and an internal diameter of 5.3 cm. The teflon liner was used to contain the reaction mixtures, which were fly ash and water/AMD wastewater, before being placed inside the steel jacket of the reactor. It was important to size the teflon liner accurately to ensure a perfect fit within the steel jacket of the reactor. The accuracy in the sizing of the teflon liner ensured that the reactor was closed properly to prevent any CO_2 from escaping out of the reaction vessel.

3.3.1 Methodology

Reaction solutions made of water/AMD wastewater, and fly ash were carefully prepared using the desired S/L ratio of 0.5 g/mL or 0.2 g/mL. The reaction solutions were placed inside the teflon liner, which was subsequently placed inside the steel jacket of the reactor. The reactor was closed and sealed properly and the body of the reactor was then placed into the heater assembly. Thermocouple, magnetic stirrer drive system, and controlled water coolant supply for the reactor introduced, and the assembly was sealed. The monitor was switched on and the temperature (^{0}C) was adjusted to the desired temperature (^{0}C). The reaction mixture was then stirred at the desired stirring speed (rpm). Initially, preliminary experiments were conducted.

The first of these baseline experiments involved the investigation of the dissolution behaviour of calcium (Ca^+) in water from pure $Ca(OH)_2$. Pure $Ca(OH)_2$ was dissolved in water for 10 min using different S/L ratios between 0.2 g/L and 1.2 g/L to determine whether calcium (Ca^{2+}) from the $Ca(OH)_2$ fully dissolves. To know this, the actual concentration of dissolved calcium (Ca^{2+}) was determined from ICP-OES analysis. The second of these baseline experiments was used to determine the amount of calcium (Ca^{2+}) leachable from the fly ash. The first parameter investigated for the second set of preliminary experiments was the temperature (^{0}C) and its effect on the leachability of calcium (Ca^{2+}). The temperature was varied between 30 ^{0}C, 50 ^{0}C, 70 ^{0}C, 90 ^{0}C, and 110 ^{0}C at 100 rpm for 60 min using a S/L ratio of 0.5 g/mL, and the optimum temperature (^{0}C) was obtained. The optimum temperature (^{0}C) obtained of 70 ^{0}C was used for experiments involving the effect of time (min) on the leachability of calcium (Ca^{2+}) wherein time (min) was varied between 30 min, 60 min, 90 min, and 120 min with the stirring speed set at 100 rpm with a S/L ratio of 0.5 g/mL used. The optimum reaction times (min) were then obtained. The effect of particle size (μm) on the leachability of calcium (Ca^{2+}) was also investigated, where the bulk size fly ash, 25 (μm), 45 (μm), and 125 (μm) particle sizes were considered using the optimum temperature of 70 ^{0}C, highest reaction time of 120 min, stirring speed of 100 rpm and S/L ratio of 0.5 g/mL.

Following preliminary experiments, carbonation experiments were then carried out using the optimum conditions from the preliminary experiments which were the conditions that resulted in higher leachability of calcium (Ca^{2+}). These conditions were assumed to be ideal for achieving optimum carbonation performance. Based on the calcium (Ca^{2+}) extraction from preliminary experiments, a reaction temperature of 70 ^{0}C, bulk particle size (μm), and reaction times of 30 min, 90 min, and then 120 min were used for carbonation experiments.

For carbonation experiments, after the reaction mixtures were placed inside the reactor with temperature (^{0}C) and stirring speed (rpm) adjusted to the desired speed, CO_2 was introduced into the reactor, and the initial CO_2 pressure was varied between 1 Mpa and 4 Mpa over 30 min, 90 min and 120 min. Optimization of other process parameters such as temperature (^{0}C), stirring speed (rpm), and the S/L ratio was done during carbonation experiments. For each experimental run, the reactor was closed and sealed properly to prevent any CO_2 from escaping. The CO_2 pressure coming into the line was controlled by the CO_2 tank, which had a pressure indicator. The pressure control valve on the reactor was shut off when the desired CO_2 pressure (Mpa) was reached. This allowed CO_2 gas to be trapped inside the vessel for the duration of the experiment. The pressure drop after each experiment was recorded. After each experimental run, the reactor was allowed to cool and then disassembled. The solid and liquid mixtures were separated using a vacuum pump. All experiments were duplicated to ensure the accuracy of the results. The appropriate sample analysis was then carried out, including Chittick tests to find out how much CO_2 in the fly ash slurry under the given conditions was transformed into $CaCO_3$.

3.3.2 Experimental procedure

3.3.2.1 Preliminary experiments

3.3.2.1.1 Dissolution of calcium (Ca^{2+}) in water from $Ca(OH)_2$

- A given mass of calcium hydroxide ($Ca(OH)_2$) was dissolved into a 1L beaker with distilled water.
- The mixture was stirred for 10 min at room temperature.
- After 10 min, the stirring was stopped, and the mixture was allowed to settle for 30 min.
- The mixture was filtered using a 0.45 (μm) membrane filter paper.
- The leachate from the mixture was sent for ICP-OES analysis to determine the concentration of calcium (Ca^{2+}) in the leachate.
- By obtaining the concentration of dissolved calcium (Ca^{2+}) in the leachate from the $Ca(OH)_2$ weighed, a calibration curve was generated.

Procedure for calculating the mass of $Ca(OH)_2$ weighed

Considering the reaction:

$$Ca(OH)_{2(s)} \rightarrow Ca^{2+}_{(aq)} + 2OH^{-}_{(aq)})$$

At a stoichiometric ratio of 1:1, the mass of calcium hydroxide ($Ca(OH)_2$) weighed to make a concentration of 200 mg/L of elemental calcium (Ca^{2+}) was determined through the calculation provided:

$$\text{Mass of } Ca(OH)_2 = \left(\frac{mass\ of\ elemental\ calcium}{molar\ mass\ of\ elemental\ calcium}\right) \times molar\ mass\ of\ Ca(OH)_2$$

$$\text{Mass of } Ca(OH)_2 = \left(\frac{0.2\ g}{40.08\ g/mol}\right) \times \left(\frac{74.09\ g}{mol}\right);\ \therefore\ \text{mass of } Ca(OH)_2 = 0.37\ g$$

Thus 0.37 g of $Ca(OH)_2$ was weighed and transferred into 1 L to make a concentration of 200 mg/L elemental calcium (Ca^{2+}). This method was used for all elemental calcium (Ca^{2+}) concentrations considered.

3.3.2.1.2 Leaching of calcium (Ca^{2+}) from fly ash

- A fly ash/water mixture was prepared at the desired S/L ratio (g/mL) and placed inside the 600 mL Parr high-pressure reactor, with the body of the reactor then placed inside the heating jacket and connected to the magnetic stirrer.
- The reaction mixture was stirred at the desired stirring speed (rpm).
- The temperature (^{0}C) was set to the desired temperature (^{0}C) with the temperature (^{0}C) controller, and the water coolant supply was introduced.
- The experiment was timed (min) over the required reaction time (min), and after the reaction was complete, the fly ash/water slurry was removed from the reaction vessel.
- Using a vacuum pump, the fly ash/water slurry was then filtered for 15 minutes through a 0.45 (μm) pore membrane filter paper.
- Following filtration, the liquid samples were preserved in a fridge at 4 ^{0}C until analysis could be conducted.
- The solid was dried overnight in an oven with the temperature set at 90 ^{0}C and then stored in sealed containers until analysis.

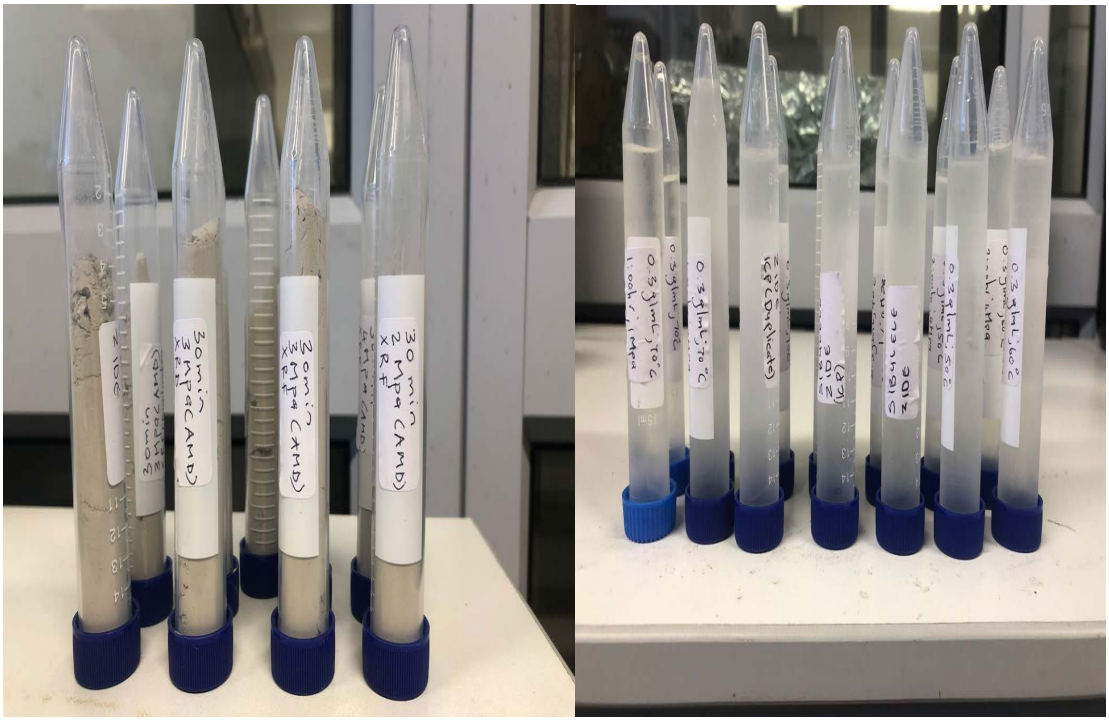

Figure 3.6: Leachate and solid residue samples from experiments contained in centrifuge tubes

- The solid residues were then taken for XRD and XRF analysis to determine the phases present while the leachate was analyzed using ICP-OES to determine the elemental compositions (ppm).

3.3.2.2 Direct carbonation experiments

- A fly ash/water mixture was prepared at the desired S/L ratio (g/mL) and placed inside the 600 mL Parr high-pressure reactor, with the body of the reactor then placed inside the heating jacket and connected to the magnetic stirrer.
- The reaction mixture was stirred at the desired stirring speed (rpm).
- The temperature (^{0}C) was set to the desired temperature (^{0}C) with the temperature (^{0}C) controller, and the water coolant supply was introduced.
- CO_2 gas was then fed into the reaction system through the line and controlled on the gas tank to obtain the desired CO_2 pressure (Mpa) for the reaction.
- After obtaining the desired pressure (Mpa) in the reaction vessel, the control valve on the reactor was then closed.
- The experiment was timed (min) over the required reaction time (min) and after the reaction was complete, the system was depressurized and allowed to cool.
- The carbonated fly ash/water slurry was then removed from the reaction vessel.
- Using a vacuum pump, the carbonated fly ash/water slurry was filtered for 15 min through a 0.45 (μm) pore membrane filter paper.
- Following filtration, the pH of the leachate was measured, and the liquid samples were preserved in a fridge at 4 ^{0}C until analysis could be conducted.
- The solid was dried overnight in an oven set at 90 ^{0}C and then stored in sealed containers until analysis.
- The solid residues were then taken for XRD and XRF analysis to determine the phases present.
- The leachate was taken for ICP-OES analysis in order to determine the elemental composition (ppm).

3.3.2.3 Indirect carbonation experiments

- A fly ash/water mixture was prepared at the desired S/L ratio (g/mL) and placed inside the 600 mL Parr high-pressure reactor, with the body of the reactor then placed inside the heating jacket and connected to the magnetic stirrer.
- The reaction mixture was stirred using the desired stirring speed (rpm).
- The temperature (^{0}C) was set to the desired temperature (^{0}C) from the monitor and the water coolant supply was introduced.
- The experiment was timed (min) over the required reaction time (min) and after the reaction was complete, the fly ash/water slurry was removed from the reaction vessel.
- Using a vacuum pump, the fly ash/water slurry was then filtered for 15 minutes through a 0.45 (μm) pore membrane filter paper.
- Following filtration, the pH of the leachate was measured before carbonation.
- The required volume (mL) for the leachate that was to be used during carbonation was measured, and the leachate was placed inside the reactor. The reactor was then placed inside the heating jacket and connected to the magnetic stirrer.
- The leachate was stirred using the desired stirring speed (rpm) and the temperature (^{0}C) was set to the desired temperature (^{0}C) on the monitor, and the water coolant supply was introduced.
- CO_2 gas was then fed into the reaction system through the line and controlled on the gas tank to obtain the desired CO_2 pressure (Mpa) for the reaction.
- After obtaining the desired pressure (Mpa) in the reaction vessel, the control valve on the reactor was then closed.
- The experiment was timed (min) over the required reaction time (min) and after the reaction was complete, the system was depressurized and allowed to cool.
- The carbonated leachate was then removed from the reaction vessel and filtered.
- Using a vacuum pump, the leachate was then filtered for 15 minutes through a 0.45 (μm) pore membrane filter paper.
- The filter paper was dried overnight with the oven temperature set at 90 ^{0}C.
- Following filtration, the pH of the leachate was measured, and the liquid samples were preserved in the fridge set at 4 ^{0}C until analysis could be conducted.
- A minuscule amount of $CaCO_3$ was recovered from the indirect aqueous carbonation process; therefore, XRD and XRF could not be performed.
- The leachate was analyzed by ICP-OES to determine the elemental composition (ppm).

CHAPTER 4

4. Results and Discussion

This results section is divided into three sections. The first section is a brief section based on results obtained from the characterisation of raw fly ash to determine the mineralogical and elemental composition of the raw fly ash used in this study. The second section provides results from preliminary experiments. Preliminary experiments were done to determine the leachability of calcium (Ca^{2+}) from the fly ash. The last section (i.e., Section 4.3) comprises results obtained from direct and indirect aqueous carbonation experiments.

4.1 Characterisation of raw fly ash

As mentioned previously, this section provides a brief discussion of the results obtained from the analysis of the raw fly ash samples. The first part of this characterisation section covers results obtained from XRD analysis for the mineralogical phases present in the fly ash, while the second section provides results from XRF analysis for the elemental composition. Figure 4.1 shows the XRD pattern for the raw fly ash:

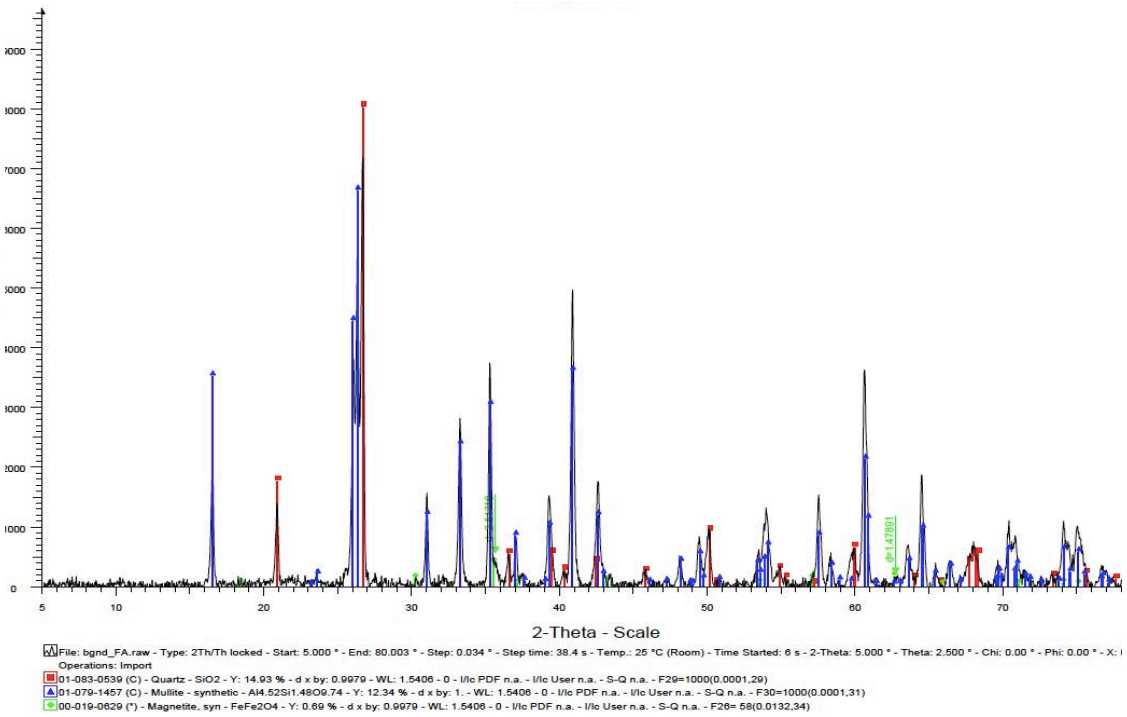

Figure 4.1: XRD analysis results for raw fly ash

4.1.1 Results from XRD

XRD analysis was initially performed on the raw fly ash to identify the mineral phases present in the fly ash. According to the XRD spectrum, Durapozz fly ash was found to be a heterogeneous material as it comprises several crystalline phases. The XRD pattern for the raw fly ash shown in Figure 4.1 consists of strong intensity peaks corresponding to quartz (SiO_2) and mullite ($Al_6O_{13}Si_2$), and overall weaker intensity peaks for magnetite ($FeFe_2O_4$). The mineralogical phases represented by the XRD pattern found in Figure 4.1 are the major mineralogical phases typically found in coal fly ash (CFA).

4.1.2 Results from XRF

XRF analysis was done to quantitatively identify the major and minor elemental compositions present in the raw fly ash. The results for the elemental compositions of the raw fly ash are presented in Table 4.1:

Table 4.1: Elemental compositions for raw fly ash from XRF

Element	Composition (wt. %)
SiO_2	54.36
Al_2O_3	34.19
CaO	4.06
Fe_2O_3	3.12
TiO_2	1.75
MgO	0.90
K_2O	0.64
P_2O_5	0.47
Na_2O	0.38
V_2O_5	0.052
Cr_2O_3	0.041
MnO	0.03
Total	100

Based on the XRF results shown in Table 4.1, the fly ash used was mainly composed of SiO_2, Al_2O_3, Fe_2O_3. From the XRF analysis results for raw fly ash, the sum of SiO_2, Al_2O_3, and Fe_2O_3 was greater than 70 %; therefore, the fly ash can be classified as Class F. The CaO (wt. %) content was 4.06 % which was within the range of typical Class F fly ash (i.e., < 10). From Table 4.1, results from XRF analysis showed that the major chemical components in the fly ash used in this work were quartz (SiO_2) and aluminium oxide (Al_2O_3) phases, and their percentage compositions were 54.36 % and 34.19 %, respectively, which was high, and this was expected for Class F fly ash. The iron oxide (Fe_2O_3) content of 3.12 % found in the fly ash was relatively low, with other mineral phases such as MgO and MnO also reporting lower compositions of 0.90 % and 0.03 %, respectively. It is worth mentioning that phases such as Fe_2O_3, MgO, and MnO also contribute to the overall consumption of CO_2 during the carbonation process with fly ash as, $FeCO_3$, $MgCO_3$, and $MnCO_3$ can be formed during the carbonation process with fly ash. However, considering the slightly higher content of CaO (wt. %) in the fly ash used in this study than FeO_3, MgO, and MnO mineral phases and bearing in mind that CaO is more soluble in water, the total $CaCO_3$ formed for direct aqueous carbonation for the present work gave a better indication of the amount of CO_2 stored in mineral form.

4.2 Preliminary Experiments

Prior to conducting experiments involving direct and indirect carbonation, baseline/preliminary experiments were first carried out to determine the amount of calcium (Ca^{2+}) leachable from the fly ash. As mentioned previously, the calcium (Ca^{2+}) extraction and subsequent dissolution constitute the main rate-limiting step for the carbonation process. Therefore, the leaching and dissolution behaviour of calcium (Ca^{2+}) in solution is quite important to understand as the concentration of calcium (Ca^{2+}) leachable from the fly ash and that can dissolve in solution has a significant effect on the rate of carbonation and the overall the percentage $CaCO_3$ formed, as well as the carbonation efficiency CE (%). The dissolution behaviour of calcium (Ca^{2+}) in water was the initial preliminary/baseline experiment using pure $Ca(OH)_2$. The experiment was used to determine whether calcium (Ca^{2+}) can fully dissolve in water, while subsequent sections were experiments used to determine the leachability of calcium (Ca^{2+}) from fly ash by investigating the effect of temperature (^{0}C), time (min), and particle size (μm) on the leaching of calcium (Ca^{2+}).

4.2.1 Dissolution of calcium (Ca^{2+}) in water from pure calcium hydroxide $Ca(OH)_2$

This section provides results from an experiment conducted to fully investigate the dissolution behaviour of calcium (Ca^{2+}) in water using pure calcium hydroxide $Ca(OH)_2$, with the complete experimental detail provided in Chapter 3, Section 3.3.2.1.1. Results presented in Figure 4.2 are from an experiment that was carried out to determine the maximum amount of calcium (Ca^{2+}) that can dissolve in water (i.e., the saturation point of calcium (Ca^{2+}) in water) using pure $Ca(OH)_2$ for a fixed reaction time (min) of 10 min with varying S/L ratios of 0.2 g/L, 0.4 g/L, 0.6 g/L, 0.8 g/L, 1 g/L, and 1.2 g/L as shown in Figure 4.2:

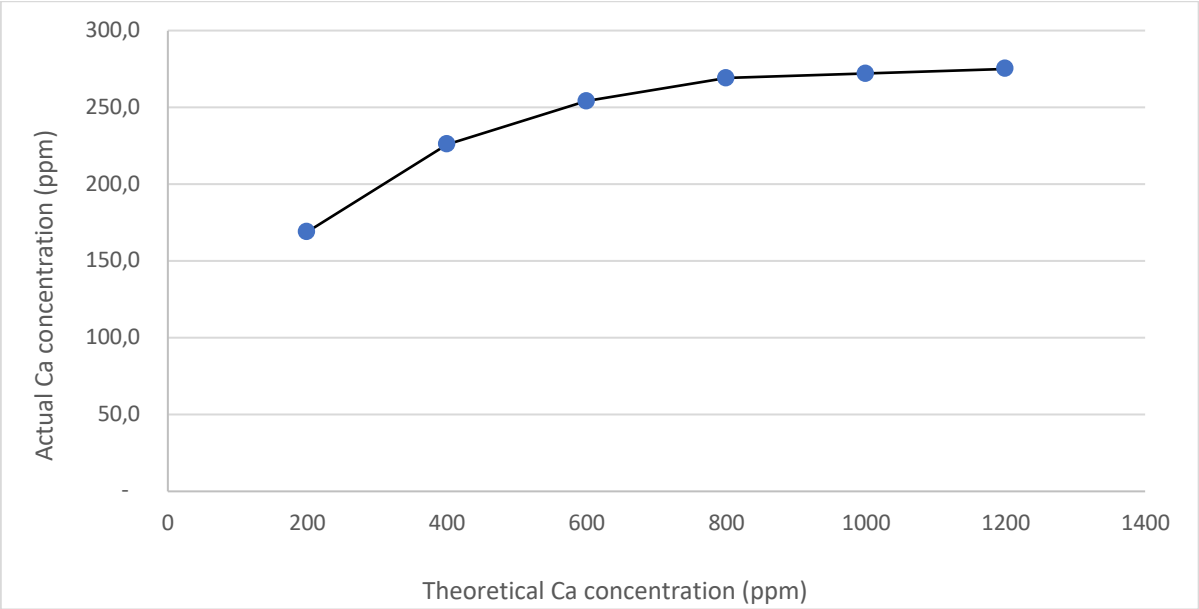

Figure 4.2: Actual saturation point of calcium (Ca^{2+}) in water from dissolving pure calcium hydroxide $Ca(OH)_2$ (reaction time: 10 min)

According to Perry et al. (2008), the theoretical saturation concentration of calcium (Ca^{2+}) is reported as 1 g/L. This means that theoretically, the maximum amount of calcium (Ca^{2+}) that can dissolve in 1 L of water is 1 g. An experiment was therefore carried out with the aim of determining whether the saturation point reported in the literature could be reached. Essentially, the experiment was used to determine whether calcium (Ca^{2+}) can fully dissolve in water, which is important to understand when it comes to the efficiency of the carbonation process.

However, results from Figure 4.2 show that the actual saturation point of calcium (Ca^{2+}) was reached at around 269 ppm after which, no more calcium (Ca^{2+}) could dissolve in water. Given that there's a 1:1 stoichiometric relationship between $Ca(OH)_2$ and calcium (Ca^{2+}) when calcium hydroxide $Ca(OH)_2$ dissociates in water, results from Figure 4.2 indicate that some of the calcium (Ca^{2+}) did not fully dissolve in the water as there was a discrepancy between the theoretical saturation concentration of calcium (Ca^{2+}) and the actual calcium (Ca^{2+}) concentration reported from ICP-OES results in all cases. This was possibly due to the lower solubility of pure $Ca(OH)_2$ in water.

4.2.2 Leaching of calcium (Ca^{2+}) from fly ash

The leachability of calcium (Ca^{2+}) from fly ash was then examined with the experimental detail given in Chapter 3, Section 3.3.2.1.2. The leachability of the calcium (Ca^{2+}) was investigated using various operating process parameters that would potentially result in the maximum extraction of calcium (Ca^{2+}) in fly ash. To determine the leachability of calcium (Ca^{+}) from fly ash, the effects of temperature (^0C) , time (min), and particle size (μm) on the leachability of calcium (Ca^{2+}) were studied.

4.2.2.1 Effect of temperature (^0C) on leachability of calcium (Ca^{2+})

The first parameter considered in determining the leachability of calcium (Ca^{2+}) from the fly ash was the temperature (^0C). The temperatures considered were 30 ^0C, 50 ^0C, 90 ^0C, and 110 ^0C over a period of 60 minutes using a S/L ratio of 0.5 g/mL and a stirring speed of 100 rpm. XRF analysis was used to determine the CaO (wt. %) content remaining in the solid residue, as shown in Figure 4.3:

4.2.2.1.1 Results from XRF analysis

XRF was used to determine the CaO (wt. %) content remaining in the solid residue for the initial set of leaching experiments involving the effect of temperature (^{0}C) on the leaching of calcium (Ca^{2+}). The effect of temperature (^{0}C) on leaching was investigated for 60 min between 30 ^{0}C and 110 ^{0}C as shown in Figure 4.3:

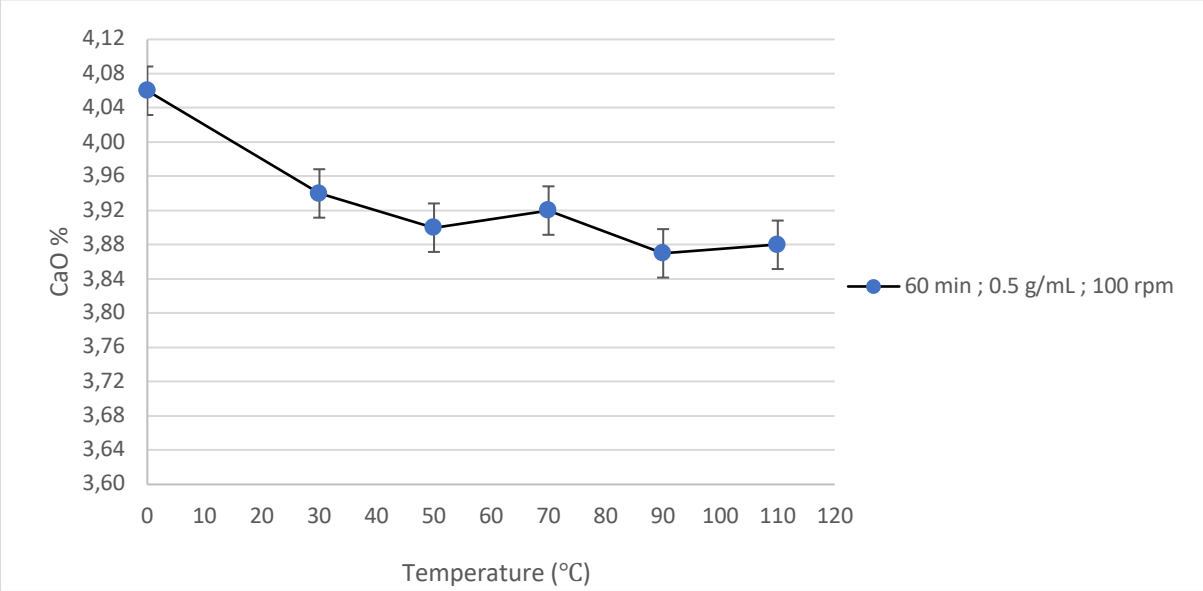

Figure 4.3: Effect of temperature (^{0}C) on CaO (wt. %) content from XRF analysis results

From Figure 4.3, it was expected that the CaO (wt. %) content that remains in the solid residue would reduce significantly from the initial composition of 4.06 wt. % in the fly ash before leaching, which is represented by the point at temperature 0 ^{0}C. However, the maximum CaO (wt. %) that dissolved was 0.19 wt. %, thus indicating that calcium (Ca^{2+}) was mostly associated with phases that did not readily dissolve in water. The results show a reduction in the CaO (wt. %) content from the initial CaO (wt.%) content for all the temperatures (^{0}C) considered, however, the concentrations obtained between 30 ^{0}C and 110 ^{0}C after 60 minutes were not significantly different and showed only a minor change in the CaO (wt. %) content remaining in the solid residue over the temperature (^{0}C) range considered with similar CaO (wt. %) weight losses observed of 0.12 wt. %, 0.16 wt. %, 0.14 wt. %, 0.19 wt. % and 0.18 wt. % at 30 ^{0}C, 50 ^{0}C, 70 ^{0}C, 90 ^{0}C and 110 ^{0}C respectively.

The negligible effect of increasing temperature (^{0}C) on the change in CaO (wt. %) after 60 min from XRF analysis was possibly due to the limitations of the XRF technique in detecting smaller concentrations. Considering that the concentration of CaO (wt. %) present in the fly ash used in this study was low and that XRF analysis is less sensitive in detecting smaller concentrations than techniques such as ICP-OES, XRF analysis was possibly less accurate in determining the CaO (wt. %) remaining in the solid residue from temperature (^{0}C) variation for leaching experiments. ICP-OES, a much more sensitive analytical technique to lower concentrations, was used to give a more precise suggestion of the temperature (^{0}C) that would result in the highest leachability of calcium (Ca^{2+}), taking into account the low concentration of CaO (wt%) accessible in the fly ash.

4.4.2.1.2 Results from ICP-OES analysis

ICP-OES analysis was performed to determine the calcium (Ca^{2+}) concentration (ppm) in the leachate. The effect of temperature (^{0}C) on leaching was investigated for 60 min between 30 ^{0}C and 110 ^{0}C as shown in Figure 4.4:

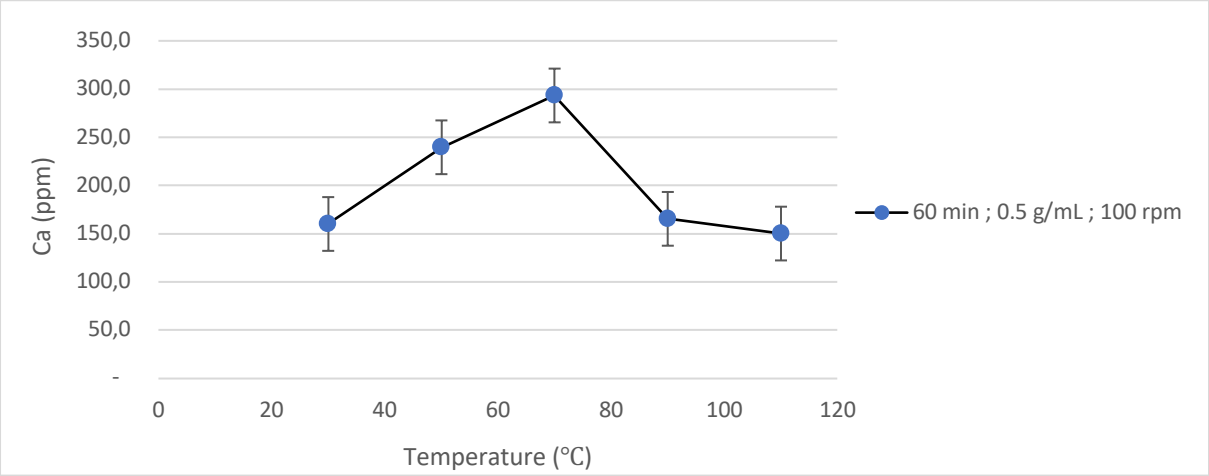

Figure 4.4: Effect of temperature (^{0}C) on leaching of calcium from ICP-OES analysis results

The results obtained from ICP-OES analysis showed a notable trend and from Figure 4.4, it can be observed that the highest calcium (Ca^{2+}) concentration obtained in the leachate was at 70 ^{0}C. Considering Bertos et al. (2004) found that the maximum uptake of CO_2 for the carbonation process increases with increasing temperature of up to 60 ^{0}C due to the opposing effect of temperature (^{0}C) on the carbonation process, the optimum temperature of 70 ^{0}C for calcium (Ca^{2+}) extraction was close enough to the maximum suitable temperature (^{0}C) for subsequent carbonation experiments. A temperature of 70 ^{0}C can also be considered ideal, as higher temperatures would prove wasteful of energy and contribute to CO_2 being emitted.

When considering the opposing effect of temperature (^{0}C), the optimum temperature of 70 ^{0}C was high enough to achieve effective calcium (Ca^{2+}) extraction but not exceedingly high to hinder the solubility of CO_2 in the liquid phase for carbonation experiments. The maximum calcium (Ca^{2+}) concentration leached when considering the effect of temperature (^{0}C) on calcium (Ca^{2+}) extraction was 293.4 ppm after 60 min, as shown in Figure 4.4, in relation to the baseline experiment conducted previously using pure $Ca(OH)_2$ where the saturation concentration of calcium (Ca^{2+}) was around 269 ppm, this discrepancy can be explained by the difference in the experimental conditions used for the leaching experiment compared to the conditions used for investigating the dissolution of calcium in water using pure $Ca(OH)_2$. The maximum amount of calcium (Ca^{2+}) extracted of 293.4 ppm was lower than the maximum theoretical saturation concentration of calcium (Ca^{2+}) of 1 g/L, which meant that the calcium (Ca^{2+}) leached did not reach the saturation limit, which is the point where the maximum amount of calcium (Ca^{2+}) can be leached. This can be attributed to the calcium (Ca^{2+}) being locked in the major mineral phases present in the fly ash, namely the quartz (SiO_2) and mullite ($Al_6O_{13}Si_2$) phases.

The presence of other phases was also detected from the first set of leaching experiments, and Figure 4.5 shows the increase in the concentration of one of the anionic phases present in higher concentration in the form of sulfate (SO_4^{2-}):

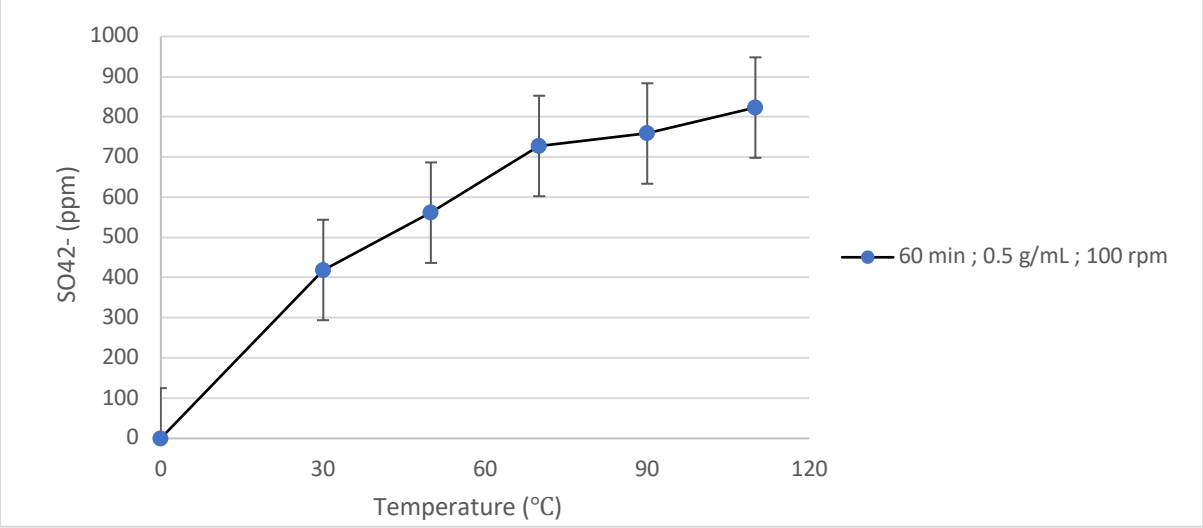

Figure 4.5: Effect of temperature (^{0}C) on sulfate concentration

Figure 4.5 shows that there was a relatively high concentration of sulfate in solution after 60 min of leaching at varying temperatures (^{0}C). The concentration of sulfate was seen to increase gradually as the temperature (^{0}C) increased until about 70 ^{0}C.

The increase in concentration of SO_4^{2-} and the presence of other ionic species such as nitrates (NO_3^{2-}) and phosphates, though in smaller concentrations (i.e., 0.64 ppm and <20 ppm, respectively, at 70 ^{0}C) from IC analysis, indicate that the solution was possibly saturated with competing ionic species, and this can be attributed to the higher S/L ratio used of 0.5 g/mL, which possibly limited the dissolution of calcium (Ca^{2+}).

The mineral phases present in the solid residue after leaching at what was observed to be the optimum temperature of 70 ^{0}C were examined and are presented in Figure 4.6:

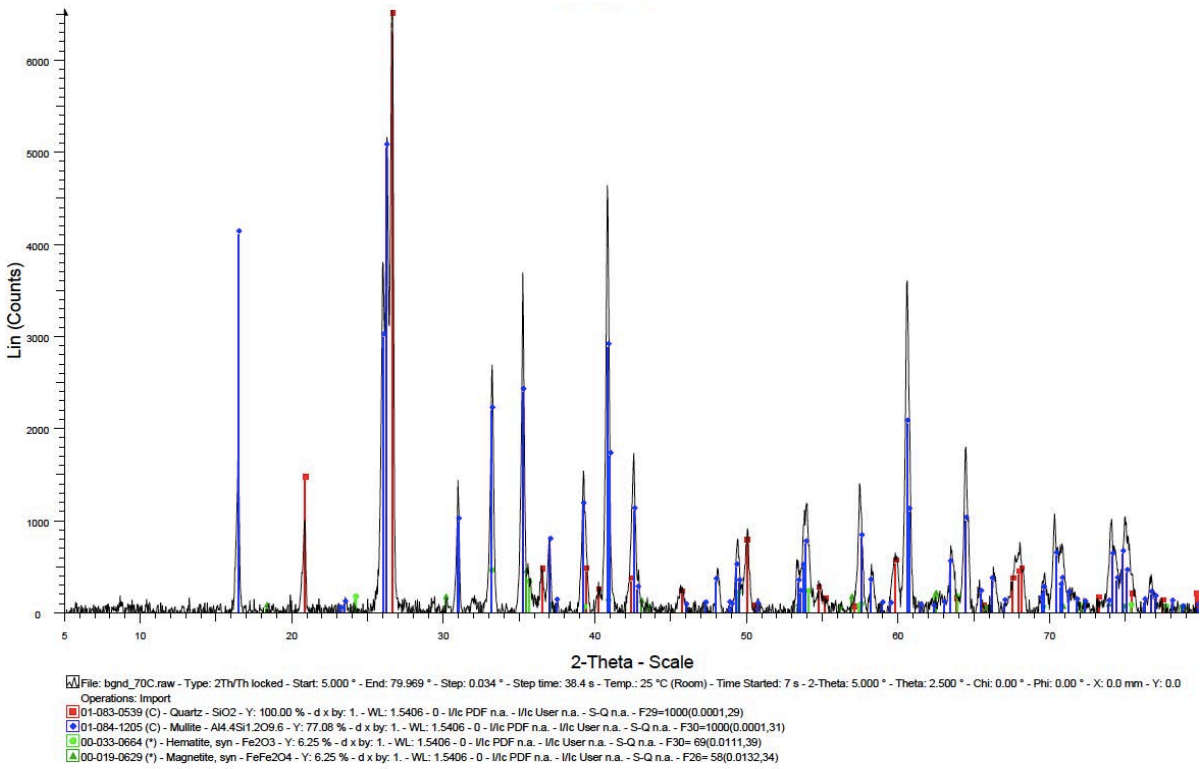

Figure 4.6: Effect of temperature on mineralogical phases from XRD analysis results

XRD analysis was used to identify the mineralogical phases remaining in the fly ash after each temperature (^{0}C) considered. Figure 4.6 shows the XRD pattern for the optimum temperature of 70 ^{0}C. The XRD pattern shown in Figure 4.6 for the preliminary run using the optimum temperature of 70 ^{0}C was similar to the XRD pattern obtained for the raw fly ash, as the same phases were identified. The XRD pattern shows the presence of quartz (SiO_2), and mullite ($Al_6O_{13}Si_2$) with high intensity peaks. It also depicts weaker intensity peaks for hematite (Fe_3O_3) and magnetite ($FeFe_2O_4$). This indicates that the temperature (^{0} C) had no effect on the mineral phases of the fly ash.

The mineral phases present at other temperatures were also considered, and Figure 4.7 shows the XRD pattern for the solid residue after leaching at 30 ^{0}C:

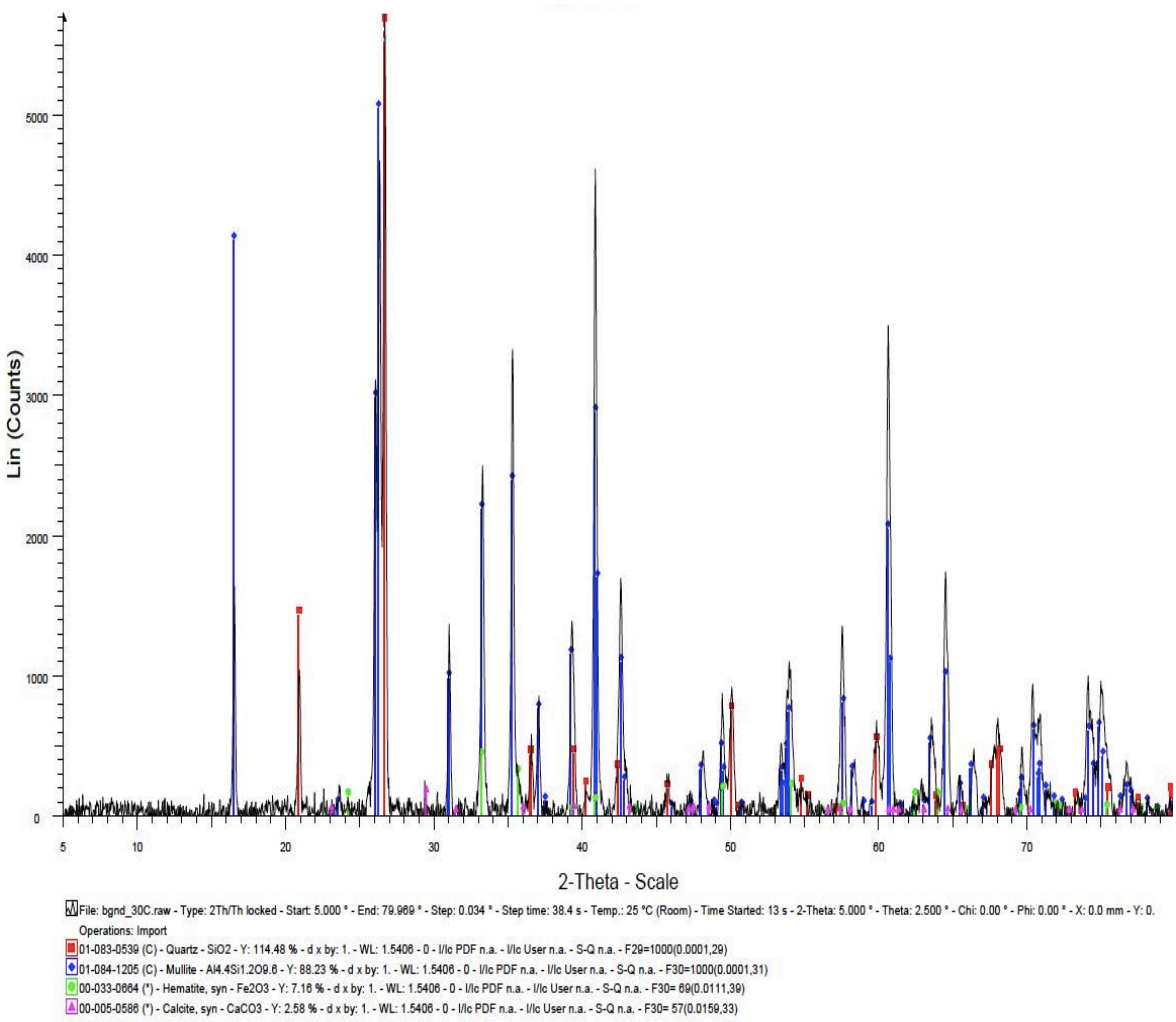

Figure 4.7: Effect of temperature(^{0}C) on mineralogical phases from XRD analysis results

Although the initial results from XRD detected no traces of calcite ($CaCO_3$) in the raw fly ash, the presence of calcite was detected at 30 ^{0}C, 50 ^{0}C, 90 ^{0}C, and 110 ^{0}C. Figure 4.7 shows the XRD pattern for just the temperature of 30 ^{0}C. The pattern shows similar mineralogical phases to those reported at 50 ^{0}C, 90 ^{0}C, and 110 ^{0}C (see Appendix C) except for the microcline ($KAlS_3O_8$) phase reported at 50 ^{0}C. With no CO_2 introduced into the system, traces of calcite ($CaCO_3$) in the solid residue were due to the interaction of the fly ash with CO_2 from the surrounding air, leading to the formation of $CaCO_3$. The $CaCO_3$ formed before the carbonation was conducted can also be attributed to the system not being purged with nitrogen (N_2) gas.

4.2.3 Effect of time (min) on leachability of calcium (Ca^{2+})

The next set of leaching experiments considered the effect of time (min) on the leaching of calcium (Ca^{2+}) from the fly ash using the optimum temperature of 70 ^{0}C determined previously, and a S/L ratio of 0.5 g/mL with stirring at 100 rpm, as shown in Figure 4.8:

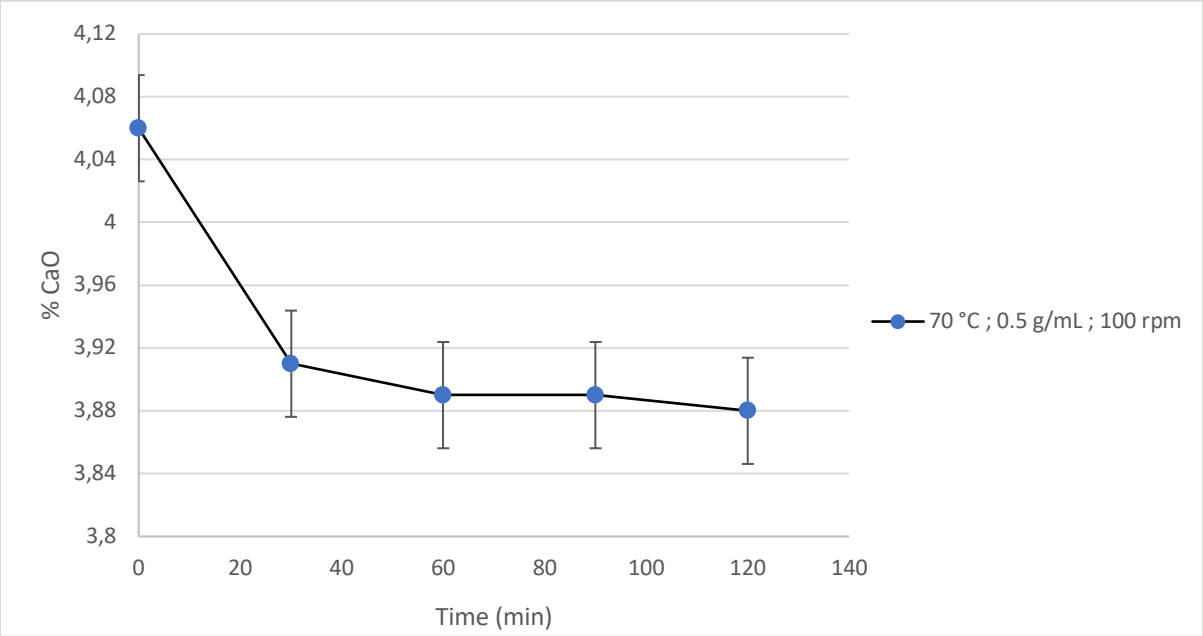

Figure 4.8: Effect of time (min) on CaO (wt. %) from XRF analysis results

Following the investigation of the effect of temperature (^{0}C) on the leaching of calcium (Ca^{2+}), the effect of time (min) on the leachability of calcium (Ca^{2+}) was then considered. Applying the optimum temperature of 70 ^{0}C over a time period of 30 min, 60 min, 90 min, and 120 min proved to have a minor effect on the change in the % CaO (wt. %) remaining in the fly ash solid residue, as the CaO (wt. %) concentration was not significantly different after 30 min, 60 min, 90 min, and 120 min, as shown by the XRF analysis results presented in Figure 4.8. Again, considering that the XRF technique is less sensitive at detecting smaller concentrations, the ICP-OES was then used to give a better indication of the effect of time (min) on the leachability of calcium (Ca^{2+}) into solution.

The effect of time (min) on the leachability of calcium (Ca^{2+}) at 70 ^{0}C using a S/L ratio of 0.5 g/mL and a stirring speed of 100 rpm was investigated more comprehensively by considering the concentration of calcium (Ca^{2+}) remaining in the leachate from ICP-OES analysis, as shown in Figure 4.9:

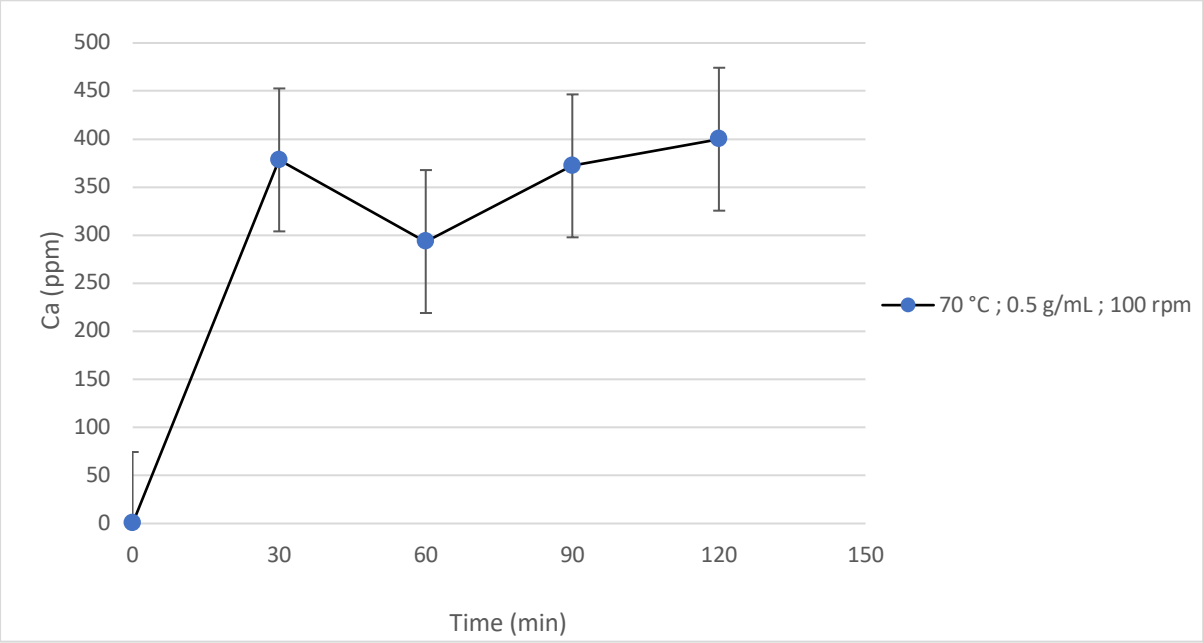

Figure 4.9: Effect of time (min) on leaching of calcium (Ca^{2+}) from ICP-OES analysis results

Figure 4.9 shows the results of the ICP-OES analysis after taking into account the impact of time (min) on the leachability of calcium (Ca^{2+}) from the fly ash. The results indicate that the calcium (Ca^{2+}) extraction was significant during the first 30 min, however, after 30 min the concentration of calcium (Ca^{2+}) leached did not change significantly, as similar concentrations of 378.3 ppm, 293.4 ppm, 372.1 ppm, and 399.8 ppm were reported after 30 min, 60 min, 90 min, and 120 min respectively, as shown in Figure 4.9. The initial increase in the concentration of calcium (Ca^{2+}) was caused by the dissolution of readily soluble calcium (Ca^{2+}) phases such as CaO and $CaSO_4$, whereas the decrease in the concentration observed after 60 min was possibly due to the precipitation of new calcium (Ca^{2+}) - containing mineral phases. The trend observed in Figure 4.9 for the leaching of calcium (Ca^{2+}) over time with fly ash was similar to the results obtained by Iizuka et al. (2004), who used a different alkaline-rich feedstock but found that for a high cement-to-water ratio of 2.9 wt. %, the solution was supersaturated with respect to calcium (Ca^{2+}) even at the early stages of the reaction, and after 10 min of extraction, the concentration of calcium (Ca^{2+}) leveled off for the duration of the 120 min reaction time.

Considering the various existing competing ionic species in fly ash and hence the possibility of oversaturation when 0.5 g/mL was initially used for calcium (Ca^{2+}) extraction and also the oversaturation, caused by the higher cement-to-water ratios from the study done by Iizuka et al. (2004), this indicates that under oversaturated conditions, the calcium (Ca^{2+}) gets extracted to reach a point of oversaturation but after a certain period in time, the change in the calcium (Ca^{2+}) extraction does not show variation because the calcium (Ca^{2+}) continually precipitates and dissolves again, hence the plateau observed after 30 min in Figure 4.9.

The maximum amount of calcium (Ca^{2+}) concentration leached when considering the effect of time (min) on calcium (Ca^{2+}) extraction was 399.8 ppm and was achieved after 120 min. In relation to the preliminary/baseline experiment conducted using pure $Ca(OH)_2$, where the saturation concentration of calcium (Ca^{2+}) was around 269 ppm, this discrepancy can be explained by the difference in the experimental conditions used for the leaching experiment compared to the conditions used for the dissolution of calcium (Ca^{2+}) in water using pure $Ca(OH)_2$. The maximum amount of calcium (Ca^{2+}) extracted at 399.8 ppm after 120 min was lower than the maximum theoretical saturation concentration of calcium (Ca^{2+}) of 1 g/L, which meant that the calcium (Ca^{2+}) leached did not reach the saturation limit of calcium (Ca^{2+}). This can be attributed to the calcium (Ca^{2+}) being locked in water-insoluble phases or the major phases present in the fly ash, namely quartz (SiO_2), and mullite ($Al_6O_{13}Si_2$) phases.

The ICP-OES analysis results also showed that the least amount of calcium (Ca^{2+}) leached was after 60 min and that more calcium (Ca^{2+}) was leachable after 30 min, 60 min, and 120 min, although the calcium (Ca^{2+}) concentrations obtained after all of these time periods were not significantly different. The Dixon's Q-Test was used to determine whether the calcium (Ca^{2}) concentration after 60 min was a potential outlier when considering the closeness in calcium (Ca^{2+}) concentrations observed at 30 min, 90 min, and 120 min. From the test, it was found that at the 90 % confidence level the test statistic (i.e., Q_{TS} = 0.768) was higher than the critical value (i.e., Q_{CV} = 0.765), therefore, we reject the null hypothesis meaning that there was enough evidence to suggest that there was an outlier in the data set and that the calcium (Ca^{2+}) concentration value obtained after 60 min of leaching was an outlier possibly caused by errors during conducting the experiment or analysis. Therefore, 60 minutes were not considered for subsequent experiments involving carbonation.

4.2.4 Effect of particle size (μm) on leachability of calcium (Ca^{2+})

The particle size (μm) was the final parameter considered for the leaching studies. The effect of the particle size (μm) on the leachability of calcium (Ca^{2+}) considered using the optimum temperature of 70 ^{0}C, a S/L ratio of 0.5 g/mL, and a stirring speed of 100 rpm. The particle size was varied between the bulk size fly ash, which was the fly ash before sieving, of 25 (μm), 45 (μm), and 125 (μm). The concentration of CaO (wt. %) after leaching for varying particle sizes was determined by XRF analysis with results presented in Figure 4.10:

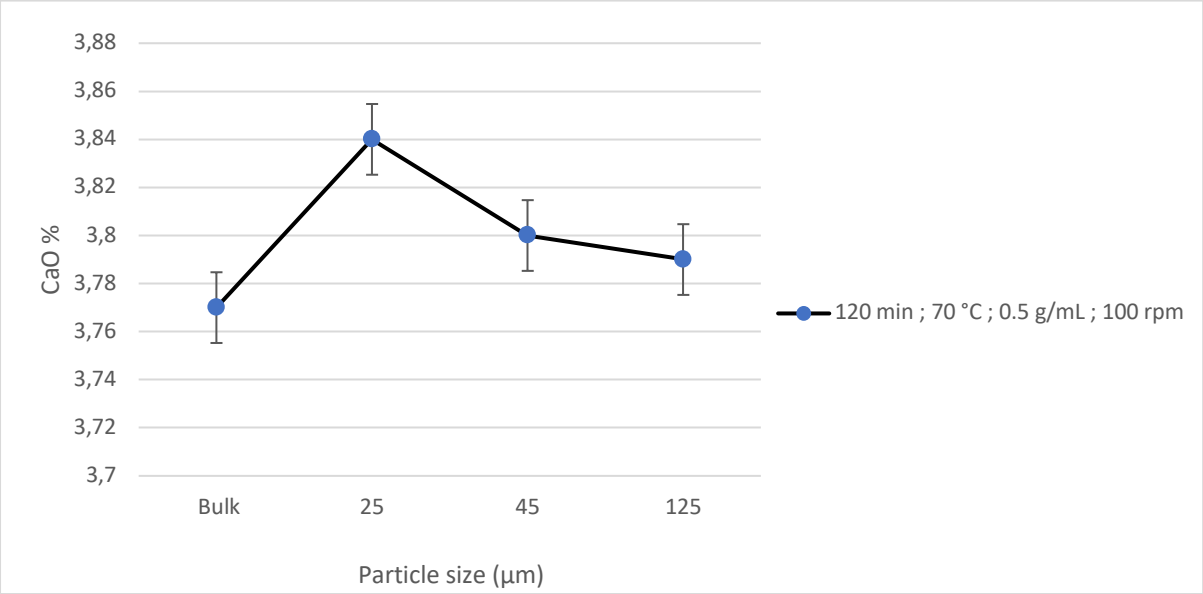

Figure 4.10: Effect of particle size (μm) on CaO (wt. %) from XRF results

The effect of the particle size (μm) was considered using the optimum temperature of 70 ^{0}C, as mentioned previously, and over 120 min, as a slightly higher concentration of calcium (Ca^{2+}) was leached over the 120 min. For varying particle sizes (μm), there were still negligible changes in the CaO (wt.%) remaining in the fly ash solid residue as reported from the XRF results provided in Figure 4.10, although a higher amount of CaO (wt. %) was still remaining for the 25 (μm) size.

This showed that a lower amount of calcium (Ca^{2+}) was leached from this particle size (μm), and this was confirmed by the ICP-OES data (see Figure 4.11). Again, owing to the difference in sensitivity between the two analytical techniques, the ICP-OES technique was then used to help give a more accurate indication of the effect of all the particle sizes (μm) on the leachability of calcium (Ca^{2+}).

The effect of the particle size (μm) on the leachability of calcium (Ca^{2+}) was also investigated by observing the concentration of calcium (Ca^{2+}) present in the leachate using results obtained from ICP-OES analysis. The particle size (μm) was varied between the bulk fly ash which, was the fly ash before sieving, 25 (μm),45 (μm), and 125 (μm), while a leaching time of 120 min, a S/L ratio of 0.5 g/mL, and a stirring speed of 100 pm were used, as shown in Figure 4.11:

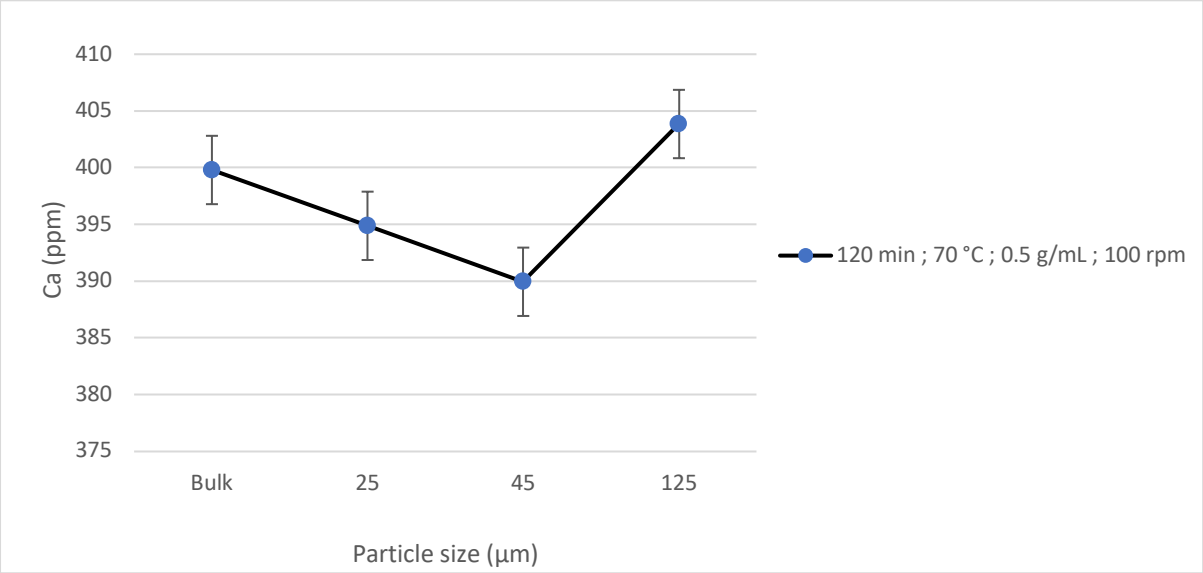

Figure 4.11: Effect of particle size (μm) on leaching of calcium (Ca^{2+}) from ICP-OES analysis results

The results obtained from ICP-OES analysis shown in Figure 4.11 indicate that there was a maximum calcium (Ca^{2+}) concentration leached from the fly ash using a particle size of 125 (μm). However, the calcium (Ca^{2+}) concentration obtained for the 125 (μm) particle size was not significantly different from the calcium (Ca^{2+}) concentration obtained for the bulk fly ash, which was the fly ash used before the sieving process. When considering the added energy consumption (MW) and potential added process costs ($/$CO_2$ stored) from the sieving process, the trade-off between the calcium (Ca^{2+}) extracted at 125 (μm) of 403.85 ppm, which was not significantly higher than the maximum calcium (Ca^{2+}) extracted of 399.8 ppm when using the bulk ash (i.e., fly ash without sieving) and the additional energy that could arise from sieving, the potential energy consumption (MW) due to sieving thus made it unjustifiable to conduct subsequent experiments (i.e., carbonation experiments) using particle sizes of 25 (μm), 45 (μm) and 125 (μm) which required sieving that would result in an added energy requirement.

Section 4.3: Direct and Indirect aqueous carbonation

This section provides results from direct and indirect aqueous carbonation and a discussion of the results in relation to previous studies.

4.3.1 Direct aqueous carbonation

This section provides a discussion of the results obtained using direct aqueous carbonation with the detailed experimental procedure given in Chapter 3, Section 3.3.2.2. The first section under this current section is based on the determination of the specific metal oxide phase that was predominately responsible for the storage of CO_2 in mineral carbonate form. The mineral carbonate form of this metal oxide phase, which is mostly responsible for the CO_2 uptake, was then used as the main measure of CO_2 storage in the fly ash material. The following sections then cover discussions around the results obtained from the measures used to determine the CO_2 uptake from the direct aqueous carbonation process.

4.3.1.1 Determination of the measure of CO_2 uptake from aqueous carbonation process

This section provides a demonstration of how the main measure of CO_2 uptake in fly ash was determined. Given the multiple oxide phases existing in fly ash that can contribute to the overall sequestration of CO_2 in the form of $CaCO_3$, $FeCO_3$, $MgCO_3$, $MnCO_3$, and K_2CO_3, it was, therefore, necessary to determine which of these phases was predominantly responsible for the storage of CO_2 in mineral carbonate form by considering the concentrations of species such as Fe^{2+}, Mg^{2+}, and also Ca^{2+} after leaching and after direct aqueous carbonation. Mn^{2+} and K^{2+} could not be considered as the elements were not detectable from ICP-OES analysis after leaching.

4.3.1.1.1 Effect of time (min) on leachability of Ca^{2+}, Fe^{2+}, Mg^{2+}

To demonstrate how the main measure of CO_2 uptake in the fly ash was determined for the direct aqueous carbonation process, the concentrations of Fe^{2+}, Mg^{2+}, and Ca^{2+} after leaching over 30 min, 60 min, 90 min, and 120 min were initially considered. This was done because the concentration of these species after leaching gave an indication of the amount that was available to react with CO_2 during the carbonation process. From there, the degree to which CO_2 reacted with a particular element could be determined. The experimental detail for the leaching was given in Chapter 3, Section 3.3.2.1.2. Figure 4.12 shows the concentration of Fe^{2+}, Mg^{2+}, and Ca^{2+} obtained from ICP-OES after leaching for 30 min, 60 min, 90 min, and 120 min at a temperature of 70 ^{0}C, using a S/L ratio of 0.5 g/mL and a stirring speed of 100 rpm:

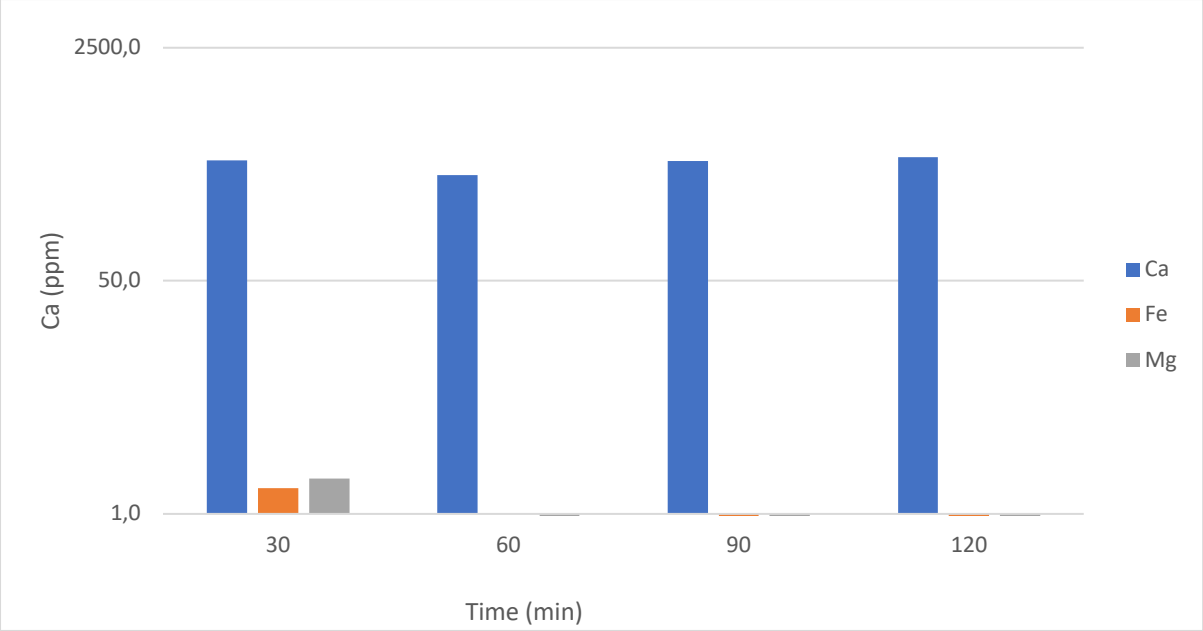

Figure 4.12: Effect of time (min) of leachability of various elements (70 ^{0}C, 0.5 g/mL, 100 rpm)

The results from Figure 4.12 show that there was a considerably higher amount of calcium (Ca^{2+}) leached over time (min) compared to the other elements considered. The calcium (Ca^{2+}) concentrations of 378.3 ppm, 293.4 ppm, 372.1 ppm, and 399.8 ppm over 30 min, 60 min, 90 min, and 120 min, respectively, were higher compared to those of iron (Fe^{2+}), which were 1.5 ppm, 0 ppm, 0.1 ppm and 0.1 and those of magnesium (Mg^{2+}), which were 1.8 ppm, 0.17 ppm, 0.1 ppm, and 0.1 ppm after 30 min, 60 min, 90 min and 120 min respectively. This was possibly due to the higher solubility of CaO in water compared to MgO and Fe_2O_3. The low amount of Mg^{2+} leached was also possibly due to the low amount of Mg^{2+} originally available in the fly hi ash (i.e., 0.90 wt. %). The leaching behaviour observed for Fe^{2+} was similar to that observed by Fatoba (2007), who also obtained a low concentration of Fe^{2+} after performing leaching studies for Secunda fly ash and attributed this to the fact that Fe^{2+} in alkaline fly ash leachates exists as oxy-hydroxides that coat the silicate grains of fly ash, thus explaining the reason for the low concentration of Fe^{2+} observed in the leachates of the fly ash.

The higher calcium (Ca^{2+}) concentrations obtained from the leaching study for time (min) in all cases compared to the other elements (i.e., Fe^{2+} and Mg^{2+}) further indicated that the CO_2 consumption due to $CaCO_3$ formation could be assumed to give a better indication of the amount of CO_2 stored in mineral carbonate form which would validate the hypothesis made that the % $CaCO_3$ would serve as the main measure for CO_2 consumption in the solid phase.

However, results from direct carbonation over 120 min were taken into consideration to corroborate this assumption by observing the concentration of Ca^{2+}, Fe^{2+}, and Mg^{2+} after the direct aqueous carbonation process in order to determine which of these elements showed the highest decrease in concentration and therefore was primarily responsible for the CO_2 uptake. This was done before the% $CaCO_3$ formed could be used as the main measure of CO_2 stored in the fly ash.

4.3.1.1.2 Effect of pressure (Mpa) on the concentration of Ca^{2+}, Fe^{2+}, Mg^{2+}

Given that fly ash contains other elements that can also be responsible for CO_2 capture in mineral carbonate form such as Fe^{2+} to form $FeCO_3$ and Mg^{2+} to form $MgCO_3$, it was important to determine the role of these species in the total amount of CO_2 stored in mineral carbonate form and to determine whether or not the assumption that the CO_2 evolved from the Chittick test was mainly due to the % $CaCO_3$ formed. To determine the role of Fe^{2+} and Mg^{2+} on the overall CO_2 stored in the fly ash, the concentration of these species after direct aqueous carbonation was considered. Figure 4.13 presents the concentrations of Ca^{2+}, $Fe^{2+,}$ and Mg^{2+} after 120 min of direct aqueous carbonation between 1 Mpa to 4 Mpa:

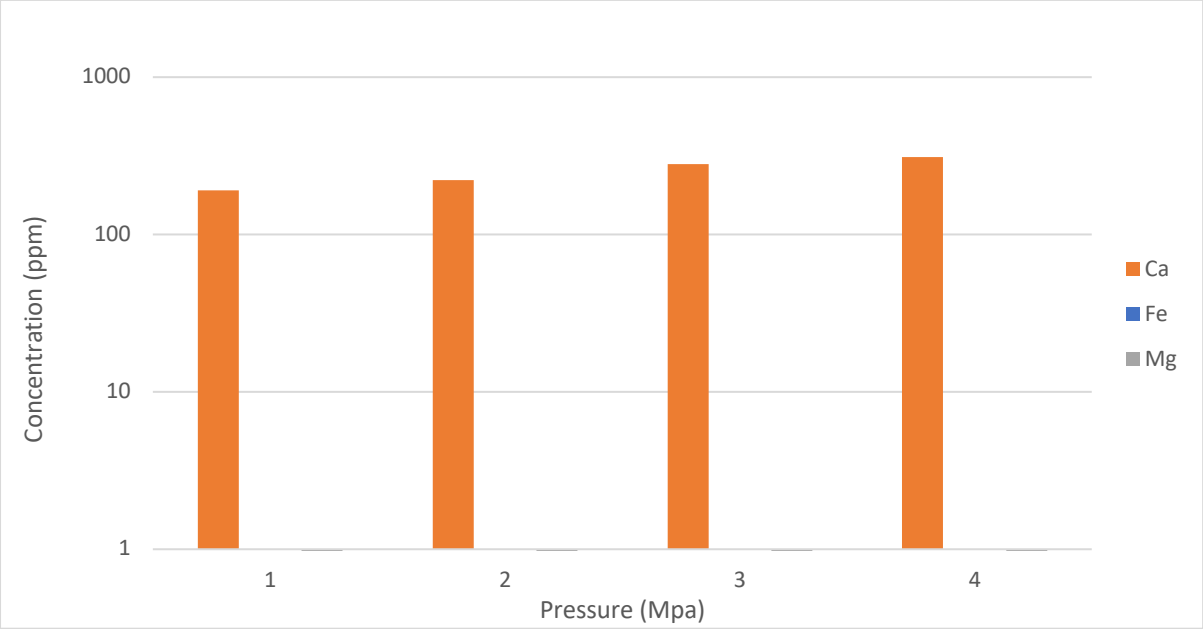

Figure 4.13: Concentration of various elements after direct aqueous carbonation (120 min, 70 ^{0}C, 0.5 g/mL, 100 rpm)

In Figure 4.13, the concentrations of Ca^{2+}, Fe^{2+}, and Mg^{2+} after direct aqueous carbonation decreased. The concentrations of Ca^{2+}, Fe^{2+}, and Mg^{2+} after 120 min of leaching (i.e., before carbonation) were 399.8, 0.1, and 0.1 respectively (see Figure 4.12). The concentrations of these species after direct aqueous carbonation decreased for all conditions of pressure (Mpa) considered, as shown in Figure 4.13. The concentration of calcium (Ca^{2+}) after leaching for 120 min was 399.8 ppm, while the concentration remaining after 120 min of direct carbonation at 1 Mpa, 2 Mpa, 3 Mpa, and 4 Mpa decreased to 190.1 ppm, 222.1 ppm, 280 ppm, and 310.1 ppm, respectively. Iron (Fe^{2+}) and magnesium (Mg^{2+}) exhibited a similar trend before and after direct carbonation.

The concentration of iron (Fe^{2+}) after leaching for 120 min was 0.1 ppm while the concentration after 120 min of direct carbonation at 1 Mpa, 2 Mpa, 3 Mpa, and 4 Mpa decreased to -0.017 ppm, -0.021 ppm, -0.0090 ppm, and -0.0055 ppm respectively. The negative concentrations after carbonation indicated that the concentration of iron (Fe^{2+}) after direct carbonation was below the detection limit of the ICP-OES instrument and could not be seen on the log scale. In the case of magnesium (Mg^{2+}), the concentration after 120 min of leaching was found to be 0.1 ppm, while the concentrations after direct carbonation for 120 min at 1 Mpa, 2 Mpa, 3 Mpa, and 4 Mpa were found to be 0.001ppm, 0.014 ppm, 0.033 ppm, and 0.022 ppm, respectively.

This shows that the percentage $CaCO_3$ was also influenced by other phases present in the fly ash that were involved in the consumption of CO_2. However, given that the decrease in calcium (Ca^{2+}) concentration after carbonation was considerably higher than other competing species due to the higher amount of calcium (Ca^{2+}) available after leaching, the assumption that the % $CaCO_3$ was the main mineral carbonate form responsible for the amount of CO_2 consumed in mineral form was accurate, and the % $CaCO_3$ therefore gave a comprehensive indication of the amount of CO_2 stored in mineral form from direct aqueous carbonation.

4.3.2. Effect of pressure (Mpa) over time (min) on % $CaCO_3$ formed

In this work, various measures were used to quantify the efficiency of the carbonation process. These carbonation performance measures were the % $CaCO_3$ formed which measured the amount of CO_2 stored as $CaCO_3$ in the fly ash, carbonation efficiency (CE %), which measured the overall CO_2 consumption based on the measured pressure drop, and the maximum CO_2 storage capacity (kg/kg fly ash), which measured the CO_2 storage potential of the fly ash used based on the initial concentration of CaO (wt. %) available in the fly ash. The % $CaCO_3$, which was determined from the Chittick test was the first carbonation performance measure to be considered. The experimental details of the Chittick test were presented in Chapter 3, Section 3.2.4. The % $CaCO_3$ was determined from direct aqueous carbonation over reaction times of 30 min, 60 min, and 120 min between 1 Mpa and 4 Mpa at 70 ^{0}C, using a S/L ratio of 0.5 g/mL, and a stirring speed of 100 rpm, as shown in Figure 4.14:

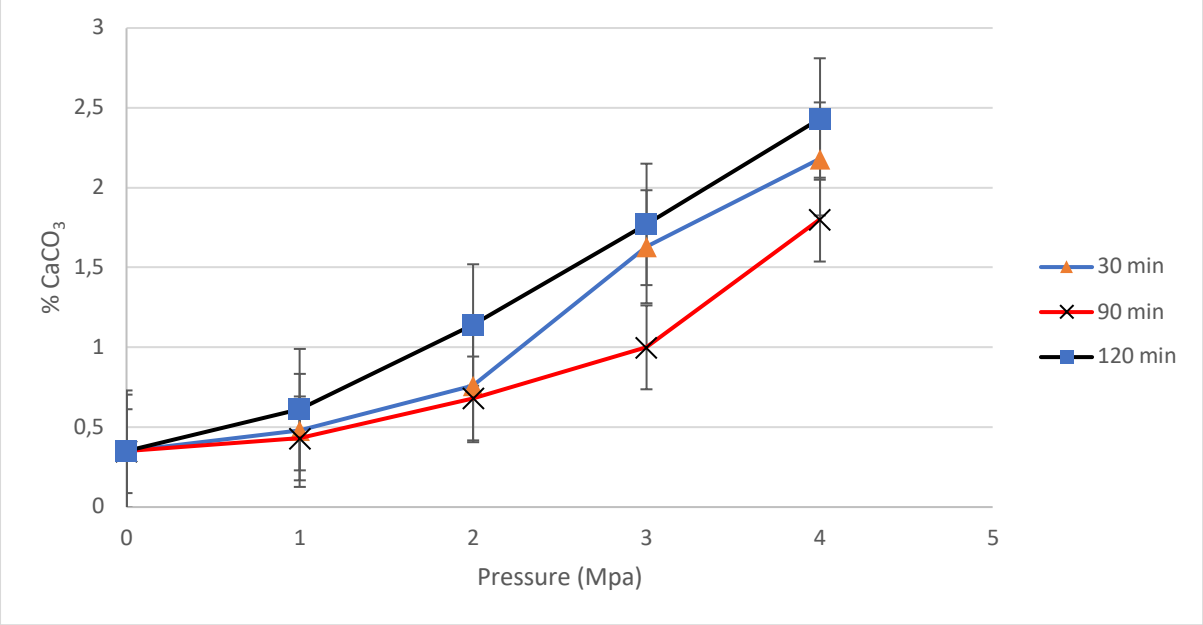

Figure 4.14: Effect of pressure (Mpa) on % $CaCO_3$ over time (min) (70 ^{0}C, 0.5 g/mL, 100 rpm)

From Figure 4.14, the percentage $CaCO_3$ formed increased gradually from its initial value of 0.35 % for all conditions of pressure (Mpa) considered. The initial $CaCO_3$ value of 0.35 % was the initial $CaCO_3$ present in the raw fly ash before the carbonation process. The formation of $CaCO_3$ in the raw fly ash can be attributed to the uptake of CO_2 from the atmosphere during handling and bulk ash storage, sample preparation, and storage of the fly ash sample.

According to Figure 4.14, there is an observable trend that an increase in the initial CO_2 pressure from 1 Mpa to 4 Mpa resulted in an increase in the percentage of $CaCO_3$ formed, and this was expected because according to Henry's law, the higher the initial CO_2 pressure, the higher the concentration of dissolved CO_2 in the liquid phase, which meant that at a higher initial CO_2 pressure, there was a higher amount of CO_2 molecules available to react with calcium (Ca^{2+}) which resulted in a faster rate of carbonation, CO_2 consumption, and overall a higher amount of CO_2 fixed as $CaCO_3$. Despite the increase in the % $CaCO_3$ formed by increasing pressure, increasing the initial CO_2 pressure from 1 Mpa, 2 Mpa, 3 Mpa, and finally 4 Mpa did not have a significant effect on the % $CaCO_3$ formed. This was possibly due to the increase in the solubility of calcium (Ca^{2+}) as the pressure (Mpa) was increased. The increase in the solubility of calcium (Ca^{2+}) caused a decrease in the rate of precipitation of $CaCO_3$. The decrease in the rate of precipitation of $CaCO_3$ with increasing pressure due to the increase in the solubility of calcium (Ca^{2+}) was consistent with findings from the study conducted by Katsuyama et al. (2005), wherein high CO_2 pressure conditions resulted in a decrease in the rate of $CaCO_3$ precipitation. Essentially, increasing the pressure (Mpa) over the same reaction time (min) slowed the precipitation of $CaCO_3$, hence the minor effect of higher pressure on the percentage of $CaCO_3$ formed, as seen in Figure 4.14.

The effect of pressure (Mpa) on the percentage $CaCO_3$ formed for direct aqueous carbonation can also be linked to calcium (Ca^{2+}) extraction. In the leaching study, when the effect of time (min) on the extraction of calcium (Ca^{2+}) was considered (see Figure 4.9), most of the calcium (Ca^{2+}) was extracted in 30 min, and due to the insignificant amount of calcium (Ca^{2+}) leached after 30 min, increasing the pressure did not have an effect on the % $CaCO_3$ formed after 30 min of the 90 min and 120 min reactions. This means that the effect of increasing the pressure (Mpa) on the percentage $CaCO_3$ formed over the 90 min and 120 min reactions was limited by the insignificant amount of additional calcium (Ca^{2+}) extracted beyond 30 min of these reactions. This can also explain why, overall, the effect of pressure (Mpa) had a minor impact on the percentage of $CaCO_3$ formed for increasing initial CO_2 pressure (Mpa) for the 90 min and 120 min reactions considered. It is worth mentioning that because it was difficult to track the calcium (Ca^{2+}) extraction during the carbonation reaction when using the autoclave reaction system, the rate of carbonation and CO_2 consumption due to the available calcium (Ca^{2+}) during the carbonation process was postulated based on the calcium (Ca^{2+}) extraction experiments/baseline experiments.

The effect of pressure on the % $CaCO_3$ formed for direct aqueous carbonation was similar to findings from the study conducted by Ukwattage et al. (2013) and Muriithi (2009) who in their studies found that increasing the initial CO_2 pressure did not affect the amount of CO_2 stored as $CaCO_3$ and that although the increase in the initial CO_2 pressure (Mpa) caused a slight increase in the % $CaCO_3$ formed, the effect of increasing the initial CO_2 pressure (Mpa) had a minor effect on the % $CaCO_3$ formed.

When considering the effect of time (min) on the % $CaCO_3$ formed from the direct aqueous carbonation process, the results indicate that there was no significant difference in the % $CaCO_3$ formed after 30 min, 90 min and 120 min at 1 Mpa to 4 Mpa. As mentioned previously, from preliminary experiments (see Figure 4.9), the effect of time (min) on the leachability of calcium (Ca^{2+}) was considered and the results showed that most of the calcium (Ca^{2+}) was extracted in the first 30 min and that no significant amount of calcium (Ca^{2+}) leached beyond 30 min. This could explain the similar amount of % $CaCO_3$ formed after 30 min, 90 min, and 120 min at 1 Mpa to 4 Mpa because the calcium (Ca^{2+}) extraction was high in the first 30 min of the carbonation reaction but did not change significantly after 30 min.

The carbonation reaction had almost finished within 30 min of the 90 min and 120 min carbonation reactions, because there was very little calcium (Ca^{2+}) leached from the fly ash after that point. As a result, the rate of CO_2 consumption because of the reaction with calcium (Ca^{2+}) to form $CaCO_3$ did not change significantly after 30 min because there was very little calcium (Ca2+) leached from the fly ash. Therefore, there was no significant amount of $CaCO_3$ formed after 30 min of the 90 min and 120 min reactions and this thus explains the comparable amount of % $CaCO_3$ observed over the reaction times of 30 min, 90 min, and 120 min at 1 Mpa to 4 Mpa. For the case of direct aqueous carbonation, this means that the calcium (Ca^{2+}) extraction step can be considered the rate-limiting step for the formation % $CaCO_3$ because no significant amount of $CaCO_3$ formed after 30 min of the carbonation reaction, and this can be attributed to the minor amount of calcium (Ca^{2+}) extracted after 30 min of carbonation.

Figure C1 (see Appendix C) shows the theoretical saturation concentration of calcium (Ca^{2+}) for a Ca-H_2O-CO_2 system from thermodynamic considerations under various temperature (^0C) and pressure (Mpa) conditions. From the graph, the theoretical saturation concentration of calcium (Ca^{2+}) at 343.15 K (i.e., the temperature (^0C) used for direct aqueous carbonation reactions) and 3 Mpa is approximately 408 ppm. Given that the actual saturation concentration of calcium (Ca^{2+}) after the 30 min, 90 min, and 120 min of the carbonation reaction at 3 Mpa was 198.1 ppm, 200.1 ppm, and 280.1 ppm respectively (see Figure 4.15), which were all less than the theoretical saturation concentration of calcium (Ca^{2+}) at 3 Mpa, this shows that calcium (Ca^{2+}) was not easily extracted from the fly ash over time (min) and that the calcium (Ca^{2+}) extraction was not as effective over the course of the carbonation reaction. This further indicates that the calcium (Ca^{2+}) extraction was the limiting factor in the carbonation reaction and the reason for this was that it did not effectively dissolve in solution, which was possibly due to the CaO being trapped in the major phases of the fly ash.

The maximum amount of % $CaCO_3$ formed of 2.43 % for direct aqueous carbonation which was obtained after 120 min at the highest initial CO_2 pressure of 4 Mpa was slightly higher compared to the 2.18 % and 1.8 % obtained after 30 min and 90 min respectively under the same conditions. However, the highest $CaCO_3$ percentage of 2.43 % was still relatively low. The release of species such as Si (refer to Table B2 of Appendix B) and the interaction of calcium (Ca^{2+}) with other species possibly resulted in less calcium (Ca^{2+}) available for the reaction with CO_2, which resulted in a reduced amount of $CaCO_3$ formed. The relatively small maximum % $CaCO_3$ formed of 2.43 % was also possibly due to the higher S/L ratio of 0.5 g/mL that was used for direct aqueous carbonation experiments. Previous studies, such as the one conducted by Dri et al. (2014), showed that the production of $CaCO_3$ was higher at lower S/L ratios because of improved calcium (Ca^{2+}) extraction efficiency due to an increase in the solubility of the calcium (Ca^{2+}). Similar results were found in this study after the effect of lowering the S/L ratio was considered (see Figure 4.23). The results indicate that a lower S/L ratio of 0.2 g/mL resulted in a significant increase in the percentage of $CaCO_3$ formed over the reaction times (min) considered.

Overall, the results obtained for direct aqueous carbonation were consistent with findings from the studies conducted by Ukwattage et al. (2013) and Muriithi (2009), who found that although the increase in the initial CO_2 pressure (Mpa) caused a slight increase in the % $CaCO_3$ formed, the effect of the initial CO_2 pressure (Mpa) had a minor effect on the % $CaCO_3$ formed. In this work, when considering direct aqueous carbonation experiments, this was mainly due to the calcium (Ca^{2+}) concentration not being high enough over the course of the reaction.

4.3.2.1 Effect of pressure (Mpa) over time (min) on calcium (Ca^{2+}) concentration (ppm) in leachates

When attempting to ascertain whether calcium (Ca^{2+}) extraction was in fact the rate-limiting phase, the amount of calcium (Ca^{2+}) that was present in the leachate following direct aqueous carbonation was crucial to take into account. Figure 4.15 shows the effect of the initial CO_2 pressure (Mpa) on the calcium concentration (Ca^{2+}) after direct aqueous carbonation. The pressure was varied from 1 Mpa to 4 Mpa at 70 ^{0}C, using a S/L ratio of 0.5 g/mL and a stirring speed of 100 rpm:

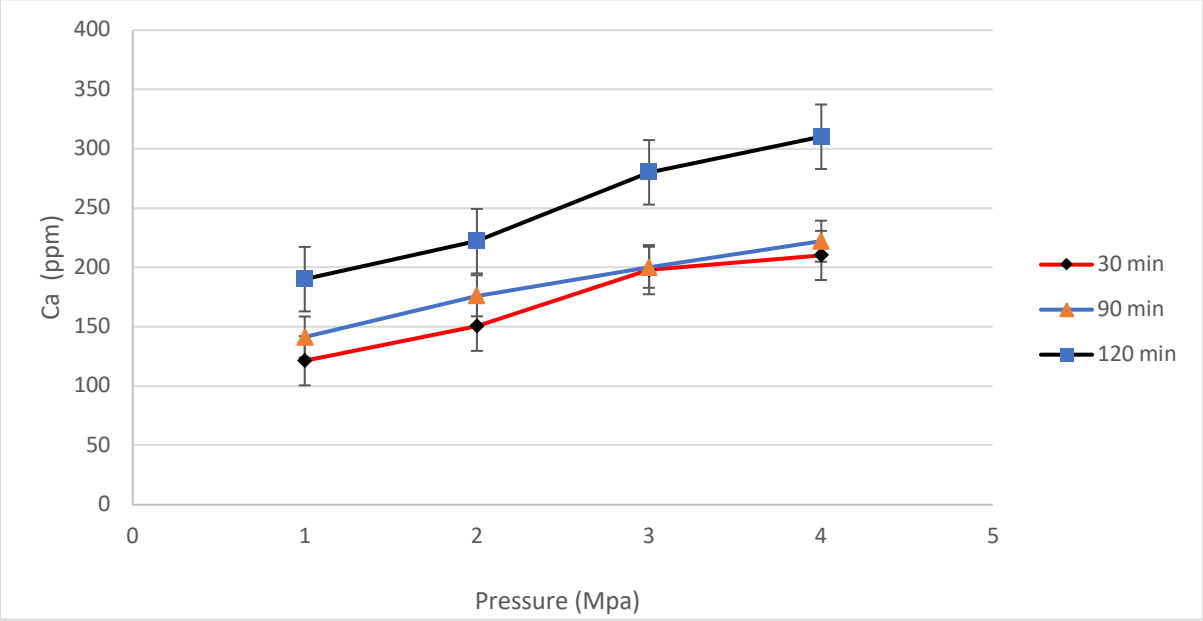

Figure 4.15: Effect of pressure (Mpa) on calcium (Ca^{2+}) concentration (ppm) in leachate over time (min) from ICP-OES analysis results (70 ^{0}C, 0.5 g/mL, 100 rpm)

Figure 4.15 shows the concentration of calcium (Ca^{2+}) remaining in the leachate after direct aqueous carbonation. From the ICP-OES analysis results, the calcium (Ca^{2+}) concentration after 120 min of direct aqueous carbonation at a pressure of 1 Mpa, 2 Mpa, 3 Mpa, and 4 Mpa was 190.1 ppm, 222.1 ppm, 280.1 ppm, and 310.1 ppm, respectively (refer to Table B6 of Appendix B). The calcium (Ca^{2+}) concentration after 120 min of direct aqueous carbonation was lower for all cases compared to the concentration of 399.1 ppm obtained from direct leaching experiments without carbonation after 120 min (see Figure 4.9). The concentration of calcium (Ca^{2+}) after 90 min of direct aqueous carbonation at 1 Mpa, 2 Mpa, 3 Mpa, and 4 Mpa was 141.3 ppm, 176.1 ppm, 200.1 ppm, and 222.1 ppm, respectively. The calcium (Ca^{2+}) concentration remaining after 90 min of direct aqueous carbonation was also lower in all cases compared to the concentration of 372.1 ppm obtained from direct leaching experiments after

90 min. Similarly, after 30 min of direct aqueous carbonation reactions, the calcium (Ca^{2+}) concentration reported at 1 Mpa, 2 Mpa, 3 Mpa, and 4 Mpa was 121.3 ppm, 150.4 ppm, 198.1 ppm, and 210.1 ppm, respectively, and these concentrations were lower in all cases compared to the concentration of 378.3 ppm obtained from direct leaching experiments after 30 min. The decrease in the calcium (Ca^{2+}) concentration after direct aqueous carbonation from the concentration obtained from leaching experiments can be attributed to the reaction of calcium (Ca^{2+}) with CO_2 during the carbonation reaction. When CO_2 pressure was introduced into the system, CO_2 molecules dissolved into the liquid phase, resulting in the availability of carbonate ions (CO_3^{2-}) that reacted with calcium (Ca^{2+}) for $CaCO_3$ formation. Maleka (2015) also found that sparging CO_2 during the carbonation reaction resulted in a decrease in calcium (Ca^{2+}) concentration due to the formation of $CaCO_3$.

Compared to the calcium (Ca2+) concentrations obtained after 30 min, 90 min, and 120 min of calcium (Ca2+) extraction, the concentration of calcium (Ca2+) after 30 min, 90 min, and 120 min of direct aqueous carbonation was lower for all conditions of pressure considered; however, the concentration of calcium (Ca2+) showed an increase as the initial CO2 pressure (Mpa) was increased. The higher calcium (Ca^{2+}) concentration obtained after direct aqueous carbonation for higher pressure (Mpa) can be attributed to the increase in the solubility of calcium (Ca^{2+}) at higher CO_2 pressure conditions.

Given that a higher initial CO_2 pressure creates a more acidic environment, the solubility of calcium (Ca^{2+}) was thus favoured more at a higher pressure during the carbonation reaction. The increase in solubility also caused a decrease in the rate of $CaCO_3$ precipitation, as observed previously, as $CaCO_3$ precipitation is not favoured at lower pHs because calcium (Ca^{2+}) can be dissolved in the solution while the $CaCO_3$ is formed over time (min). Therefore, it was expected to obtain a higher calcium (Ca^{2+}) concentration after carbonation with a higher initial CO_2 pressure. The results also indicate that there was a higher concentration of calcium (Ca^{2+}) found in the leachate after a longer reaction time of 120 min for all conditions of pressure considered and this was expected because the longer the reaction proceeded, the greater the increase in the solubility of calcium (Ca^{2+}) for increasing pressure (Mpa), thus the higher the overall amount of calcium (Ca^{2+}) found in the leachate after 120 min for increasing CO_2 pressure as seen in Figure 4.15. The ICP-OES results obtained in Figure 4.15 for calcium (Ca^{2+}) extraction after carbonation are consistent with findings from the study conducted by Iizuka et al. (2004) who in their study found that an increase in the initial CO_2 pressure caused an increase in the calcium extraction rate due to the higher solubility of calcium (Ca^{2+}) at a higher pressure.

4.3.3 Effect of pressure (Mpa) over time (min) on CE (%)

The carbonation efficiency (CE %) was used to determine the degree of CO_2 consumption due to $CaCO_3$ formation and was dependent on the pressure drop (refer to Table B15 of Appendix B) which was determined by taking the difference between the initial CO_2 pressure (Mpa) and the final CO_2 pressure (Mpa) observed. As mentioned previously, the CE (%) was also dependent on the initial CaO (wt. %) content of the fly ash material (see Appendix A for CE % calculation). The CE (%) was determined for direct aqueous carbonation over reaction times of 30 min, 90 min, and 120 min from 1 Mpa to 4 Mpa, using a S/L of 0.5 g/mL and a stirring speed of 100 rpm as shown in Figure 4.16:

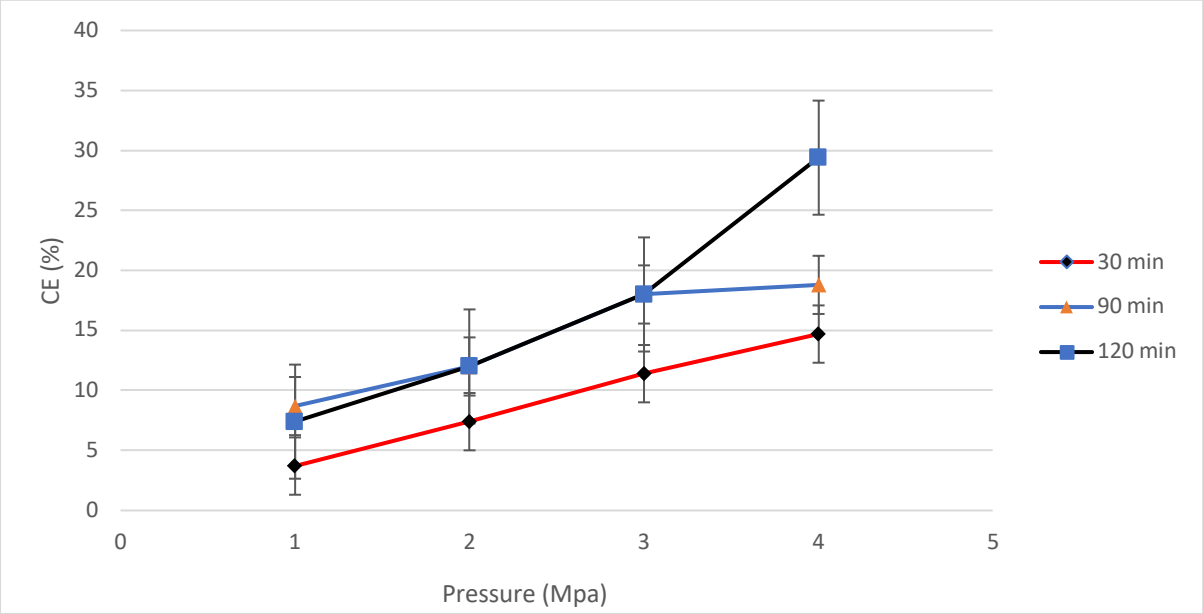

Figure 4.16: Effect of pressure (Mpa) over time (min) on CE (%) (70 ^{0}C, 0.5 g/mL, 100 rpm)

Figure 4.16 shows that the carbonation efficiency (CE %) increases with increasing initial CO_2 pressure (Mpa) for all cases. Given that the CE (%) in this study was directly proportional to the pressure drop due to $CaCO_3$ formation ($i.e. P_{carbonation\_pressure\ drop}$), a higher CE (%) at a higher initial CO_2 pressure (Mpa) was expected because according to Henry's law, a higher initial CO_2 pressure (Mpa) increases the amount of CO_2 dissolved in the liquid phase. This means that there were more CO_2 molecules available to react with the calcium (Ca^{2+}) which resulted in a higher rate of carbonation and CO_2 consumption, therefore, causing a higher overall pressure drop due to the reaction with calcium ions (Ca^{2+}), hence the higher CE (%) obtained for increasing pressure (Mpa).

The highest CE (%) of 29.4 % was obtained at 4 Mpa over 120 min. The findings presented in Figure 4.16 were consistent with findings from the study conducted by Muriithi (2009), who also achieved the highest CE (%) of 75.5 % at a higher initial CO_2 pressure of 4 Mpa. Montes-Hernandez et al. (2009) also achieved the highest CE (%) of 82 % at the highest initial CO_2 pressure of 4 Mpa. The highest CE (%) achieved from these studies was higher compared to the 29.4 % achieved for direct aqueous carbonation in this work, and this can be attributed to the use of brine as a reaction medium by Muriithi (2009) which provided an additional calcium (Ca^{2+}) source, and the longer reaction time of 1080 min used by Montes-Hernandez et al. (2009). Although the CE (%) showed an increase as the CO_2 pressure (Mpa) was increased for the same reaction time (min), the CE (%) achieved after 30 min, 90 min, and also 120 min at 1 Mpa to 4 Mpa was not significantly different except for the significantly higher CE (%) achieved at 4 Mpa for the reaction time of 120 min.

The higher CO_2 pressure of 4 Mpa was possibly a contributing factor to the highest CE (%) of 29.4 % achieved after 120 min at 4 Mpa. Even though calcium (Ca^{2+}) extraction is the rate-limiting step for the direct aqueous carbonation process, an elevated pressure (Mpa) could still contribute to the overall CO_2 consumption, as shown by the results obtained. Essentially, at the highest CO_2 pressure applied of 4 Mpa, there was a higher degree of CO_2 consumption due to the reaction with calcium ions (Ca^{2+}), which resulted in a higher pressure drop, hence the significant effect of the highest CO_2 pressure on the CE (%) over the longest reaction time of 120 min observed.

The similar CE (%) achieved after 30 min, 90 min, and 120 min at 1 Mpa to 4 Mpa for direct aqueous carbonation can be attributed to the leaching behaviour of calcium (Ca^{2+}) over time (min) because the CE (%) depends on the pressure drop due to the reaction of CO_2 with calcium (Ca^{2+}) and given that most calcium (Ca^{2+}), was extracted during the first 30 min for direct aqueous carbonation, the pressure drop was observed to drop considerably quickly over 30 min, as expected. Therefore, there was a higher overall pressure drop over the 30 minutes of the carbonation reaction.

However, after 30 min of the 90 min and 120-minute reactions, the pressure started to decrease quite slowly and eventually reached a plateau. This was due to the negligible amount of calcium (Ca^{2+}) leached after 30 min, and given that less calcium (Ca^{2+}) was available to react with CO_2 after 30 min, the rate of carbonation and CO_2 consumption were similar after 30 min of the 90 min and 120 min reactions. In this case, given that no significant amount of CO_2 was being consumed due to the reaction with calcium (Ca^{2+}) after 30 min, this resulted in the overall pressure drop due to the reaction of CO_2 with calcium (Ca^{2+}) being similar after 30 min, 90 min, and 120 min at 1 Mpa, 2 Mpa, 3 Mpa, and 4 Mpa, hence the similar CE (%) observed after 30 min, 90 min, and 120 min at 1 Mpa to 4 Mpa of the direct aqueous carbonation reaction.

Ukwattage et al. (2013) noted a considerably similar trend in their study, wherein the pressure drop increased rapidly in the first 120 min of the reaction due to the faster rate of carbonation but reached a plateau after 120 min until after 60 min of carbonation, which means that the fly ash used in their work was quite reactive in the initial stages as well. Despite the similarities in the CE (%) obtained after 30 min, 90 min, and 120 min at 1 Mpa to 4 Mpa, Figure 4.16 shows that there is a significantly higher CE (%) of 29.4 % after 120 min at 4 Mpa. The overall pressure drop was slightly higher over the 120 min reaction, possibly due to the slightly higher calcium (Ca^{2+}) extracted of approximately 400 ppm after 120 min (see Figure 4.9), which gave an indication that although most calcium (Ca^{2+}) had been leached after 30 min, there was still a small amount of calcium (Ca^{2+}) extracted after 30 min that was involved in the reaction with CO_2 thus causing a slightly higher overall pressure drop and hence the slightly higher CE (%) reported after 120 min.

Overall, compared to the results obtained for the % $CaCO_3$ formed (see Figure 4.14), the CE (%) results presented in Figure 4.16 show a similar trend to the % $CaCO_3$ for all the initial CO_2 pressures considered (i.e.,1 Mpa to 4 Mpa) over all the reaction times (min) considered. This shows an expected correlation between CE (%) and % $CaCO_3$ formed because the pressure drop due to $CaCO_3$ formation ($i.e. P_{carbonation\_pressure\ drop}$), determines the amount of CO_2 fixed as $CaCO_3$ as well as the CE (%) achieved. This explains the similar % $CaCO_3$ formed and the similar CE (%) achieved over 30 min, 90 min, and 120 min at 1 Mpa to 4 Mpa for direct aqueous carbonation, as the pressure drop due to calcium (Ca^{2+}) reacting with CO_2 was not significant beyond 30 min. Although there is a correlation between the percentage of $CaCO_3$ formed and the CE (%), a higher carbonation efficiency (CE %) can be achieved at a higher pressure due to the higher rate of carbonation, however, a higher pressure can decrease the rate of $CaCO_3$ formation due to the increase in the solubility of calcium (Ca^{2+}). This can also explain the significantly higher CE (%) achieved after 120 min at 4 Mpa, whereas the % $CaCO_3$

formed after 120 min at 4 Mpa was similar to the % $CaCO_3$ formed after 90 min and 30 min at 4 Mpa.

4.3.4 Effect of reaction temperature (^{0}C) on % $CaCO_3$ formed

Although the temperature of 70 ^{0}C was found to be the optimum temperature (^{0}C) from preliminary experiments due to the higher concentration of calcium (Ca^{2+}) leached, the effect of lowering the reaction temperature (^{0}C) on the overall % $CaCO_3$ formed determined from Chittick tests was still investigated for direct aqueous carbonation to validate findings from preliminary experiments using a reaction time of 120 min, an initial CO_2 pressure of 4 Mpa, a S/L ratio of 0.5 g/mL, and a stirring rate of 100 rpm as shown in Figure 4.17:

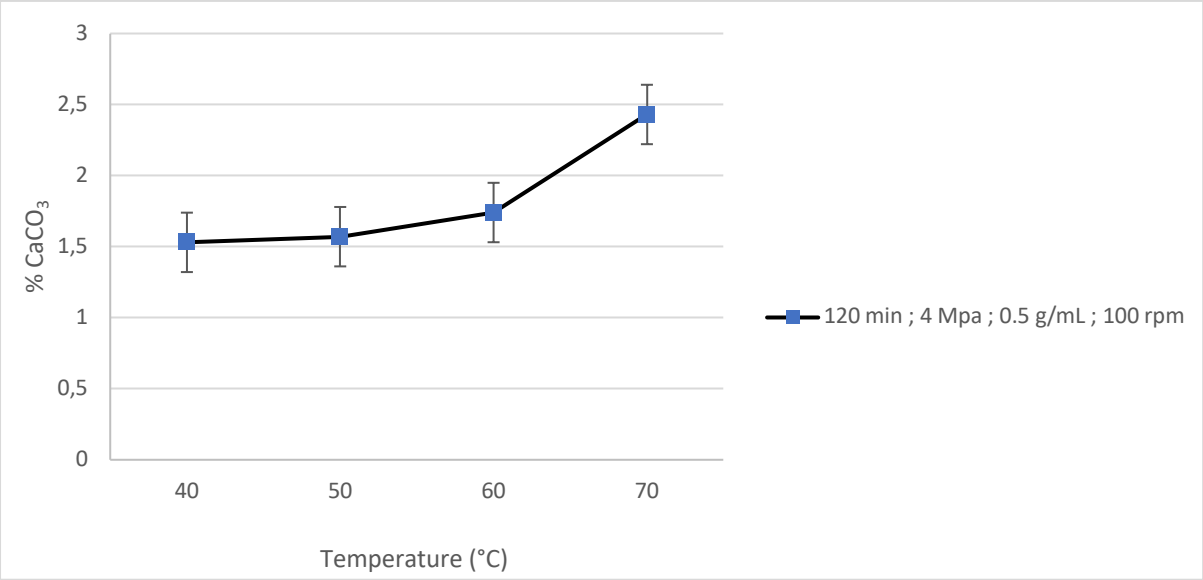

Figure 4.17: Effect of temperature (^{0}C) on % $CaCO_3$ formed from Chittick tests

From Figure 4.17, the highest percentage of $CaCO_3$ formation was achieved at 70 ^{0}C which validated the assumption made from preliminary experiments. The higher percentage of $CaCO_3$ achieved at 70 ^{0}C was because, at 70 ^{0}C, the molecules had enough kinetic energy to participate effectively in the reaction, and the extraction of calcium (Ca^{2+}) is known to proceed faster with increased temperature (^{0}C), as mentioned by Ukwattage et al. (2015). This, therefore, led to a higher amount of calcium (Ca^{2+}) ions available to react with CO_2, and thus a faster rate of carbonation and CO_2 consumption was achieved, which overall resulted in a higher percentage of $CaCO_3$ formed. In addition, a temperature of 70 ^{0}C is not exceedingly high to hinder the solubility of CO_2 in the liquid phase; therefore, there could still be an effective reaction between calcium (Ca^{2+}) and CO_2 for effective carbonation.

Ukwattage et al. (2015), in their study, also used a similar temperature of 60 ^{0}C to achieve the highest CO_2 sequestration capacity. However, results obtained from their study indicated that the sequestration capacity started decreasing for temperatures beyond 60 ^{0}C. The decrease in the sequestration capacity for temperatures above the optimum temperature (i.e., > 60 ^{0}C) was attributed to the decrease in the solubility of CO_2 in the liquid phase at slightly elevated temperatures (^{0}C). Therefore, based on the temperature (^{0}C) effects, the study found the leaching of calcium (Ca^{2+}) to be rate-determining between 20 ^{0}C and 60 ^{0}C, and that for temperatures above 60 ^{0}C, a reaction involving CO_2 then becomes rate-limiting.

In the study conducted by Patel et al. (2017), it was also found that the CO_2 storage (%) decreased above 50 ^{0}C due to CO_2 dissolution in water being hindered by an increase in temperature (^{0}C). The results obtained by Ukwattage et al. (2015), Patel et al. (2017), as well as other previous work, seem to indicate that the ideal temperature (^{0}C) for the carbonation reaction is in the range of 20 ^{0}C to 60 ^{0}C and that a temperature (^{0}C) that is significantly above this range deters the carbonation performance. Given that the temperature of 70 ^{0}C was not significantly above this range (i.e., 20 ^{0}C to approximately 60 ^{0}C), a higher percentage of $CaCO_3$ when investigating the effect of temperature (^{0}C) could still be achieved in this study at 70 ^{0}C as shown in Figure 4.17.

However, it is important to note that Muriithi (2009) used a high temperature of 90 ^{0}C and still achieved a high CE (%) using a brine solution. Ji et al. (2017) found that increasing the temperature (^{0}C) while also increasing the initial CO_2 pressure (Mpa) was effective, as a higher CE (%) was achieved in their study under these conditions. This could explain why Muriithi (2009) also obtained the highest CE (%) at a higher temperature (^{0}C), because the highest CE (%) obtained by Muriithi (2009) was found at the highest initial CO_2 pressure (Mpa). This suggests that the effect of temperature (^{0}C) on the carbonation performance should be investigated further to accurately determine the most effective temperature (^{0}C) for the carbonation reaction, as the use of a higher temperature (^{0}C) and pressure (Mpa) to achieve a higher efficiency could offset the CO_2 stored due to the higher energy input (MW) which would potentially result in CO_2 being emitted.

4.3.4.1 Effect of temperature (^{0}C) on CE (%)

The effect of temperature (^{0}C) on the CE (%) was also investigated for a reaction time of 120 min using an initial CO_2 pressure of 4 Mpa, a S/L ratio of 0.5 g/mL, and a stirring speed of 100 rpm:

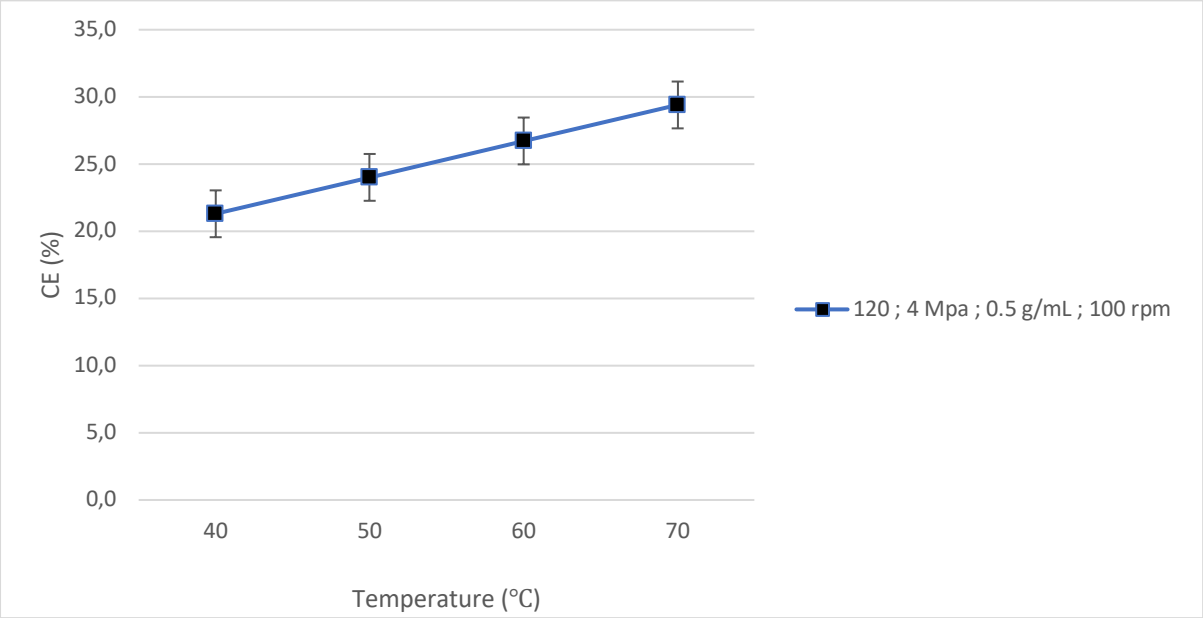

Figure 4.18: Effect of temperature (^{0}C)on the CE (%)

The results from Figure 4.18 indicate that the highest CE (%) was achieved at 70 ^{0}C, which was a suitable temperature (^{0}C) for achieving higher extraction of calcium (Ca^{2+}) and yet still allowed for the effective dissolution of CO_2 in the liquid phase, which resulted in a faster rate of carbonation and a higher pressure drop due to $CaCO_3$ formation and hence a higher CE (%) at this temperature (^{0}C). Again, this result was consistent with findings from studies such as the one conducted by Ukwattage et al. (2015), who achieved the highest sequestration capacity at a temperature of 60 ^{0}C which was close to the optimum temperature of 70 ^{0}C reported for this work.

4.3.5 Characterisation of carbonated solid residues through XRD for direct aqueous carbonation

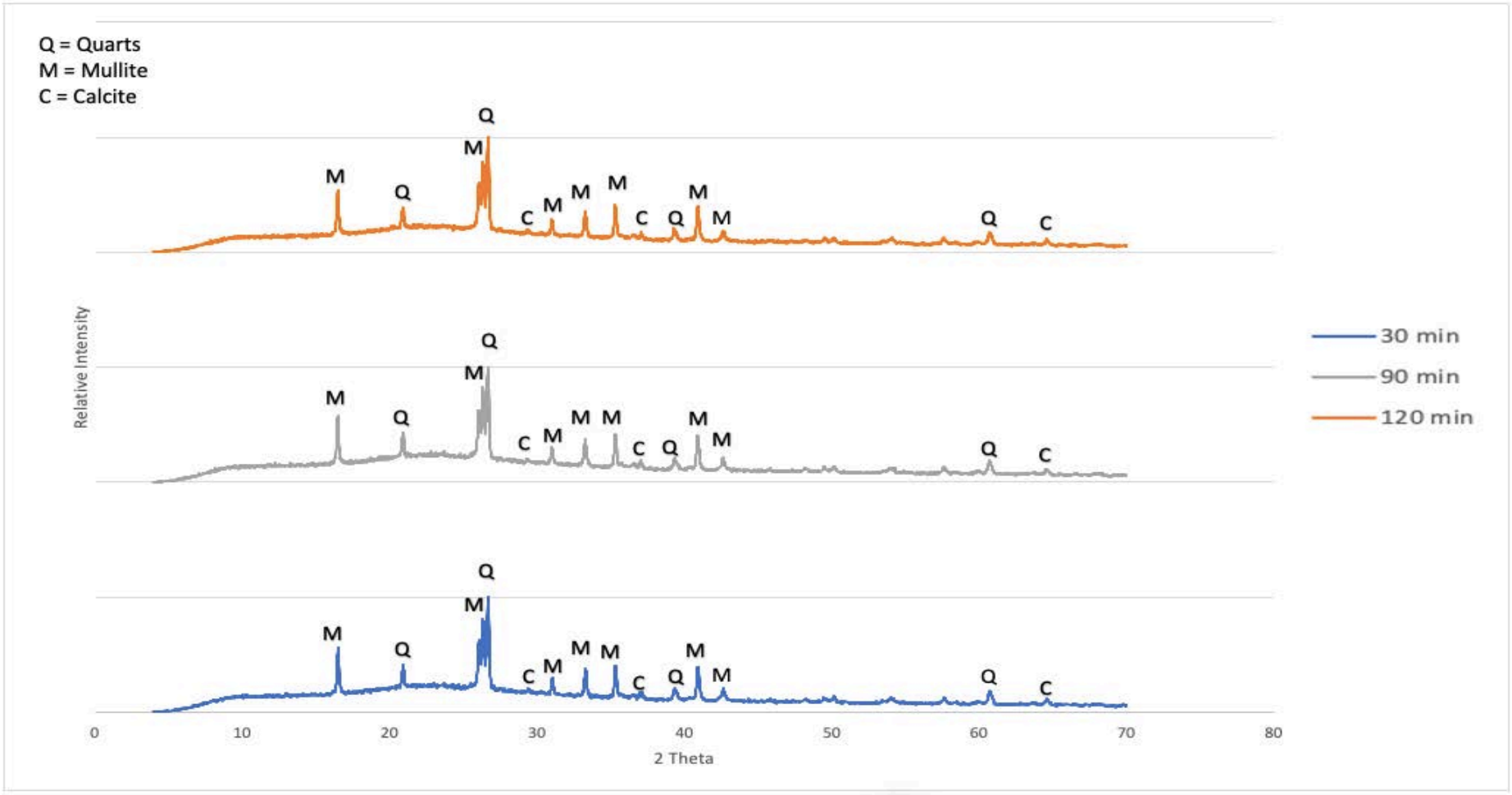

Figure 4.19: XRD pattern obtained from direct aqueous carbonation process (4 Mpa, 0.5 g/mL, 100 rpm)

4.3.5.1 Results from XRD analysis

This section provides XRD analysis results from the direct aqueous carbonation process, with the relevant mineral phases identified using the peaks obtained from the XRD pattern. The XRD was conducted on samples with applied conditions of 30 min, 90 min, and 120 min, a CO_2 pressure of 4 Mpa, a S/L ratio of 0.5 g/mL, and a stirring speed of 100 rpm, as shown in Figure 4.19. The XRD spectrum presented in Figure 4.19 showing the mineral phases present in the solid residue after direct aqueous carbonation, depicts strong intensity peaks identified between 15 to 30 (2 theta) after 30 min, 90 min, and 120 min of direct aqueous carbonation at 4 Mpa. These peaks were for quartz and mullite, which was expected as these constitute the major crystalline phases of fly ash. Calcite was also identified, and its low peaks were found before 30, 40, and 65 (2 theta). The peaks after 40 (2 theta) were characterised by amorphous phases. The presence of a small amount of calcite was due to the interaction of calcium (Ca^{2+}) with CO_2 during the carbonation reaction which further shows that there was an amount of CO_2 that was sequestrated during the direct aqueous carbonation process as $CaCO_3$.

4.3.5.2 Results from XRF analysis

XRF analysis of carbonated solid residues was conducted to determine the concentration of species after direct aqueous carbonation after 120 min at 4 Mpa as shown in Table 4.2:

Table 4.2: Analysis of elemental compositions from XRF analysis for direct aqueous carbonation

Element	Composition (wt. %)
SiO_2	54.02
Al_2O_3	34.97
CaO	3.79
Fe_2O_3	3.08
TiO_2	1.65
MgO	0.90
K_2O	0.64
P_2O_5	0.43
Na_2O	0.34
Cr_2O_3	0.041
MnO	0.03
Total	100

Table 4.2 shows results from XRF for direct aqueous carbonation after 120 min at 4 Mpa. The results indicate that there was a decrease in the CaO (wt. %) content in the solid residue as expected because there was a concentration of 3.79 wt. % remaining after the direct aqueous carbonation process compared to the original concentration of 4.06 wt. % found in the raw fly ash. This decrease can be attributed to the extraction of the calcium oxide (CaO) phase into solution from the fly ash, which was then involved in the direct aqueous carbonation reaction and resulted in a lower concentration of CaO (wt %) in the solid residue after direct aqueous carbonation due to the precipitation to form $CaCO_3$.

4.3.6 Indirect aqueous carbonation

The indirect aqueous carbonation route was also considered for CO_2 storage in this work with the experimental detail given in Chapter 3, Section 3.3.2.3, however, no significant amount of $CaCO_3$ was recovered from the process to measure the percentage of $CaCO_3$ formed. Given that Chang et al. (2017) mentioned that forming the desired polymorph of $CaCO_3$, namely calcite, from indirect carbonation requires a high concentration of calcium (Ca^{2+}) and a higher solution pH (i.e., > 11), the maximum calcium (Ca^{2+}) extracted of 422.23 ppm (see Figure 4.21) from the indirect aqueous route and the solution pH of 8.13 before carbonation were not high enough, and this was possibly the reason for the minuscule amount of $CaCO_3$ formed from indirect aqueous carbonation. In addition, due to the small volume of the reaction system used for this work (ie., 600 mL), a small volume of the supernatant was therefore used for indirect aqueous carbonation, and this could have also been a contributing factor to the minuscule amount of $CaCO_3$ recovered from the indirect aqueous carbonation process. However, the CE (%) was still determined in order to estimate the extent of carbonation due to the interaction of the calcium (Ca^{2+}) rich supernatant and the CO_2.

4.3.6.1 Effect of stirring speed (rpm) on the leachability of calcium (Ca^{2+}) before indirect aqueous carbonation

The optimization of certain process parameters was a key component in investigating how carbonation performance could be improved. Hence, the effect of stirring speed (rpm) on the leaching of calcium (Ca^{2+}) was considered before conducting experiments involving indirect aqueous carbonation. The stirring speed was varied between 100 rpm, 200 rpm, 300 rpm, and 400 rpm at 70 ^{0}C, using a S/L ratio of 0.5 g/mL over 120 min, as shown in Figure 4.20:

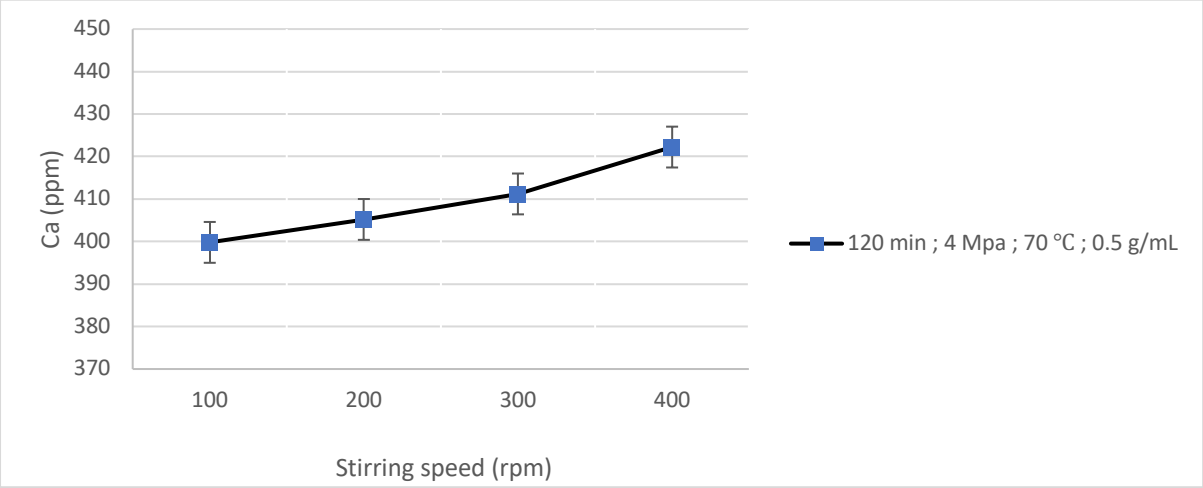

Figure 4.20: Effect of stirring speed on leachability of calcium (Ca^{2+}) from ICP-OES analysis

Prior to conducting indirect aqueous carbanion experiments, the effect of the stirring speed (rpm) on calcium (Ca^{2+}) extraction was first investigated over 120 min, as there was a slightly higher calcium (Ca^{2+}) concentration of 399.8 ppm reported previously after 120 min of calcium (Ca^{2+}) extraction from preliminary experiments (see Figure 4.9). Results presented in Figure 4.20 clearly indicate that the concentration of calcium (Ca^{2+}) extracted increased as the stirring speed was increased up to 400 rpm, with the highest calcium (Ca^{2+}) concentration obtained being 422.23 ppm at the highest stirring speed considered of 400 rpm. These results were expected as the increase in the stirring speed (rpm) increases the diffusion of metal ions into solution, thus increasing the concentration of calcium (Ca^{2+}) that is leached. The results were consistent with the findings from the study conducted by Mayoral et al. (2013), who utilized relatively higher stirring speeds (i.e., up to 1200 rpm) to achieve maximum percentage (%) efficiency for their process.

4.3.6.2 Effect of time (min) on the leachability of calcium (Ca^{2+}) before carbonation

A further investigation into the leachability of calcium (Ca^{2+}) over time (min) at 70 ^{0}C, using a S/L ratio of 0.5 g/mL and the optimum stirring speed of 400 rpm was done. Figure 4.21 shows the concentration of calcium (Ca^{2+}) that was present in the leachate after 30 min, 60 min, 90 min, and 120 min:

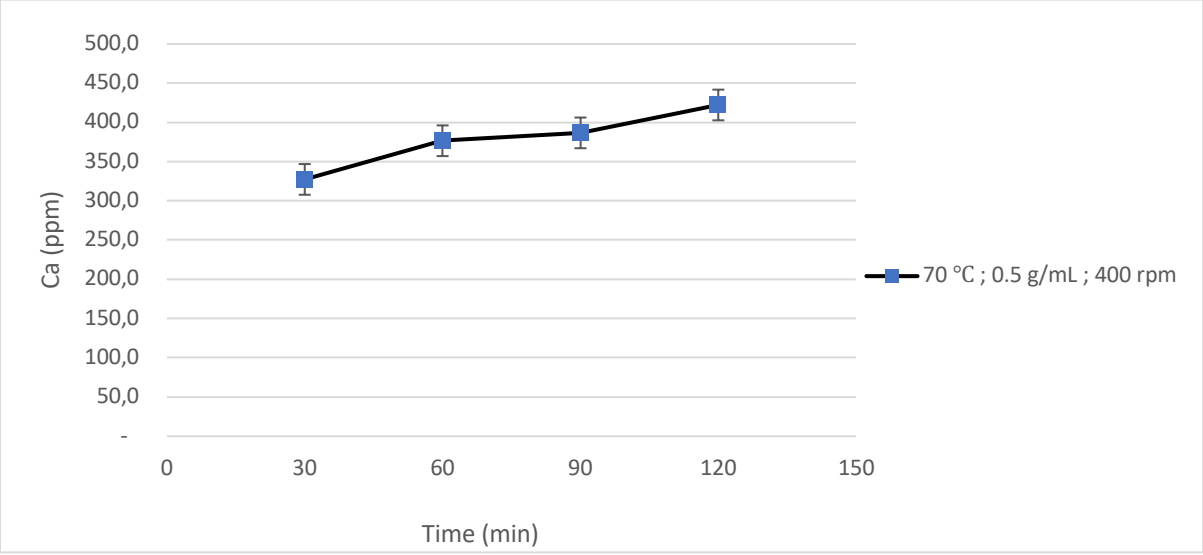

Figure 4.21: Effect of time (min) on leachability of calcium (Ca^{2+}) before carbonation

Figure 4.21 shows that the calcium (Ca^{2+}) extraction increased with time (min). This meant that when water was used as the reaction medium, the calcium (Ca^{2+}) extraction was affected by the stirring speed (rpm) because the highest concentration of calcium (Ca^{2+}) obtained using a stirring speed of 400 rpm after 120 min was 422.23 ppm, which was higher compared to the concentration of 399.8 ppm obtained when a stirring speed of 100 rpm was applied for the calcium (Ca^{2+}) extraction time of 120 min.

Figure 4.21 shows that a higher stirring speed (rpm) results in an increase in the calcium (Ca^{2+}) extraction because the maximum calcium (Ca^{2+}) concentration extracted at 400 rpm after 120 min of extraction was 422.23 ppm and was higher than the maximum calcium (Ca^{2+}) extracted of 399.8 ppm at 100 rpm for the same calcium (Ca^{2+}) extraction time of 120 min (see Figure 4.9). The results depicted in Figure 4.21 for leaching before carbonation of the leachate, which show that the concentration of calcium (Ca^{2+}) in the leachate increased with increasing time (min) at 400 rpm, were consistent with findings from the study conducted by Jo, Kim, et al. (2012), who found that leaching over a longer time (min) resulted in higher calcium (Ca^{2+}) extraction efficiency.

4.3.6.3 Effect of pressure (Mpa) over time (min) on CE (%) achieved for indirect aqueous carbonation

For indirect aqueous carbonation, the leaching was done for 30 min, 90 min, and 120 min, with the leaching time (min) equivalent to the time used to carbonate the leachate. Figure 4.22 displays results obtained for the calculated CE (%) from the indirect aqueous carbonation process over 30 min, 90 min, and 120 min of carbonation at 70 ^{0}C, using a S/L ratio of exactly 0.5 g/mL, and the optimum stirring speed of 400 rpm obtained from leaching experiments:

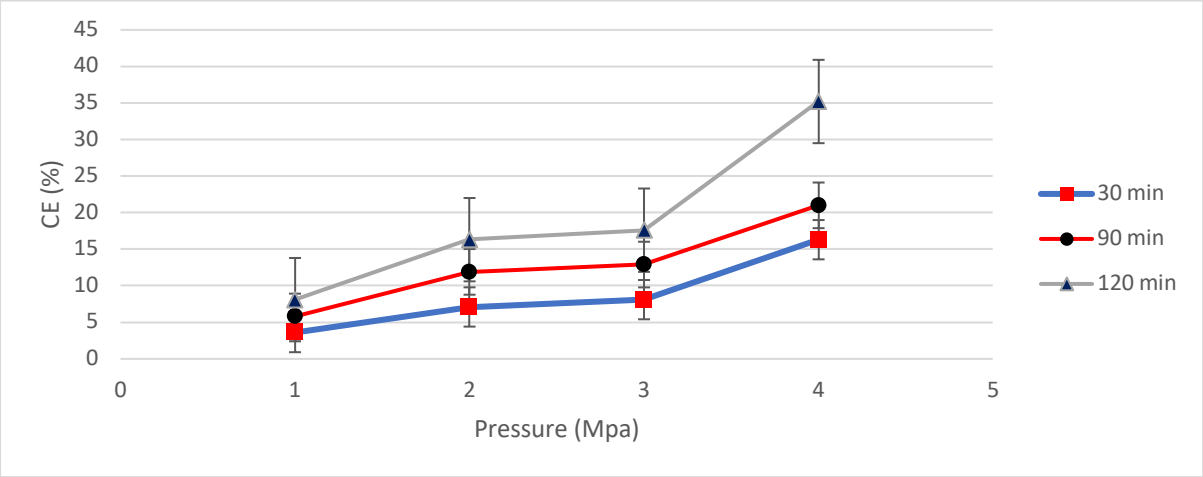

Figure 4.22: Effect of pressure (Mpa) over time (min) on CE (%) (70 ^{0}C, 0.5 g/mL, 400 rpm)

For the indirect aqueous carbonation process, the carbonation efficiency (CE %) showed an increase with increasing initial CO_2 pressure (Mpa) as expected. This was due to the higher concentration of CO_2 molecules dissolved in the liquid phase that could react with calcium (Ca^{2+}) for a higher CO_2 pressure (Mpa). The higher availability of CO_2 molecules in solution resulted in an increased rate of carbonation and higher CO_2 consumption due to the reaction with calcium (Ca^{2+}) ions for the precipitation reaction to form pure $CaCO_3$. Therefore, the higher rate of CO_2 consumption and higher overall pressure drop (see Table B16 in Appendix B) due to the reaction of CO_2 with calcium (Ca^{2+}) to form precipitated $CaCO_3$ at higher initial CO_2 pressures (Mpa) explains the higher CE (%) reported for higher CO_2 pressures (Mpa) in all cases.

Over the 120 minutes carbonation of the leachate, the CE (%) at 3 Mpa was 17.6 % and when the CO_2 pressure was increased to 4 Mpa, the CE (%) achieved increased to 35.2 %. This meant that increasing the initial CO_2 pressure to 4 Mpa had a significant effect on the CE (%) over the 120 min reaction. The significant increase in the CE (%) at the highest initial CO_2 pressure of 4 Mpa over the same reaction time of 120 min can be explained by the higher concentration of calcium (Ca^{2+}) over the 120 min reaction and the higher amount of CO_2 molecules available at a pressure of 4 Mpa.

Given that the results from Figure 4.22 indicate that lower initial CO_2 pressures of 1 Mpa and 2 Mpa had a minor effect on the CE (%) over the same reaction time (min) for most cases and that the significant effect of pressure on CE (%) started to be apparent at the highest CO_2 pressure, this, therefore, indicates that a higher CO_2 pressure (Mpa) was required for the indirect aqueous carbonation process to obtain the maximum CE (%). The effect of using a higher initial CO_2 pressure to obtain maximum CE (%) for the indirect carbonation process was consistent with findings from the study conducted by Dananjayan et al. (2016), whereby for their CO_2 sequestration process, using a higher initial CO_2 pressure of up to 0.4 Mpa resulted in a higher CO_2 sequestration capacity.

From Figure 4.22, the effect of reaction time (min) on the overall CE (%) can be observed, wherein an increase in the reaction time (min) resulted in an increase in the CE (%) achieved at 1 Mpa to 4 Mpa. The increase in CE (%) achieved over time (min) can also be attributed to the calcium (Ca^{2+}) extraction. Figure 4.21 shows that the extraction of calcium (Ca^{2+}) from leaching experiments before carbonation of the calcium (Ca^{2+}) rich leachate increased with increasing time (min) as previously stated.

This explains the slightly higher CE (%) achieved over 120 min of indirect aqueous carbonation compared to the CE (%) achieved after 30 min and 90 min of carbonation and also the slightly higher CE (%) over 90 min compared to 30 min at 1 Mpa, 2 Mpa, 3 Mpa, and 4 Mpa because there was higher calcium (Ca^{2+}) extracted for the 120 min and the 90 min reactions compared to the 30 min reactions, as suggested by the results obtained for the calcium (Ca^{2+}) extraction over time (min) presented in Figure 4.21. Essentially, there was a higher overall pressure drop over the indirect aqueous carbonation reaction, especially over 120 min, which resulted in a higher rate of CO_2 consumption compared to the total CO_2 consumption achieved after 30 min and 90 min thus resulting in a higher CE (%) achieved over the 120 min reaction compared to the CE (%) obtained after 30 min and 90 min of carbonation.

Due to the increase in calcium (Ca^{2+}) extraction over time (min), the effect of time (min) on the CE (%) was apparent for indirect aqueous carbonation unlike in the case of direct aqueous carbonation. This was because the gradual increase in the calcium (Ca^{2+}) concentration over the longer reaction time (min) for indirect aqueous carbonation meant that once the leachate was separated from the solid residues and subjected to carbonation more calcium (Ca^{2+}) reacted with the CO_2 and thus more CO_2 was consumed due to the carbonation reaction which led to a higher overall pressure drop and hence CE (%) which also explains the slightly higher maximum CE (%) of 35.2 % which was achieved for indirect aqueous carbonation compared to the maximum CE (%) of 29.4 % achieved for direct aqueous carbonation.

The calcium (Ca^{2+}) extraction for direct aqueous carbonation did not change significantly after 30 min which meant that the CE (%) achieved remained similar after 30 min, 90 min and finally 120 min at 1 Mpa to 4 Mpa, whereas in the case of indirect aqueous carbonation, because the calcium (Ca^{2+}) extraction gradually increased over the time (min), the effect of time (min) could be observed because the longer the reaction time (min) was, the more CO_2 was consumed due to the higher calcium (Ca^{2+}) availability over a longer reaction time (min).

Jo, Kim, et al. (2012) in their study using indirect aqueous carbonation found the carbonation efficiency (CE %) to be directly related to the calcium (Ca^{2+}) extraction efficiency and that the higher the calcium (Ca^{2+}) extraction efficiency, the higher the carbonation efficiency (CE %). This agrees with the findings from this study because higher carbonation efficiencies were achieved when there was a higher concentration of calcium (Ca^{2+}) in the leachate. Considering that the leaching and carbonation for this work were done over the same amount of time (min), Figure 4.21 shows that the highest amount of calcium (Ca^{2+}) leached was after 120 min when stirring at 400 rpm, and with the highest CE (%) from Figure 4.22 also achieved after 120 min of carbonation, this showed the correlation between the calcium (Ca^{2+}) concentration in the leachate and CE (%).

This indicated that the higher the amount of calcium (Ca^{2+}) extracted, the higher the degree of CO_2 consumption due to the reaction between calcium (Ca^{2+}) and CO_2 for the precipitation to form pure $CaCO_3$ which resulted in a higher CE (%). Essentially, the maximum CE (%) was achieved when there was a higher amount of calcium (Ca^{2+}) in the leachate and for a higher initial CO_2 pressure (Mpa) due to an increase in the rate of carbonation under these conditions which resulted in higher pressure drop and therefore a higher CE (%).

Hosseini et al. (2014) also found that the availability of calcium (Ca^{2+}) ions in the leachate was one of the main factors influencing the efficiency of carbonation through the indirect method and in their study, they found that as the percentage (%) leaching of calcium (Ca^{2+}) increased, so did the carbonation percentage (%) and it reached a maximum of approximately 90 %. The results obtained by Han et al. (2015) also showed a similar trend wherein an increase in the leaching efficiency of calcium (Ca^{2+}) resulted in an increase in the overall CO_2 sequestration capacity with the highest capacity being 0.031 kg CO_2/kg fly ash.

4.4 Further process optimization

As mentioned previously, due to calcium (Ca^{2+}) extraction being identified as the rate-limiting step from direct aqueous experiments, certain process parameters were varied during the experimental work to improve the calcium (Ca^{2+}) extraction and therefore potentially optimize on the % $CaCO_3$ formed and CE (%).

4.4.1 Effect of S/L ratio on % $CaCO_3$ formed

Figure 4.23 presents results obtained from Chittick tests for examination of the effect of using a lower S/L ratio on the % $CaCO_3$ formed during direct aqueous carbonation over the reaction times of 30 min, 60 min, 90 min, and 120 min, at the optimum pressure of 4 Mpa and optimum stirring speed of 400 rpm:

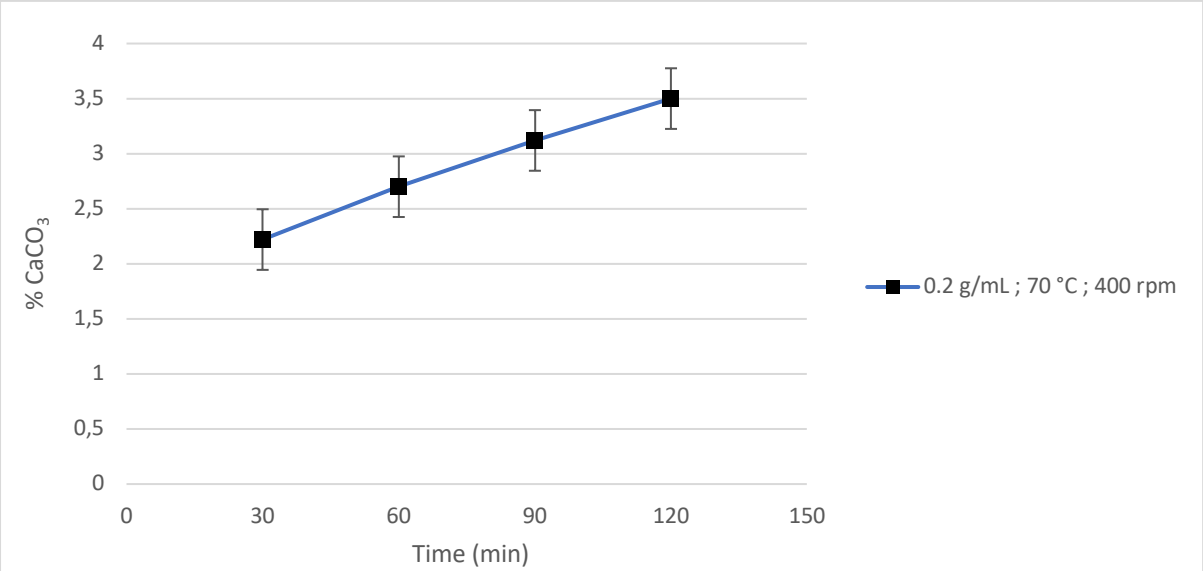

Figure 4.23: Effect of lower S/L ratio on $CaCO_3$ formed from Chittick tests

The effect of using a lower S/L ratio of 0.2 g/mL compared to the original S/L ratio of 0.5 g/mL on the % $CaCO_3$ formed was considered with results obtained presented in Figure 4.23. The experiments were conducted over reaction times of 30 min, 60 min, 90 min, and 120 min for an initial CO_2 pressure of 4 Mpa. The reaction time of 60 min was still considered in this case in order to have a clearer observation of the effect of time (min) on the % $CaCO_3$ formed when the S/L ratio was lowered to 0.2 g/mL. As the time increased at the S/L ratio of 0.2 g/mL, the % $CaCO_3$ formed also increased to reach a maximum of 3.5 %. It is evident that for a lower S/L ratio, a higher % $CaCO_3$ can be achieved when considering that the maximum % $CaCO_3$ formed when a S/L ratio of 0.5 g/mL was used was 2.43 (see Figure 4.14).

Back et al. (2008) also achieved the highest degree of % $CaCO_3$ formed at the lowest S/L ratio (0.025 g/mL) which shows that through the dilution effect, a lower S/L ratio produces a higher volume of water which increases the solubility and hence the availability of calcium (Ca^{2+}) ions in solution causing a higher rate of CO_2 consumption due to $CaCO_3$ formation and hence more $CaCO_3$ formed over time (min). Although a higher % $CaCO_3$ was achieved for a lower S/L ratio, it is important to consider that the higher % $CaCO_3$ reported for the lower S/L ratio of 0.2 g/mL can also be attributed to the use of a higher stirring speed (i.e., 400 rpm) compared to the stirring rate of 100 rpm, used when a S/L ratio of 0.5 g/mL was originally used.

4.4.2 Effect of S/L ratio on CE (%)

Figure 4.24 presents results obtained for the determination of the effect of using a lower S/L ratio on the calculated CE (%) from direct aqueous carbonation over reaction times of 30 min, 60 min, 90 min, and 120 min, at the optimum pressure of 4 Mpa and optimum stirring speed of 400 rpm:

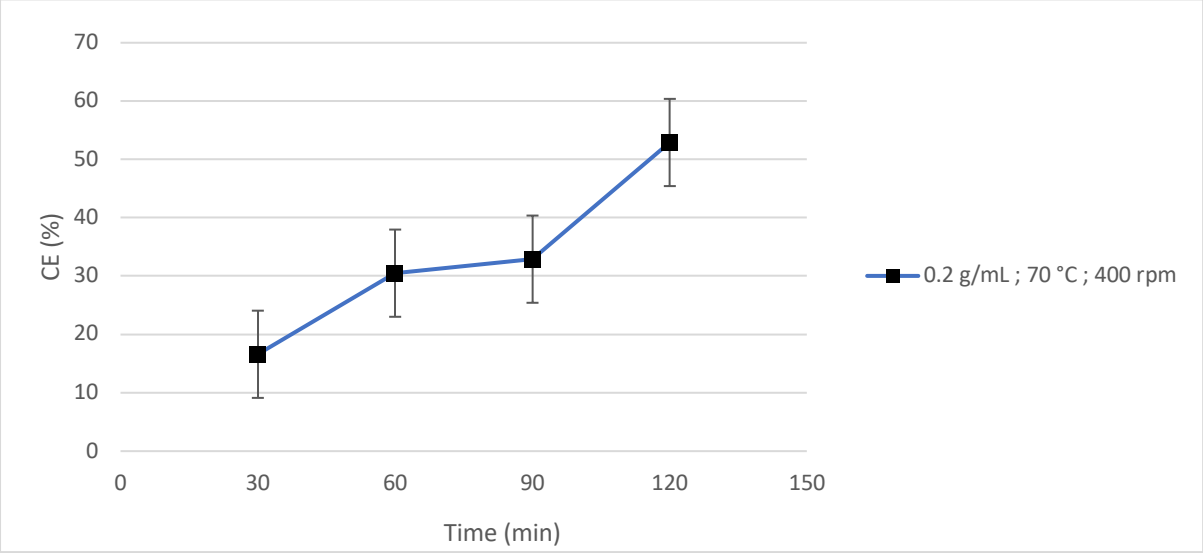

Figure 4.24: Effect of lower S/L ratio on CE (%)

The results from Figure 4.24 show that the CE (%) achieved increased for a lower S/L ratio of 0.2 g/mL as time increased from 30 min to 120 min at an applied CO_2 pressure of 4 Mpa. The reaction time of 60 min was still considered in this case to have a clearer observation of the effect of time (min) on the CE (%) as the S/L ratio was lowered to 0.2 g/mL. The maximum CE (%) achieved for a lower S/L ratio of 0.2 g/mL was 52.9 % and was higher compared to the 29.4 % attained for the higher S/L ratio of 0.5 g/mL originally used.

The higher CE (%) achieved for the lower S/L ratio of 0.2 g/mL can also be attributed to the effective solubility of calcium (Ca^{2+}) at a lower S/L ratio. Given that the pressure drop due to $CaCO_3$ formation also depends on the concentration of calcium (Ca^{2+}), a higher CE (%) over time (min) was expected for a lower S/L ratio of 0.2 g/mL compared to that of 0.5 g/mL because of the effective solubility of calcium (Ca^{2+}) during the direct aqueous carbonation reaction through the dilution effect. The effective solubility of calcium (Ca^{2+}) over time (min) at a lower S/L ratio, therefore, resulted in a higher degree of CO_2 consumption and a higher overall pressure drop over a longer reaction time (min) due to a higher amount of calcium (Ca^{2+}) being available over time (min) at a lower S/L ratio. Essentially, the higher availability of calcium (Ca^{2+}) over time (min) at a lower S/L ratio meant that there was a faster rate of carbonation as more calcium (Ca^{2+}) was available to react with CO_2 which led to a higher degree of CO_2 consumption as mentioned, and a higher overall pressure drop over time (min), which then resulted in a higher CE (%) achieved over time (min) as seen in Figure 4.24.

CHAPTER 5

5. Results and Discussion

This results section provides results for direct and indirect carbonation with acid mine drainage (AMD) wastewater used as a reaction solvent. It provides discussions based on the results obtained from the direct and indirect carbonation studies when AMD wastewater was used, with the viewpoint of comparing the results from the direct and indirect carbonation approaches. The results are also compared to the results obtained in Chapter 4 when water was used as the reaction solvent, with the viewpoint of ascertaining which process was more effective for CO_2 storage.

5.1.1 Characterisation of AMD wastewater

Before conducting carbonation experiments involving AMD wastewater, the wastewater was first analysed to determine the concentration of elemental species present in the wastewater. through ICP-OES analysis with results presented in Table 5.1:

Table 5.1: Elemental composition of AMD wastewater from ICP-OES analysis

pH	2.63
Element	Concentration (ppm)
SO_4^{2-}	990.1
Fe	1899
Ca	362.5
Mg	329.9
Mn	65.7
Mg	61.2
Si	36.4
K	33.7
Na	18.3
Zn	7.8
Ni	0.81
Co	0.76
Cu	0.39
Sr	0.35
Li	0.22

Element	Concentration (ppm)
Se	0.16
Pb	0.11
Cd	0.058
Ti	-0.017
As	-0.021
Mo	-0.041
Cr	-0.063
P	-0.095

Table 5.1 shows the concentration of major elements (i.e., Al, Fe, Mg, Mn, Ca), minor elements (i.e., Na, Si, Zn), and trace elements in the AMD wastewater used. From the viewpoint of CO_2 sequestration, the presence of metals such as Ca^{2+}, Fe^{2+}, and Mg^{2+} could all contribute to the overall CO_2 stored in mineral carbonate form as CO_2 can interact with these metals to form mineral carbonates in the form of $CaCO_3$, $FeCO_3$, and $MgCO_3$. Therefore, it was important to determine which of these elemental species was predominantly responsible for the overall CO_2 storage in mineral carbonate form. The pH of the AMD was reported as 2.63 and was within the expected range for typical AMD. The neutralization of the acidic pH coupled with the removal of toxic elements from the wastewater was achieved through the carbonation process using fly ash and was important to ensuring that the AMD wastewater met TWQR standards.

5.1.2 Determination of the measure of CO_2 uptake from carbonation using AMD

To determine the carbonation performance measure that could be used for CO_2 storage, the concentration of species that could contribute to the overall amount of CO_2 stored in mineral carbonate form, namely Fe^{2+}, Mg^{2+}, and also Ca^{2+}, before and after the carbonation process was also considered for the CO_2 sequestration using AMD wastewater as the reaction solvent.

5.1.2.1 Leaching of elements with AMD wastewater as a solvent

This section provides results from leaching experiments using AMD wastewater with the experimental details given in Chapter 3, Section 3.3.2.1.2. The leaching using AMD wastewater as a reaction solvent was conducted over 30 min, 60 min, 90 min, and 120 min at 70 ^{0}C using the optimum S/L ratio and stirring speed of 0.2 g/mL and 400 rpm, respectively, as shown in Figure 5.1:

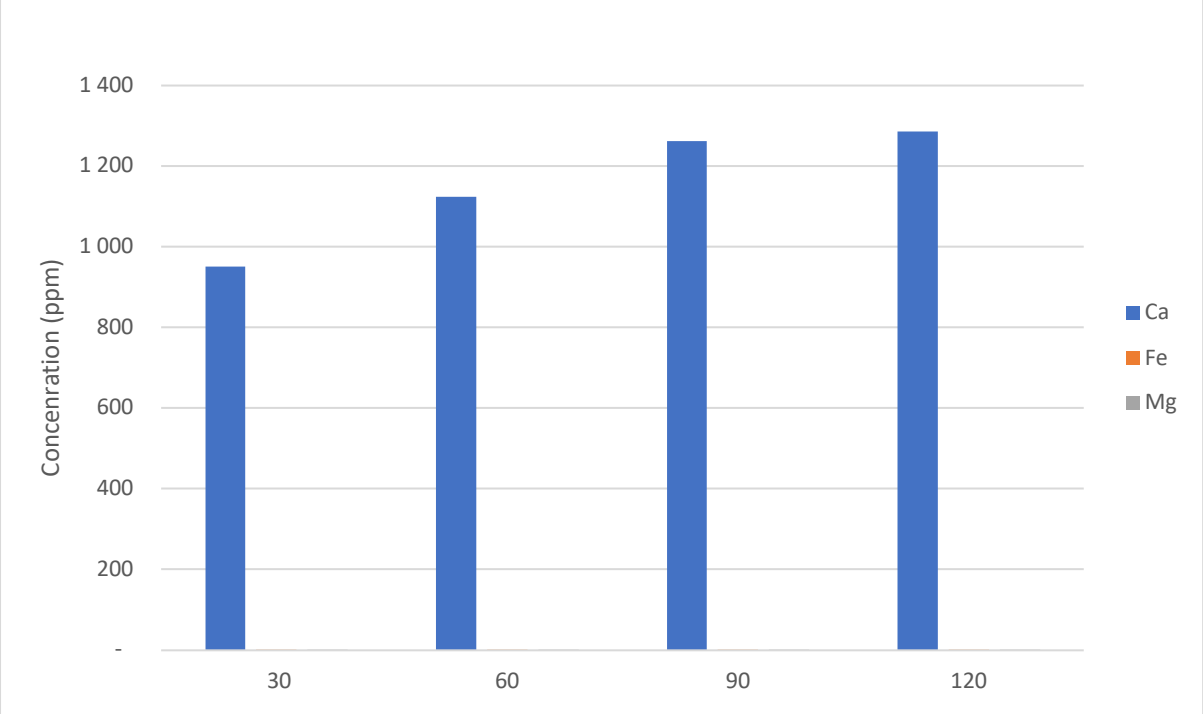

Figure 5.1: Concentration of Ca^{2+}, Fe^{2+}, Mn^{2+} after leaching using AMD wastewater (70 ^{0}C, 0.2 g/mL, 400 rpm)

Figure 5.1 shows the concentration of the elements Ca^{2+}, $Fe^{2+,}$ and Mg^{2+} after leaching with AMD wastewater. Considering the initial concentration of 1899 ppm for Fe^{2+} and 329.9 ppm for Mg^{2+}, the results presented in Figure 5.1 indicate that there was a significant decrease in the concentration of Fe^{2+} and Mg^{2+} after leaching in all cases investigated, as concentrations of 0.0549 ppm, 0.05 ppm, 0.0389 ppm, and 0.007 ppm over 30 min, 60 min, 90 min, and 120 min, respectively, for Fe^{2+} were reported, while the concentrations of Mg^{2+} were 0.0081 ppm, 0.0079 ppm, 0.0073 ppm, and 0.0068 ppm over 30 min, 60 min, 90 min, and 120 min, respectively. This was possibly due to hydrolysis (redox reactions), which resulted in the precipitation of Fe^{2+} as well as Mg^{2+} into insoluble metal hydroxides. On the other hand, the results show that there was a higher calcium (Ca^{2+}) concentration than the 362.9 ppm present in the AMD after leaching in all cases, and this can be attributed to the extraction of the readily available calcium (Ca^{2+}) from the fly ash that resulted in the dissolution of $Ca(OH)_2$ in solution, thus causing an increase in the calcium (Ca^{2+}) concentration over time (min).

5.1.2.2 Concentration of elements after carbonation with AMD wastewater as a solvent

The concentration of the elemental species that could potentially contribute to the overall CO_2 uptake in mineral carbonate form namely iron (Fe^{2+}), magnesium (Mg^{2+}), and calcium (Ca^{2+}) was considered after indirect carbonation in order to observe the extent to which the concentration of these species would decrease upon interaction with CO_2 after carbonation of the leachate. The experimental details for indirect carbonation were given in Chapter 3, Section 3.3.2.3. Figure 5.2 shows the concentrations of Fe^{2+}, Mg^{2+}, and Ca^{2+} after indirect carbonation over 120 min from 1 Mpa to 4 Mpa, at 70 ^{0}C, using a S/L ratio of 0.2 g/mL and a stirring speed of 400 rpm:

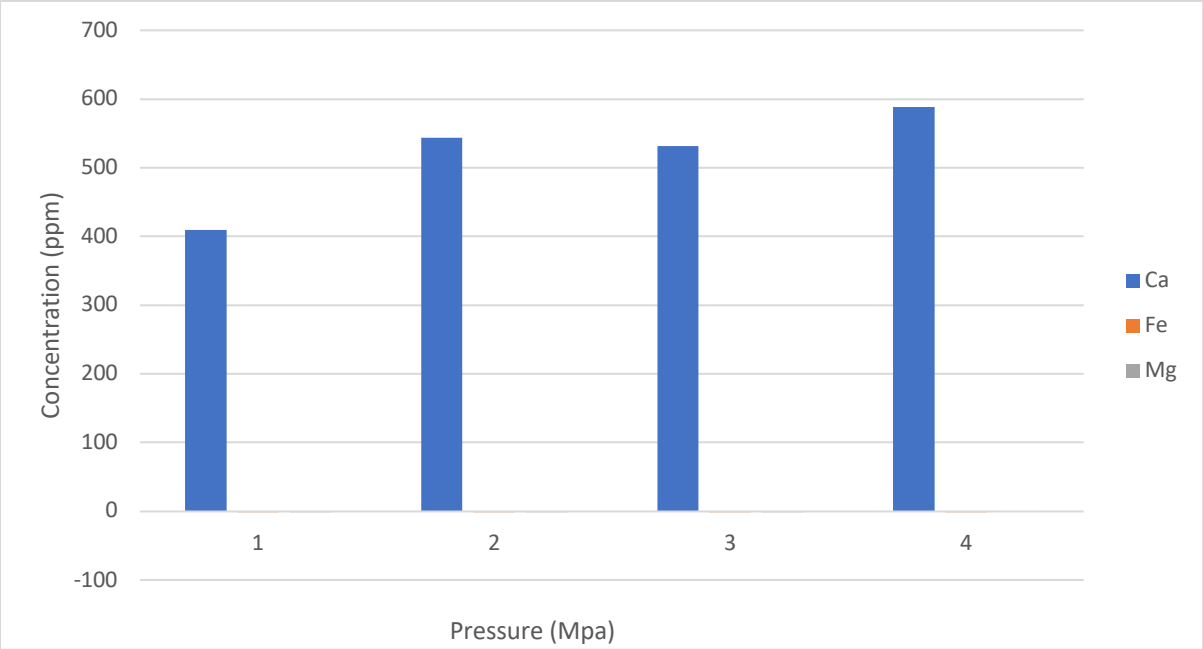

Figure 5.2: Concentration of Ca^{2+} , Fe^{2+}, and Mg^{2+} after carbonation with AMD wastewater (120 min, 70 ^{0}C, 0.2 g/mL, 400 rpm)

Figure 5.2 displays the concentration of Ca^{2+}, Fe^{2+}, and Mg^{2+} after 120 minutes of carbonation to illustrate how the indirect carbonation approach was employed to provide the key measure of CO_2 uptake in mineral carbonated form when AMD was used as a reaction solvent. From the results obtained after leaching for 120 min presented in Figure 5.1, the concentrations of Fe^{2+} and Mg^{2+} of 0.007 ppm and 0.0068 ppm, respectively, decreased to concentrations below the detection limit of the ICP-OES instrument after carbonation for all cases of CO_2 pressure (Mpa) considered. The further reduction of Fe^{2+} and Mg^{2+} although minor, was possibly due to the interaction with CO_2. In the case of calcium (Ca^{2+}), the concentration of 1268 ppm obtained after 120 min before carbonation decreased to 410 ppm, 544 ppm, 532 ppm, and 294 ppm at 1 Mpa, 2 Mpa, 3 Mpa, and 4 Mpa, respectively. This shows that there was a higher decrease in calcium (Ca^{2+}) concentration after carbonation compared to other elements such as Fe^{2+} and Mg^{2+}. The higher reduction in calcium (Ca^{2+}) after carbonation suggests that the calcium (Ca^{2+}) was mostly responsible for the CO_2 stored in mineral form, hence the use of % $CaCO_3$ as the main measure of CO_2 storage for carbonation with AMD.

5.1.2.3 Effect of time (min) on the calcium (Ca^{2+}) extraction with water compared to AMD wastewater

Given that it was demonstrated that calcium (Ca^{2+}) was the element predominantly responsible for CO_2 capture in mineral carbonate form from the concentrations obtained before and after indirect carbonation with AMD wastewater, it was also important to highlight the leaching behaviour of calcium (Ca^{2+}) over time (min) when AMD was used as the reaction solvent. Figure 5.3 shows a comparison between the concentration of calcium (Ca^{2+}) leached over time (min) first when deionized water was used and subsequently when AMD wastewater was used as the reaction solvent. The comparison could be used to highlight the importance of the concentration of calcium (Ca^{2+}) on the overall carbonation performance for the carbonation experiments involving AMD. Figure 5.3 provides a comparison between the calcium (Ca^{2+}) extraction over extraction times of 30 min, 60 min, 90 min, and 120 min when water was used and when AMD wastewater was used. Again, the experimental detail for the leaching was presented in Chapter 3 Section 3.3.2.1.2. The experimental conditions for the leaching when water was used were: 70 ^{0}C, using a S/L ratio of 0.5 g/mL and stirring speed of 100 rpm while those for AMD wastewater were: 70 ^{0}C, using a S/L ratio of 0.2 g/mL and a stirring speed of 400 rpm as shown in Figure 5.3:

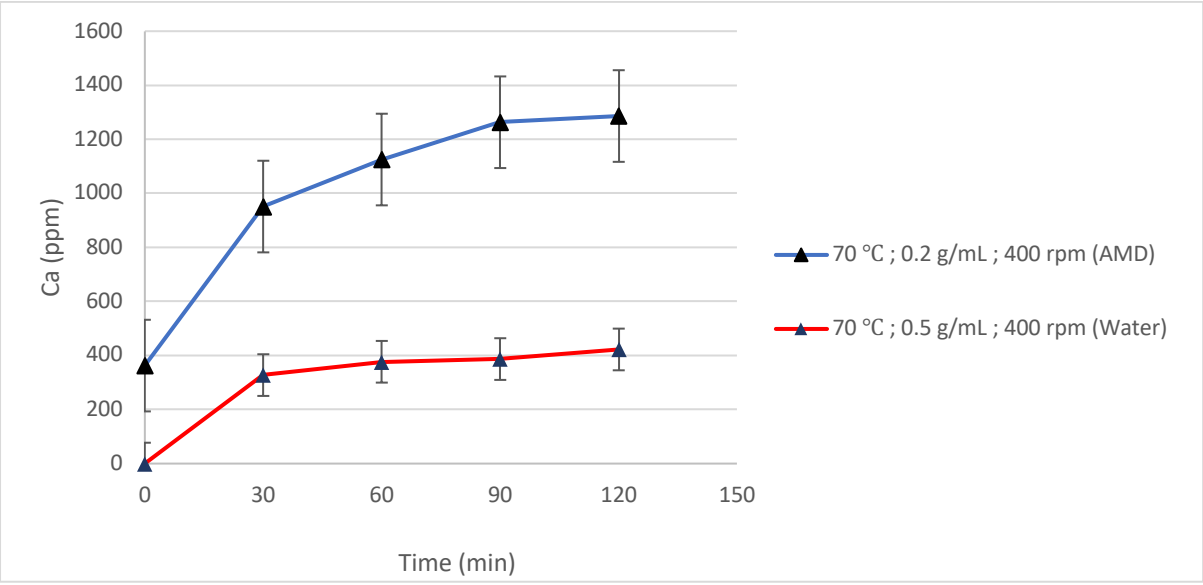

Figure 5.3: Effect of time on the leachability of calcium (Ca^{2+}) with water and AMD wastewater

The comparison provided in Figure 5.3 between the calcium (Ca^{2+}) extraction when water was used compared to when AMD wastewater was used as the reaction medium shows that there was a higher calcium (Ca^{2+}) concentration present in the leachate over time (min) when AMD was used in all cases. The concentrations of calcium (Ca^{2+}) leached when AMD was used were 951 ppm, 1125 ppm, 1263 ppm, and 1286 ppm over 30 min, 60 min, 90 min, and 120 min respectively while the concentrations obtained when water was used were 327.4 ppm, 376.7 ppm, 386 ppm, and 422.23 ppm over 30 min, 60 min, 90 min, and 120 min respectively. The higher calcium (Ca^{2+}) concentrations obtained when using AMD wastewater were mainly due to the initial concentration of 362.5 ppm available in the AMD wastewater as well as the total calcium (Ca^{2+}) extracted from the fly ash because there was an increase of 261.2 ppm, 385.8 ppm, 513.5 ppm, and 480.3 ppm from the experiments involving the AMD wastewater over 30 min, 60 min, 90 min, and 120 min respectively compared to when water was used when the calcium (Ca^{2+}) concentration of 362.5 ppm originally found in the AMD wastewater was not considered. The additional calcium (Ca^{2+}) extracted from the fly ash material can be attributed to the lower S/L ratio of 0.2 g/mL used for AMD leaching which meant that the calcium (Ca^{2+}) extraction from the fly ash was therefore more effective compared to when the S/L ratio of 0.5 g/mL was used for leaching experiments with water.

From Figure 5.3, It is important to note that the calcium (Ca^{2+}) extraction slowed down after 30 min of extraction because the calcium (Ca^{2+}) concentration leached in the first 30 min was 588.5 ppm while the concentrations reported after 60 min, 90 min, and 120 min increased by 174 ppm, 312 ppm and 335 ppm respectively. The decrease in the rate of calcium (Ca^{2+}) extraction was possibly due to the reaction of calcium (Ca^{2+}) with phases such as the sulfates (SO_4^{2-}) present in the AMD wastewater.

5.2. Direct carbonation with AMD wastewater

This section provides results from the direct carbonation process using AMD wastewater, with detailed discussions of the results in relation to previous studies. The experimental detail for direct carbonation was provided in Chapter 3, Section 3.3.2.2.

5.2.1 Effect of pressure (Mpa) over time (min) on % $CaCO_3$ formed

The % $CaCO_3$ formed using Chittick tests was determined for direct carbonation using AMD wastewater as a reaction solvent. The experimental detail for the Chittick test was given in Chapter 3 Section 3.2.4. The results presented in Figure 5.4 show the % $CaCO_3$ formed from direct carbonation with AMD over 30 min, 60 min, 90 min, and 120 min of carbonation, at 70 ^{0}C, using a S/L ratio of 0.2 g/mL and stirring speed of 400 rpm:

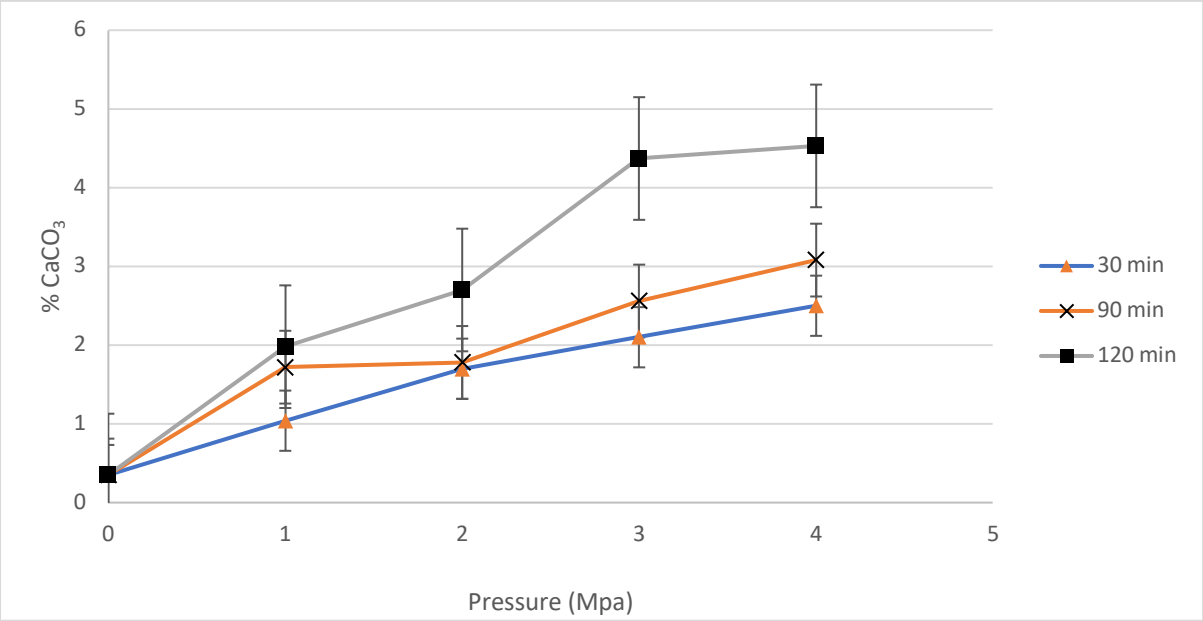

Figure 5.4: Effect of pressure (Mpa) over time (min) on the % $CaCO_3$ formed (70 ^{0}C, 0.2 g/mL, 400 rpm)

Figure 5.4 shows results from direct carbonation with AMD wastewater. The reaction times of 30 min, 90 min, and 120 min were selected for the purpose of comparison with direct aqueous carbonation results. Results from direct carbonation with AMD show that the % $CaCO_3$ formed increased with increasing initial CO_2 pressure (Mpa) in all cases as expected due to the increase in the availability of dissolved CO_2 molecules that could react with calcium (Ca^{2+}) in solution.

The results also indicate that there was a significant increase in the % $CaCO_3$ formed for the 120 min direct carbonation reaction when the initial CO_2 pressure was increased from 2 Mpa to 3 Mpa. For an initial CO_2 pressure of 2 Mpa after 120 min, the % $CaCO_3$ achieved was 2.70 % and when the pressure was increased to 3 Mpa, the % $CaCO_3$ formed increased to 4.37 % meaning that increasing the initial CO_2 pressure to 3 Mpa had a significant effect on the % $CaCO_3$ formed over the 120 min reaction.

The significant effect of pressure (Mpa) on the increase in the % $CaCO_3$ achieved over the same reaction time of 120 min for a higher initial CO_2 pressure of 3 Mpa can be attributed to the higher amount of CO_2 molecules available and the continual increase in the calcium (Ca^{2+}) extraction until 90 min when AMD wastewater was used (see Figure 5.3). The increase in calcium (Ca^{2+}) extraction for the most part of the 120 min reaction meant that an effective rate of carbonation and $CaCO_3$ formation was maintained over the course of the carbonation reaction and considering the higher concentration of CO_2 that was available at 3 Mpa compared to 2 Mpa, this ensured an effective rate of carbonation hence the significant effect of increased pressure on the % $CaCO_3$ observed in Figure 5.4.

Due to the higher rate of calcium (Ca^{2+}) extraction in 30 min observed in Figure 5.3, this meant that there was effective calcium (Ca^{2+}) extraction in the first 30 min of the 120 min carbonation reaction, and for a higher initial CO_2 pressure of 3 Mpa, more CO_2 could be dissolved under the alkaline conditions in the initial stages of the direct carbonation reaction due to the higher concentration and hence availability of CO_2 molecules at higher pressure (Mpa). In addition, there was still a significant increase in the calcium (Ca^{2+}) extraction even after 30 min of the 120 min reaction until the rate of calcium (Ca^{2+}) extraction reached a plateau after 90 min, meaning the rate of carbonation was still effective enough even after 30 min of the 120 min reaction and the overall CO_2 consumption at higher initial CO_2 pressure was higher, hence the significant effect of the initial CO_2 pressure on the % $CaCO_3$ formed especially for a higher initial CO_2 pressure of 3 Mpa and 4 Mpa over the same reaction time (min) as observed in Figure 5.4.

Although results from Figure 5.4 show that increasing the pressure to 3 Mpa and 4 Mpa from 2 Mpa had a significant effect on the % $CaCO_3$ formed over 120 min, the results also indicate that increasing the pressure beyond 3 Mpa (i.e., to 4 Mpa) had a minor effect on the % $CaCO_3$ formed as the % $CaCO_3$ of 4.37 % at 3 Mpa was similar to the % $CaCO_3$ formed of 4.53 % at 4 Mpa. The minor increase in the % $CaCO_3$ can be attributed to the decrease in the rate of $CaCO_3$ precipitation at a higher pressure of 4 Mpa. Due to the increase in solubility of calcium (Ca^{2+}) at a higher pressure, this meant that as $CaCO_3$ was forming over the 120 min reaction, at a higher CO_2 pressure of 4 Mpa, its dissociation was also potentially favoured meaning that as $CaCO_3$ was forming, it possibly dissociated during the reaction because of the increase in solubility of calcium (Ca^{2+}) and calcium (Ca^{2+}) re-dissolved in solution.

This, therefore, decreased the rate of $CaCO_3$ precipitation at 4 Mpa hence the similar % $CaCO_3$ found at 3 Mpa and 4 Mpa. This implies that because increasing the pressure beyond 3 Mpa did not favour an increased rate of $CaCO_3$ precipitation and thus did not have a significant effect on the % $CaCO_3$ and when also considering the potential additional energy (MW) due to pressurization at 4 Mpa, the pressure of 3 Mpa can be considered the optimum pressure for $CaCO_3$ precipitation when using AMD wastewater as the solvent.

Jo, Ahn, et al. (2012) found that for lower CO_2 pressures (Mpa), the precipitation to $CaCO_3$ was preferred as the highest % $CaCO_3$ in their study was achieved at 0.1 Mpa. Iizuka et al. (2004) also found that $CaCO_3$ precipitation was favoured at a lower initial CO_2 pressure. In this study, although a slightly lower pressure than 4 Mpa was favoured for precipitation, the pressure of 3 Mpa, however, was still high enough to promote an effective rate of carbonation but not too high to hinder $CaCO_3$ precipitation.

This indicates that a balance between pressure conditions that promote an effective rate of carbonation without hindering the precipitation process to form $CaCO_3$ is critical for ensuring an effective carbonation process because results from Figure 5.4 indicate that although a high % $CaCO_3$ was achieved at 4 Mpa, there was no significant increase in the % $CaCO_3$ formed when the initial CO_2 pressure was increased from 3 Mpa to 4 Mpa as the % $CaCO_3$ formed was 4.37 % and 4.53 % respectively. As mentioned previously, this was possibly due to the fact that over the reaction time of 120 min at the highest pressure of 4 Mpa, the solubility of calcium (Ca^{2+}) increased as higher pressure creates a more acidic environment, which favours the solubility of calcium (Ca^{2+}) but not the $CaCO_3$ precipitation.

As the solubility of calcium (Ca^{2+}) was favoured at a higher pressure, this meant that calcium (Ca^{2+}) from the $CaCO_3$ formed could dissolve back into solution causing a decrease in the rate of $CaCO_3$ formation. This implies that the rate of $CaCO_3$ formation decreased at a higher pressure as expected because higher pressure does not favour the precipitation of carbonates as observed by Ji & Yu (2018). Ultimately, the $CaCO_3$ precipitation was favoured at a slightly lower pressure which was 3 Mpa and as mentioned, the pressure of 3 Mpa can thus be considered the optimum pressure for $CaCO_3$ precipitation as it was high enough to promote an effective rate of carbonation but did not hinder the precipitation of $CaCO_3$. Overall, the effect of pressure on the total amount of % $CaCO_3$ formed for direct carbonation with AMD was consistent with the effect of initial CO_2 pressure (Mpa) observed in the studies previously mentioned including the study conducted by Dananjayan et al. (2016), whereby a slightly higher initial CO_2 pressure (Mpa) of up to 0.4 Mpa resulted in a higher sequestration capacity compared to lower initial CO_2 pressures of 0.1 Mpa, 0.2 Mpa and 0.3 Mpa used in their study.

The effect of the reaction time (min) on the % $CaCO_3$ formed can also be observed from Figure 5.4 whereby a higher amount of $CaCO_3$ was formed over the longer reaction time of 120 min. This can also be attributed to calcium (Ca^{2+}) extraction. The calcium (Ca^{2+}) extraction results obtained when AMD was used (see Figure 5.3), show that there was a higher rate of calcium (Ca^{2+}) extraction in the first 30 min as the calcium (Ca^{2+}) concentration increased from the initial concentration of 362.5 ppm to 951.1 ppm, however, there was still a significant increment in the calcium (Ca^{2+}) concentration beyond 30 min as the concentration between 30 min and 120 min increased from 951.1 ppm to 1265 ppm.

This means that there was still a significant rate of calcium (Ca^{2+}) extraction after 30 min which resulted in more consumption of CO_2 to form more $CaCO_3$ after 30 min of the 120 min long carbonation reaction. This, therefore, explains the higher amount of % $CaCO_3$ formed over 120 min because the rate of carbonation and rate of CO_2 consumption were consistently high throughout the 120 min reaction, hence the significantly higher amount of % $CaCO_3$ formed after 120 min.

This shows that because there was high enough calcium (Ca^{2+}) extraction throughout the reaction, a significant rate of carbonation was maintained throughout the 120 min carbonation reaction and thus more $CaCO_3$ could form over 120 min of direct carbonation. Therefore, for the current work, when effective calcium (Ca^{2+}) extraction was achieved over time (min), it was expected that a higher % $CaCO_3$ would form after the longest reaction time of 120 min and at a higher initial CO_2 pressure (Mpa) because the calcium (Ca^{2+}) extraction was the rate-limiting step. When considering the effect of reaction time (min), the study by Dananjayan et al. (2016) also found that a higher reaction time of 600 min resulted in an increase in the sequestration capacity.

Although there was a higher % $CaCO_3$ formed after 120 min, the % $CaCO_3$ formed after 90 min was still close to the % $CaCO_3$ formed after 120 min for most cases and this was due to the minor amount of calcium (Ca^{2+}) extracted after 90 min (see Figure 5.3). In addition, results from Figure 5.4 show that due to the higher calcium (Ca^{2+}) concentration obtained from AMD leaching, the solution during the carbonation process was highly saturated, therefore, more $CaCO_3$ could form through precipitation under the highly saturated conditions. The results from direct carbonation with AMD indicate that there was more effective storage of CO_2 as $CaCO_3$ compared to direct aqueous carbonation. This result was expected because of the additional calcium (Ca^{2+}) concentration provided by the AMD wastewater. Furthermore, using a lower S/L ratio of 0.2 g/mL for AMD carbonation experiments ensured better solubility of calcium (Ca^{2+}) and a faster degree of CO_2 consumption due to a higher concentration of calcium (Ca^{2+}) available. This explains the higher % $CaCO_3$ formed for direct carbonation with AMD.

The higher amount of $CaCO_3$ formed as a result of using AMD wastewater as a reaction medium was consistent with findings from the study such as the one conducted by Lee et al. (2016) where a high % $CaCO_3$ of 33.46 % was achieved when AMD wastewater was used for the CO_2 storage process. The use of a higher stirring speed of 400 rpm was also an important contributing factor to the higher % $CaCO_3$ formed for direct carbonation with AMD wastewater compared to direct aqueous carbonation as it improved mass transfer of CO_2 and diffusion of calcium (Ca^{2+}) for more effective $CaCO_3$ formation.

Overall, for direct carbonation with AMD wastewater, the effect of a higher initial CO_2 pressure (Mpa) and a longer reaction time can be observed to have a significant effect on the amount of % $CaCO_3$ formed. The highest increase in the % $CaCO_3$ formed was found to be 4.53 % at 4 Mpa after 120 min of direct carbonation and this was higher than the maximum % $CaCO_3$ of 2.43 % formed for direct aqueous carbonation for the same conditions of CO_2 pressure (Mpa) applied and reaction time (min).

Again, this can be attributed to additional calcium (Ca^{2+}) provided by the AMD wastewater and more effective calcium (Ca^{2+}) extraction achieved due to the optimization process of certain parameters. However, although the % $CaCO_3$ achieved was higher for carbonation using AMD wastewater compared to when water was used, the CO_2 stored as $CaCO_3$ was possibly slightly reduced due to the small concentration of other elemental species such as Fe^{2+} and Mg^{2+} present in the AMD, as these elements also contain the ability to be converted into mineral form thereby storing CO_2. The total % $CaCO_3$ formed was also influenced by the formation of mineral phases, such as gypsum and ettringite, as shown in the results obtained from XRD analysis as the formation of these phases resulted in a reduced amount of calcium (Ca^{2+}) available for the reaction with CO_2, which resulted in a reduced amount of % $CaCO_3$ formed.

5.2.2 Effect of pressure (Mpa) over time (min) on CE (%)

The CE (%) (refer to Appendix A for calculation) was also considered for direct carbonation with AMD wastewater over 30 min, 60 min, and 120 min, at 70 ^{0}C, using a S/L ratio of 0.2 g/mL and a stirring speed of 400 rpm, as shown in Figure 5.5:

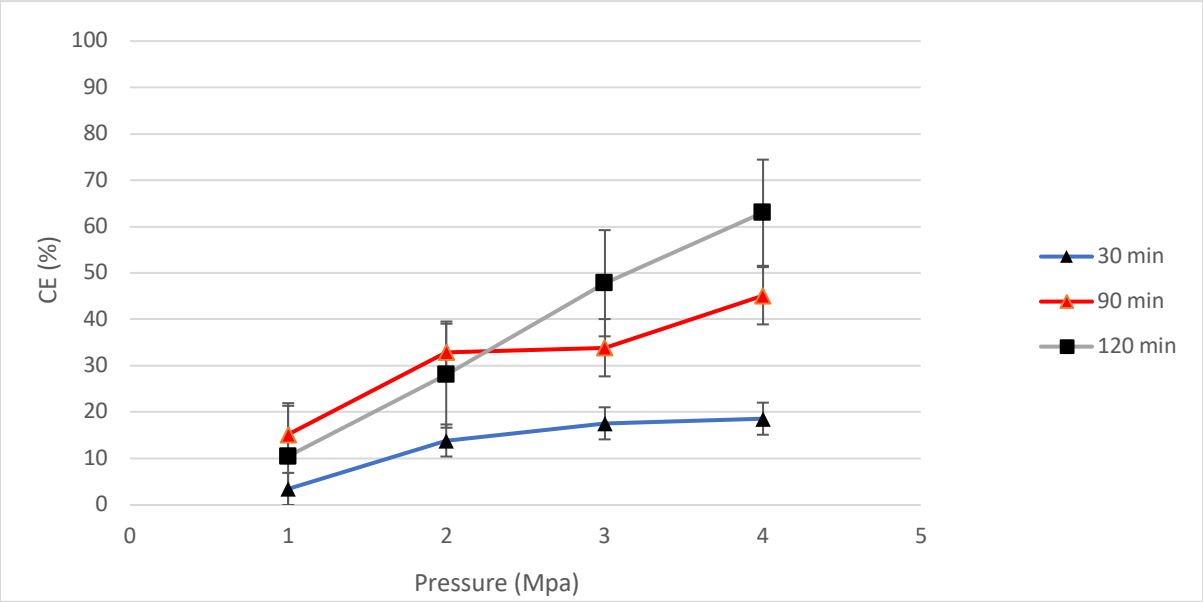

Figure 5.5: Effect of pressure (Mpa) over time (min) on the CE (%) (70 ^{0}C, 0.2 g/mL, 400 rpm)

The effect of initial CO_2 pressure (Mpa) after a reaction time of 30 min, 90 min, and 120 min is shown in Figure 5.5, and the CE (%) shows a similar trend to the one observed from previous results, whereby the CE (%) increased with increasing initial CO_2 pressure (Mpa) for the same reaction time (min). The CE (%) can be seen to increase considerably from 3 Mpa to 4 Mpa for the 120 min and 90 min reactions. The higher increase in the CE (%) for increasing CO_2 pressure after 120 min and 90 min compared to the CE (%) obtained after 30 min, was due to higher concentration of CO_2 molecules available and also the calcium (Ca^{2+}) extraction (see Figure 5.3) as there was still a significant amount of calcium (Ca^{2+}) extracted after 30 min of the 120 min and 90 min reaction which meant that because more calcium (Ca^{2+}) was still being extracted into solution, the solution was still relatively alkaline after 30 min for both these reactions meaning more CO_2 could dissolve and react with calcium (Ca^{2+}) thus promoting a faster degree of CO_2 consumption, higher overall pressure drop and hence the higher CE (%) observed for increasing CO_2 pressure after 120 min and 90 min of direct carbonation. Due to the insignificant increase in the calcium (Ca^{2+}) concentration after 120 min and 90 min (see Figure 5.3), the maximum CE (%) achieved over 120 min and 90 min was not significantly different as shown in Figure 5.5.

The maximum CE (%) achieved after 120 min and 90 min were significantly higher compared to the maximum CE (%) achieved after 30 min of direct carbonation at 3 Mpa and 4 Mpa. Given that CO_2 dissolution is promoted under alkaline conditions and there was a continual increase in the calcium (Ca^{2+}) concentration for the 120 min and 90 min reactions, more CO_2 could still be dissolved especially at the higher initial CO_2 pressures of 3 Mpa and 4 Mpa as more CO_2 molecules were available meaning that the rate of carbonation, as well as CO_2 consumption were still relatively high after 30 min of the 120 min and 90 min reaction for a pressures of 3 Mpa and 4 Mpa. This explains the higher CE (%) achieved at 3 Mpa and 4 Mpa over the 120 min and 90 min because there was a higher overall pressure drop due to the total CO_2 consumption for a higher CO_2 pressure over the same reaction time (min).

The effect of the reaction time (min) on the CE (%) formed can also be observed from Figure 5.5 wherein a higher amount of CE (%) was achieved over the longer reaction times of 120 min and 90 min compared to 30 min at 3 Mpa and 4 Mpa. This can also be attributed to the calcium (Ca^{2+}) extraction, as the calcium (Ca^{2+}) extraction results obtained when AMD wastewater was used (see Figure 5.3), show that there was still a significant increment in the calcium (Ca^{2+}) concentration beyond 30 min as the concentration between 30 min and 120 min increased from 951.1 ppm to 1265 ppm. This means that there was still a significant rate of calcium (Ca^{2+}) extraction after 30 min, which resulted in the consumption of CO_2 to form more $CaCO_3$ after 30 min of the 120 min and 90 min direct carbonation reaction. This, therefore, resulted in a significantly higher overall pressure drop, hence the significantly higher CE (%) obtained over the 120 min and 90 min reactions compared to the 30 min direct carbonation reaction for all cases.

This shows the benefit of a longer reaction time (min) when the calcium (Ca^{2+}) extraction is effective over time (min) because for a longer reaction time (min), the overall pressure drop due to $CaCO_3$ formation was higher and subsequently the CE (%) increased. In addition, the highest CE (%) of 63 % observed after 120 min was when an initial CO_2 pressure of 4 Mpa was used, which was the highest initial CO_2 pressure used. This was expected because of the higher availability of CO_2 molecules that could react with calcium (Ca^{2+}) in solution over the longer reaction time (min) which resulted in a faster rate of carbonation and overall a higher pressure drop due to $CaCO_3$ formation, hence the higher CE (%) reported after 120 min at a pressure of 4 Mpa.

This also agrees with the results for the % $CaCO_3$ as the highest % $CaCO_3$ was formed at the same conditions (i.e., 120 min at 4 Mpa) which again shows the correlation between the two carbonation performance measures (i.e., % $CaCO_3$ formed and the CE %). The highest CE (%) achieved of 63 % for direct carbonation using AMD wastewater was notably higher than the CE (%) of 29.4 % and 35.2 % achieved for direct and indirect aqueous carbonation respectively and this was due to the AMD wastewater providing an additional source of calcium (Ca^{2+}). The increase in calcium (Ca^{2+}) concentration when AMD wastewater was used thus promoted a faster rate of carbonation and CO_2 consumption resulting in a higher overall pressure drop due to $CaCO_3$ formation and hence the higher CE (%) reported for reactions involving AMD wastewater. As mentioned previously the increase in the stirring speed up to 400 rpm and the lower S/L ratio for experiments with AMD wastewater were also contributing factors to the higher CE (%) achieved for direct carbonation with AMD wastewater.

Additionally, the CE (%) achieved for direct carbonation with AMD wastewater of 63 % was higher than the CE (%) of 53.9 % achieved for indirect carbonation with AMD. The reason for the higher CE (%) achieved for direct carbonation using AMD was that calcium (Ca^{2+}) could still be leached from the fly ash during direct carbonation, whereas for indirect carbonation, the process relies on only the calcium (Ca^{2+}) extracted with no additional extractable calcium (Ca^{2+}) from the fly ash over the course of the reaction.

5.3 Maximum CO_2 storage capacity (kg/kg fly ash)

The theoretical maximum CO_2 storage capacity for this work was found to be 0.042 kg/kg fly ash. Theoretically, if all oxides react to form carbonates, the sequestration capacity of the Durapozz fly ash is 4.2 %. This means that for every 1 tonne or kg of fly ash, 0.042 tonnes or kg of CO_2 can be sequestered by the fly ash. From the theoretical CO_2 storage capacity and considering the highest carbonation efficiency (CE %) of 63 % achieved in this study from direct carbonation with AMD, the maximum CO_2 storage capacity was found to be 0.026 kg/kg fly ash and was similar to the storage capacity achieved by Montes-Hernandez et al. (2009). Given that the actual maximum amount of CO_2 that can be sequestered depends on the CaO (wt. %) content of the material, the storage capacity reported in this study was similar to the storage capacity reported by Montes-Hernandez et al. (2009) due to similar CaO (wt. %) content. The fly ash used in this study contains a CaO (wt. %) content of 4.06 % while the CaO (wt. %) from the study conducted by Montes-Hernandez et al. (2009) was 4.1 %.

Muriithi (2009) found that for Secunda fly ash, the maximum CO_2 storage capacity for the Secunda fly ash was 0.062 kg/kg fly ash which was higher than the 0.026 kg/kg fly ash obtained for this work. The maximum CO_2 storage capacity of the Secunda fly ash was higher than the Durapozz fly ash that was used for this work due to the higher CaO (wt. %) content of 9.198 % that was available in the Secunda fly ash. The Durapozz fly ash used in this study had a lower CaO (wt. %) content of 4.06 %, hence the maximum CO_2 storage capacity was lower than the one found by Muriithi (2009).

Dananjayan et al. (2016) also achieved a slightly higher CO_2 storage capacity of 0.05 kg/kg fly ash compared to the 0.026 kg/kg fly ash obtained in this study and this was due to the higher CaO (wt. %) content in the coal fly ash (CFA) used in their study which was 6.74 % compared to the lower 4.06 CaO (wt. %) content in the fly ash used in this work. The study conducted by Jo, Ahn, et al. (2012) also showed the importance of the CaO (wt. %) content on the CO_2 storage capacity as a higher CO_2 storage capacity of 0.071 kg/kg fly ash was achieved in their work due to the higher CaO (wt. %) content of 15 % found in the fly ash used in their study.

5.4 Characterisation of carbonated solid residues for direct carbonation with AMD

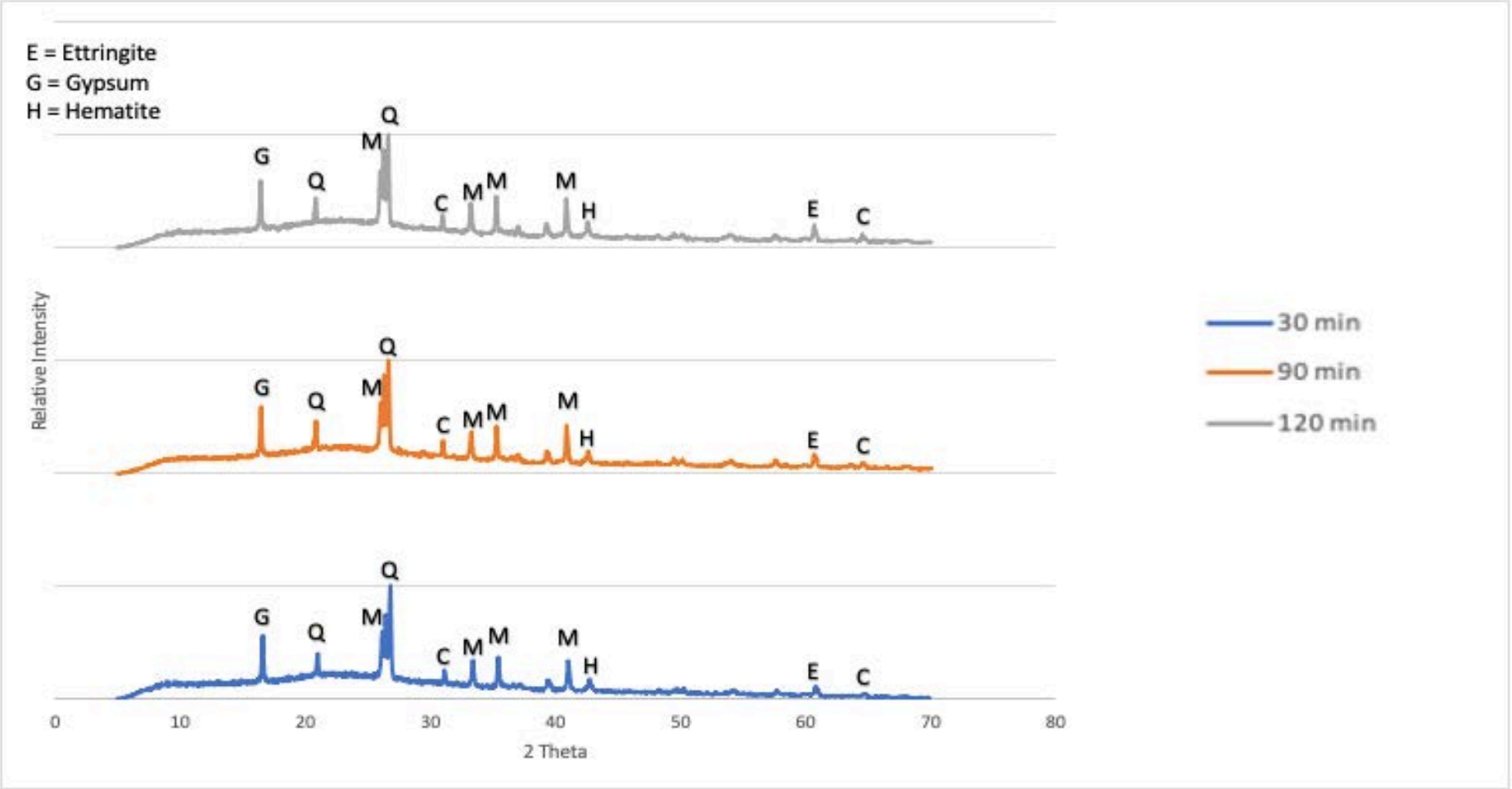

Figure 5.6: XRD pattern from direct carbonation with AMD (70 ^{0}C, 4 Mpa, 0.2 g/mL, 400 rpm)

5.4.1 Results from XRD analysis

The results from Figure 5.6 show the XRD pattern for carbonated solid residues after 30 min, 90 min, and 120 min of direct carbonation with AMD wastewater at an initial CO_2 pressure of 4 Mpa, at 70 ^{0}C, using a S/L ratio of 0.2 g/mL at a stirring speed of 400 rpm. The XRD pattern for the fresh fly ash shown in Figure 4.1 shows that the fly ash was originally composed of crystalline phases in the form of quartz and mullite with weaker peaks identified for magnetite. The XRD pattern displayed in Figure 5.6 shows newly identifiable phases for the solid residues after carbonation with AMD wastewater, and while the XRD pattern still showed the presence of major crystalline phases such as quartz and mullite, which were contained in the raw fly ash sample, new phases in the form of gypsum ($CaSO_4$), hematite (Fe_2O_3), and calcite ($CaCO_3$) were present as well. The presence of gypsum ($CaSO_4$) was further confirmed by the decrease in the concentration of sulfate (SO_4^{2-}) from its original concentration of 990.1 ppm (see Table 5.1), to lower concentrations of 210.1 ppm, 189.9 ppm, and 151.2 ppm over 30 min, 90 min, and 120 min, respectively, after carbonation at 4 Mpa, which therefore suggests that calcium (Ca^{2+}) reacted with SO_4^{2-}, thus resulting in the formation of the new phase, namely gypsum.

5.4.2 Results from XRF analysis

XRF analysis of carbonated solid residues was conducted to determine the concentration of species after direct carbonation with AMD wastewater as shown in Table 5.2:

Table 5.2: Analysis of elemental compositions from XRF analysis for direct carbonation with AMD

Element	Composition (wt. %)
SiO_2	52.2
Al_2O_3	33.67
Cr_2O_3	3.9
CaO	3.35
Fe_2O_3	3.2
TiO_2	1.7
MgO	0.81
K_2O	0.67
P_2O_5	0.44
Na_2O	0.31
MnO	0.04
Total	100

Table 5.2 shows results from XRF for direct carbonation with AMD wastewater after 120 min at 4 Mpa. The results indicate that there was a decrease in the CaO content in the solid residue as there was an amount of 3.35 wt. % after carbonation compared to the original 4.06 wt. % found in the raw fly ash. This can be attributed to the calcium (Ca^{2+}) extraction step during the precipitation to form $CaCO_3$ during the carbonation reaction which resulted in a reduced CaO (wt %) content.,

5.5 AMD neutralization by direct carbonation

The neutralization of AMD wastewater through the direct carbonation process was considered. This section provides results for the neutralization of AMD wastewater under various conditions.

5.5.1 pH neutralization

Figure 5.7 presents the pH results obtained after direct carbonation of with AMD wastewater over 30 min, 90 min, and 120 min at 70 ^{0}C, using a S/L ratio of 0.2 g/mL and a stirring speed of 400 rpm:

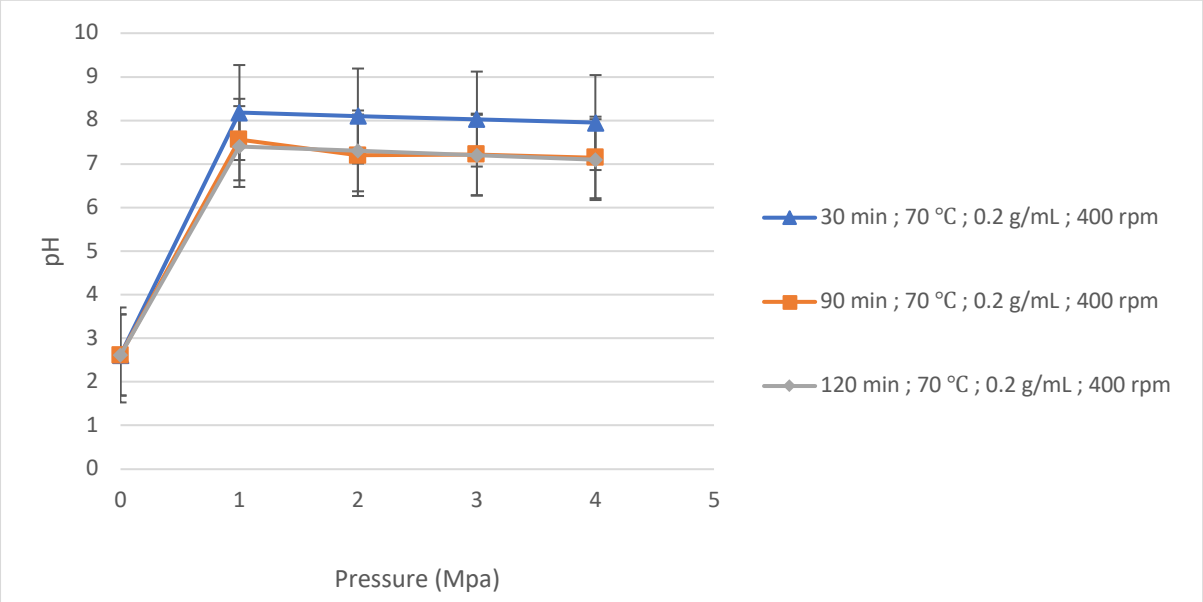

Figure 5.7: Effect of pressure on pH measured

Given that an autoclave system was used for this work, it was difficult to track the pH of the solution over the duration of the experiments. However, the behaviour of the pH over the course of the reaction was postulated from results obtained from the calcium (Ca^{2+}) extraction (see Figure 5.3) and also from the known effect of CO_2 pressure on the pH. Figure 5.7 shows that the initial pH of the AMD wastewater used was 2.63, which was within the expected range for AMD wastewater.

As the fly ash was stirred with the AMD, the pH increased, and based on leaching experiments (see Figure 5.3), there was a higher increase in alkalinity of the solution during direct carbonation with AMD in the initial stages of the reaction as there was a high rate of calcium (Ca^{2+}) extraction in the first 30 min of the reaction. It is worth noting that over the course of the reaction, the hydrolysis of AMD components such as Fe^{2+} and Al^{3+} caused an offset in the pH increase. Given that the rate of calcium (Ca^{2+}) extraction decreased over time (min) and with CO_2 present in the system, the pH decreased due to the dissolved CO_2 and generation of H^+ ions in solution. From results obtained in Figure 5.7, the solution pH approaches neutrality for all cases as the initial CO_2 pressure (Mpa) increases however for a higher initial CO_2 pressure, the pH was driven slightly more closer to neutral pH and this can be attributed to the higher concentration of CO_2 molecules present for a higher CO_2 pressure.

For a higher initial CO_2 pressure (Mpa), more CO_2 was dissolved under alkaline conditions at the initial stages of the reaction therefore at the latter stages of the reaction as calcium (Ca^{2+}) extraction decreased, for a higher CO_2 pressure, the higher concentration of CO_2 meant that there was still more CO_2 available at the latter stages of the reaction and more H_2CO_3 was available that dissociated to form HCO_3^- and $2H^+$ thus causing a decrease in solution pH until it approached neutrality.

The closest pH to a neutral pH was 7.1 and was achieved after 120 min at 4 Mpa which shows that for a longer reaction time (min) and higher initial CO_2 pressure (Mpa), more effective neutralization of pH was achieved. The pH variation over the different conditions of pressure considered for the present work was similar to the trend observed by Lee et al. (2016). In their feasibility study of CO_2 storage through the neutralization process of AMD, they found the pH to increase sharply in the initial stages of the reaction but approached a more neutral pH over time upon carbonation.

5.5.2 % Removal of metal ions from direct carbonation with AMD

Figure 5.8 shows the % removal of metal ions in solution during direct carbonation with AMD over 120 min, at 70 ^{0}C, using a S/L ratio of 0.5 g/mL and a stirring speed of 400 rpm:

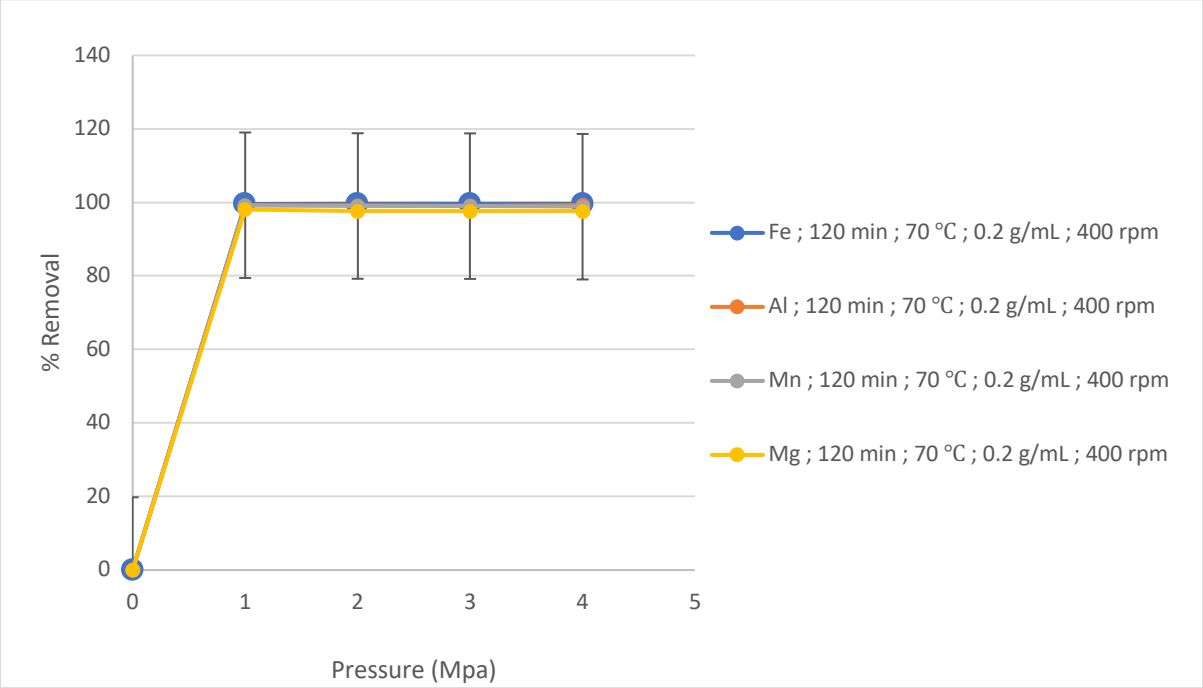

Figure 5.8: % Removal of various metal ions from AMD wastewater

Figure 5.8 shows the effect of the direct carbonation process on the % removal of certain metal ions from AMD wastewater. Overall, there was effective removal of all metal ions as a high % removal was achieved in all cases over 120 min. However, the increase in pressure (Mpa) did not seem to have a significant effect on the % removal of metal ions. The % removal of metal ions was mainly due to the precipitation of metal hydroxides. The hydrolysis of Al^{3+}, Fe^{2+}, Mg^{2+}, and Mn^{2+} resulted in the precipitation of these metals to form insoluble hydroxides which led to their removal. Gitari et al. (2018) also found that the hydrolysis of metal ions such as Al^{3+}, Fe^{2+}, Mg^{2+}, and Mn^{2+} causes the precipitation of these metal ions as insoluble hydroxides thus leading to their removal. The high % removal of close to 100 % for all elements considered suggests that the concentration of these elements after treatment was within the target water quality range.

5.6 Indirect carbonation with AMD

This section presents results related to indirect carbonation with AMD wastewater with the experimental detail given in Chapter 3, Section 3.3.2.3.

5.6.1 Effect of time (min) on calcium (Ca^{2+}) leaching with AMD before carbonation

The calcium (Ca^{2+}) extraction was done as required before carbonation of the leachate for indirect carbonation with AMD wastewater and the leaching was done over 30 min, 60 min, 90 min, and 120 min, at 70 ^{0}C, using a S/L ratio of 0.2 g/mL and at a stirring speed of 400 rpm as shown in Figure 5.9:

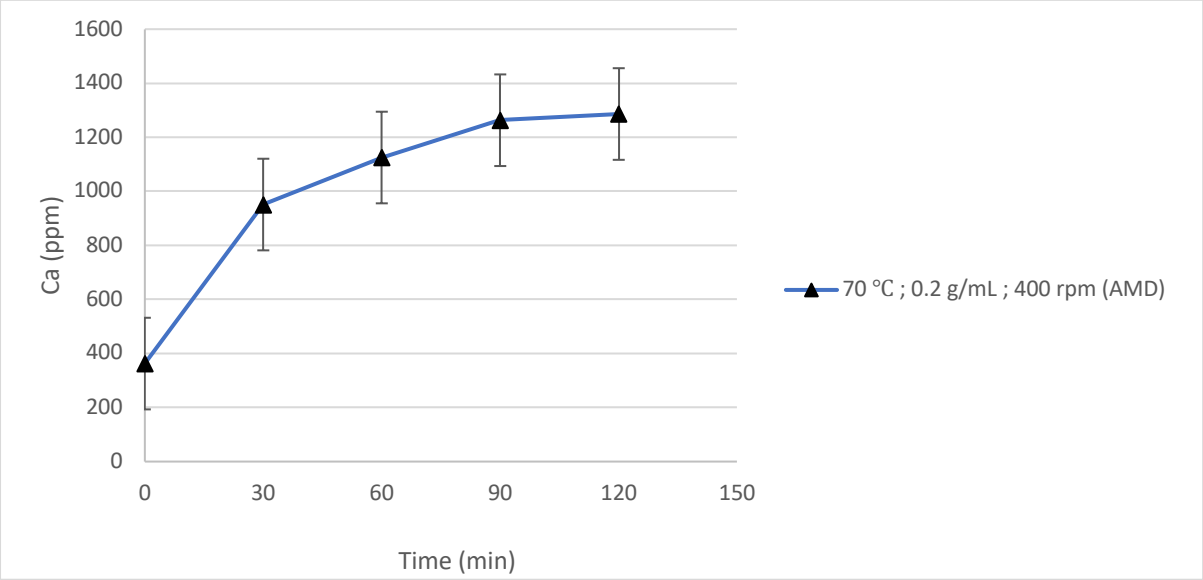

Figure 5.9: Effect of time (min) on calcium (Ca^{2+}) extraction from ICP-OES analysis

Figure 5.9 shows the results from leaching experiments when AMD wastewater was used. The results indicate that there was a higher rate of calcium (Ca^{2+}) extraction in the first 30 min as the concentration increased significantly from the initial calcium (Ca^{2+}) concentration of 362.5 ppm present in the AMD to 951.1 ppm. Notably, there was still an increment in the calcium (Ca^{2+}) concentration after 30 min as the concentration between 30 min and 120 min increased from 951.1 ppm to 1265 ppm. This means that there was still a relatively high rate of calcium (Ca^{2+}) extraction after 30 min.

5.6.2 Effect of pressure (Mpa) over time (min) on CE (%)

Similar to experiments done using water, the % $CaCO_3$ formed could not be considered for CO_2 storage using AMD wastewater as there was not enough solid recovered, however, the CE (%) was considered for the process and the results presented in Figure 5.10 were for the calculated CE (%) from indirect carbonation with AMD over 30 min, 90 min, and 120 min, at a temperature of 70 ^{0}C, using a S/L ratio of 0.2 g/mL and a stirring speed of 400 rpm as shown in Figure 5.10:

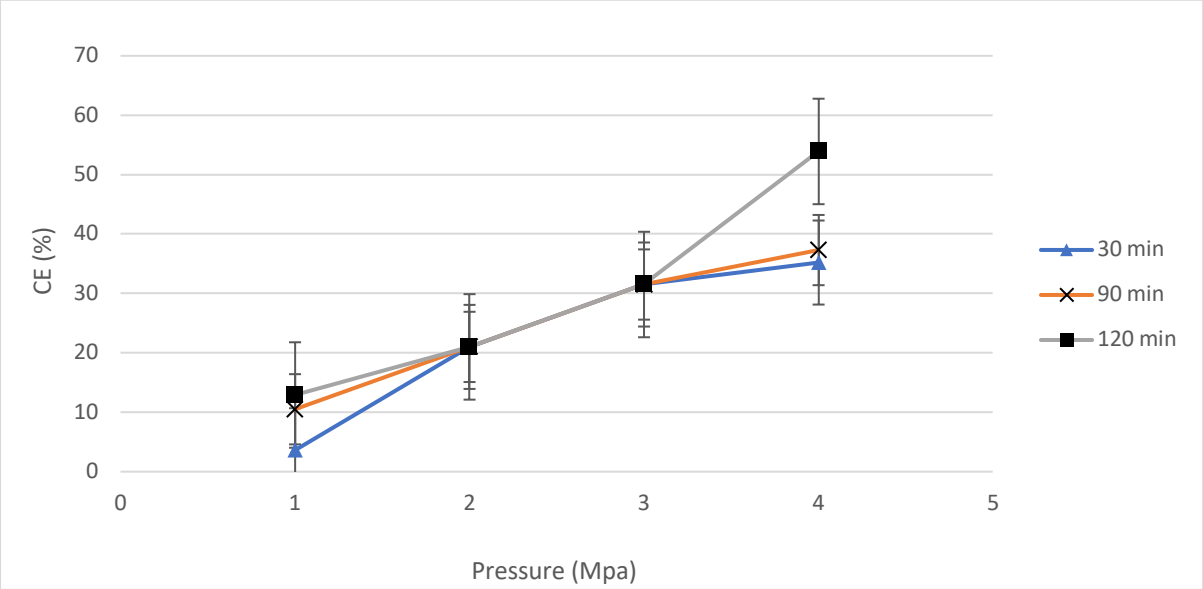

Figure 5.10: Effect of pressure (Mpa) on the CE (%) achieved (70 ^{0}C, 0.2 g/mL, 400 rpm)

Figure 5.10 exhibited a similar trend to results reported previously for the CE (%). For indirect carbonation with AMD wastewater, the CE (%) increased with increasing initial CO_2 pressure (Mpa) in all cases, with the highest CE (%) of 53.9 % obtained after 120 min of carbonating the leachate at 4 Mpa. The results indicate that as expected, the CE (%) was dependent on the amount of CO_3^{2-} molecules that were available in solution and could react with calcium (Ca^{2+}) to form precipitated $CaCO_3$ and that the higher the CO_2 pressure, the higher the concentration of CO_2 molecules available for the reaction with calcium (Ca^{2+}) which resulted in a faster rate of carbonation and hence a higher CE (%). The CE (%) obtained from indirect carbonation with AMD wastewater was notably higher than that obtained for both direct and indirect aqueous carbonation processes.

Similar to the indirect aqueous carbonation process, the CE (%) for indirect carbonation with AMD wastewater was a function of the calcium (Ca^{2+}) content in the leachate and given the additional calcium (Ca^{2+}) provided by AMD wastewater to enhance the carbonation process, it was expected that a higher carbonation efficiency CE (%) of 53.9 % would be achieved for the indirect carbonation route involving AMD wastewater compared to the lower CE (%) of 29.4 % and 35.2 % achieved for direct and indirect aqueous carbonation respectively.

The significant increase in the CE (%) at the highest initial CO_2 pressure of 4 Mpa over the same reaction time of 120 min observed in Figure 5.10 can be attributed to the higher calcium (Ca^{2+}) concentration in the leachate for the 120 min carbonation reaction. Given that CO_2 dissolution is promoted under alkaline conditions, more CO_2 could still be dissolved especially at the higher initial CO_2 pressure of 4 Mpa as more CO_2 molecules were available meaning that the rate of carbonation, as well as CO_2 consumption, was consistently higher throughout the 120 min carbonation of the leachate at 4 Mpa, hence the significant effect of pressure (Mpa) on the CE (%) at 4 Mpa after 120 min observed in Figure 5.10.

The effect of the reaction time (min) on the CE (%) can also be observed from Figure 5.10 whereby a higher CE (%) was achieved over the longer reaction time of 120 min at 4 Mpa. This was also due to the calcium (Ca^{2+}) concentration present in the leachate for the 120 minute reaction. As mentioned previously, from the calcium (Ca^{2+}) extraction results obtained when AMD was used (see Figures 5.3 and 5.9), there was higher calcium (Ca^{2+}) extraction in the first 30 min as the calcium (Ca^{2+}) concentration increased from the initial concentration of 362.5 ppm to 951.1 ppm, however, there was still a significant increment in the calcium (Ca^{2+}) concentration after 30 min as the concentration between 30 min and 120 min increased from 951.1 ppm to 1265 ppm.

This, therefore, explains the higher CE (%) achieved over 120 min at 4 Mpa because the rate of carbonation and rate of CO_2 consumption were consistently high throughout the 120 min reaction which led to a higher overall pressure drop, hence the significantly higher amount of CE (%) achieved over 120 min at a CO_2 pressure of 4 Mpa. The results in Figure 5.10 indicate that there was similar CE (%) observed at 2 Mpa after 30 min, 90 min and, 120 min and this was possibly due to the lower CO_2 initial pressure (Mpa) applied.

This meant that the carbonation reaction was possibly not fast enough for the lower initial CO_2 pressures as less CO_2 molecules were available to react with calcium (Ca^{2+}). This implies that even though calcium (Ca^{2+}) extraction is the rate limiting step for the process, a lower pressure (Mpa) can still affect the rate of carbonation and hence CE (%). When considering the increase in calcium (Ca^{2+}) extraction over time (min) when AMD was used as the reaction solvent and the fact that the pressure at 3 Mpa was high enough, the overall CE (%) achieved was expected to increase over time at 3 Mpa.

However, the results presented in Figure 5.10 show that there was a similar CE (%) achieved at 3 Mpa after 30 min, 90 min and 120 min. This deviation was possibly caused errors in the experiment which could have possibly been from the leakage of CO_2 from the reaction system when the experimental runs were carried out as well as incorrect recording of the final pressure reading after the experiment was conducted.

5.7 AMD neutralization by indirect carbonation

The neutralization of AMD wastewater through indirect carbonation was also considered. This section provides results for the neutralization of AMD wastewater for various conditions.

5.7.1 pH neutralization after carbonation

Figure 5.11 presents the pH results obtained after carbonation of the leachate for the indirect carbonation process with AMD wastewater over 30 min, 90 min, and 120 min, at 70 ^{0}C, using a S/L ratio of 0.2 g/mL and a stirring speed of 400 rpm:

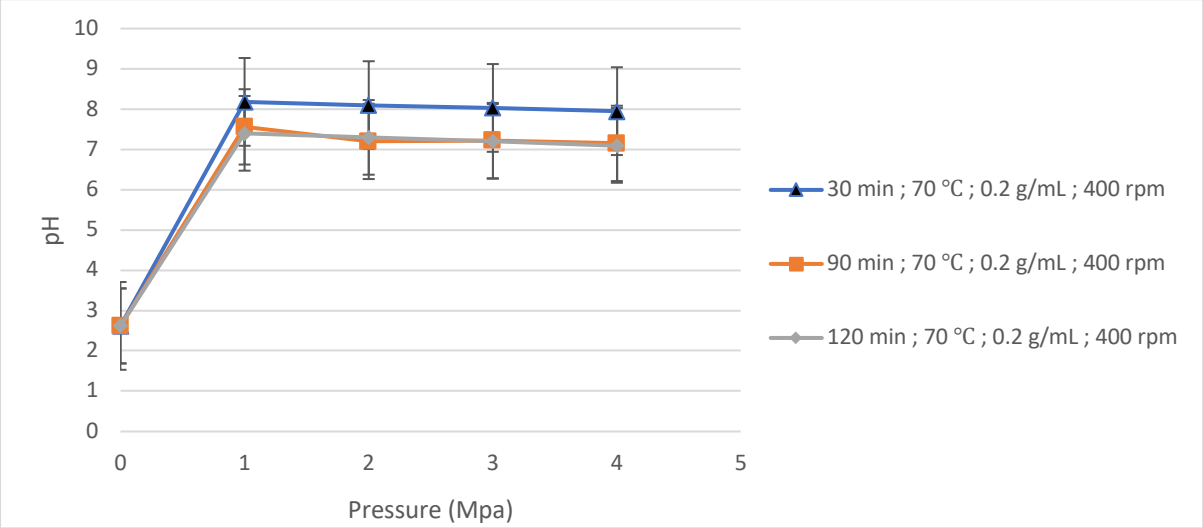

Figure 5.11: Effect of pressure (Mpa) on pH measured

Figure 5.11 shows the results of solution pH after the carbonation of the leachate for indirect carbonation with AMD wastewater. The results indicate that an effective neutralization of AMD wastewater was achieved in all cases for increasing initial CO_2 pressure (Mpa). For the indirect carbonation process with AMD wastewater, the pH obtained from the leachate after the initial step which was the calcium (Ca^{2+}) extraction step over 30 min, 90 min, and 120 min was 8.55, 8.20, and 8.22 respectively.

When considering that the pH obtained after carbonation at 4 Mpa after 30 min, 90 min, and 120 min was 7.95, 7.15, and 7.1 respectively, this shows that the carbonation with CO_2 for the sequestration step was effective in neutralizing the AMD wastewater used. The closest pH to a neutral pH which was 7.1 was obtained for the highest pressure of 4 Mpa and this was expected because given that for a higher initial CO_2 pressure (Mpa), more CO_2 was dissolved under alkaline conditions at the initial stages of the reaction, meaning there was still more CO_2 available at the latter stages of the reaction to form H_2CO_3 that dissociated to form HCO_3^- and $2H^+$ thus causing a decrease in solution pH until it approached neutrality.

The reaction time also had an effect on the neutralization process as the closest pH to a neutral pH was achieved after 120 min which shows that for a longer reaction time (min) and higher initial CO_2 pressure (Mpa), more effective neutralization of pH can be achieved. Maleka (2015) also conducted a carbonation study following the neutralization process of AMD and found the pH to decrease from 9.85 to 7.72 upon carbonation. This was attributed to the dissociation of aqueous CO_2 to carbonic acid (H_2CO_3).

5.7.2 % Removal of metal ions after carbonation

Figure 5.12 shows the % removal of metal ions in solution during carbonation of the leachate from the indirect carbonation process with AMD wastewater over 120 min, at 70 ^{0}C, using a S/L ratio of 0.5 g/mL and a stirring speed of 400 rpm:

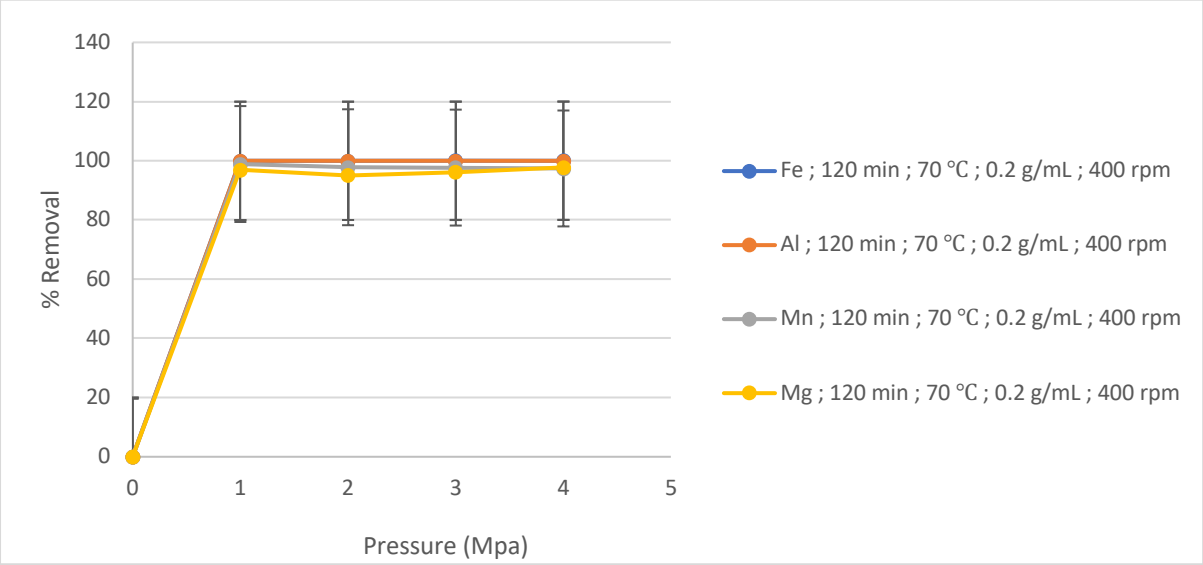

Figure 5.12: % Removal of various metal ions

Figure 5.12 shows the effect of the indirect carbonation process on the % removal of certain metal ions from AMD wastewater. The % removal obtained was close to a 100 % in all cases and the results were similar to the % removal achieved for Fe^{2+}, Al^{3+}, Mn^{2+}, Mg^{2+} for direct carbonation with AMD. Overall, there was effective removal of all metal ions as a high % removal was achieved in all cases over 120 min.

However, the increase in pressure did not have a significant effect on the % removal of metals. Again, as observed with direct carbonation with AMD, the % removal of metal ions can be attributed to the precipitation of metal hydroxides. The hydrolysis of Al^{3+}, Fe^{2+}, Mg^{2+}, and Mn^{2+} resulted in the precipitation of these metals to form insoluble hydroxides which led to their removal and again, this was consistent with findings from Gitari et al. (2018) who also found that the hydrolysis of metal ions such as Al^{3+}, Fe^{2+}, Mg^{2+}, and Mn^{2+} causes the precipitation of these metal ions as insoluble hydroxides thus leading to their removal. Maleka (2015) also achieved a high % removal of some of the major elements present in Kundalila Gold Mine water as a 100 % removal of Al^{3+}, Fe^{2+}, Mg^{2+}, and Mn^{2+} was achieved after 210 min during the various treatment combinations.

5.8 Results Summary

The results obtained for the various carbonation performance measures used in this study were summarised. Table 5.3 shows a summary of results for the highest percentage $CaCO_3$ formed from direct aqueous carbonation and direct carbonation with AMD wastewater achieved after 120 min of direct carbonation for CO_2 at a pressure of 4 Mpa. Table 5.3 also presents results for the maximum carbonation efficiency (CE %) achieved from direct aqueous carbonation, direct carbonation with AMD wastewater, indirect aqueous carbonation, and indirect carbonation with AMD wastewater after 120 min at 4 Mpa. The maximum CO_2 storage capacity (kg/kg fly ash) was also presented, as were the pH values that were closest to reaching neutrality obtained from the AMD neutralization process using direct and indirect carbonation.

Table 5.3: Results Summary

	Direct aqueous carbonation	Indirect aqueous carbonation	Direct carbonation with AMD	Indirect carbonation with AMD
% $CaCO_3$	2.43	-	4.53	-
CE (%)	29.4	35.2	63	53.9
Maximum CO_2 storage capacity (kg/kg fly ash)	-	-	0.026	-
pH			7.1	7.1

When considering the % $CaCO_3$, results from Table 5.3 indicate that there was a maximum % $CaCO_3$ formed of 2.43 % from the direct aqueous carbonation process while there was a maximum % $CaCO_3$ formed of 4.53 % from direct carbonation with AMD wastewater. It was found that the higher % $CaCO_3$ formed for direct carbonation with AMD wastewater was due to the lower S/L ratio used for the process which led to higher extraction of calcium (Ca^{2+}), the additional calcium (Ca^{2+}) concentration of 362.5 ppm which was originally present in the AMD wastewater and the higher stirring speed used for experiments involving AMD wastewater.

The highest CE (%) was 63 % and was achieved from direct carbonation with AMD wastewater after 120 min of direct carbonation at 4 Mpa. This was followed by the second highest CE (%) of 53.9 % achieved from indirect carbonation with AMD under the same process conditions. The higher CE (%) through the direct route was possibly due to the continued extraction of calcium (Ca^{2+}) from the fly ash during the direct carbonation reaction. There was a notably lower CE (%) achieved when pure water was used as the solvent compared to when AMD wastewater was utilized. The carbonation efficiency CE (%) from direct aqueous carbonation was 29.4 % while the CE (%) achieved from the indirect aqueous route was 35.2 % after 120 min of carbonation at 4 Mpa. This can also be attributed to the lower S/L ratio applied for the AMD carbonation study, the additional calcium (Ca^{2+}) concentration provided by the AMD wastewater as well as the higher stirring speed of 400 rpm for the AMD carbonation study.

The higher CE (%) achieved from the indirect aqueous route compared to the CE (%) achieved from the direct aqueous route was due to the higher stirring rate (rpm) used for indirect aqueous carbonation which improved the calcium (Ca^{2+}) extraction. Considering the higher CE (%) achieved for the indirect aqueous carbonation route, the increase in the stirring speed from 100 rpm to 400 rpm before indirect aqueous carbonation experiments were conducted was justifiable because the total energy consumed due to the increase in the stirring speed did not significantly affect the total energy output of the process. The maximum CO_2 storage which gave an indication of the maximum CO_2 storage potential of the fly ash per 1 kg of fly ash used was also measured and it was found to be 0.026 kg/kg fly ash. It was in the expected range for fly ash material with a CaO (wt. %) of 4.06 %. A pH of 7.1 was achieved for direct and indirect carbonation with AMD wastewater after 120 min and for CO_2 pressure of 4 Mpa. The pH under these conditions was close to a neutral pH of 7.

CHAPTER 6

6.1 Material balance: CO_2 mass balance

From the general mass balance

$$Input + Generation = Accumulation + Consumption + Output$$

The molecular species balance was considered for the process:

$$\therefore Generation = 0$$

Steady-state was assumed for the carbonation reaction as there was no material build-up within the system over time:

$$\therefore Accumulation = 0$$

Therefore the mass balance reduces to:

$$Input = Consumption + Output$$

The CO_2 mass balance was used to account for the CO_2 uptake in the reaction system. It was assumed that the CO_2 fed into the reaction system $(i.e., Input: \sum CO_{2(in)})$ was equivalent to the sum of the CO_2 consumed due to the carbonation reaction $(i.e., \sum CO_{2(consumption)})$ and the unreacted CO_2 from the carbonation process $(i.e., Output: \sum CO_{2(out)})$. The CO_2 mass balance was therefore given as:

$$\sum CO_{2(in)} = \sum CO_{2(\text{consumption})} + \sum CO_{2(out)}$$

The optimum conditions from the direct aqueous carbonation process were also used for the material balance instead of the optimum conditions from direct carbonation with AMD wastewater because they provided a more accurate estimate of the total energy output from the process and because the physical properties of pure water are known. This was because the total mass of CO_2 used for the energy balance was determined from material balance considerations, therefore, the conditions used for both calculations needed to be consistent.

Therefore, by using the optimum process conditions for direct aqueous carbonation of 120 min and 4 Mpa, the mass of CO_2 fed was calculated as:

$\sum CO_{2(in)}$:

$$PV = nRT$$

where V is the reactor volume of 600 mL;

and;

$$P_{CO_2} = 4 \text{ Mpa}$$

For the calculation the pressure (Mpa) was converted to bar, hence:

$$P_{CO_2} = 40 \text{ bar}$$

$$\therefore n = \frac{(40\ bar)(0.6\ L)}{(0.08314472\ L\ bar/K\ mol)\ (343.15\ K)}$$

$$\therefore n_{CO_2} = \ 0.84\ mol$$

$$\therefore Grams\ of\ CO_2 = 0.84\ mol\ \times 44.01\ g/mol\ = 36.97\ g$$

$\sum CO_{2(consumption)}$:

$$n = \frac{P_{carbonation\_pressure\ drop} V}{RT}$$

$$\therefore n = \frac{(15.2\ bar)(0.6\ L)}{(0.08314472\ L\ bar/K\ mol)\ (343.15\ K)}$$

$$\therefore n_{CO_2} = \ 0.32\ mol$$

$$\therefore Grams\ of\ CO_2 = 0.32\ mol\ \times 44.01\ g/mol = 14.08\ g$$

$\sum CO_{2(out)}$:

$$\sum CO_{2(out)} = \sum CO_{2(in)} - \sum CO_{2(consumption)} \ (Dissolved\ CO_2 + \ CO_2\ stored\ as\ CaCO_3)$$

$$\sum CO_{2(out)} = 36.97\ g - (12.0\ g + 2.08\ g) = 22.89\ g$$

The material entering and leaving the system after the carbonation reaction were accounted for in Figure 6.1:

Where;

M represents the total mass entering and leaving the system

X represents the mass fraction of each component within each stream

W reprents the weight fraction of water

The mass of CO_2 entering the system, which was MCO_2, was the total mass of CO_2 fed into the system, and was calculated from the material balance. The mass of water fed, which was MH_2O was determined from the S/L ratio and was 200 g. The mass of water leaving the system was 186 g, meaning that the fraction of water leaving the system (i.e., $X1H_20$) was equivalent to a fraction of 0.93. This means that there was a fraction of water that remained in the solid residue, before drying of the solid and this fraction was $X2H_20$ and was equivalent to 0.07. The fractions of elemental species in fly ash entering and leaving the system were obtained from the XRF results before and after direct aqueous carbonation, while the input and output fractions of $CaCO_3$ (i.e., XCO_2 as $CaCO_3$) were determined from the Chittick test.

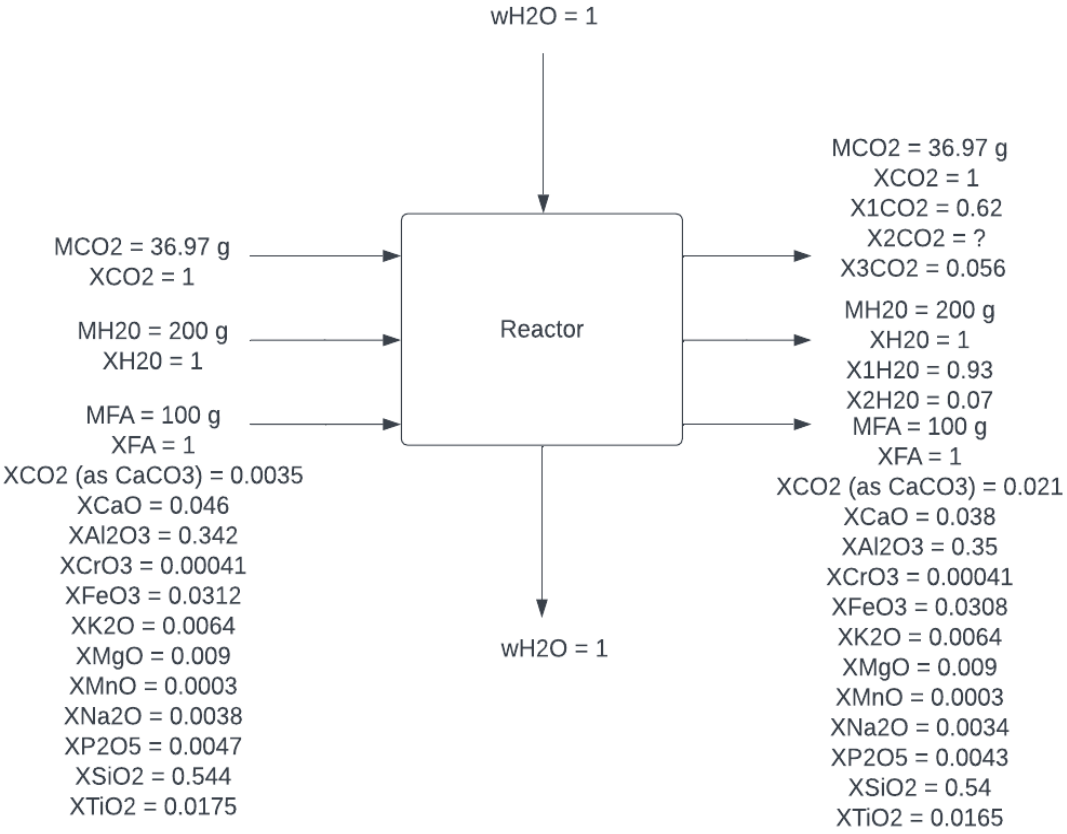

Figure 6.1: PFD for input and output material for carbonation reaction

From the CO_2 component balance:

$$\left(X_{CO_2}\right)\left(M_{CO_2}\right) = \left(\left(X_{1CO_2}\right)\left(M_{1CO_2}\right) + \left(X_{2CO_2}\right)\left(M_{2CO_2}\right) + \left(X_{3CO_2}\right)\left(M_{3CO_2}\right)\right.$$

∴ To determine the fraction of unreacted CO_2 (i.e., X_{1CO_2}), we can substitute for the relevant mass and mass fraction values for input CO_2, CO_2 consumed and CO_2 out:

$$\therefore (1)(36.97\ g) = \left(\left(X_{1CO_2}\right)\left(36.97\ g\right) + (0.32)(36.97) + (0.056)(36.97)\right.$$

$$\therefore 36.97\ g - 11.83\ g - 2.07\ g = \left(X_{1CO_2}\right)\left(36.97\ g\right)$$

$$\therefore X_{1CO_2} = \frac{23.07\ g}{36.97\ g}$$

$$\therefore X_{1CO_2} = 0.62$$

From material balance considerations, the mass and mass fraction of CO_2 that did not react were 22.89 g and 0.62, respectively. This was higher than the total mass obtained for the CO_2 that was consumed of 14.08 g, which was able to participate in the precipitation reaction to form calcium carbonate ($CaCO_3$). This means that there was a higher amount of CO_2 that was undissolved from the process, and given that the main interest for this work was to determine the amount of CO_2 permanently stored in mineral carbonate form as $CaCO_3$, the highest percentage of $CaCO_3$ obtained from direct aqueous carbonation of 2.43 % was low, which means that more CO_2 needed to dissolve. To improve the dissolution of CO_2 so that there are more CO_3^{2-} ions available to react with calcium (Ca^{2+}), fly ash material with a higher CaO (wt. %) content could be used because, due to Le Chatelier's principle, higher dissolution of CO_2 is normally favoured under alkaline conditions. Therefore, using coal fly ash material with a higher CaO (wt. %) concentration would create a more alkaline environment during the carbonation reaction, thus increasing the dissolution of CO_2, which could benefit the formation of more $CaCO_3$.

6.2 Energy balance (Required power)

The energy balance was conducted to determine the power requirement of the process using the optimum conditions for direct aqueous carbonation. As mentioned previously, the reason for using the optimum conditions from the direct aqueous carbonation process instead of the optimum conditions from direct carbonation with AMD was because the physical properties of pure water that are required for the energy balance calculation are known and would thus give a more reliable estimation of the total energy consumed. The energy balance focused mainly on the power requirement due to the carbonation reaction.

From the general energy balance:

$$\Delta \dot{E}_{system} = \dot{Q} + \dot{W}$$

Where $\dot{Q}$ for the Ca-H_2O-CO_2 system is the power required for heating ($\dot{Q}_{heat}$) and $\dot{W}$ is the power required for stirring and pressurization $\dot{W}_{system}$.

Power for heating

$$\dot{Q}_{heat} = \dot{Q}_{water} + \dot{Q}_{fly\ ash} + \dot{Q}_{CO_2}$$

$$\dot{Q}_{water} = mc_p\Delta T$$

Given that the mass of water and fly ash for the S/L of 0.5 g/mL (100 g fly ash: 200 mL water) was 200 g and 100 g respectively, it follows that:

$$\dot{Q}_{water} = (200\ g)(4.182\ J/g\ ℃)(70\ ℃) = 58548\ J/s$$

$$\dot{Q}_{fly\ ash} = (100\ g)(0.9497 J/g\ ℃)(70\ ℃) = 6650\ J/s$$

The mass of CO_2 determined from the CO_2 mass balance was 36.97 g, therefore;

$$\dot{Q}_{CO_2} = (36.97\ g)(0.84\ J/g\ ℃)(70\ ℃) = 2173.8\ J/s$$

$$\therefore \dot{Q}_{heat} = 58548\ \frac{J}{s} + 6650\ \frac{J}{s} + 2173.8\ \frac{J}{s} = 67371.84\ \frac{J}{s} = \frac{0.067\ MJ}{s} = 0.067\ MW$$

Power for stirring

Energy consumption for stirring at 100 rpm is given by:

$W = N_p \rho n^3 d^5$ where;

W = energy consumption from stirring

N_p = power number (dimensionless)

ρ = density of fluid (kg/m^3)

n (rps) = stirring rate per second (s^{-1})

d = diameter of paddle (m)

Calculating the power number N_p form Nagata's equation:

$$N_p = \frac{A}{Re} + B \left(\frac{1000 + 1.2\ Re^{0.66}}{1000 + 3.2\ Re^{0.66}}\right)^P \left(\frac{Z}{D}\right)^{0.35 + \frac{b}{D} sin\theta^{1.2}}$$

Calculating the Reynold's number (Re):

Given: n = 100 rpm =1.67 rps and;

Diameter of paddle = 0.035 m

and;

μ : Viscosity of fluid

$$\therefore Re = \frac{\rho n d^2}{\mu} = \frac{(1000\ kg/m^3)(1.67\ s^{-1})(0.035\ m)^2}{4.04 \times 10^{-4}\ kg/ms}$$

$$= 5058.73$$

$$A = 14 + \frac{b}{D}\left(670\left(\frac{d}{D} - 0.6\right)^2 + 185\right)$$

$$b = height\ of\ paddle = 0.13\ m$$

$$D = diameter\ of\ reaction\ vessel = 0.063\ m$$

$$d = diameter\ of\ paddle = 0.035\ m$$

$$\therefore A = 14 + \frac{0.13}{0.063}\left(670\left(\frac{0.035}{0.063} - 0.6\right)^2 + 185\right) = 398.5$$

$$log\ B = 1.3 - 4\left(\frac{b}{D} - 0.5\right)^2 - 1.4\left(\frac{d}{D}\right)$$

$$log\ B = 1.3 - 4\left(\frac{0.13}{0.063} - 0.15\right)^2 - 1.14\left(\frac{0.035}{0.063}\right) = -13.98$$

$$\therefore B = 10^{-13.98} = 1.05 \times 10^{-14}$$

$$P = 1.1 + 4\left(\frac{b}{D}\right) - 2.5\left(\frac{d}{D} - 0.5\right)^2 - 7\left(\frac{b}{D}\right)^4$$

$$\therefore P = 1.1 + 4\left(\frac{0.13}{0.063}\right) - 2.5\left(\frac{0.035}{0.063} - 0.5\right)^2 - 7\left(\frac{0.13}{0.063}\right)^4 = -117.57$$

Given $Z = height\ of\ reactor\ vessel = 0.147\ m$ and θ is the paddle gradient:

$$N_p = \frac{398.5}{5058.73} + (1.05 \times 10^{-14})\left(\frac{1000 + 1.2\,(5058.73)^{0.66}}{1000 + 3.2\,(5058.73)^{0.66}}\right)^{-117.57}\left(\frac{0.147}{0.063}\right)^{0.35 + \frac{0.13}{0.063} sin 90^{0}}{}^{1.2}$$

$$= 0.079$$

$$\therefore W = (0.079)(1000\,\tfrac{kg}{m^3})(1.67\,s^{-1})^3(0.035\,m)^5 = 1.93 \times 10^{-11}\ MW$$

Power for pressurization

$$P = nRTlog\frac{P1}{P2}$$

$$P = (0.84\,mol)\left(8.314\frac{J}{K}mol\right)(343.15\,K)log\frac{30\,bar}{40\,bar} = 299.4\,\frac{J}{s} = 0.000299\,MW$$

Total power consumption

$$\Delta\dot{E}_{system} = 0.067\,MW + 1.93 \times 10^{-11}\,MW + 0.000299\,MW = 0.068\,MW$$

The energy output determined from the energy balance was 0.068 MW, and the power due to heating contributed largely to this total energy (MW) consumption, meaning that the power due to heating contributed largely to the calcium (Ca^{2+}) extraction for the process. The 0.068 MW consumed after 120 min of direct aqueous carbonation at an applied CO_2 pressure of 4 Mpa was lower than the total energy consumption of 420 kW h/t of CO_2 stored for the CO_2 treatment from the study conducted by Iizuka et al. (2004). This was attributed to the energy requirement of 89 kW hr/t of CO_2 stored for CO_2 separation from flue gas as well as the energy required for pulverization of 104 kW hr/t of CO_2 stored, which was not considered in this work as pure CO_2 was used with no pre-treatment of the fly ash required.

Power for stirring at 400 rpm

Given that the stirring speed was increased to 400 rpm at the start of indirect aqueous carbonation experiments, which were part of process optimization, the energy output at 400 rpm was also considered.

∴ Energy consumption for stirring at 400 rpm is given by:

Firstly calculating the Reynold's number (Re):

Given: n = 400 rpm = 6.68 rps

$$\therefore Re = \frac{\rho n d^2}{\mu} = \frac{(1000\ kg/m^3)(6.68\ s^{-1})(0.035\ m)^2}{4.04 \times 10^{-4}\ kg/ms}$$

$$= 20234.92$$

$$\therefore N_p = \frac{398.5}{20234.92} + (1.05\ \times\ 10^{-14})\left(\frac{1000 + 1.2\ (20234.92)^{0.66}}{1000 + 3.2\ (20234.92)^{0.66}}\right)^{-117.57}\left(\frac{0.147}{0.063}\right)^{0.35 + \frac{0.13}{0.063} sin 90^{0}}{}^{1.2}$$

$$= 0.0197$$

$$\therefore\ W = (0.0197)(1000\frac{kg}{m^3})(6.68\ s^{-1})^3(0.035\ m)^5 = 3.08\ \times\ 10^{-10}\ MW$$

<u>Total power consumption</u>

$$\therefore \Delta\dot{E}_{system}\ =\ 0.067\ MW +\ 3.08\ \times\ 10^{-10}\ MW + 0.000299\ MW =\ 0.068\ MW$$

There was an observable increase of $2.89\ \times\ 10^{-10}\ MW$ in power due to stirring when the stirring speed was increased from 100 rpm up to 400 rpm, although this had a negligible effect on the total energy (MW) consumption for the carbonation process. This means that considering the trade-off between increasing the stirring speed (rpm) and the potential benefit this increase would have to the carbonation performance, increasing the stirring speed (rpm) was justifiable, especially considering that the highest carbonation efficiency (CE %) for the aqueous process at 100 rpm was 29.4 % during direct aqueous carbonation, while this increased to 35.2 % once a stirring speed of 400 rpm was applied during indirect aqueous carbonation.

CHAPTER 7

7.1 Conclusions

Carbon Capture and Storage (CCS) through accelerated MC is among the most practical methods sought for the effective capture and storage of CO_2 in efforts to create a decarbonized society, however, the energy consumption, and in turn, the costs associated with the process continue to hinder its widespread implementation. Hence, the main focus of this study was the optimization of several process parameters, which included the temperature (^0C), reaction time (min), particle size (μm), the S/L ratio, CO_2 pressure (Mpa), and the stirring speed (rpm) and also the use of an alkaline rich industrial waste feedstock in the form of fly ash to improve the carbonation performance thereby reducing the energy consumption (MW) of the MC process.

The carbonation performance for this work was measured through the % $CaCO_3$ formed, the CE (%) achieved, and also the maximum CO_2 storage capacity (kg/kg fly ash). Given that the overall carbonation performance depends on the extraction and dissolution of calcium (Ca^{2+}), the CO_2 dissolution in the liquid phase and precipitation to form calcium carbonate ($CaCO_3$), the dissolution behaviour of calcium (Ca^{2+}), and the leachability of calcium (Ca^{2+}) from the fly ash used in this study were initially investigated and formed part of a preliminary/baseline study to determine how effectively calcium (Ca^{2+}) dissolved in water and how much calcium (Ca^{2+}) was leachable from the fly ash. From the preliminary study, it was found that calcium (Ca^{2+}) did not dissolve completely in water when using pure $Ca(OH)_2$ due to the notable discrepancy between the theoretical saturation concentration of calcium (Ca^{2+}) of 1 g/L and the actual calcium (Ca^{2+}) that was dissolved. The actual calcium (Ca^{2+}) concentration dissolved for the S/L ratio of 1000 mg/L was 272 mg/L. The leachability of calcium (Ca^{2+}) from fly ash was then investigated.

The parameters investigated for the calcium (Ca^{2+}) extraction study were the temperature (^0C), time (min), and particle size (μm). Conditions leading to the highest concentration of calcium (Ca^{2+}) leached were considered the optimum conditions from the leaching study and were subsequently used for carbonation experiments. The optimum temperature was found to be 70 ^0C and the optimum reaction times were 30 min, 90 min, and 120 min due to the lower concentration obtained after 60 min, which from the Dixon's Q-Test proved to be an outlier potentially caused by errors while conducting the experiment.

Given that coal fly ash is a finer material and also considering the potential additional energy consumption (MW) due to the sieving process, the trade-off between the maximum calcium (Ca^{2+}) extracted at 125 (μm) made it unjustifiable to conduct subsequent experiments (i.e., carbonation experiments) using particle sizes of 25 (μm), 45 (μm), and 125 (μm) which required sieving that would result in an added energy requirement.

Considering that there were other mineral phases in fly ash such as Fe_2O_3 and MgO that could possibly contribute to the overall CO_2 stored in mineral carbonate form, results from leaching which was before carbonation and after the carbonation process indicated that the % $CaCO_3$ formed provided the best indication of the amount of CO_2 stored in mineral carbonate form. This was based on the higher amount of calcium (Ca^{2+}) concentration depleted after the direct aqueous carbonation and indirect carbonation processes with AMD wastewater, which indicated that the CO_2 fixed as $CaCO_3$ gave a better indication of the amount of CO_2 stored in mineral carbonate form. This also corroborated the initial assumption made.

Given that the main interest of the present work was to determine the potential of fly ash to permanently store CO_2, the % $CaCO_3$ formed was considered the most important carbonation performance measure as it demonstrated the amount of CO_2 that could be fixed in the fly ash in mineral carbonate form or could form precipitated $CaCO_3$ from the recovered leachate. The % $CaCO_3$ formed was thus considered first. The maximum % $CaCO_3$ of 4.53 % formed through the direct carbonation route with AMD wastewater was higher than that formed through the direct aqueous route as a maximum % $CaCO_3$ of 2.43 % was achieved for direct aqueous carbonation for the same reaction time of 120 min and CO_2 pressure of 4 Mpa. This was mainly attributed to the lower S/L ratio used for AMD carbonation experiments, the additional calcium (Ca^{2+}) provided by the AMD wastewater, and the increase in the stirring speed up to 400 rpm upon process optimization for the AMD carbonation study. The maximum % $CaCO_3$ formed of 4.53 % from direct carbonation with AMD wastewater was comparable with the maximum amount of % $CaCO_3$ formed of 6.5 % from the study conducted by Muriithi (2009) even though the CaO (wt.%) content in the fly ash used in this study was lower than Secunda fly ash used by Muriithi (2009). Although Muriithi (2009) made use of brine which also has an additional concentration of calcium (Ca^{2+}), the higher concentration of calcium (Ca^{2+}) in AMD wastewater explains the comparable amount of % $CaCO_3$ achieved in this study to the one achieved by Muriithi (2009).

The calcium (Ca^{2+}) extraction step was found to be the rate-limiting step from direct aqueous carbonation and had a significant role in the % $CaCO_3$ formed. For direct aqueous carbonation, there were similar amounts of % $CaCO_3$ formed after 30 min, 90 min, and 120 min due to most calcium (Ca^{2+}) being extracted in 30 min, whereas in the case of direct carbonation with AMD, the % $CaCO_3$ increased over time (min) in some cases due to more effective extraction of calcium (Ca^{2+}) and in turn, the higher calcium (Ca^{2+}) concentration obtained over time (min). The highest % $CaCO_3$ formed for direct carbonation utilizing AMD wastewater of 4.53 % for 120 min at 4 Mpa compared to the 2.43 % achieved for direct aqueous carbonation was therefore due to the effective calcium (Ca^{2+}) extraction including the additional calcium (Ca^{2+}) concentration of 362.5 ppm found in the AMD wastewater.

Parameters such as the S/L ratio and stirring speed had a significant effect on the calcium (Ca^{2+}) extraction and hence the % $CaCO_3$ formed. The higher % $CaCO_3$ formed in this work for direct carbonation with AMD can be attributed to the lower S/L ratio used which improved the solubility of calcium (Ca^{2+}) and as mentioned previously, the higher stirring rate of 400 rpm compared to the 100 rpm used for direct aqueous carbonation which improved the diffusion of metal ions from the fly ash into solution thus increasing the concentration of calcium (Ca^{2+}) in solution. There was a minuscule amount of $CaCO_3$ recovered from the indirect carbonation route to measure the % $CaCO_3$ formed and this was possibly due to the small volume of the leachate used due to the small volume of the autoclave reactor used (i.e., 600 mL) in this study. Also, the conditions were possibly not effective enough to form a considerable amount of the desired polymorph of $CaCO_3$ which in this case is calcite.

Apart from the % $CaCO_3$ formed, which gave the best indication of the amount of CO_2 actually stored permanently from the process, the CE (%) which gave a measure of the CO_2 consumed due to the reaction with calcium (Ca^{2+}) was still measured. The highest CE (%) achieved in this study was 63 % and was achieved for direct carbonation with AMD wastewater. This was comparable to the CE (%) of 67.3 achieved by Dananjayan et al. (2016) despite their fly ash having a slightly higher CaO (wt. %) compared to the CaO (%) content from the fly ash used in this study, which showed the benefit of the additional calcium (Ca^{2+}) provided by AMD wastewater. The highest CE (%) of 63 % achieved from direct carbonation with AMD was then followed by the second highest CE (%) of 53.9 % achieved through indirect carbonation with AMD wastewater for the same reaction time of 120 min and CO_2 pressure of 4 Mpa. The higher CE (%) through the direct route was possibly due to the continued extraction of calcium (Ca^{2+}) from the fly ash during the direct carbonation reaction.

There were lower carbonation efficiencies CE (%) reported when water was used as a solvent compared to when the AMD wastewater was utilized. The carbonation efficiency CE (%) from direct aqueous carbonation was 29.4 %, while the CE (%) achieved from the indirect aqueous route was 35.2 % for the same reaction time of 120 min and CO_2 pressure of 4 Mpa. Again, this can be attributed to the additional calcium (Ca^{2+}) concentration of 362.5 ppm provided by the AMD wastewater, the lower S/L ratio of 0.2 g/mL employed for experiments involving AMD wastewater as the solvent, as well as the higher stirring speed (rpm) of 400 rpm.

The higher CE (%) achieved from the indirect aqueous route compared to the CE (%) achieved from the direct aqueous route was due to the higher stirring speed of 400 rpm used for indirect aqueous carbonation which improved the calcium (Ca^{2+}) extraction. Considering the higher CE (%) achieved for the indirect aqueous carbonation route, the increase in the stirring speed from 100 rpm to 400 rpm for indirect aqueous carbonation experiments was justifiable because the total energy (MW) consumed due to the increase in the stirring speed did not significantly affect the total energy output (MW) as only $3.08 \times 10^{-10}\ MW$ at 400 rpm was due to increase in stirring at 400 rpm. The maximum CO_2 storage capacity was also measured and it gave an indication of the maximum CO_2 storage potential of the fly ash per 1 kg of fly ash used. The maximum CO_2 storage potential of 0.026 kg/kg fly ash achieved in this study was the same as the CO_2 storage potential of 0.026 kg/kg fly ash achieved by Montes-Hernandez et al. (2009) due to the similar CaO (wt. %) content in the fly ash.

From material balance considerations, there was a considerable amount of undissolved CO_2 in the liquid phase because from the total mass of CO_2 introduced into the reaction system (i.e., $\sum CO_{2(in)}$) of 36.97 g, it was found that the total mass of undissolved CO_2 (i.e., $\sum CO_{2(out)}$) was 22.89 g which meant that the fraction of undissolved CO_2 was high and was 0.62. The total mass of dissolved CO_2 was lower and was 14.08 g with only 2.08 g stored as $CaCO_3$ in total. To improve CO_2 dissolution, a feedstock of higher calcium (Ca^{2+}) content could be used. The energy balance indicated that a total of 0.068 MW was consumed from the process and a high amount of the energy from the total energy output was due to the power for heating. The energy consumed of 0.068 MW was relatively lower compared to the total energy output of 420 kW hr/ t CO_2 found by Iizuka et al. (2004) and was mostly due to the non-pre-treatment (i.e., crushing, grinding, sieving, etc) of the fly ash.

Overall, considering the lower CaO (wt.%) in the fly ash used in this study, the CO_2 storage process using Durapozz fly ash was effective because the highest % $CaCO_3$ achieved was 4.53 %, the highest CE (%) achieved was 63 % and the maximum CO_2 storage obtained was 0.026 kg/kg fly ash, which was all comparable with other studies. This was mostly due to the additional calcium (Ca^{2+}) concentration from the AMD wastewater and given that the amount of calcium (Ca^{2+}) available in solution had a significant effect on the carbonation performance, the sequestration potential of Durapozz fly ash was improved by using AMD wastewater as the reaction solvent. However, considering that a higher reaction time (min) and CO_2 pressure (Mpa) were required to achieve optimum results, the overall efficiency of the process remains questionable and perhaps can be further improved by using calcium (Ca^{2+}) extraction agents or fly ash material with higher CaO (wt. %) content.

The initial CO_2 pressure (Mpa) was also seen to influence the rate of the carbonation process. However, although an increase in pressure improved the rate of carbonation and hence the CE (%) due to higher CO_2 consumption, increasing the pressure (Mpa) did not favour the precipitation to form $CaCO_3$ as the highest % $CaCO_3$ of 4.53 % achieved at 4 Mpa was considerably similar to the % $CaCO_3$ of 4.37 % achieved at 3 Mpa, which suggests that the increase in pressure possibly decreased the rate of $CaCO_3$ formation due to the increase in the solubility of calcium (Ca^{2+}). This, therefore, implies that a slightly lower pressure of 3 Mpa was more suitable for the carbonation reaction because a pressure of 3 Mpa was high enough to ensure an effective rate of carbonation, but was not too high to hinder the precipitation of $CaCO_3$. Also, when considering the additional energy due to pressurization, a slightly lower pressure of 3 Mpa can be considered the optimum operating pressure for the process.

The process was also quite successful in the neutralization and treatment of AMD wastewater as effective neutralization of the AMD wastewater was achieved after 120 min of carbonation for CO_2 pressure of 4 Mpa for both direct and indirect carbonation with AMD wastewater. A pH of 7.1 was achieved under these conditions which was close to a neutral pH of 7. The percentage (%) removal of most elements was close to 100 % which suggested that most of the concentrations after treatment met the target water quality range (TWQR).

7.2 Recommendations and Implications

Given that calcium (Ca^{2+}) was mostly responsible for the storage of CO_2 in mineral carbonate form and that its extraction and dissolution had a significant effect on the overall carbonation performance of the process investigated, materials with a higher CaO (wt.%) content should be considered more for the CO_2 storage process, as this can result in better overall carbonation performance. The use of materials with higher CaO (wt. %) content could also be beneficial towards improving the dissolution of CO_2 in the liquid phase, as there was a high amount of undissolved CO_2 found in this process. However, when considering the abundance, low pre-treatment costs, etc., the use of fly ash as a feedstock for this process is still worthwhile. The use of coal fly ash (CFA) for the CO_2 storage process would also minimize the environmental hazard caused by stockpiled coal fly ash. Considering the significance of the calcium (Ca^{2+}) extraction step for the current process, the use of effective metal-extracting reagents such as recyclable ammonium salts (i.e., CH_3COONH_4) can be considered in future studies. However, there is an additional process cost coupled with recovery issues associated with extraction agents. The dissolution behaviour of calcium (Ca^{2+}) in water can be better understood by using salts that are more soluble than $Ca(OH)_2$.

The use of CO_2 pressure that is not too low to achieve an effective rate of carbonation but not too high to hinder the precipitation process to form precipitated $CaCO_3$ would be more recommended for the CO_2 storage process through MC when also considering the potential additional energy due to pressurization, even though a slightly higher% $CaCO_3$ and significantly higher CE (%) could be achieved at the highest pressure (Mpa). Using lower temperatures (^0C) is recommendable for the process and could also be beneficial as a high amount of the energy consumed from this process was due to the power from heating. In addition, lower temperatures (^0C) have been known to favour the precipitation that forms $CaCO_3$ more than higher temperatures.

The use of AMD wastewater as a reaction solvent for the process of CO_2 storage should be investigated more, given the higher carbonation performance achieved compared to when pure water is used. Also, given that South Africa has experienced problems with water shortages, the use of alternative reaction mediums such as AMD for such a process is recommendable in order to prevent such shortages. However, considering that the $CaCO_3$ produced from this process has a potential market value that can help offset the energy output and costs associated with the mineral carbonation process, the use of AMD wastewater as a solvent can be disadvantageous because the toxic metals that are removed from the wastewater through precipitation into metal hydroxides could potentially result in a $CaCO_3$ product of lesser purity that does not meet the purity standards for industries that have the potential to use the $CaCO_3$ product from this process. Given the proven benefit and advantage of using AMD wastewater for the carbonation performance of this process, using indirect carbonation when using AMD wastewater as the solvent would be more recommendable, as the wastewater would first be neutralized and treated in the initial stage which is the calcium (Ca^{2+}) extraction step, with the leachate then carbonated, which could result in a purer $CaCO_3$ product. Future work should, therefore, consider the use of indirect carbonation for CO_2 storage through MC and focus closely on strategies to minimize the energy consumption for this process route. Reactors of bigger volumes such as a jet loop system should be considered, when investigating the indirect carbonation process route to recover enough precipitated $CaCO_3$ for measuring the percentage $CaCO_3$ formed.

CO_2 emitting industries such as the cement industry could benefit from this process, and it is thus recommendable that the $CaCO_3$ product from MC processes is used in industries such as the cement industry. Apart from the benefit of the CO_2 capture that this process would offer in such industries, the reuse of the $CaCO_3$ from this process in such industries would ensure that the cement industry saves on the cost of mining limestone for their cement production process. However, it is also important to consider that the process of reusing $CaCO_3$ in the cement industry could present the potential issue of releasing CO_2 back into the atmosphere as $CaCO_3$ would require heating to retrieve the active ingredient for cement production, which is limestone. This would prove counterproductive for the process of CO_2 storage, as CO_2 would be reemitted. Although the aim of this study was to demonstrate the CO_2 storage potential of fly ash, future studies should also focus on the emission of CO_2 from the process in order to have a holistic evaluation of the efficiency of the CO_2 storage process. This is because if the amount of CO_2 stored is not significantly higher than the CO_2 emitted, then the entire storage process would prove ineffective. Future work should also consider the use of synthesised flue gas instead of pure CO_2 to carry out the process under more realistic conditions.

Policies should be developed towards enforcing the implementation of CCS in parallel with other capture and storage methods, such as geological storage. This will be more practical and effective in ensuring a larger capacity of CO_2 capture and storage on a global scale. This will also work well towards creating a decarbonised society and will also ensure small- and large-scale emitters save on the considerably high amounts paid towards carbon tax while gaining green credibility in the process.

However, future work must consider the economic feasibility of retrofitting CCS facilities into CO_2 emission sources and the possibility of re-emitting CO_2, while for large scale emitters, the environmental issues surrounding geological storage need to be addressed. Furthermore, to create an even more decarbonised society to meet the net zero CO_2 global emission target by 2050, less reliance should be placed on non-renewable energy sources such as coal, natural gas, etc. Policies should be in place to ensure the phasing in and integration of renewable energy sources such as solar energy to ensure that there is an energy mix and hence less reliance on non-renewable energy sources, which, in turn, would reduce net global CO_2 emissions. Finally, the widespread implementation of this process on a larger scale should be considered, as it will advance the effort towards the implementation of a circular economy in South Africa.

References

Ajayi, T., Gomes, J. S., & Bera, A. (2019). A review of CO_2 storage in geological formations emphasizing modeling, monitoring and capacity estimation approaches. *Petroleum Science*, *16*(5), 1028–1063.

Akcil, A., & Koldas, S. (2006). Acid Mine Drainage (AMD): causes, treatment and case studies. *Journal of Cleaner Production*, *14*(12-13 SPEC. ISS.), 1139–1145.

Alterary, S. S., & Marei, N. H. (2021). Fly ash properties, characterization, and applications: A review. *Journal of King Saud University - Science*, *33*(6), 101536.

American Coal Ash Association. (2013). Fly Ash Facts for Highway Engineers. *Journal of Chemical Information and Modeling*, *53*(9), 1689–1699.

Back, M., Kuehn, M., Stanjek, H., & Peiffer, S. (2008). Reactivity of alkaline lignite fly ashes towards CO_2 in water. *Environmental Science and Technology*, *42*(12), 4520–4526.

Bandilla, K. W. (2020). Carbon capture and storage. In *Future Energy: Improved, Sustainable and Clean Options for Our Planet*.

Bauer, M., Gassen, N., Stanjek, H., & Peiffer, S. (2011). Carbonation of lignite fly ash at ambient T and P in a semi-dry reaction system for CO_2 sequestration. *Applied Geochemistry*, *26*(8), 1502–1512.

Beck, B., Surridge, T., & Hietkamp, S. (2013). The South African centre for carbon capture and storage delivering CCS in the developing world. *Energy Procedia*, *37*, 6502–6507.

Ben Ghacham, A., Cecchi, E., Pasquier, L. C., Blais, J. F., & Mercier, G. (2015). CO_2 sequestration using waste concrete and anorthosite tailings by direct mineral carbonation in gas-solid-liquid and gas-solid routes. *Journal of Environmental Management*, *163*, 70–77.

Board, E. A., Mitchell, M., Mahanti, P. K., Garhyan, P., Shahbazi, M., Chai, J., Rajagopalan, R., Park, S., Elnashaie, S., Chowdhury, S., Omrani, G., Ray, A. K., Nafi, M., Ayadi, F., Sawhney, B., Wang, D., Los, C. A., Pancholi, J., Smith, T., Nasira, G. M. (2012). *European Journal of Scientific Research*. *73*(4).

Bobicki, E. R., Liu, Q., Xu, Z., & Zeng, H. (2012). Carbon capture and storage using alkaline industrial wastes. *Progress in Energy and Combustion Science*, *38*(2), 302–320.

Chang, R., Kim, S., Lee, S., Choi, S., Kim, M., & Park, Y. (2017). Calcium carbonate precipitation for CO_2 storage and utilization: A review of the carbonate crystallization and polymorphism. *Frontiers in Energy Research*, *5*(JUL), 1–12.

Cloete, M. (2010). *ATLAS on geological storage of carbon dioxide in South Africa*. *January 2010*, 1–61.

CSIR. (2009). *Acid Mine Drainage in South Africa, Briefing Note 2009/02*. *August*, 1–2.

Doeff, M. M., Wilcox, J. D., Yu, R., Aumentado, A., Marcinek, M., & Kostecki, R. (2008). Impact of carbon structure and morphology on the electrochemical performance of LiFePO4/C composites. *Journal of Solid State Electrochemistry*, *12*(7–8), 995–1001.

Dri, M., Sanna, A., & Maroto-Valer, M. M. (2014). Mineral carbonation from metal wastes: Effect of solid to liquid ratio on the efficiency and characterization of carbonated products. *Applied Energy*, *113*, 515–523.

DWAF. (1996). South African Water Quality Guidelines: Volume 1 Domestic Use. In *Department of Water Affairs and Forestry* (Vol. 1, Issue 2nd ed.).

Fatoba, O. J. O. O. (2007). *Chemical compositions and leaching behaviour of some South African fly ashes*. *November*.

Fernández Bertos, M., Simons, S. J. R., Hills, C. D., & Carey, P. J. (2004). A review of accelerated carbonation technology in the treatment of cement-based materials and sequestration of CO_2. *Journal of Hazardous Materials*, *112*(3), 193–205.

Ford. (2003). T echnical Not e 409 April 2003. *Management*, *April*.

Funston, W., Ndou, H., & Reynolds-Clausen, K. (2021). Beneficiation of Eskom Ash: Fact Sheet. *Risk and Sustainability*, *1*(May), 1–2.

Gerdemann, S. J., O'Connor, W. K., Dahlin, D. C., Penner, L. R., & Rush, H. (2007). Ex situ aqueous mineral carbonation. *Environmental Science and Technology*, *41*(7), 2587–2593.

Gianoncelli, A., Zacco, A., Struis, R. P. W. J., Borgese, L., Depero, L. E., & Bontempi, E. (2013). *Fly Ash Pollutants, Treatment and Recycling*.

Gitari, M., Petrik, L., Etchebers, O., Key, D., Iwuoha, E., & Okujeni, C. (2006). Treatment of acid mine drainage with fly ash: Removal of major contaminants and trace elements. *Journal of Environmental Science and Health - Part A Toxic/Hazardous Substances and Environmental Engineering*, *41*(8), 1729–1747.

Gitari, M. W., Petrik, L. F., Etchebers, O., Key, D. L., Iwuoha, E., & Okujeni, C. (2006). Treatment of Acid Mine Drainage with Fly Ash: Removal of Major Contaminants and Trace Elements. *Journal of Environmental Science and Health, Part A*, *41*(8), 1729–1747.

Gitari, W M, Somerset, V. S., Petrik, L. F., Key, D., Iwuoha, E., & Okujeni, C. (2005). Treatment of Acid Mine Drainage with Fly Ash : Removal of Major , Minor Elements, SO_4 And Utilization of the Solid Residues for Wastewater. *World of Coal Ash (WOCA)*, *January*, 1–23.

Gitari, Wilson Mugera, Petrik, L. F., & Akinyemi, S. A. (2018). Treatment of Acid Mine Drainage with Coal Fly Ash: Exploring the Solution Chemistry and Product Water Quality. *Coal Fly Ash Beneficiation - Treatment of Acid Mine Drainage with Coal Fly Ash*.

Global CCS Institute (GCCSI). (2020). Global Status of CCS 2020. *Global CCS Institute*, *June*, 1–44.

Goodman, P. D., Skipper, R., & Aitken, N. (2015). Modern instruments for characterizing degradation in electrical and electronic equipment. In *Reliability Characterisation of Electrical and Electronic Systems*. Elsevier Ltd.

Gupta, A. K. (2011). *Copyright by Abhishek Kumar Gupta Understanding the Plume Dynamics and Risk Associated with CO_2 Injection in Deep Saline Aquifers*

Han, S. J., Im, H. J., & Wee, J. H. (2015). Leaching and indirect mineral carbonation performance of coal fly ash-water solution system. *Applied Energy*, *142*, 274–282.

Hannan, J. (2017). Thermo Scientific iCAP 7000 Plus Series ICP-OES: Innovative ICP-OES optical design. *Technical Note 43333*, 1–4.

He, L., Yu, D., Lv, W., Wu, J., & Xu, M. (2013). A novel method for CO_2 sequestration via indirect carbonation of coal fly ash. *Industrial and Engineering Chemistry Research*, *52*(43), 15138–15145.

Himmelblau, D. and Riggs, J. - 2004 - Basic Principles and Calculations in Chemical Engineering, 7E.

Ho, H., Iizuka, A., Shibata, E., Tomita, H., Takano, K., & Endo, T. (2020). *CO_2 Utilization via Direct Aqueous Carbonation of Synthesized Concrete Fines under Atmospheric Pressure*.

Hosseini, T., Selomulya, C., Haque, N., & Zhang, L. (2014). Indirect carbonation of victorian brown coal fly ash for CO_2 sequestration: Multiple-cycle leaching-carbonation and magnesium leaching kinetic modeling. *Energy and Fuels*, *28*(10), 6481–6493.

Huijgen, W.J.J., & Comans, R. N. J. (2003). Carbon dioxide sequestration by mineral carbonation. In *Environmental science & technology* (Vol. 43, Issue 6).

Huijgen, Wouter J.J., Witkamp, G. J., & Comans, R. N. J. (2005). Mineral CO_2 sequestration by steel slag carbonation. *Environmental Science and Technology*, *39*(24), 9676–9682.

Huntzinger, D. N., Gierke, J. S., Kawatra, S. K., Eisele, T. C., & Sutter, L. L. (2009). Carbon dioxide sequestration in cement kiln dust through mineral carbonation. *Environmental Science and Technology*, *43*(6), 1986–1992.

Iizuka, A., Fujii, M., Yamasaki, A., & Yanagisawa, Y. (2004a). *Development of a New CO_2 Sequestration Process Utilizing the*. 7880–7887.

Iizuka, A., Fujii, M., Yamasaki, A., & Yanagisawa, Y. (2004b). Development of a new CO_2 sequestration process utilizing the carbonation of waste cement. *Industrial and Engineering Chemistry Research*, *43*(24), 7880–7887.

Iizuka, A., Yamasaki, A., & Yanagisawa, Y. (2013). Cost evaluation for a carbon dioxide sequestration process by aqueous mineral carbonation of waste concrete. *Journal of Chemical Engineering of Japan*, *46*(4), 326–334.

IPCC. (2005). *IPCC Special Report on Carbon Dioxide Capture and Storage* (L. A. M. Metz, B., O. Davidson, H. C. de Coninck, M. Loos.

Jain, M., & Dwivedi, A. (2014). Fly ash – waste management and overview : A Review Fly ash – waste management and overview : A Review. *Recent Research in Science and Technology 2014*, *6(1)* (January), 30–35.

Jansen, D., Gazzani, M., Manzolini, G., Dijk, E. Van, & Carbo, M. (2015). Pre-combustion CO_2 capture. *International Journal of Greenhouse Gas Control*, *40*, 167–187.

Ji, L., & Yu, H. (2018a). Carbon dioxide sequestration by direct mineralization of fly ash. In *Carbon Dioxide Sequestration in Cementitious Construction Materials*. Elsevier Ltd.

Ji, L., & Yu, H. (2018b). Carbon dioxide sequestration by direct mineralization of fly ash. In *Carbon Dioxide Sequestration in Cementitious Construction Materials*. Elsevier Ltd.

Ji, L., Yu, H., Wang, X., Grigore, M., French, D., Gözükara, Y. M., Yu, J., & Zeng, M. (2017). CO_2 sequestration by direct mineralisation using fly ash from Chinese Shenfu coal. *Fuel Processing Technology*, *156*, 429–437.

Jo, H. Y., Ahn, J. H., & Jo, H. (2012). Evaluation of the CO_2 sequestration capacity for coal fly ash using a flow-through column reactor under ambient conditions. *Journal of Hazardous Materials*, *241–242*, 127–136.

Jo, H. Y., Kim, J. H., Lee, Y. J., Lee, M., & Choh, S. J. (2012). Evaluation of factors affecting mineral carbonation of CO_2 using coal fly ash in aqueous solutions under ambient conditions *Chemical Engineering Journal*, *183*, 77–87.

Jones, S. N., & Cetin, B. (2017). Evaluation of waste materials for acid mine drainage remediation. *Fuel*, *188*, 294–309.

Kaliyavaradhan, S. K., & Ling, T. C. (2017). Potential of CO_2 sequestration through construction and demolition (C&D) waste - An overview. *Journal of CO_2 Utilization*, *20* (May), 234–242.

Kalombe, R. M., Ojumu, T. V., Katambwe, V. N., Nzadi, M., Bent, D., Nieuwouldt, G., Madzivire, G., Kevern, J., & Petrik, L. F. (2020). Treatment of acid mine drainage with coal fly ash in a jet loop reactor pilot plant. *Minerals Engineering*, *159* (February), 106611.

Karla Kruse, A., Jasso, A., Folliard, K., Ferron, R., Juenger, M., & Drimalas, T. (2012). *Characterizing Fly Ash (Report 0-6648-1)*. *7*, 172.

Katsuyama, Y., Yamasaki, A., Iizuka, A., Fujii, M., Kumagai, K., & Yanagisawa, Y. (2005). Development of a process for producing high-purity calcium carbonate ($CaCO_3$) from waste cement using pressurized CO_2. *Environmental Progress*, *24*(2), 162–170.

Kheirinik, M., Ahmed, S., & Rahmanian, N. (2021). Comparative techno-economic analysis of carbon capture processes: Pre-combustion, post-combustion, and oxy-fuel combustion operations. *Sustainability (Switzerland)*, *13*(24).

Kirby, D. (2014). Effective Treatment Options for Acid Mine Drainage in the Coal Region of West Virginia. *Theses, Dissertations and Capstones*, *Paper 857*.

Lal, R. (2008). Carbon sequestration. In *Philosophical Transactions of the Royal Society B: Biological Sciences* (Vol. 363, Issue 1492, pp. 815–830).

Lee, H. C., Min, K. W., & Seo, E. Y. (2016). A feasibility study on CO_2 sequestration using the neutralization process of acid mine drainage. *Geosystem Engineering*, *19*(6), 293–301.

Lichtschlag, A., Pearce, C. R., Suominen, M., Blackford, J., Borisov, S. M., Bull, J. M., de Beer, D., Dean, M., Esposito, M., Flohr, A., Gros, J., Haeckel, M., Huvenne, V. A. I., James, R. H., Koopmans, D., Linke, P., Mowlem, M., Omar, A. M., Schaap, A., Connelly, D. P. (2021). Suitability analysis and revised strategies for marine environmental carbon capture and storage (CCS) monitoring. *International Journal of Greenhouse Gas Control*, *112* (December 2020), 103510.

Madzivire, G., Maleka, R. M., Tekere, M., & Petrik, L. F. (2019). Cradle to cradle solution to problematic waste materials from mine and coal power station: Acid mine drainage, coal fly ash and carbon dioxide. *Journal of Water Process Engineering*, *30* (August 2017), 100474.

Mathieu, P. (2006). The IPCC special report on carbon dioxide capture and storage. In *ECOS 2006 - Proceedings of the 19th International Conference on Efficiency, Cost, Optimization, Simulation and Environmental Impact of Energy Systems*.

Mayoral, M. C., Andrés, J. M., & Gimeno, M. P. (2013). Optimization of mineral carbonation process for CO_2 sequestration by lime-rich coal ashes. *Fuel*, *106*, 448–454.

Mazzotti, M., Carlos, J., Allam, R., Lackner, K. S., Meunier, F., Rubin, E. M., Sanchez, J. C., Yogo, K., & Zevenhoven, R. (2005). Mineral carbonation and industrial uses of carbon dioxide. *IPCC Special Report on Carbon Dioxide Capture and Storage*, *October*, 319–338.

Montes-Hernandez, G., Pérez-López, R., Renard, F., Nieto, J. M., & Charlet, L. (2009). Mineral sequestration of CO_2 by aqueous carbonation of coal combustion fly-ash. *Journal of Hazardous Materials*, *161*(2–3), 1347–1354.

Mortezaei, K., Amirlatifi, A., Ghazanfari, E., & Vahedifard, F. (2017). Potential CO_2 leakage from geological storage sites: Advances and challenges. *Environmental Geotechnics*, *8*(1), 3–27.

Muriithi, G., Gitari, M. W., & Petrik, L. F. (2009). Brine remediation using fly ash and accelerated carbonation. *Proceedings of the International Mine Water Conference*, *October*, 671–679.

Muriithi, Grace N., Petrik, L. F., Fatoba, O., Gitari, W. M., Doucet, F. J., Nel, J., Nyale, S. M., & Chuks, P. E. (2013). Comparison of CO_2 capture by ex-situ accelerated carbonation and in in-situ naturally weathered coal fly ash. *Journal of Environmental Management*, *127*, 212-220.

Muriithi, Grace Nyambura. (2009). *CO_2 sequestration using brine impacted fly ash Magister Scientiae in the Chemistry Department , University of the Western Cape Supervisor : Dr Leslie F . Petrik*. *November*.

Ncongwane, M. S. (2016). *Assessment of the potential carbon footprint of engineered processes for the mineral carbonation of PGM tailings*. University of Cape Town.

Neeraj, & Yadav, S. (2020). Carbon storage by mineral carbonation and industrial applications of CO_2. *Materials Science for Energy Technologies*, *3*, 494–500.

Nkongolo, E. B. (2020). *Passive treatment of acid mine drainage using South African coal fly ash in a column reactor .*

Nomhle Ngwenya. (2019). Is carbon capture and storage still a feasible option for South Africa? *20 May 2019*.

Nyambura, M. G., Mugera, G. W., Felicia, P. L., & Gathura, N. P. (2011). Carbonation of brine impacted fractionated coal fly ash: Implications for CO_2 sequestration. *Journal of Environmental Management*, *92*(3), 655–664.

Olajire, A. A. (2013). A review of mineral carbonation technology in sequestration of CO_2. *Journal of Petroleum Science and Engineering*, *109*, 364–392.

Pan, S. Y., Chang, E. E., & Chiang, P. C. (2012). CO_2 capture by accelerated carbonation of alkaline wastes: A review on its principles and applications. *Aerosol and Air Quality Research*, *12*(5), 770–791.

Pat-Espadas, A. M., Portales, R. L., Amabilis-Sosa, L. E., Gómez, G., & Vidal, G. (2018). Review of constructed wetlands for acid mine drainage treatment. *Water (Switzerland)*, *10*(11).

Patel, A., Basu, P., & Acharya, B. (2017). An investigation into partial capture of CO_2 released from a large coal/petcoke fired circulating fluidized bed boiler with limestone injection using its fly and bottom ash. *Journal of Environmental Chemical Engineering*, *5*(1), 667–678.

Perdana, M. C., Sutanto, H. B., & Prihatmo, G. (2018). Vertical Subsurface Flow (VSSF) constructed wetland for domestic wastewater treatment. *IOP Conference Series: Earth and Environmental Science*, *148*(1).

Pérez-López, R., Nieto, J. M., & de Almodóvar, G. R. (2007). Utilization of fly ash to improve the quality of the acid mine drainage generated by oxidation of a sulphide-rich mining waste: Column experiments. *Chemosphere*, *67*(8), 1637–1646.

Perry, S., Perry, R. H., Green, D. W., & Maloney, J. O. (2008). *CHEMICAL ENGINEERS ' HANDBOOK SEVENTH*.

Potgieter-Vermaak, S. S., Potgieter, J. H., Monama, P., & Van Grieken, R. (2006). Comparison of limestone, dolomite and fly ash as pre-treatment agents for acid mine drainage. *Minerals Engineering*, *19*(5), 454–462.

Puthiya Veetil, S. K., Rebane, K., Yörük, C. R., Lopp, M., Trikkel, A., & Hitch, M. (2021). Aqueous mineral carbonation of oil shale mine waste (limestone): A feasibility study to develop a CO_2 capture sorbent. *Energy*, *221*.

Rabiu, K. O., Han, L., & Bhusan Das, D. (2017). CO_2 Trapping in the Context of Geological Carbon Sequestration. In *Encyclopedia of Sustainable Technologies* (Vol. 3). Elsevier.

Ramogohlo Martha Maleka. (2015). *Acid mine drainage treatment with coal fly ash, lime and aluminium hydroxide: Potential CO_2 sequestration*. University of the Western Cape.

Reddy, K., Weber, H., Bhattacharyya, P., Morris, A., Taylor, D., Christensen, M., Foulke, T., & Fahlsing, P. (2010). Instantaneous Capture and Mineralization of Flue Gas Carbon Dioxide: Pilot Scale Study. *Nature Precedings*, *December*.

Reklaitis, G. V, & Schneider, D. (1986). *Introduction to material and energy balances*. *239*, 683.

Reynolds-Clausen, K., & Singh, N. (2019). South Africa's Power Producer's Revised Coal Ash Strategy and Implementation Progress. *Coal Combustion and Gasification Products*, *11*(1), 1–10.

Rushendrarevathy, T. D., Pavithra, E., Palanivelu, K., & Ramachandran, A. (2014). National Conference on Green Engineering and Technologies for Sustainable Future-2014. CO_2 sequestration by lime mud through direct mineral carbonation National *Journal of Chemical and Pharmaceutical Sciences*, *4*, 15–17.

Sanna, A., Uibu, M., Caramanna, G., Kuusik, R., & Maroto-Valer, M. M. (2014). A review of mineral carbonation technologies to sequester CO_2. *Chemical Society Reviews*, *43*(23), 8049–8080.

Saran, R. K., Arora, V., & Yadav, S. (2018). *CO_2 sequestration by mineral carbonation : a review*. *20*(3), 497–503.

Sett, R. (2017). Flyash : Characteristics, Problems and Possible Utilization. *Advances in Applied Science Research*, *8*(3), 32–50.

Sikhakhane, J. (2020). *Climate explained: could the world stop using fossil fuels today?* 2020–2023.

Smith, E., Morris, J., Kheshgi, H., Teletzke, G., Herzog, H., & Paltsev, S. (2021). The cost of CO_2 transport and storage in global integrated assessment modeling. *International Journal of Greenhouse Gas Control*, *109*, 103367.

Smith, K. (1997). Constructed Wetlands for Treating Acid Mine Drainage. *Restoration and Reclamation Review*, 1–7.

Soong, Y., Fauth, D. L., Howard, B. H., Jones, J. R., Harrison, D. K., Goodman, A. L., Gray, M. L., & Frommell, E. A. (2006). CO_2 sequestration with brine solution and fly ashes. *Energy Conversion and Management*, *47*(13–14), 1676–1685.

Stumm, W. and Morgan, J. J. (1996). *Aquatic Chemistry, Chemical Equilibria and Rates in Natural Waters* (3rd Editio). John Wiley & Sons.

Sun, Y., Parikh, V., & Zhang, L. (2012). Sequestration of carbon dioxide by indirect mineralization using Victorian brown coal fly ash. *Journal of Hazardous Materials*, *209–210*, 458–466.

Tamilselvi Dananjayan, R. R., Kandasamy, P., & Andimuthu, R. (2016). Direct mineral carbonation of coal fly ash for CO_2 sequestration. *Journal of Cleaner Production*, *112*, 4173–4182.

Taylor, J., Pape, S., & Murphy, N. (2005). A Summary of Passive and Active Treatment Technologies for Acid and Metalliferous Drainage (AMD). *Proceedings of the 5th Australian Workshop on Acid Drainage*, *29*, 1–49.

Tomiyama, S., Igarashi, T., Baltazar, C., & Tangviroon, P. (2019). Acid mine drainage sources and hydrogeochemistry at the Yatani mine , Yamagata , Japan : A geochemical and isotopic study. *Journal of Contaminant Hydrology*, *225*(January), 103502.

Ukwattage, N. L., Ranjith, P. G., & Wang, S. H. (2013). Investigation of the potential of coal combustion fly ash for mineral sequestration of CO_2 by accelerated carbonation. *Energy*, *52*, 230–236.

Ukwattage, N. L., Ranjith, P. G., Yellishetty, M., Bui, H. H., & Xu, T. (2015). A laboratory scale study of the aqueous mineral carbonation of coal fly ash for CO_2 sequestration. *Journal of Cleaner Production*, *103*, 665–674.

Vellemu, E. (2017). *The Ecological Risk of Acid Mine Drainage in a Salinising Landscape*. *October*, 190.

Vilakazi, A. Q., Ndlovu, S., Chipise, L., & Shemi, A. (2022). The Recycling of Coal Fly Ash: A Review on Sustainable Developments and Economic Considerations. *Sustainability (Switzerland)*, *14*(4), 1–32.

W Seifritz. (1990). CO_2 disposal by means of silicates. *Nature*, *345*(June), 486.

Wardhono, A. (2018). Comparison Study of Class F and Class C Fly Ashes as Cement Replacement Material on Strength Development of Non-Cement Mortar. *IOP Conference Series: Materials Science and Engineering*, *288*(1), 0–6.

Yadav, S., & Mehra, A. (2021). A review on ex situ mineral carbonation. *Environmental Science and Pollution Research*, *28*(10), 12202–12231.

Appendix A

Sample Calculations:

1. Elemental compositions from XRF without LOI

$$Sum\ without\ LOI = Sum\ of\ elemental\ compositions\ for\ all\ elements\ present\ in\ sample\ (\%) - LOI\ (\%)$$

$$Elemental\ composition\ (without\ LOI) = \frac{Composition\ of\ element\ with\ LOI\ (\%)}{Sum\ without\ LOI\ (\%)} \times 100$$

CaO (wt. %) in raw fly ash

$$Sum\ without\ LOI = 97.23\ \% - 0.73\ \%$$

$$= 96.5\ \%$$

$$Elemental\ composition\ (without\ LOI) = \frac{3.92\ \%}{96.50\ \%} \times 100 = 4.06\ wt.\ \%$$

2. Theoretical maximum CO_2 storage capacity

$$CO_2\ (\%) = 0.785 \times (\%\ CaO - 0.7\ \%\ SO_3) + 1.09\ \%\ Na_2O + 0.93\ \%\ K_2O$$

$$CO_2\ (\%) = 0.785 \times \big(4.06 - 0.7(0)\big) + 1.09(0.38) + 0.93(\ 0.64) = 4.2\ \%$$

$$\therefore 0.042\ \ tommes\ of\ \ CO_2\ \ is\ sequestrated/\ tonne\ of\ fly\ ash$$

2. Dixon's Q-Test

Considering the following data set from preliminary experiments for the effect of time (min) on leachability of calcium (Ca^{2+}):

293.4 ppm, 375.1 ppm, 378.3 ppm, 399.8 ppm

The Dixon's Q-Test was used to determine whether there was an outlier in the data set. The null and alternative hypothesis were as follows:

H_0 There are no outliers present in the data set
H_1 There is one outlier present (i.e., the lowest value 293.4 ppm)

The test statistic for the procedure was given by:

$$Q_{Ts} = \frac{Gap}{Range}$$

Gap = Difference between the outlier and the next value

$$\therefore Gap = 375.1 - 293.4 = 81.7$$

Range = Difference between the maximum and minimum value

$$\therefore Range = 399.8 - 293.4 = 106.4$$

$$\therefore Q_{Ts} = \frac{81.7}{106.4} = 0.768$$

From Table C1 (see Appendix C), the critical value (Q_{CV}) at 90 % confidence level for n = 4 is 0.765. The 90 % confidence level was chosen because of the small data set.

If the test statistic is greater than the critical value $Q_{Ts} > Q_{CV}$ we reject the null hypothesis. Otherwise, we fail to reject the null hypothesis.

Given that $Q_{Ts} > Q_{CV}$ (i.e., 0.768 > 0.765), we reject the null hypothesis therefore there was enough evidence to suggest that there was an outlier in the data set which was 293.4 ppm.

3. Maximum CO_2 storage capacity

Given that the highest CE (%) achieved in the study was 63 %, it follows that the maximum CO_2 storage capacity (kg/ fly ash) of the fly ash used was given by:

$$Maximum\ CO_2\ storage\ capacity = 63\ \%\ \times 0.042$$

$$= 0.026\ tonnes\ of\ CO_2\ /\ tonne\ of\ fly\ ash\ of\ fly\ ash$$

4. % $CaCO_3$ formed for direct aqueous carbonation

To determine the % $CaCO_3$ formed, correction factors were calculated for each reading and subsequently used to determine the % $CaCO_3$ formed:

$$f = \frac{W \times T}{1.22 \times V}$$

$$W = 0.10\ g\ of\ pure\ CaCO_3$$

$$T = 292.95\ K$$

$$V = CO_2\ evolved\ after\ 1\ min\ (R_1)\ for\ pure\ CaCO_3 + CO_2\ evolved\ after\ 20\ min\ (R_{20})\ for\ pure\ CaCO_3$$
$$= 3.9 + 7.1\ mL$$
$$= 11\ mL$$

$$\therefore f = \frac{(0.10)(292.95)}{(1.22)(11)}$$

$$= 2.18$$

The correction factor was used to calculate the % $CaCO_3$ (based on 1.7 g of fly ash samples).

Given that $F = CR_1 - (0.04)\ (CR_{20} - CR_1)$ and $\%\ CaCO_3 = 0.232F$

Where;

CR_1 = $R_1\ (reading\ after\ 1\ min) \times f$

CR_{20} = $R_{20}\ (reading\ after\ 20\ min) \times f$

The % $CaCO_3$ formed using the optimum conditions of 120 min at the initial CO_2 pressure of 4 Mpa for direct aqueous carbonation:

$R_1(reading\ for\ volumetric\ CO_2\ evolved\ after\ 1\ \text{min}) = 4.8$

$R_{20}\ (reading\ for\ volumetric\ CO_2\ evolved\ after\ 20\ \text{min}) = 4.7$

$\therefore\ CR_1 = 4.8\ \times\ 2.18$

$= 10.48$

$CR_{20} = 4.7\ \times\ 2.18$

$= 10.26$

$\therefore\ F\ = 10.48\ -\ (0.04)\ (10.26\ -10.48)$

$= 10.49$

$\therefore\ \%\ CaCO_3\ = (0.232)\ (10.49)$

$= 2.43\ \%$

The same method was used to calculate % $CaCO_3$ for direct carbonation with AMD wastewater.

5. Carbonation Efficiency (CE %) for direct aqueous carbonation

The CE (%) calculation in this study was adopted from the study conducted by Muriithi (2009). The pressure drop due to $CaCO_3$ formation $(i.e., P_{carbonation\_pressure\ drop})$ which gave an indication of the amount of CO_2 stored in mineral form was used to determine the number of moles of CO_2 (n_{CO_2}) consumed due to CO_2 mineralization and was assumed to be dependent on the initial and final CO_2 pressure (Mpa).

Therefore;

Given that $CE\% = \frac{n_{CO_2} M_{CO_2}}{\left(\frac{w_{Cao}}{M_{CaO}}\right) M_{CO_2}} \times 100$

and;

$$n_{CO_2} = \frac{P_{carbonation\_pressure\ drop} V}{RT}$$

Using optimum conditions of 120 min at the initial CO_2 pressure of 4 Mpa (converted to bar for the purpose of the CE (%) calculations) for direct aqueous carbonation:

$$Initial\ pressure\ (bar) = 40\ bar$$

$$Final\ pressure\ (bar) = 24.8\ bar$$

$$\therefore\ P_{carbonation\_pressure\ drop} = Final\ \ pressure\ (bar)\ - initial\ prssure\ (bar)$$

$$P_{carbonation\_pressure\ drop} = 40\ bar\ - 24.8\ bar$$

$$= 15.2\ bar$$

In this study, the reaction system used was similar to the reaction system utilized by Muriithi et al. (2009). Given that the reactor steel jacket and the teflon liner were not a tight fit, the volume of gaseous CO_2 for this work was also given as:

$$Volume\ of\ the\ steel\ jacket - volume\ of\ the\ teflon\ liner - the\ volume\ occupied\ by\ the\ solid\ and\ liquid\ mixture\ in\ the\ teflon\ liner$$

- $Volume\ of\ the\ steel\ jacket = \pi r^2 h$

Given that the height of the steel jacket is given as:

$$H_{steel\ jacket} = 14.7\ cm;$$

with the steel jacket internal diameter given as:

$$d_{(i)steel\ jacket} = 6.3\ cm;$$

The radius (r) therefore becomes:

$$r_{steel\ jacket} = \frac{1}{2} \times d_{(i)steel\ jacket)}$$

$$r_{steel\ jacket} = \frac{1}{2} \times 6.3\ cm$$

$$= 3.15\ cm$$

$\therefore\ Volume\ of\ the\ steel\ jacket = \pi(3.1\ cm)^2(16.38\ cm)$

$= 458.24\ cm^3$

- $Volume\ of\ the\ teflon\ liner$

The volume of the teflon liner was calculated by a displacement experiment where the volume displaced by the teflon liner in water was taken to be its volume:

$Volume\ of\ the\ teflon\ liner = 160\ cm^3$

- $Volume\ occupied\ by\ the\ solid\ and\ liquid\ mixture\ in\ the\ teflon\ liner$

$Volume\ occupied\ by\ the\ solid\ and\ liquid\ mixture = \pi r^2 h$

Given that the height of the solid and liquid mixture was:

$H_{solid,liquid\ mixture} = 11.75cm;$

with the teflon liner internal diameter given as:

$d_{teflon} = 5.3\ cm;$

The radius (r) therefore becomes:

$r_{teflon} = \frac{1}{2} \times d_{teflon}$

$r_{teflon} = \frac{1}{2} \times 5.3\ cm$

$= 2.65\ cm$

$\therefore\ Volume\ of\ solid\ and\ liquid\ mixture = \pi(2.65\ cm)^2(11.75\ cm)$

$= 259.22\ cm^3$

$\therefore V = 458.24\ cm^3 - 160\ cm^3 - 259.22\ cm^3$

$= 39.02\ cm^3$

$= 0.04\ L$

$\therefore n_{CO_2} = \frac{(15.2\ bar)(0.04\ L)}{(0.08314472\ L\ bar/K\ mol)\ (343.15\ K)}$

$= 0.0213\ mol$

$\therefore$ From $CE\ (\%) = \frac{n_{CO_2} M_{CO_2}}{\left(\frac{w_{Cao}}{M_{CaO}}\right) M_{CO_2}} \times 100$

Given;

$M_{CO_2} = 44.01\ g/mol$ (molecular weight of CO_2) and;

$w_{Cao}(wt.\%) = 4.06\ \%$ (CaO (wt. %) content in fly ash) and;

$M_{CaO} = 56.007\ g/mol$ (molecular weight of calcium (Ca^{2+}))

The carbonation efficiency then CE (%) becomes:

$CE\% = \frac{(0.0213\ mol)(44.01 \frac{g}{mol})}{\left(\frac{4.06}{56.007\ g/mol}\right)(44.01\ \frac{g}{mol})} \times 100$

$= 29.4\ \%$

6. Carbonation Efficiency (CE %) for direct carbonation with AMD wastewater

Given that a lower S/L ratio of 0.2 g/mL was used for experiments with AMD wastewater, the height of the solid and liquid mixture was different and therefore the volume occupied by the solid and liquid mixture was also different. Therefore, the calculation for CE (%) in this case was given as:

Using the optimum conditions of 120 min at the initial CO_2 pressure of 4 Mpa (converted to bar for the purpose of the CE (%) calculations) for direct carbonation with AMD wastewater:

$$Initial\ pressure\ (bar) = 40\ bar$$

$$Final\ pressure\ (bar) = 18.6\ bar$$

$$\therefore\ P_{carbonation\_pressure\ drop} = Final\ \ pressure\ (bar)\ - initial\ prssure\ (bar)$$

$$P_{carbonation\_pressure\ drop} = 40\ bar\ - 21.4\ bar$$

$$= 18.6\ bar$$

And;

$$Volume\ of\ the\ steel\ jacket - volume\ of\ the\ teflon\ liner - the\ volume\ occupied\ by\ the\ solid\ and\ liquid\ mixture\ in\ the\ teflon\ liner$$

- $Volume\ of\ the\ steel\ jacket = \pi r^2 h$

Given that the height of the steel jacket is given as:

$$H_{steel\ jacket} = 14.7\ cm;$$

with the steel jacket internal diameter given as:

$$d_{(i)steel\ jacket} = 6.3\ cm;$$

The radius (r) therefore becomes:

$$r_{steel\ jacket} = \frac{1}{2} \times d_{(i)steel\ jacket)}$$

$$r_{steel\ jacket} = \frac{1}{2} \times 6.3\ cm$$

$$= 3.15\ cm$$

$$\therefore\ Volume\ of\ the\ steel\ jacket = \pi(3.1\ cm)^2(16.38\ cm)$$

$$= 458.24\ cm^3$$

- $Volume\ of\ the\ teflon\ liner$

The volume of the teflon liner was calculated by a displacement experiment where the volume displaced by the teflon liner in water was taken to be its volume:

$$Volume\ of\ the\ teflon\ liner = 160\ cm^3$$

- $Volume\ occupied\ by\ the\ solid\ and\ liquid\ mixture\ in\ the\ teflon\ liner$

$$Volume\ occupied\ by\ the\ solid\ and\ liquid\ mixture = \pi r^2 h$$

Given that the height of the solid and liquid mixture was:

$$H_{solid,liquid\ mixture} = 10.5\ cm;$$

with the teflon liner internal diameter given as:

$$d_{teflon} = 5.3\ cm;$$

The radius (r) therefore becomes:

$$r_{teflon} = \frac{1}{2} \times d_{teflon}$$

$$r_{teflon} = \frac{1}{2} \times 5.3\ cm$$

$$= 2.65\ cm$$

$$\therefore\ Volume\ of\ solid\ and\ liquid\ mixture = \pi(2.65\ cm)^2(10.5\ cm) = 231.7\ cm^3$$

$\therefore V = 458.24\ cm^3 - 160\ cm^3 - 231.7\ cm^3$

$= 66.54\ cm^3$

$= 0.07\ L$

$\therefore n_{CO_2} = \frac{(18.6\ bar)(0.07\ L)}{(0.08314472\ L\ bar/K\ mol)\ (343.15\ K)}$

$= 0.0456\ mol$

$\therefore$ From $CE\ (\%) = \frac{n_{CO_2} M_{CO_2}}{\left(\frac{w_{Cao}}{M_{CaO}}\right) M_{CO_2}} \times 100$

Given;

$M_{CO_2} = 44.01\ g/mol$ (molecular weight of CO_2) and;

$w_{Cao}(wt.\%) = 4.06\ \%$ (CaO (wt. %) content in fly ash) and;

$M_{CaO} = 56.007\ g/mol$ (molecular weight of calcium (Ca^{2+}))

The carbonation efficiency then CE (%) becomes:

$CE\% = \frac{(0.0456\ mol)(44.01 \frac{g}{\text{mol}})}{\left(\frac{4.06}{56.007\ g/mol}\right)(44.01\ \frac{g}{mol})} \times 100$

$= 63\ \%$

The same method was used to determine the CE (%) for indirect aqueous carbonation and indirect carbonation with AMD wastewater using a height of 10.4 cm for the leachate which meant that the height when calculating the volume of the solution was 10.4 cm.

7. % Removal of metal ions from AMD treatment

$Fe^{2+}\ \%\ removal = \left(\frac{conc.of\ ionic\ species\ in\ raw\ AMD - conc.of\ species\ after\ reaction\ time\ (hr)}{concentration\ of\ ionic\ species\ in\ raw\ AMD}\right) \times 100$

$= \frac{1899 - (-0..5480)}{1899} \times 100$

$= 100\ \%$

Appendix B

Raw Data:

Table B 1: Baseline experiment: Dissolution of calcium (Ca^{2+}) from $Ca(OH)_2$

Theoretical Ca^{2+} concertation (mg/L)	Actual Ca^{2+} concentration from ICP-OES results (ppm)	Averaged Ca^{2+} concentration from ICP-OES results (ppm)	Mass of $Ca(OH)_2$ weighed (g)	Mass of $Ca(OH)_2$ from ICP-OES results (g)	Mass of undissolved $Ca(OH)_2$ (g)
200	168.5	169	0.37	0.31	0.06
	170.7		0.37	0.32	0.05
	166.7		0.37	0.31	0.06
400	233.4	226	0.73	0.43	0.30
	226.8		0.73	0.42	0.32
	219.2		0.73	0.41	0.33
600	256.6	254	1.1	0.47	0.63
	253.5		1.1	0.47	0.64
	250.7		1.1	0.46	0.65
800	272.8	269	1.48	0.50	0.98
	268.5		1.48	0.50	0.98
	266.6		1.48	0.49	0.98
1000	273.7	272	1.85	0.50	1.34
	271.0		1.85	0.50	1.35
	270.3		1.85	0.50	1.35
1200	275.1	275	2.2	0.50	1.71
	277.2		2.2	0.51	1.71
	272.5		2.2	0.50	1.71

Baseline Experiments: Effect of temperature (^{0}C)

Table B 2: ICP-OES Raw Data (Dup: Duplicate)

ppm	30 ^{0}C (Run)	30 ^{0}C (Dup)	50 ^{0}C (Run)	50 ^{0}C (Dup)	70 ^{0}C (Run)	70 ^{0}C (Dup)	90 ^{0}C (Run)	90 ^{0}C (Dup)	110 ^{0}C (Run)	110 ^{0}C (Dup)
Ca	118.9	201.5	253.1	226.3	301.7	285.1	43.12	288	6.05	294.5
Al	7.07	4,00	3.93	4.02	1.85	0.71	0.06	15.67	6,04	1.15
Si	7.15	2.82	2.08	3.17	3.12	1.70	0.58	0.42	0,16	1.06
Mg	2.07	0.14	0.01	0.07	0.01	0.32	0.02	0.92	0,19	0.20
Na	2.04	10.84	9.28	14.27	11.43	16.22	2.33	19.67	0,08	20.57
Pb	0,01	0.14	-0.02	0.00	-0.03	0.00	-0.03	0.00	0,09	0.07
Cu	2.97	0.00	0.00	0.01	-0.00	0.01	0.02	0.02	-0,02	0.01
As	6.42	-0.06	-0.02	0.46	-0.02	-0.74	0.00	-0.8	-6,32	-0.02
Zn	0.02	-0.14	-0.01	0.07	-0.01	-0.16	0.03	-0.10	9,97	-0.15
Mo	-0.00	-0.12	0.34	0.21	0.51	-0.32	0.11	-0.39	0,02	0.27
Co	-0.00	-0.29	-0.00	0.35	-0.00	-0.28	0.02	-0.21	0,00	-0.26
Cr	0.00	0.12	0.92	0.82	1.36	1.26	0.26	0.20	0,00	0.00
Ni	-0.01	-0.29	0.00	0.01	0.00	0.00	0.03	0.01	0,00	0.00
Ta	0.25	3.25	6.32	5.23	3.68	2.88	-0.63	0.00	-0,01	0.00
Se	-0.01	-0.07	0.09	0.08	0.10	0.09	0.00	0.00	0,10	0.00
P	0.65	-0.09	-0.01	0.00	-0.01	0.00	0.00	0.00	-0,01	0.00
Cd	-0,01	0.21	0.00	0.01	0.01	0.00	0.06	0.04	0,21	0.10
Be	0,15	4.00	0,00	0.02	0.00	0.00	0.03	0.00	-0,01	0.00
Mn	-0,01	-0.07	0.00	0.06	-0.00	-0.15	0.03	-0.06	0,37	-0.07
Ti	-0.00	-0.09	-0.00	0.00	-0.00	-0.09	0.03	-0.09	0,05	-0.05
Sr	-0.00	5.15	3.61	3.00	5.57	8.93	0.03	8.08	0,03	10.12
Fe	1.10	0.12	-0.00	0.00	-0.00	-0.08	1.09	0.09	-0,01	0.28

Table B 3: XRF Raw Data

%	Raw FA	30 ^{0}C (Run)	30 ^{0}C (Dup)	50 ^{0}C (Run)	50 ^{0}C (Dup)	70 ^{0}C (Run)	70 ^{0}C (Dup)	90 ^{0}C (Run)	90 ^{0}C (Dup)	110 ^{0}C (Run)	110 ^{0}C (Dup)
Fe_2O_3	3.01	3.00	3.01	3.01	2.96	2.98	3.00	3.05	3.05	3.01	2.98
MnO	0.03	0.03	0.03	0.03	0.03	0.03	0.03	0.03	0.03	0.03	0.03
Cr_2O_3	0.04	0.04	0.05	0.05	0.05	0.05	0.06	0.04	0.05	0.05	0.05
V_2O_5	0.05	0.05	0.05	0.05	0.05	0.04	0.05	0.06	0.04	0.05	0.05
TiO_2	1.69	1.71	1.73	1.71	1.65	1.70	1.70	1.70	1.71	1.67	1.70
CaO	3.92	3.83	3.84	3.77	3.76	3.82	3.77	3.81	3.76	3.74	3.75
K_2O	0.62	0.63	0.63	0.59	0.60	0.63	0.60	0.62	0.60	0.60	0.58
P_2O_5	0.45	0.43	0.45	0.43	0.43	0.44	0.43	0.42	0.43	0.44	0.44
SiO_2	52.46	52.74	52.78	52.55	52,65	52,72	53.10	53.30	52.97	52.36	52.55
Al_2O_3	32.99	33.52	33.38	33.46	33.87	33.64	33.91	33.91	33.50	33.16	32.99
MgO	0.87	0.90	0.81	0.82	0.91	0.95	0.91	0.97	0.94	0.94	0.93
Na_2O	0.37	0.23	0.37	0.19	0.64	0.56	0.19	0.40	0.35	0.36	0.37
LOI	0.73	0.42	0.88	0.49	0.96	0.25	0.91	0.26	0.89	0.21	0.80

Baseline Experiments: Effect of time (min)

Table B 4: ICP-OES Raw Data (Brackets: negative concentration; ND: not detectable)

ppm	30 min (Run)	30 min (Dup)	60 min (Run)	60 min (Dup)	90 min (Run)	90 min (Dup)	120 min (Run)	120 min (Dup)
Ca	384.4	372.2	301.68	285.05	374.6	369.6	396.7	403
Al	10.5	11.6	1.85	0.71	4.2	4.1	2.1	2.4
Mg	1.9	1.7	0.01	0.32	0.1	0.1	0.1	0.1
Na	16.2	15.3	11.43	16.32	19.4	18.8	12.6	13.1
Pb	0.1	0.1	(0.03)	0.01	ND	ND	ND	ND
Cu	ND	ND	(0.00)	0.01	ND	ND	ND	ND
As	ND	ND	(0.02)	(0.74)	ND	ND	ND	ND
Zn	ND	ND	(0.01)	(0.16)	ND	ND	ND	ND
Mo	ND	ND	(0.51)	(0.32)	ND	ND	ND	ND
Co	ND	ND	(0.00)	(0.28)	ND	ND	ND	ND
Cr	5.7	5.5	1.36	1.35	2.1	2.1	2.9	3.0
Ni	ND	ND	0.00	0.00	ND	ND	ND	ND
P	0.6	0.7	(0.01)	0.00	ND	ND	ND	ND
Cd	ND	ND	0.00	0.00	ND	ND	ND	ND
Be	ND	ND	(0.00)	0.00	ND	ND	ND	ND
Mn	ND	ND	(0.00)	(0.15)	ND	ND	ND	ND
Ti	0.6	0.6	(0.00)	(0.09)	ND	ND	ND	ND
Sr	12.4	12.0	5.57	8.93	8.4	8.1	8.7	8.9
Fe	1.3	1.8	(0.00)	(0.08)	ND	0.00	0.1	0.1

Table B 5: XRF Raw Data

%	30 min (Run)	30 min (Dup)	90 min (Run)	90 min (Dup)	120 min (Run)	120 min (Dup)
Fe_2O_3	2.91	2.95	2.93	2.90	2.94	2.89
MnO	0.03	0.03	0.02	0.03	0.03	0.03
Cr_2O_3	0.04	0.05	0.04	0.05	0.04	0.05
V_2O_5	0.05	0.06	0.04	0.05	0.07	0.04
TiO_2	1.66	1.68	1.66	1.65	1.68	1.67
CaO	3.80	3.82	3.82	3.76	3.76	3.78
K_2O	0.63	0.66	0.61	0.62	0.63	0.62
P_2O_5	0.47	0.43	0.43	0.44	0.42	0.41
SiO_2	53.23	53.35	53.27	53.12	53.10	53.32
Al_2O_3	33.39	33.55	33.40	33.13	33.52	33.40
MgO	0.96	0.90	0.91	1.00	0.93	0.77
Na_2O	0.23	0.10	0.40	0.35	0.48	<0.01
LOI	1.04	1.01	1.13	1.13	0.95	0.96

Direct aqueous carbonation: Effect of pressure (Mpa) over time (min)

Table B 6: ICP-OES Raw Data

ppm	30 min 1Mpa (Run)	30 min 1Mpa (Dup)	30 min 2Mpa (Run)	30 min 2Mpa (Dup)	30 min 3Mpa (Run)	30 min 3Mpa (Dup)	30 min 4Mpa (Run)	30 min 4Mpa (Dup)	90 min 1Mpa (Run)	90 min 1Mpa (Dup)	90 min 2Mpa (Run)	90 min 2Mpa (Dup)	90 min 3Mpa (Run)	90 min 3Mpa (Dup)	90 min 4Mpa (Run)	90 min 4Mpa (Dup)	120min 1Mpa (Run)	120min 1Mpa (Dup)	120min 2Mpa (Run)	120min 2Mpa (Dup)	120min 3Mpa (Run)	120min 3Mpa (Dup)	120min 4Mpa (Run)	120min 4Mpa (Dup)
Ca	123.6	119.0	155.8	145.0	201.2	195.0	211.9	208.3	140.0	142.6	174.1	178.1	198.2	202.0	220.2	224.0	188.2	192.0	215.2	229.0	279.0	281.2	320.0	300.2
Al	(0.05)	0.06	(0.01)	0.02	(0.03)	(0.05)	(0.02)	(0.04)	(0.05)	(0.04)	(0.04)	(0.03)	(0.04)	(0.04)	(0.06)	(0.05)	0,02	0.01	0.03	0.03	(0.001)	(0.002)	0.08	0.05
Si	13.86	13.45	24.33	24.45	11.64	13.34	19.38	18.47	18.24	17.02	12.23	11.08	12.89	12.89	15.40	13.97	13.51	12.47	21.10	21.10	12.31	12.06	21.50	18.19
Mg	11.23	9.14	14.71	16.11	7.48	11.38	13.71	17.84	15.32	15.39	10.81	11.65	13.60	13.60	12.63	9.35	0.001	0.001	0.0014	0.0014	0.03	0.03	0.05	0.05
Na	1.19	1.15	3.45	0.24	(0.03)	2.17	0.84	(2.77)	(0.68)	(1.88)	0.28	0.79	(0.36)	(0.36)	2.76	2.52	1.13	(2.53)	2.79	2.79	2.31	1.82	1.80	4.24
K	10.94	9.70	15.05	15.62	11.25	9.50	10.91	15.38	12.34	13.29	13.15	14.70	13.58	13.58	11.56	10.26	14.09	17.11	14.32	14.32	12.07	14.07	12.85	16.45
Pb	0.00	0.00	0.01	0.04	0.01	0.04	0.03	0.00	(0.01)	0.02	(0.01)	0.01	0.01	0.01	0.01	0.00	0.01	0.03	0.01	0.01	0.01	0.00	(0.01)	0.03
Cu	0.00	0.00	0.00	0.01	0.00	0.00	0.00	0.01	0.01	0.01	0.00	0.00	0.00	0.00	0.00	(0.00)	0.00	0.00	0.00	0.00	0.00	0.01	0.00	0.01
As	0.23	0.23	0.32	0.32	0.19	0.22	0.34	0.28	0.30	0.28	0.08	0.08	0.10	0.10	0.07	0.06	0.13	0.11	0.30	0.30	0.80	0.03	0.30	0.22
Zn	(0.01)	0.01	(0.01)	(0.01)	(0.01)	(0.01)	0.07	(0.00)	(0.01)	(0.01)	0.01	0.20	(0.01)	(0.01)	(0.01)	0.01	0.01	(0.01)	0.08	0.08	0.00	0.00	(0.01)	(0.01)
Mo	0.38	0.31	0.50	0.51	0.25	0.39	0.39	0.39	0.44	0.40	0.37	0.35	0.45	0.45	0.53	0.46	0.39	0.34	0.55	0.55	0.24	0.81	0.47	0.41
Co	0.00	0.00	(0.00)	0.00	0.00	(0.00)	0.00	(0.00)	0.00	(0.00)	(0.00)	(0.00)	(0.00)	(0.00)	(0.00)	(0.00)	0.00	(0.00)	0.00	0.00	0.03	0.00	0.00	0.00
Cr	1.20	0.98	1.47	1.46	0.75	1.26	1.15	1.18	1.27	1.17	0.95	0.89	1.19	1.19	1.44	1.19	1.03	0.91	1.63	1.63	1.05	0.24	1.09	0.93
Ni	0.01	0.01	0.02	0.03	0.01	0.02	0.01	0.03	0.03	0.04	0.01	0.02	0.03	0.03	0.01	0.01	0.03	0.03	0.01	0.01	0.05	0.03	0.04	0.06
Ta	0.70	0,63	1.03	0.67	1.07	1.05	0.93	0.63	0.80	0.54	0.54	0.38	0.55	0.55	1.05	1.05	0.13	0.20	1.55	1.55	0.44	0.80	0.87	0.47
Se	0.29	0,26	0.26	0.41	0.19	0.28	0.20	0.46	0.44	0.51	0.23	0.34	0.37	0.37	0.26	0.22	0.38	0.39	0.37	0.37	(0.00)	0.05	0.28	0.41
P	(0.04)	0.04	1.39	1.24	0.77	1.04	1.06	0.81	0.96	0.86	(0.05)	0.08	0.20	0.20	(0.01)	(0.01)	0.41	0.29	2.09	2.09	1.99	0.40	1.68	1.21
Cd	0.00	0.00	0.00	0.00	0.00	0.00	0.00	0.00	0,00	0.00	0.00	0.00	0.00	0.00	0.00	(0.00)	0.00	(0.00)	0.00	0.00	0.00	0.00	0.00	(0.00)
Li	1.16	0.94	1.56	1.71	0.80	1.10	1.32	1.63	1.60	1.63	1.47	1.55	1,57	1,57	1.53	1.38	1.82	1.75	1.69	1.69	1.99	2.09	1.73	1.83
Be	0.00	0.00	0.00	0.00	0.00	0.00	0.00	0.00	0.00	0.00	0.00	0.00	0.00	0.00	0.00	0.00	0.00	0.00	0.00	0.00	0.00	0.00	0.00	0.00
Mn	(0.00)	0,00	0.06	0.06	0.04	0.06	0.04	0.04	0.04	0.04	0.01	0.02	0.02	0.02	0.00	(0.00)	0.05	0.04	0.06	0.06	0.06	0.06	0.05	0.05
Ti	(0.00)	0,00	0.00	(0.00)	(0.00)	(0.00)	(0.00)	(0.00)	(0.00)	(0.00)	(0.00)	(0.00)	(0.00)	(0.00)	(0.00)	(0,00)	0,00	(0.00)	(0.00)	(0.00)	0.00	0.00	0.00	0.00
Sr	1.97	1.66	3.20	3.44	1.38	2.42	2.07	2.55	2.55	2.56	1.98	2.10	2.49	2.49	2.19	1.74	2.43	2.12	2.29	2.29	2.66	2.68	2.62	2.56
Fe	(0.02)	0,02	(0.00)	(0.02)	(0.02)	(0.02)	(0.02)	(0.02)	(0.02)	(0.02)	(0.02)	(0.02)	(0.01)	(0.01)	(0.02)	(0.02)	(0.0187)	(0.0147)	(0.0120)	(0.0126)	(0.002)	(0.016)	(0.0021)	(0.0081)

Table B 7: XRF Raw Data

%	120 min 1Mpa (Run)	120 min 1Mpa (Dup)	120 min 2Mpa (Run)	120 min 2Mpa (Dup)	120 min 3Mpa (Run)	120 min 3Mpa (Dup)	120 min 4Mpa (Run)	120 min 4Mpa (Dup)
Fe_2O_3	3.02	3.02	3.02	3.00	3.03	2.99	3.04	3.04
MnO	0.06	0.03	0.04	0.04	0.03	0.03	0.03	0.03
Cr_2O_3	0.04	0.04	0.04	0.04	0.04	0.04	0.04	0.04
TiO_2	1.64	1.64	1.63	1.62	1.64	1.63	1.63	1.63
CaO	3.76	3.75	3.72	3.71	3.71	3.71	3.73	3.74
K_2O	0.72	0.61	0.68	0.66	0.61	0.68	0.61	0.66
P_2O_5	0.43	0.42	0.42	0.42	0.43	0.43	0.43	0.42
SiO_2	53.44	53.55	53.40	53.29	53.55	53.30	53.50	53.29
Al_2O_3	34.55	34.65	34.40	34.47	34.54	34.28	34.50	34.56
MgO	0.89	0.89	0.89	0.89	0.89	0.89	0.89	0.89
Na_2O	0.32	0.33	0.31	0.32	0.33	0.34	0.31	0.37
LOI	1.31	1.31	1.31	1.31	1.31	1.31	1.31	1.31

Indirect aqueous carbonation: Effect of time (min) on leaching

Table B 8: ICP-OES Raw Data

ppm	30 min (Run)	30 min (Dup)	60 min (Run)	60 min (Dup)	90 min (Run)	90 min (Dup)	120 min (Run)	120 min (Dup)
Ca	340	314.71	370.2	383.1	380.2	393.14	420.23	424.23
Al	0.63	0.60	0.68	0.65	5.85	5.80	13.86	13.81
Si	1.06	1.00	0.94	0.90	0.78	0.70	0.85	0.80
Mg	0.02	0.00	0.02	0.00	0.18	0.10	0.25	0.20
Na	28.51	26.97	30.29	30.01	25.41	25.01	36.82	36.77
Pb	0.29	0.10	0.25	0.20	0.24	0.21	0.26	0.21
Cu	(0.00)	(0.01)	0.00	0.01	(0.00)	0.01	0.0004	(0.05)
As	(0.02)	(0.03)	0.02	0.02	0.03	0.03	(0.01)	(0.06)
Zn	(0.00)	(0.00)	0.02	0.01	(0.00)	0.00	(0.005)	(0.06)
Mo	0.77	0.66	0.74	0.70	0.73	0.71	0.95	0.90
Co	(0.01)	(0.01)	0.01	0.00	(0.01)	0.00	(0.009)	(0.06)
Cr	1.86	1.70	1.79	1.80	1.91	1.70	2.70	2.65
Ni	(0.01)	(0.00)	0.01	0.00	(0.01)	0.00	(0.009)	(0.06)
Ta	0.40	0.30	0.38	0.20	0.55	0.50	0.58	0.60
Se	0.20	0.15	0.15	0.10	0.14	0.14	0.30	0.25
P	(0.02)	(0.01)	0.02	0.01	(0.01)	0.00	(0.04)	(0.09)
Pb	(0.02)	(0.00)	0.01	0.00	(0.02)	0.00	(0.004)	(0.05)
Cd	(0.00)	(0.01)	0.00	0.01	(0.00)	0.02	(0.0008)	(0.005)
Li	2.07	2.06	2.04	2.00	2.18	2.20	2.58	2.53
Be	(0.00)	(0.01)	0.00	(0.00)	(0.00)	(0.01)	(0.0014)	(0.05)
Mn	(0.00)	(0.00)	0.00	0.01	(0.00)	0.001	(0.0007)	(0.05)
Ti	(0.00)	(0.00)	0.00	0.01	(0.00)	0.00	0.009	(0.04)
Sr	6.95	6.01	6.77	6.07	6.26	6.76	6.14	6.09
Fe	(0.05)	(0.01)	0.05	0.04	(0.05)	0.00	(0.04)	(0.09)

Direct carbonation with AMD: Effect of pressure (Mpa) over time (min)

Table B 9: ICP-OES Raw Data

ppm	120 min 1Mpa (Run)	120 min 1Mpa (Dup)	120 min 2Mpa (Run)	120 min 2Mpa (Dup)	120 min 3Mpa (Run)	120 min 3Mpa (Dup)	120 min 4Mpa (Run)	120 min 4Mpa (Dup)
Ca	1411.8	1452.08	1241.6	1431.8	1393.6	1350	1978	1785.6
Al	4.9	4.8	4.7	5	5.3	5.6	4.41	4.4
Si	191.4	190.4	182.3	180.2	179.3	189.2	145.3	140.2
Mg	6.2	6.5	7.1	8.5	7.3	8.6	7.7	7.98
Na	15.1	14.1	16.2	16.1	14.1	13.9	13.59	13.40
Pb	45.8	40.9	34.5	32.4	30.1	29.0	22.01	22.0
Cu	(0.21)	(0.01)	0.02	0.01	0.00	0.01	(0.04)	(0.02)
As	(0.10)	0.10	0.22	0.21	0.4	0.45	(0,09)	0.00
Zn	0.18	0.16	0.89	0.70	0.15	0.14	0.15	0.20
Mo	0.73	0.70	1.2	1.3	1.1	1.5	0.74	0.78
Co	1.87	1.85	1.62	1.60	1.59	1.50	1.94	1.80
Cr	(0.09)	(0.08)	0.01	0.012	0.89	0.80	(0.06)	(0.01)
Ni	0.28	0.20	0.21	0.21	0.34	0.35	0.6	0.5
Ta	20.86	19.8	19.67	13.4	13.1	12.3	11.9	11.7
Se	1.96	1.80	1.60	1.50	1.40	1.30	1.29	1.20
P	(0.21)	(0.01)	1.21	1.42	1.76	1.56	2.81	2.87
Pb	0.09	0.08	0.67	0.65	0.57	0.50	0.42	0.41
Cd	4.99	5.1	5.6	5.8	9.1	9.5	10.1	10.3
Be	0.09	0.10	0.11	0.15	0.20	0.25	0.90	0.91
Mn	0.5	0.5	0.64	0.66	0.68	0.69	0.76	0.77
Ti	(0.10)	0.10	0.60	0.50	0.12	0.01	(0.09)	(0.01)
Sr	(0.65)	(0.78)	0.34	0.45	0.67	0.50	0.59	0.71
Fe	6.5	6.7	6.2	6.5	6.44	6.40	6.45	6.5

Table B 10: XRF Raw Data

%	120 min 1Mpa (Run)	120 min 1Mpa (Dup)	120 min 2Mpa (Run)	120 min 2Mpa (Dup)	120 min 3Mpa (Run)	120 min 3Mpa (Dup)	120 min 4Mpa (Run)	120 min 4Mpa (Dup)
Fe_2O_3	3.24	3.25	3.24	3.25	3.23	3.23	3.17	3.16
MnO	0.04	0.03	0.03	0.03	0.03	0.04	0.04	0.04
Cr_2O_3	0.04	0.04	0.04	0.04	0.04	0.04	0.04	0.04
TiO_2	1.64	1.64	1.64	1.64	1.64	1.63	1.64	1.63
CaO	3.24	3.23	3.18	3.17	3.35	3.38	3.30	3.31
K_2O	0.63	0.65	0.63	0.63	0.65	0.65	0.66	0.66
P_2O_5	0.42	0.42	0.42	0.43	0.43	0.43	0.43	0.44
SiO_2	53.36	53.58	53.64	53.36	53.48	53.51	53.0	53.31
Al_2O_3	34.6	34.68	34.4	34.59	34.51	34.62	34.93	34.93
MgO	0.79	0.79	0.79	0.79	0.78	0.78	0.78	0.81
Na_2O	0.32	0.30	0.34	0.30	0.29	0.30	0.32	0.30
LOI	1.54	1.52	1.74	1.76	1.71	1.67	1.67	1.65

Indirect carbonation with AMD: Effect of time (min) on leaching

Table B 11: ICP-OES Raw Data

ppm	30 min (Run)	30 min (Dup)	60 min (Dup)	60 min (Run)	90 min (Dup)	90 min (Run)	120 min (Dup)	120 min (Dup)
Ca	940	962.1	1110	1140.2	1262	1264	1285	1286
Al	0.41	0.40	0.39	0.30	0.12	0.13	0.12	0.05
Si	0.54	0.55	0.43	0.40	0.34	0.30	0.23	0.20
Mg	0.0081	0.008	0.01	0.015	0.0071	0.0074	0.0067	0.0069
Na	11.5	11.4	10.4	10.3	8.4	8.3	7.2	4.5
Pb	0.19	0.18	0.017	0.016	0.001	0.00	(0.001)	0.00
Cu	0.01	0.02	0.001	0.0012	ND	ND	ND	ND
As	0.009	0.008	0.007	0.006	0.005	0.004	0.002	0.003
Zn	0.019	0.018	0.017	0.018	0.019	0.013	0.014	0.015
Mo	0.24	0.23	0.17	0.16	0.03	0.02	0.01	0.00
Co	0.012	0.011	0.0012	0.0011	0.00	0.00	ND	ND
Cr	0.94	0.94	0.93	0.92	0.80	0.79	0.56	0.51
Ni	(0.02)	0.00	ND	ND	ND	ND	ND	ND
Ta	0.34	0.32	0.28	0.27	0.26	0.25	0.27	0.23
Se	0.15	0.14	0.13	0.12	0.14	0.13	0.12	0.11
P	0.05	0.04	0.03	0.02	0.01	0.00	ND	ND
Pb	0.005	0.004	0.005	0.004	0.003	0.004	0.005	0.003
Li	0.61	0.60	0.059	0.058	0.040	0.031	0.020	0.019
Be	(0.05)	(0.04)	ND	ND	ND	ND	ND	ND
Mn	0.008	0.009	0.008	0.007	0.005	0.004	0.003	0.002
Ti	0.006	(0.007)	0.005	0.004	0.003	0.002	0.001	0.00
Sr	1.24	1.23	1.01	1.00	0.99	0.89	0.20	0.21
Fe	0.054	0.054	0.05	0.04	0.038	0.039	0.007	0.006

Indirect carbonation with AMD: Effect of pressure (Mpa) over time (min)

Table B 12: ICP-OES Raw Data

ppm	120 min 1Mpa (Run)	120 min 1Mpa (Dup)	120 min 2Mpa (Run)	120 min 2Mpa (Dup)	120 min 3Mpa (Run)	120 min 3Mpa (Dup)	120 min 4Mpa (Run)	120 min 4Mpa (Dup)
Ca	410	409	542	546	531	532	589	588
Al	0.018	0.017	0.016	0.015	0.014	0.013	0.012	0.013
Si	1.80	1.79	1.70	1.69	1.60	1.50	1.30	1.29
Mg	(0.002)	(0.0021)	(0.0035)	(0.0034)	(0.0043	0.0044)	0.004	0.0045
Na	58.1	57.9	40.2	40.1	39.8	37.2	37.1	38
Pb	0.062	0.061	0.059	0.059	ND	ND	ND	ND
Cu	0.0074	0.0073	0.0069	0.0060	0.0058	0.0055	0.0040	0.0039
As	0.0014	0.0013	0.0012	0.0011	0.0010	0.0011	ND	ND
Zn	0.0023	0.0024	0.0020	0.0019	0.0018	0.0017	0.0015	0.0014
Mo	0.14	0.13	0.11	0.10	0.09	0.08	0.05	0.04
Co	0.011	0.011	0.09	0.08	0.07	0.06	0.05	0.04
Cr	0.51	0.50	0.049	0.045	0.040	0.039	0.037	0.030
Ni	0.0063	0.0062	0.0061	0.0062	0.0052	0.0040	0.0039	0.0037
Ta	0.40	0.39	0.30	0.29	0.028	0.27	0.20	0.19
Se	0.019	0.018	0.017	0.015	0.015	0.012	0.011	0.010
P	0.024	0.023	0.011	0.010	0.009	0.008	0.006	0.006
Cd	0.62	0.61	ND	ND	ND	ND	ND	ND
Be	0.0082	0.0080	0.0079	0.0078	0.0070	0.006	0.005	0.004
Mn	ND	ND	ND	ND	ND	ND	ND	ND
Ti	0.0067	0.0066	0.0064	0.0060	0.0059	0.0054	0.0053	0.005
Sr	1.28	1.26	1.02	1.00	0.90	0.85	0.56	0.70
Fe	(0.002)	(0.001)	(0.0035)	(0.0034)	(0.0043)	(0.0044)	0.0045	0.0046

Chittick test

W = 0.10 grams weighed of pure $CaCO_3$

T (temperature of measurement in K) = 292.95 K

V (mL produced CO_2): R_1 = 3.9 mL and R_{20} = 7.1 mL ∴ V = 3.9 mL + 7.1 mL = 11 mL

Table B 13: Raw data from Chittick test (direct aqueous carbonation)

Conditions	R1	R2
30 min, 1 Mpa	1	2.4
30 min, 2 Mpa	1.5	1.7
30 min, 3 Mpa	3.2	2.7
30 min, 4 Mpa	4.3	4.1
90 min, 1Mpa	0.9	2.1
90 min, 2 Mpa	1.4	2.8
90 min, 3 Mpa	1.5	2.8
90 min, 4 Mpa	3.5	3.9
120 min, 1 Mpa	1.2	1.1
120 min, 2 Mpa	2.3	3.5
120 min, 3 Mpa	3.5	3.6
120 min, 4 Mpa	4.8	4.7

Table B 14: Raw data from Chittick test (direct carbonation with AMD)

Conditions	R1	R2
30 min, 1 Mpa	2	0.8
30 min, 2 Mpa	3.2	1.1
30 min, 3 Mpa	4	1.5
30 min, 4 Mpa	4.8	2.6
90 min, 1Mpa	3.3	0.7
90 min, 2 Mpa	3.5	3.2
90 min, 3 Mpa	5.9	1.5
90 min, 4 Mpa	3.5	3.9
120 min, 1 Mpa	3.9	1.5
120 min, 2 Mpa	5.3	4.6
120 min, 3 Mpa	8.5	5.4
120 min, 4 Mpa	8.8	5.1

Pressure drop

Table B 15: Raw data for initial and final pressure (direct aqueous carbonation)

Conditions	Initial pressure (Mpa)	Final pressure (Mpa)	Pressure drop (Mpa)
30 min, 1 Mpa	1	0.83	0.17
30 min, 2 Mpa	2	1.72	0.28
30 min, 3 Mpa	3	2.41	0.59
30 min, 4 Mpa	4	3.24	0.76
90 min, 1 Mpa	1	0.55	0.45
90 min, 2 Mpa	2	1.38	0.62
90 min, 3 Mpa	3	2.07	0.93
90 min, 4 Mpa	4	3.03	0.97
120 min, 1 Mpa	1	0.62	0.38
120 min, 2 Mpa	2	1.38	0.62
120 min, 3 Mpa	3	2.07	0.93
120 min, 4 Mpa	4	2.48	1.52

Table B 16: Raw data for initial and final pressure (indirect aqueous carbonation)

Conditions	Initial pressure (Mpa)	Final pressure (Mpa)	Pressure drop (Mpa)
30 min, 1 Mpa	1	0.9	0.1
30 min, 2 Mpa	2	1.79	0.21
30 min, 3 Mpa	3	2.76	0.24
30 min, 4 Mpa	4	3.52	0.48
90 min, 1 Mpa	1	0.83	0.17
90 min, 2 Mpa	2	1.65	0.35
90 min, 3 Mpa	3	2.62	0.38
90 min, 4 Mpa	4	3.38	0.62
120 min, 1 Mpa	1	0.76	0.24
120 min, 2 Mpa	2	1.52	0.48
120 min, 3 Mpa	3	2.48	0.52
120 min, 4 Mpa	4	2.96	1.04

Table B 17: Raw data for initial and final pressure (direct carbonation with AMD)

Conditions	Initial pressure (Mpa)	Final pressure (Mpa)	Pressure drop (Mpa)
30 min, 1 Mpa	1	0.9	0.1
30 min, 2 Mpa	2	1.59	0.41
30 min, 3 Mpa	3	2.48	0.52
30 min, 4 Mpa	4	3.45	0.55
90 min, 1 Mpa	1	0.55	0.45
90 min, 2 Mpa	2	1.03	0.97
90 min, 3 Mpa	3	2	1
90 min, 4 Mpa	4	2.67	1.33
120 min, 1 Mpa	1	0.69	0.31
120 min, 2 Mpa	2	1.17	0.83
120 min, 3 Mpa	3	1.59	1.41
120 min, 4 Mpa	4	2.14	1.86

Table B 18: Raw data for initial and final pressure (indirect carbonation with AMD)

Conditions	Initial pressure (Mpa)	Final pressure (Mpa)	Pressure drop (Mpa)
30 min, 1 Mpa	1	0.9	0.1
30 min, 2 Mpa	2	1.38	0.62
30 min, 3 Mpa	3	2.07	0.93
30 min, 4 Mpa	4	2.96	1.04
90 min, 1 Mpa	1	0.69	0.31
90 min, 2 Mpa	2	1.38	0.62
90 min, 3 Mpa	3	2.07	0.93
90 min, 4 Mpa	4	2.9	1.1
120 min, 1 Mpa	1	0.62	0.38
120 min, 2 Mpa	2	1.38	0.62
120 min, 3 Mpa	3	2.07	0.93
120 min, 4 Mpa	4	2.41	1.59

Appendix C

Table C 1: Critical values for the rejection quotient, Q (Q-test)

N	80 %	90 %	95 %	96 %	98 %	99 %
4	0.679	0.765	0.829	0.846	0.889	0.926

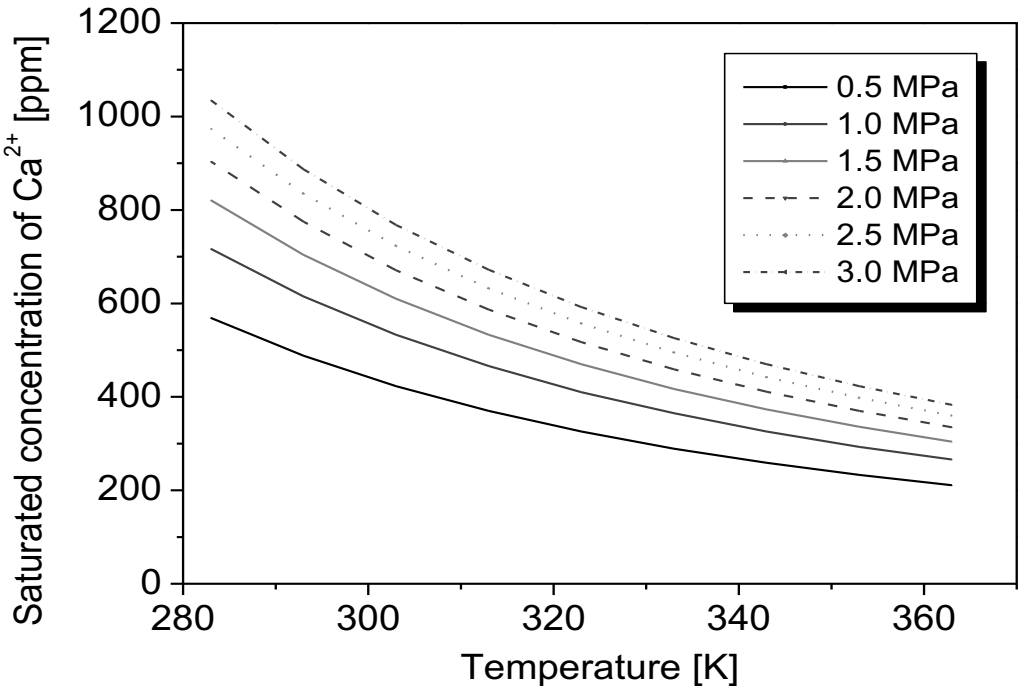

Figure C 1: Saturation concentration of calcium (Ca^{2+}) for a Ca-H_2O-CO_2 at various pressures (Mpa) (Stumm, W. and Morgan, 1996)

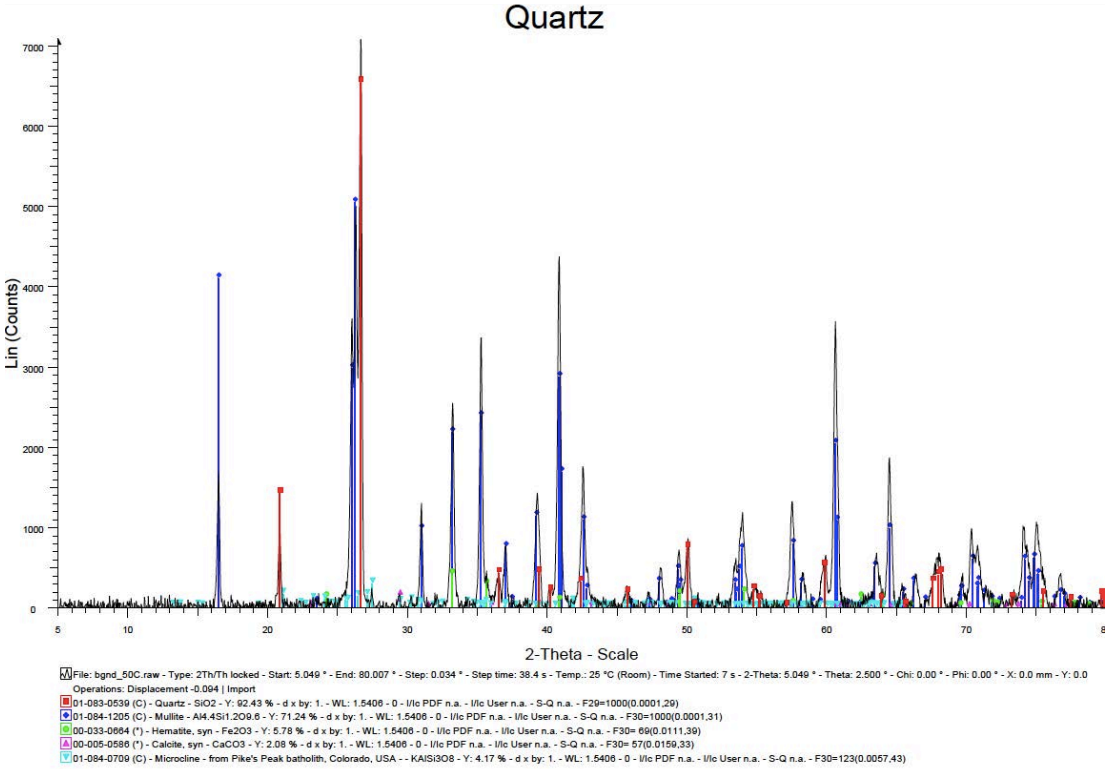

Figure C 2: XRD pattern for solid residue at 50 ^{0}C

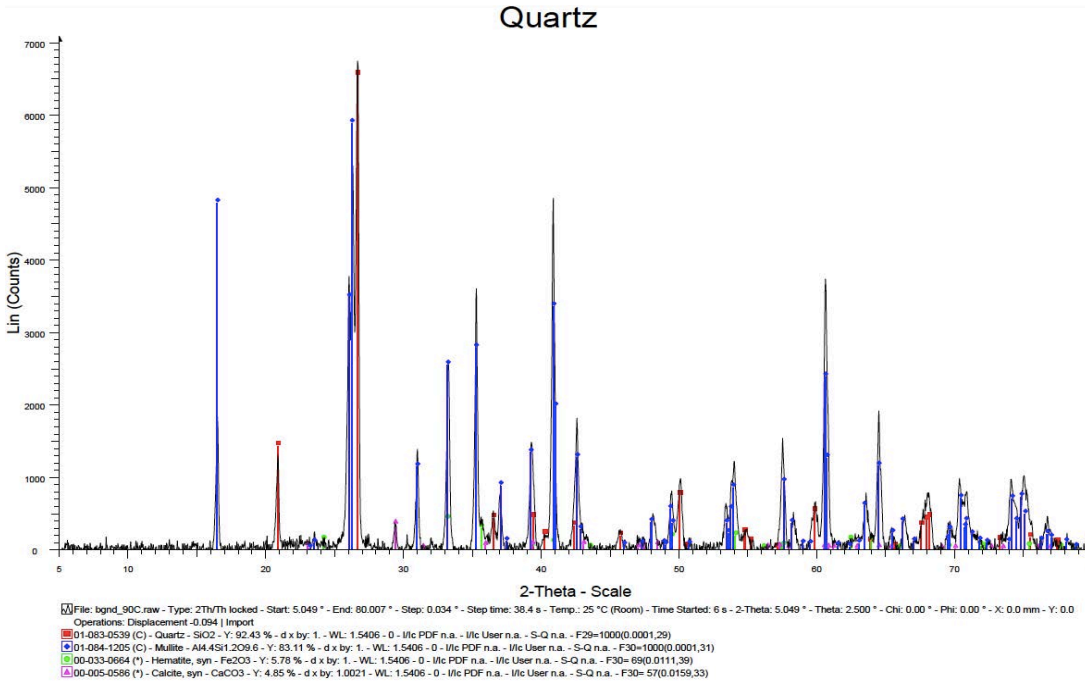

Figure C 3: XRD pattern for solid residue at 90 ^{0}C

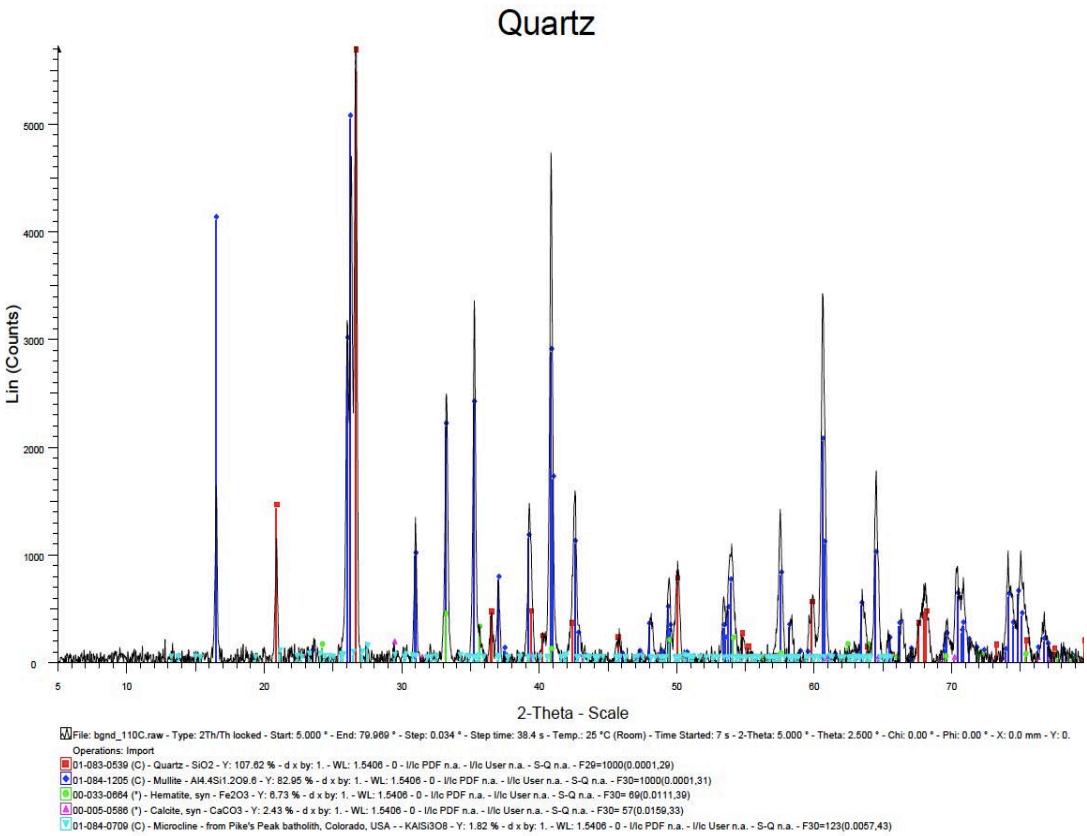

Figure C 4: XRD pattern for solid residue at 110 ^{0}C